



VNIVERSITAT DE VALÈNCIA

**Facultat de Farmàcia**

*Departament de Medicina Preventiva i Salut Pública, Ciències de l'Alimentació,  
Toxicologia i Medicina Legal*

**Programa de Doctorado con Mención hacia la Excelencia  
en Ciencias de la Alimentación**

**MECANISMOS DE ACCIÓN CITOTÓXICA  
PRODUCIDOS POR LA ESTERIGMATOCISTINA EN  
LAS CÉLULAS SH-SY5Y DE NEUROBLASTOMA  
HUMANO**

**STERIGMATOCYSTIN-INDUCED CYTOTOXIC MECHANISMS  
OF ACTION ON HUMAN NEUROBLASTOMA SH-SY5Y CELLS**

**Tesis Doctoral Internacional**

**Valencia, Julio 2021**

Presentada por:

**Veronica Zingales**

Dirigida por:

**Dra. María José Ruiz Leal**

**Dra. Mónica Fernández-Franzón**



La **Dra. María José Ruiz Leal**, Catedrática del área de Toxicología y la **Dra. Mónica Fernández-Franzón**, Profesora Titular del área de Toxicología,

**CERTIFICAN QUE:**

La Licenciada en Ciencias Biológicas y Biología Sanitaria **Dña. Veronica Zingales** ha realizado bajo su dirección el trabajo que lleva por título “Mecanismos de acción citotóxica producidos por la esterigmatocistina en las células sh-sy5y de neuroblastoma humano” y autorizan su presentación para optar al título de Doctora por la Universidad de Valencia.

Y para que así conste, expiden y firman el presente certificado

Burjassot (Valencia), julio 2021.

Dra. María José Ruz Leal

Dra. Mónica Fernández-Franzón



La presente tesis doctoral ha dado lugar a 8 artículos publicados o que si publicarán en las siguientes revistas:

1. Sterigmatocystin-induced cytotoxicity via oxidative stress induction in human neuroblastoma cells. (2020). *Food and Chemical Toxicology*. 136:110956. doi: 10.1016/j.fct.2019.110956. Impact factor: 6.023
2. The role of mitochondria in sterigmatocystin-induced apoptosis on SH-SY5Y cells. (2020). *Food and Chemical Toxicology*. 142:111493. doi: 10.1016/j.fct.2020.111493. Impact factor: 6.023
3. Cytotoxic effects of individual and combined sterigmatocystin and nivalenol on liver hepatocellular carcinoma cells. (2020). *Food and Chemical Toxicology*. 143:11147. doi: 10.1016/j.fct.2020.111473. Impact factor: 6.023
4. Sterigmatocystin: Occurrence, toxicity and molecular mechanisms of action - A review. (2020). *Food and Chemical Toxicology*. 146:111802. doi: 10.1016/j.fct.2020.111802. Impact factor: 6.023
5. Occurrence, mitigation and in vitro cytotoxicity of nivalenol, a type B trichothecene mycotoxin - Updates from the last decade (2010-2020). (2021). *Food and Chemical Toxicology*. 52:112182. doi: 10.1016/j.fct.2021.112182. Impact factor: 6.023
6. Sterigmatocystin-induced DNA damage triggers cell-cycle arrest via MAPK in human neuroblastoma cells. (2021). *Toxicology Mechanisms and Methods*, 26, 1-10. doi: 10.1080/15376516.2021.1916801. Impact factor: 2.987

7. Role of quercetin on sterigmatocystin-induced oxidative stress-mediated toxicity. (2021). *Food and Chemical Toxicology*. Under review. Impact factor: 6.023
8. Development of an in vitro neuroblastoma 3D model and its application for sterigmatocystin-induced cytotoxicity testing. (2021). *Food and Chemical Toxicology*. Under review. Impact factor: 6.023



La doctoranda agradece a la Generalitat Valenciana, Conselleria d'Educació, Investigació, Cultura i Esport:

La beca de investigación de carácter predoctoral del Programa Santiago Grisolia de la (GRISOLIAP/2018/092) CPI-18-117. [2018/4821]

La presente Tesis Doctoral Internacional se engloba dentro de los siguientes proyectos y una red nacional de excelencia:

- ✓ Mitigación, biomarcadores, y toxicidad de micotoxinas legisladas y emergentes (AGL2016-77610-R).
- ✓ Programa Prometeo para grupos de investigación de excelencia (Prometeo 2018/126).
- ✓ Exposición combinada a micotoxinas y plaguicidas. Evaluación del riesgo, seguridad y estrategias de mitigación (PID2020-115871RB-I00-ALI)
- ✓ Red Nacional sobre las micotoxinas y hongos micotoxigénicos y de sus procesos de descontaminación (MICOFOOD).





*“Perseverance is what makes  
the impossible possible, the  
possible probable, and the  
probable certain”*

Robert Half



*Ad Alessandro,  
per trasformare i miei sogni in realtà*



Llegado al final de este camino, pienso en las muchas veces que me han preguntado si estaba realmente segura de que quería emprender el camino del doctorado. Sin dudas, puedo decir que no es un camino fácil, hubo momentos buenos y no tan buenos, muchos sacrificios y ciertamente no faltó el trabajo duro. Pero no ha habido un solo día en el que me arrepienta de mi elección. Y esto gracias a las personas que me acompañaron en este viaje y que merecen ser agradecidas.

En primer lugar, a mis directoras de tesis por haberme guiado durante esta etapa, conduciéndome a un importante desarrollo profesional y personal. A la Dra. María José Ruiz, por el tiempo que me has dedicado, por los consejos, la comprensión y la confianza que me has demostrado, por haber sido más que una directora. A la Dra. Mónica Fernández-Franzón por tenderme tu mano, por tu profesionalidad, apoyo y disponibilidad.

Gracias al Dr. Jordi Mañes y a la Dra. Guillermina Font por acogerme y hacerme sentir parte de este grupo de investigación desde el primer día y por devolverme la esperanza en la meritocracia.

A mis compañeros de este viaje que han hecho inolvidable esta experiencia; gracias por los muchos recuerdos bonitos que guardaré siempre. A Noelia, que con tu bondad infinita y tu energía has hecho cada día más dulce y ligero: gracias por lo que haces y has hecho por mí, nunca te agradeceré lo suficiente. A Mercedes, por estar siempre ahí, por tus infalibles consejos, por tus abrazos y tu espontaneidad; tu amistad ha jugado un papel importante en esta mi etapa: tienes un lugar especial en mi corazón. A Alessandra y Fojan, que habéis traído alegría y luz incluso a los días más oscuros: gracias por los momentos felices que me habéis regalado, nunca los olvidaré. A Fran, por tu apoyo durante los primeros días de este viaje y por ser un apoyo con el que siempre se puede contar. A Claudia y Massimo, por hacerme sentir cerca de nuestra querida Sicilia. A Luna y Agnese que, a pesar de vuestra corta estancia, habéis dejado una huella imborrable en mi corazón. A Dio, por haberme acompañado con tus consejos durante los primeros tiempos de esta etapa y por haberme hecho sentir parte de una familia desde el primer momento.

## Agradecimientos

---

A Bea, Alfonso, Víctor, Valentina, Tiago, Raquel, Carlos, Juanma, Manu y todos los demás compañeros que he tenido el placer de conocer a lo largo de los años.

Gracias a todos los profesores del laboratorio que día a día habéis enriquecido mi amor por la ciencia, al personal de cultivos y a todos los compañeros con los que he compartido muchas horas de trabajo, perdiendo la noción de tiempo entre un pase y una siembra de placas.

Al personal que forma parte de la secretaría de este departamento y, en particular, *gràcies* a Carmen Escrivá por tu infinita disponibilidad y por llevar el peso de muchas responsabilidades con absoluta ligereza.

Grazie alla Prof.ssa Elisa Cimetta, a Rosaria, Pina, Noemi, Anna e a tutto il gruppo NBTECH dell'Università di Padova per la vostra gentilezza e generosità, per il vostro impegno e per il tempo dedicatomi. Grazie per avermi accolta con calore sin da subito, tra un aperitivo ed un prosecco tra le vie di Padova.

Un ringrazio va anche a coloro che hanno fatto nascere in me questa passione per la scienza, a Luca e Alfio, il cui appoggio rimane una certezza nonostante il tempo e la distanza.

Grazie alla mia amica Sabrina, per aver sempre creduto in me più di quanto io stessa ci credessi e per insegnarmi ogni giorno a vedere il lato positivo delle cose.

Un grazie speciale va alla mia famiglia ed in particolare ai miei genitori, che ha permesso che arrivassi fin qui. Grazie per avermi resa quella che sono. E grazie per appoggiarmi sempre in tutte le mie scelte, anche in quelle più difficili. Non é stato facile affrontare la lontananza da voi; sono stati tanti i giorni segnati dalla vostra mancanza e dalla consapevolezza che il tempo trascorso lontani non ci verrà più restituito. Grazie per aver affrontato tutto questo per me. La voglia di rendervi ogni giorno sempre più orgogliosi di me é stata una delle forze motrici di questo viaggio.

Grazie a mia sorella Iolanda, dalla quale mai avrei pensato dovermi allontanare. Il nostro rapporto ha dimostrato saper superare qualsiasi lontananza. Ci sei sempre stata per me e sempre ci sarai, così come io per te.

Grazie ai miei suoceri e ai miei cognati per aver sempre creduto in me e per aver fatto sentire sempre il vostro appoggio.

Ed infine, *dulcis in fundo*, grazie al mio amore Alessandro. Grazie per aver reso possibile tutto questo. Grazie per accompagnarmi in ogni fase della mia vita. Grazie per esserci sempre, pronto a reggermi, consolarmi, confortarmi e regalarmi un sorriso. Grazie per aver accettato di condividere quest'esperienza con me, per fidarti ciecamente. Grazie per supportarmi e sopportarmi. Con te vicino tutto è piú facile ed è anche grazie a te se oggi posso realizzare un sogno. Sei la parte migliore di me. Grazie.

*Gràcies a tots i totes per donar-me una part de vosaltres.*

*Valencia siempre será un lugar especial en mi corazón: aquí siempre estaré en casa, junto a mi pequeña familia española.*





---

**Table of contents**

<b>LIST OF TABLES</b>	<b>XIX</b>
<b>LIST OF FIGURES</b>	<b>XXI</b>
<b>LIST OF ABBREVIATIONS</b>	<b>XXXIII</b>
<b>RESUMEN</b>	<b>1</b>
<b>SUMMARY</b>	<b>3</b>
<b>1. INTRODUCTION</b>	<b>5</b>
1.1. Mycotoxins: Generalities	7
1.2. References	11
1.3. Sterigmatocystin: Occurrence, toxicity and molecular mechanisms of action – A review	13
1.4. Occurrence, mitigation and in vitro cytotoxicity of nivalenol, a type B trichothecene mycotoxin - Updates from the last decade (2010-2020)	79
<b>2. OBJECTIVES</b>	<b>117</b>
<b>3. RESULTS</b>	<b>123</b>
3.1. Cytotoxic effects of individual and combined sterigmatocystin and nivalenol on liver hepatocellular carcinoma cells	125
3.2. Sterigmatocystin-induced cytotoxicity via oxidative stress induction in human neuroblastoma cells	169
3.3. Role of quercetin on sterigmatocystin-induced oxidative stress-mediated toxicity	213
3.4. The role of mitochondria in sterigmatocystin-induced apoptosis on SH-SY5Y cells	251
3.5. Sterigmatocystin-induced DNA damage triggers cell-cycle arrest via MAPK in human neuroblastoma cells	293

---

<b>3.6. Development of an in vitro neuroblastoma 3D model and its application for sterigmatocystin-induced cytotoxicity testing</b>	329
<b>4. GENERAL DISCUSSION</b>	375
<b>4.1. Viabilidad celular</b>	378
4.1.1. Efectos tóxicos de las micotoxinas individuales	378
4.1.2. Efectos tóxicos de combinaciones de micotoxinas	379
<b>4.2. Estrés oxidativo</b>	381
<b>4.3. Sistemas de defensa antioxidante</b>	383
4.3.1. Niveles de glutatión	383
4.3.2. Actividades enzimáticas	385
4.3.3. Quercetina	386
<b>4.4. Toxicidad mitocondrial</b>	388
<b>4.5. Muerte celular: apoptosis y necrosis</b>	389
<b>4.6. Potencial de membrana mitocondrial (<math>\Delta\Psi_m</math>)</b>	391
<b>4.7. Proliferación celular</b>	392
<b>4.8. Genotoxicidad</b>	394
<b>4.9. Respuesta inflamatoria</b>	395
<b>4.10. Citotoxicidad en un modelo de cultivo 3D</b>	396
<b>4.11. Referencias</b>	398
<b>6. CONCLUSIONES</b>	405
<b>ANEXO I Difusión de Resultados</b>	411

## List of Tables

**1.INTRODUCTION****1.3. Sterigmatocystin: Occurrence, toxicity and molecular mechanisms of action – A review**

Tabla 1. <i>In vitro</i> STE toxicity studies.	43
--	----

Tabla 2. <i>In vivo</i> toxicity studies.	51
---	----

**1.4. Occurrence, mitigation and in vitro cytotoxicity of nivalenol, a type B trichothecene mycotoxin - Updates from the last decade (2010-2020)**

Tabla 1. Reports on the occurrence of NIV genotypes since last decade	90
---	----

Tabla 2. Comparative IC <sub>50</sub> values of NIV in different cell lines	98
---	----

**3.RESULTS****3.1. Cytotoxic effects of individual and combined sterigmatocystin and nivalenol on liver hepatocellular carcinoma cells**

Table 1. The IC <sub>50</sub> (μM) ± SEM ( <i>n</i> =2) values of NIV and STE in HepG2 cells determined by MTT assay after 24, 48 and 72 h of exposure..	143
--	-----

Table 2. Dose–effect relationship parameters and mean combination index (CI) values (as a function of fractional inhibition of proliferation) of binary mixture of NIV and STE on HepG-2 cells.	147
---	-----

**3.3. Role of quercetin on sterigmatocystin-induced oxidative stress-mediated toxicity**

Table 1. Gene-specific primers for <i>q</i> PCR experiments.	226
--	-----

**3.4. The role of mitochondria in sterigmatocystin-induced apoptosis on SH-SY5Y cells**

Table 1. Gene-specific primers for <i>q</i> PCR experiments.	266
--	-----

**3.5. Sterigmatocystin-induced DNA damage triggers cell-cycle arrest via MAPK in human neuroblastoma cells**

Table 1. The tail DNA %, tail length and olive tail moment in SH-SY5Y cells exposed to STE at 0.78, 1.56 and 3.12 μM for 24 h.	307
--	-----

**3.6. Development of an in vitro neuroblastoma 3D model and its application for sterigmatocystin-induced cytotoxicity testing**

Table 1. The tail DNA %, tail length and olive tail moment in SH-SY5Y cells obtained from spheroids exposed to 2.5 μM STE for 3 days.	358
---	-----

Table 1. LC-ESI- <i>q</i> TOF-MS data (MS1) of the degradation products obtained in juice and smoothie samples after PEF treatment.	308
---	-----



## List of Figures

**1. INTRODUCTION****1.3. Sterigmatocystin: Occurrence, toxicity and molecular mechanisms of action – A review**

Fig. 1. Conversion of sterigmatocystin to aflatoxin B1 and aflatoxin G1 26

Fig. 2. Sterigmatocystin-induced molecular mechanisms of action. 60

**3.RESULTS****3.1. Cytotoxic effects of individual and combined sterigmatocystin and nivalenol on liver hepatocellular carcinoma cells**

Fig. 1. Chemical structures of Nivalenol (A) and Sterigmatocystin (B). 133

Fig. 2. Cytotoxic effects of individual and binary combination of NIV and STE in HepG2 cells performed by MTT assay after 24 h (a), 48 h (b) and 72 h (c) of exposure; NIV (--▲--), STE (••••) and NIV+STE (-\*-). (\*)  $p \leq 0.05$  indicates significant difference between the mixture and STE assayed individually. (#)  $p \leq 0.05$  indicates significant difference between the mixture and NIV assayed individually. 145

Fig. 3. Fractional effect ( $fa$ )/combination index (CI) curve as described by Chou and Talalay model on HepG2 cells exposed to 24 h (a), 48 h (b) and 72 h (c). Each point represents the CI  $\pm$  SD at a  $fa$  by computer simulation (from  $fa = 0.25$  to  $0.90$ ) as determined in our experiments. The dotted line indicates additive, the area under the dotted line synergism, and the area above of the dotted line antagonism. 146

Fig. 4 Effect of the binary combination NIV + STE on HepG2 cells. a) Single agent dose response curves induced by NIV or STE on HepG2 cells. b) Single-agent and combination dose-response shift. c-e) Surface plots of HepG2 cells treated with NIV, STE or combined NIV + STE shown in 2D and 3D. Each point represents the mean of two independent measurements. Plots were generated using Combeneft program by applying three methods for combined treatments: Loewe additivity model (c), HSA model (d) and Bliss independence model (e). Level of antagonism or synergism is represented by color scale bar. 149

Fig. 5. Time dependence of ROS-induced fluorescence in HepG2 cells exposed to NIV (a), STE (b) and NIV + STE (c). Results are expressed as mean  $\pm$  SEM ( $n=2$ ). (\*)  $p \leq 0.05$  indicates significant difference from the time 0 minutes; (#)  $p \leq 0.05$  indicates significant difference from the control. 151

Fig. 6. Measurement of mitochondrial membrane potential ( $\Delta\Psi_m$ ) in HepG2 cells after 24 h of exposure to different concentrations of NIV (a), STE (b) and NIV + STE (c). Results are expressed as mean  $\pm$  SEM ( $n=2$ ). (\*)  $p \leq 0.05$  indicates significant difference from the control. 152

### 3.2. Sterigmatocystin-induced cytotoxicity via oxidative stress induction in human neuroblastoma cells

Fig. 1. Chemical structure of sterigmatocystin. 177

Fig. 2. Time dependence of ROS-induced fluorescence in SH-SY5Y cells exposed to STE at 0.78, 1.56 and 3.12  $\mu\text{M}$ . The H2-DCFDA was added to SH-SY5Y cells and left for 20 min previously to STE addition from 0 to 120 min. Results are expressed as mean  $\pm$  SEM ( $n=2$ ). There were no significant differences between the concentrations and the control. 186

Fig. 3. The ROS-induced fluorescence in SH-SY5Y cells exposed to STE at 0.78, 1.56 and 3.12  $\mu\text{M}$  during 24 h. Cells were stained with CellROX Deep Red Reagent and subjected to ROS analysis by flow cytometry. a) Data are expressed as mean  $\pm$  SEM ( $n=3$ ). (\*)  $p \leq 0.005$  indicates a significant difference from the control. b) Dot plot representative of control SH-SY5Y cells and c) Dot plot representative of SH-SY5Y cells exposed to 3.12  $\mu\text{M}$  of STE. 187

Fig. 4. The LPO as measured by MDA production in SH-SY5Y cells incubated for 24h with 0.78, 1.56 and 3.12  $\mu\text{M}$  of STE. Results are expressed as mean  $\pm$  SEM ( $n=2$ ) in ng of MDA/mg of protein measured by Lowry method. (\*)  $p \leq 0.005$ , (\*\*)  $p \leq 0.000$  indicates a significant difference from solvent control. (#)  $p \leq 0.01$  indicates a significant difference from 0.78  $\mu\text{M}$  of STE. 188

Fig. 5. Effect of STE (0.78, 1.56 and 3.12  $\mu\text{M}$ ) with and without NAC or BSO pre-treatment on GSH levels (a), GSSG levels (b), and on the GSH/GSSG ratio (c) after 24 h of exposure. Data are expressed as mean values  $\pm$  SEM of two independent experiments with 4 replicates each. \*  $p \leq 0.05$  indicates a significant difference from the respective control (fresh medium, BSO pre-treatment and NAC pre-treatment); #  $p \leq 0.05$  indicates a significant difference respect to the fresh medium 191

Fig. 6. Effect of STE (0.78, 1.56 and 3.12  $\mu\text{M}$ ) with and without NAC or BSO pre-treatment on glutathione peroxidase activity after 24 h of exposure. Data are expressed in % of the unexposed control. GPx activity is expressed as  $\mu\text{mol}$  of NADPH oxidized/min/mg of protein; mean  $\pm$  SEM ( $n = 3$ ). \*  $p \leq 0.05$  indicates a significant difference from the respective solvent control; #  $p \leq 0.05$  indicates a significant difference respect to the medium. 194

Fig. 7. Effect of STE (0.78, 1.56 and 3.12  $\mu\text{M}$ ) with and without NAC or BSO pre-treatment on glutathione S-transferase activity after 24 h of exposure. Data are expressed in % of the unexposed control. GST activity is expressed as mol of product formed/min/mg of protein; mean  $\pm$  SEM ( $n = 3$ ). \*  $p \leq 0.05$  indicates a significant difference from the respective solvent control; #  $p \leq 0.05$  indicates a significant difference respect to the medium. 194

Fig. 8. Effect of STE (0.78, 1.56 and 3.12  $\mu\text{M}$ ) with and without NAC or BSO pre-treatment on catalase activity after 24 h of exposure. Data are expressed in % of the unexposed control. CAT activity is expressed as  $\mu\text{mol}$   $\text{H}_2\text{O}_2$ /min/mg of protein; mean  $\pm$  SEM ( $n = 3$ ). \*  $p \leq 0.05$  indicates a significant difference from the respective solvent control; #  $p \leq 0.05$  indicates a significant difference respect to the medium. 195

Fig. 9. Effect of STE (0.78, 1.56 and 3.12  $\mu\text{M}$ ) with and without NAC or BSO pre-treatment on superoxide dismutase activity after 24 h of exposure. The SOD activity is expressed as units of SOD/mg of protein; mean  $\pm$  SEM ( $n = 3$ ). \*  $p \leq 0.05$  indicates a significant difference from the respective solvent control; #  $p \leq 0.05$  indicates a significant difference respect to the medium. 195

### 3.3. Role of quercetin on sterigmatocystin-induced oxidative stress-mediated toxicity

Fig. 1. Effect of QUE on STE-induced loss of cell viability in SH-SY5Y cell line. Cells were treated with STE (0.19 – 25  $\mu\text{M}$ ) for 24 h in the presence or absence of QUE pre-treatment (10  $\mu\text{M}$ ) for 2 h. Cell viability was assessed by MTT assay. Data are expressed as mean  $\pm$  SEM of two independent experiments ( $n = 2$ ) with 4 replicates each. (\*)  $p \leq 0.05$  indicates a significant difference compared to the corresponding solvent control. (#)  $p \leq 0.05$  indicates a significant difference respect to the corresponding STE treated cells. 228

Fig. 2. Effect of QUE on STE-induced oxidative stress in SH-SY5Y cell line. Cells were treated with STE (0.78, 1.56 and 3.12  $\mu\text{M}$ ) for 24 h in the presence or absence of QUE pre-treatment (10  $\mu\text{M}$ ) for 2 h. The ROS generation was assessed by  $\text{H}_2\text{-DCFDA}$  assay. Data are expressed as mean  $\pm$  SEM of two independent experiments ( $n = 2$ ) with 24 replicates each. (\*)  $p \leq 0.05$  indicates a significant difference compared to the corresponding solvent control. (#)  $p \leq 0.05$  indicates a significant difference respect to the corresponding STE treated cells. 229

Fig. 3. Effect of STE and QUE on NOS-2 (a) and HO-1 (b) expression in SH-SY5Y cell line. Cells were treated with STE (0.78, 1.56 and 3.12  $\mu\text{M}$ ) for 24 h in the presence or absence of QUE pre-treatment (10  $\mu\text{M}$ ) for 2 h. The relative mRNA expression levels were measured by real-time PCR. The average of the target gene values was normalized to the corresponding 18S rRNA value and expressed as fold change compared with the solvent control. Data are expressed as mean  $\pm$  SEM of three independent experiments ( $n = 3$ ) with 3 replicates each. (\*)  $p \leq 0.05$  indicates a significant difference compared to the corresponding solvent control. (#)  $p \leq 0.05$  indicates a significant difference respect to the corresponding STE treated cells. indicates a significant difference from solvent control. (#)  $p \leq 0.01$  indicates a significant difference from 0.78  $\mu\text{M}$  of STE. 231

Fig. 4. Effect of STE and QUE on NF- $\kappa\text{B}$  translocation. a) The SH-SY5Y cells were exposed to STE (0.78, 1.56 and 3.12  $\mu\text{M}$ ) for 24 h in presence or absence of QUE 10  $\mu\text{M}$  pre-treatment, fixed and studied for localization of NF- $\kappa\text{B}$  through indirect immunofluorescence using FITC conjugated secondary antibody (green). The nucleus was stained with DAPI (blue). Figures show DAPI staining, FITC staining and overlay. Images were obtained by using the automated microscope IN Cell Analyzer 2000 (40x magnification). The data shown are representative of three independent experiments. b) Quantification of the nuclei/cytoplasm ratio fluorescence intensity. Data are expressed as mean  $\pm$  SEM ( $n = 3$ ). (\*)  $p \leq 0.05$  indicates a significant difference compared to the corresponding solvent control. (#)  $p \leq 0.05$  indicates a significant difference respect to the corresponding STE treated cells.. 233- 234



Fig. 5. Effect of STE and QUE on TNF- $\alpha$  (a) and IL-6 (b) expression in SH-SY5Y cell line. Cells were treated with STE (0.78, 1.56 and 3.12  $\mu$ M) for 24 h in the presence or absence of QUE pre-treatment (10  $\mu$ M) for 2 h. The relative mRNA expression levels were measured by real-time PCR. The average of the target gene values was normalized to the corresponding 18S rRNA value and expressed as fold change compared with the solvent control. Data are expressed as mean  $\pm$  SEM of three independent experiments ( $n = 3$ ) with 3 replicates each. (\*)  $p \leq 0.05$  indicates a significant difference compared to the corresponding solvent control. (#)  $p \leq 0.05$  indicates a significant difference respect to the corresponding STE treated cells. 236

### 3.4. The role of mitochondria in sterigmatocystin-induced apoptosis on SH-SY5Y cells

Fig. 1. Effect of STE (from 0.78 to 25  $\mu$ M) on the viability of SH-SY5Y cells. Cells were grown in the presence of glucose (25 mM) or galactose (10 mM), following 24 h of exposure to STE. Measurements were performed in a microplate reader using the MTT viability assay. Data are expressed as mean  $\pm$  SEM of three independent experiments with 4 replicates each. (\*)  $p \leq 0.05$  indicates a significant difference compared to the control. (#)  $p \leq 0.05$  indicates a significant difference respect to the corresponding cells grown in glucose-supplemented medium. 269

Fig. 2. Effect of STE (from 0.78 to 25  $\mu$ M) on ATP levels in SH-SY5Y cells. Cells were grown in the presence of glucose (25 mM) or galactose (10 mM), following 24 h of exposure to STE. Measurements were performed in a microplate reader using the CellTiter-Glo<sup>®</sup> Luminescent Cell Viability Assay (Promega). Data are expressed as mean  $\pm$  SEM of three independent experiments with 4 replicates each. (\*)  $p \leq 0.05$  indicates a significant difference compared to the control. (#)  $p \leq 0.05$  indicates a significant difference respect to the corresponding cells grown in glucose-supplemented medium. 270

Fig. 3. Effect of 24 h of exposure to STE 6.24  $\mu$ M with or without antimycin A (10  $\mu$ M) or rotenone (10  $\mu$ M) on the viability of SH-SY5Y cells cultured in galactose-supplemented medium. Measurements were performed in a microplate reader using the MTT viability assay. Data are expressed as mean 271

± SEM of three independent experiments with 4 replicates each. (\*)  $p \leq 0.05$  indicates a significant difference compared to STE 6.24  $\mu\text{M}$ .

Fig. 4. Analysis of mitochondrial superoxide induction in SH-SY5Y cells after exposure to different concentrations (0.78, 1.56 and 3.12  $\mu\text{M}$ ) of STE for 24 h. Mitochondrial superoxide was measured by MitoSOX™ Red Mitochondrial Superoxide Indicator by flow cytometry. a) Data are expressed as mean ± SEM of three independent experiments. (\*)  $p \leq 0.05$  indicates a significant difference compared to the control. b) Dot plot representative of control SH-SY5Y cells and c) Dot plot representative of SH-SY5Y cells exposed to 3.12  $\mu\text{M}$  of STE. 272

Fig. 5. Effect of STE (0.78, 1.56 and 3.12  $\mu\text{M}$ ) on mitochondrial membrane potential ( $\Delta\Psi\text{m}$ ) determined by Rh123 assay. The SH-SY5Y cells were exposed to STE or control (1% methanol) for 24 h in 96-well black plate and then loaded with Rh123 for 15 min. Data are expressed as mean ± SEM of three independent experiments with 24 replicates each. There were no significant differences between the concentrations tested and the control. 273

Fig. 6. Analysis of apoptosis/necrosis induction in SH-SY5Y cells after exposure to different concentrations (0.78, 1.56 and 3.12  $\mu\text{M}$ ) of STE for 2 h. Cells were stained with Annexin V-FITC and PI to distinguish a) early apoptotic and apoptotic/necrotic cells and b) necrotic cells. Data are expressed as mean ± SEM of three independent experiments. (\*)  $p \leq 0.05$  indicates a significant difference compared to the control. 275

Fig. 7. Analysis of apoptosis/necrosis induction in SH-SY5Y cells after exposure to different concentrations (0.78, 1.56 and 3.12  $\mu\text{M}$ ) of STE for 24 h. Cells were stained with Annexin V-FITC and PI to distinguish early apoptotic, apoptotic/necrotic and necrotic cells. (a-d) Two-dimensional dot plots of FITC Annexin V vs. PI through flow cytometry. Cells stained negative for Annexin V-FITC and PI in the lower left quadrant shows alive cells. Cells stained positive for Annexin V-FITC and negative for PI in the lower right quadrant are representing early apoptosis. Cells stained negative for Annexin V-FITC and positive for PI in the upper left quadrant representing necrotic cells. Cells stained positive for both Annexin V-FITC and PI in the upper right quadrant are the late apoptotic/necrotic cells. (e) Percentage of early apoptotic, late apoptotic/necrotic and necrotic cells. Data 276

are expressed as mean  $\pm$  SEM of three independent experiments. (\*)  $p \leq 0.05$  indicates a significant difference compared to the control.

Fig. 8. Analysis of the relative mRNA expression levels of Bax, Bcl-2 and Casp-3 quantified in SH-SY5Y cells after 24 h of STE exposure using real-time PCR. The average of the target gene values was normalized to the corresponding 18S rRNA value and expressed as fold change compared with the solvent control. (\*)  $p \leq 0.05$  indicates a significant difference compared to the control. 277

### 3.5. Sterigmatocystin-induced DNA damage triggers cell-cycle arrest via MAPK in human neuroblastoma cells

Fig. 1. The DNA strand breaks in SH-SY5Y cells measured by alkaline comet assay. The cells were treated with the vehicle (a), 0.78  $\mu$ M (b), 1.56  $\mu$ M (c) and 3.12  $\mu$ M (d) for 24 h. Cells were observed under a fluorescent microscope and quantified (20x magnification). The data shown are representative of three independent experiments. 307

Fig. 2. Effect of STE exposure on histone H2AX phosphorylation. a) The SH-SY5Y cells were exposed to STE (0.78, 1.56 and 3.12  $\mu$ M) for 24 h, fixed and stained with DAPI to visualize nuclei (blue) and with anti- $\gamma$ H2AX antibody as DSBs marker (green). Figures show DAPI staining, FITC staining and overlay. Images were obtained by using the automated microscope IN Cell Analyzer 2000 (40x magnification). The data shown are representative of three independent experiments. b) Quantification of the  $\gamma$ H2AX nuclear staining intensity. Data are expressed as mean  $\pm$  SEM ( $n = 3$ ). (\*)  $p \leq 0.05$  indicates a significant difference compared to the control.. 308-  
309

Fig. 3. Genotoxicity assessment by micronucleus assay in SH-SY5Y cells exposed to STE (0.78, 1.56, and 3.12  $\mu$ M) for 48 h. Data are expressed as percentage of MN per 20 000 cells  $\pm$  SEM ( $n = 3$ ). (\*)  $p \leq 0.05$  indicates a significant difference compared to the control. 310

Fig. 4. Analysis of cell-cycle distribution of SH-SY5Y cells treated with STE at 0.78, 1.56, and 3.12  $\mu\text{M}$  for 24 h. Data are expressed as mean  $\pm$  SEM ( $n = 3$ ). (\*)  $p \leq 0.05$  indicates a significant difference compared to the control. 312

Fig. 5. Cells were exposed to STE, stained with PI and subjected to cell-cycle analysis by flow cytometry. The cell-cycle histograms are representative of SH-SY5Y cells: (a) control and (b) exposed to 3.12  $\mu\text{M}$  of STE for 24 h. 312

Fig. 6. Analysis of cell-cycle distribution of SH-SY5Y cells pre-treated with 20  $\mu\text{M}$  PD98059 (a), 20  $\mu\text{M}$  SP600125 (b), 10  $\mu\text{M}$  SB203580 (c), or 50  $\mu\text{M}$  PFT (d) and exposed to 3.12  $\mu\text{M}$  STE for 24 h. Data are expressed as mean  $\pm$  SEM ( $n = 3$ ). (\*)  $p \leq 0.05$  indicates a significant difference compared to the control; (#)  $p \leq 0.05$  indicates a significant difference compared to cells exposed to 3.12  $\mu\text{M}$  STE. 313

### 3.6. Development of an in vitro neuroblastoma 3D model and its application for sterigmatocystin-induced cytotoxicity testing

Fig. 1. Pipeline employed for spheroid segmentation. a) Routine used to segment spheroids from the background (top panel). Additional routine employed to segment regions of higher cell density within spheroids from migrated cells around (bottom panel). b) Representative image of the overlay of the generated spheroid mask over the original image. 346

Fig. 2. Bright-field images of SH-SY5Y (a) and SK-N-DZ (b) spheroids grown at the indicated time points. Images were obtained using the Light Microscope Zeiss Axio Observer (Zeiss Microscopy, Germany). Scale bars: 100  $\mu\text{m}$ . 348

Fig. 3. Morphology and volume of human neuroblastoma spheroids after exposure to STE. a) Bright-field images of SH-SY5Y spheroids after 0, 1, 2, 3 and 4 days of exposure to increasing concentrations of STE (2.5 - 20  $\mu\text{M}$ ). Scale bar: 100  $\mu\text{m}$ . Images were obtained using the Light Microscope Zeiss Axio Observer (Zeiss Microscopy, Germany). b) Bar chart showing the area growth of SH-SY5Y spheroids exposed to STE (2.5 and 5  $\mu\text{M}$ ) for 0, 2, 3 and 4 days. (\*)  $p \leq 0.05$  indicates a significant difference compared to the control. Quantitative analysis was performed using the software Zen Lite version 2.6 (Zeiss Microscopy, Germany). c) Bright-field images of SK-N- 351- 353

DZ spheroids after 0, 1, 2, 3 and 4 days of exposure to increasing concentrations of STE (2.5 - 20  $\mu\text{M}$ ). Scale bar: 100  $\mu\text{M}$ . Images were obtained using the Light Microscope Zeiss Axio Observer (Zeiss Microscopy, Germany). d) Bar chart showing the area growth of SK-N-DZ spheroids exposed to STE (2.5 - 20  $\mu\text{M}$ ) for 0, 2, 3 and 4 days. Quantitative analysis was performed using the Zen Lite version 2.6 (Zeiss Microscopy, Germany). (\*)  $p \leq 0.05$  indicates a significant difference compared to the control.

Fig. 4. Effect of STE exposure on Casp-3 and Ki-67 by immunofluorescence assay. The SH-SY5Y spheroids were exposed to STE (2.5, and 5  $\mu\text{M}$ ) for (a) 2 and (b) 3 days, fixed and stained with DAPI to visualize nuclei (blue), anti-Casp-3 antibody as marker of apoptosis (red) and anti-Ki-67 antibody as marker of proliferation (green). Images were obtained by using the confocal fluorescence microscope Zeiss LSM 800 (Zeiss Microscopy, Germany; 25x magnification). The data shown are representative of two independent experiments.

354

Fig. 5. 3D images are representative of SH-SY5Y spheroids exposed to STE 5  $\mu\text{M}$  for (a) 2 and (b) 3 days. Spheroids were exposed to STE and stained with DAPI (blue), the apoptotic marker Casp-3 (red) and the proliferation marker Ki-67 (green). Images were obtained using the software Zen Lite version 3.3 (Zeiss Microscopy, Germany).

355

Fig. 6. Effect of STE on cPARP expression. SH-SY5Y spheroids were exposed to STE at 2.5 and 5  $\mu\text{M}$  for 3 days. The samples were then subjected to western blot analysis. a) Western blot showing cleaved PARP expression. b) Densitometric analysis of cleaved PARP wester blots performed using ImageJ software version 1.53e (Java 1.8.0\_172, USA). The average of the target protein value was normalized to the corresponding GAPDH value and expressed as fold change compared with the solvent control. Data are expressed as mean  $\pm$  SEM of two independent experiments ( $n = 2$ ). (\*)  $p \leq 0.05$  indicates a significant difference compared to the control.

355

Fig. 7. Effect of STE exposure on ROS generation in SH-Y5Y spheroids. Spheroids were exposed to STE (2.5 and 5  $\mu\text{M}$ ) for 1, 2 and 3 days. The ROS generation was assessed by  $\text{H}_2\text{-DCFDA}$  probe. Data are expressed as mean  $\pm$  SEM of two independent experiments ( $n = 2$ ) with 24 replicates each. (\*)  $p \leq 0.05$  indicates a significant difference compared to the control. 357

Fig. 8. The DNA strand breaks in SH-SY5Y spheroids measured by alkaline comet assay. The cells were treated with the vehicle (a) and 2.5  $\mu\text{M}$  (b) of STE for 3 days. The cells in the single cell suspension were obtained from spheroids by mechanical degradation and enzymatic digestion. Cells were observed under a fluorescent microscope and quantified (20x magnification). 358

Fig. 9. Effect of STE (0.78, 1.56 and 3.12  $\mu\text{M}$ ) on cell migration in SH-SY5Y cells monolayer (2D). a) Representative microscopic images showing the effect of STE on cell migration in the wound healing migration assay (10x magnification). Cells were seeded in each compartment of the silicone culture insert and, after its removal, cells were photographed for evidence of cell migration 0, 1 and 2 days after the addition of the mycotoxin. b) Bar chart showing the wound closure expressed as the remaining area uncovered by the cells over the time. The area that remained clear of cells was quantified using ImageJ software version 1.53e (Java 1.8.0\_172, USA). Data are expressed as mean  $\pm$  SEM of three independent experiments ( $n = 3$ ). Three visual fields were analysed per sample in each independent experiment. (\*)  $p \leq 0,05$  indicates a significant difference with respect to the corresponding solvent control; (#)  $p \leq 0,05$  indicates a significant difference respect to the corresponding concentration at time 0 h. c) Representative microscopic images of cells that migrated through the pores of the transwell in the transwell migration assay (10x magnification). Cells exposed to STE for 2 days were seeded upper transwell chambers, incubated for 1 day, fixed and stained with crystal violet. d) Bar chart showing the number of cells that migrated through the transwell in the transwell migration assay. The number of cells that migrated through the transwell was calculated using the ImageJ software 1.53e (Java 1.8.0\_172, USA). Data are expressed as mean  $\pm$  SEM of two independent experiments ( $n = 2$ ) with 2 replicates each. Four-five visual fields were analysed per replicate in each independent experiment. No significant differences were observed between cells exposed to STE and control. 360- 362

Fig. 10. Effect of STE 2.5  $\mu\text{M}$  on cell migration in SH-SY5Y spheroids (3D). a-b) Spheroids were placed on gelatin-coated plates and exposed to 2.5  $\mu\text{M}$  STE. Control was treated with the vehicle. Images were captured for 3 days at intervals of 1 day using the inverted light microscope Zeiss Primo Vert equipped with a Zeiss camera (Axiocam 208 color, Zeiss Microscopy, Germany) at 4 $\times$  magnification and analysed with the software MATLAB R2020a (MathWorks<sup>®</sup>, Natick, MA). Scale bar: 500  $\mu\text{m}$ . c) Details of cell migration in spheroids after 3 days of exposure obtained using the inverted light microscope Zeiss Primo Vert equipped with a Zeiss camera (Axiocam 208 color, Zeiss Microscopy, Germany) at 10 $\times$  magnification. Scale bar: 100  $\mu\text{m}$ . d) Western blot showing MMP9 expression and its densitometric analysis performed using Image J software version 1.53e (Java 1.8.0\_172, USA). The average of the target protein value was normalized to the corresponding GAPDH value and expressed as fold change compared with the solvent control. Data are expressed as mean  $\pm$  SEM of two independent experiments ( $n = 2$ ). No significant differences were observed between spheroids exposed to STE and control.

363-

364





**List of abbreviations**

15-ADON	15-acetil deoxinivalenol
2D	Two-dimensional
3-ADON	3-acetil deoxinivalenol
3D	Three-dimensional
8-OHdG	8-hydroxydeoxyguanosine
A549	Adenocarcinomic human alveolar basal epithelial cells
ACHN	Adenocarcinomic human alveolar basal epithelial cells
ACI	August-Copenhagen Irish
ADN	Ácido desoxirribonucleico
AFB1	Aflatoxin B1
AFG1	Aflatoxin G1
AFs	Aflatoxins
ARNm	Ácido ribonucleico mensajero
ATM/p53	Ataxia Telangiectasia Mutated kinase/tumour protein p53
ATP	Adenosine triphosphate
BAX	Bcl-2-associated X protein
BCL-2	Bcl-2-associated X protein
BEA	Beauvericin
BEAS-2B	Human bronchial epithelial cells
BSO	L-Buthionine-(S,R)-Sulfoximine
BW	Body weight
C3H	Inbred mouse strain
CASP-3	Caspase-3
CAT	Catalase
CHK1	Checkpoint kinase 1
CHO-K1	Chinese hamster ovary cells
CTE	Cadena de Transporte Electronico
DNA	Deoxyribonucleic acid
DON	Deoxynivalenol
EFSA	European Food Safety Authority
ENNs	Eniatinas
ERK	Extracellular signal-regulated kinase

## Lista de abreviaturas

---

ERK	Extracellular signal-regulated kinase
FAO	Food Agriculture Organization
FAOSTAT	Food and Agriculture Organization Corporate Statistical Database
FBs	Fumonisin
FCM	Flow cytometry
FDA	Food and Drug Administration
GES-1	Human gastric epithelial cells
GPx	Glutathione peroxidase
GSH	Glutathione
GSSG	Glutathione Oxidized
GST	Glutathione S-transferase
Hep3B	Human hepatocellular carcinoma cells
HepG2	Human hepatocellular carcinoma cells;
Het-1A	Human esophageal epithelial cells
HL-60	Human promyelocytic leukaemia cells
HLA-I	Human leukocyte antigen-I
hMLH1	Human mutL homolog 1
HO-1	Heme Oxygenase-1
HPBMc	Human peripheral blood mononuclear cells
IARC	International Agency for Research on Cancer
IC <sub>50</sub>	mean 50% inhibitory concentration
IL	Interleukin
JNK	c-JUN N-terminal kinase
Keap-1	Kelch-like ECH-associated protein 1
L-929	Murine fibroblasts
LD <sub>50</sub>	Median lethal dose
LPO	Lipid peroxidation
LS-174T	Human epithelial colorectal adenocarcinoma cells
LY294002	PI3K inhibitor
MAPK	Mitogen activated protein kinase
MEFs	Mouse embryonic fibroblasts
MeOH	Methanol
MMP	Mitochondria membrane permeability
MMR	Mismatch repair
mPBMC	Mouse peripheral blood mononuclear cells

MTT	3-(4,5-dimethylthiazol-2-yl)-2,5-diphenyltetrazolium bromide
MYCN	v-myc myelocytomatosis viral-related oncogene, neuroblastoma-derived
NAC	N-acetyl-L-cysteine
Neuro-2a	Murine neuroblastoma cells
NF- $\kappa$ B	Nuclear Factor kappa-light-chain-enhancer of activated B cells
NOS-2	Nitric Oxide Synthase-2
NR	Neutral Red
OXPHOS	Oxidative Phosphorilation
p38	Mitogen activated protein kinase
p53	Tumour protein p53
PAT	Patulin
PD98059	ERK inhibitor
QUE	Quercetin
RASFF	Rapid Alert System for Food and Feed
RN	Rojo Neutro
ROS	Reactive oxygen species
SH-SY5Y	Human neuroblastoma cells
SK-N-DZ	Human neuroblastoma cells
SOD	Superoxide dismutase
SP600125	JNK inhibitor
SRB	Sulforhodamine B
STE	Sterigmatocystin
THP-1	Human acute monocyte leukaemia cells
TNF- $\alpha$	Tumor necrosis factor $\alpha$
WHO	World Health Organization
$\gamma$ H2AX	Phosphorylated histone H2AX
$\Delta\Psi_m$	Mitochondrial Membrane Potencial



**RESUMEN**

En la presente Tesis Doctoral se ha llevado a cabo la evaluación *in vitro* de los efectos producidos por la micotoxina esterigmatocistina (STE) en células de mamífero. El conocimiento de los efectos tóxicos y exposición a dicha micotoxina permite una mejor caracterización de los riesgos de la población.

Se ha evaluado la citotoxicidad individual de la STE en células de neuroblastoma (SH-SY5Y) y de carcinoma hepatocelular humano (HepG2), mostrando valores de IC<sub>50</sub> únicamente en las células SH-SY5Y. Debido a que la exposición simultánea o secuencial a múltiples micotoxinas podría dar lugar a efectos adversos sobre la salud del consumidor, se ha evaluado la citotoxicidad combinada de la STE con el nivalenol (NIV) en las células HepG2, mostrando efectos principalmente aditivos y sinérgicos.

A continuación, se han evaluado los mecanismos de toxicidad de la STE en las células SH-SY5Y. La exposición de las células SH-SY5Y a la STE pone de manifiesto disrupción del ciclo celular, incremento del daño al ADN y del estrés oxidativo, que podría estar relacionado con la muerte celular por apoptosis.

Tras demostrar la capacidad de la STE para generar especies reactivas del oxígeno (ROS), se ha evaluado la eficacia del sistema de defensa intracelular (enzimático y no enzimático) frente al estrés oxidativo, observándose una disminución de los niveles de glutatión, así como de la actividad de las enzimas glutatión peroxidasa, glutatión transferasa, catalasa y superóxido dismutasa, lo cual indica que las células SH-SY5Y son incapaces de contrarrestar el estrés oxidativo producido por la STE.

Por otra parte, se ha determinado el efecto de la quercetina, un antioxidante de la dieta conocido por sus múltiples propiedades biológicas, y se ha observado un efecto protector frente a la citotoxicidad, la producción de ROS y la inducción de otros marcadores de estrés oxidativo producidas por la STE en las células SH-SY5Y.

Finalmente, se han evaluado los efectos de la STE sobre procesos como proliferación, estrés oxidativo, apoptosis y daño al ADN en modelos de cultivo celular tridimensionales (3D) de neuroblastoma (esferoides) de células SH-SY5Y y se han comparado con el efecto inducido en los cultivos de las células SH-SY5Y en monocapa. Los resultados obtenidos han confirmado la citotoxicidad y la capacidad de la STE para inducir apoptosis, estrés oxidativo y daño al ADN en las células SH-SY5Y, tanto en cultivos celulares 2D como en 3D. Sin embargo, los esferoides han mostrado más resistencia que el cultivo celular en monocapa (2D) a los efectos tóxicos de la STE, ya que concentraciones y tiempos de exposición menores fueron suficientes para causar efectos tóxicos en el sistema 2D que no se observan en el sistema 3D.

Los resultados indican que la STE supone un riesgo tóxico potencial. Por lo tanto, es necesario un mayor conocimiento sobre los mecanismos de acción tóxica de la STE para poder prevenir efectos adversos sobre la salud de los individuos expuestos a esta u otras micotoxinas.

## SUMMARY

In the present Doctoral Thesis, *in vitro* evaluation of the effects induced by the mycotoxin sterigmatocystin (STE) in mammalian cells has been carried out. Elucidating the toxicological effect of STE will allow for a better assessment of the risk associated with its exposure.

Individual cytotoxicity of STE has been evaluated in human neuroblastoma (SH-SY5Y) and hepatocellular carcinoma (HepG2) cells, showing IC<sub>50</sub> values only in SH-SY5Y cells. As simultaneous or sequential exposure to multiple mycotoxins could lead to adverse effects on consumer health, the cytotoxicity of STE in combination with nivalenol (NIV) has been evaluated in HepG2 cells, resulting mainly in additive and synergistic effects.

Afterward, the mechanisms of STE toxicity cells have been evaluated in SH-SY5Y. Exposure of SH-SY5Y cells to STE reveals cell cycle disruption, increased DNA damage and oxidative stress, which could be related to apoptosis cell death.

After demonstrating the ability of STE to generate reactive oxygen species (ROS), the efficacy of the intracellular defence system (enzymatic and non-enzymatic) against oxidative stress has been evaluated, observing a decrease in glutathione levels, as well as in the activity of the enzymes glutathione peroxidase, glutathione transferase, catalase and superoxide dismutase, which suggests that SH-SY5Y cells are not able of counteracting the oxidative stress induced by STE.

Furthermore, the effect of quercetin, a dietary antioxidant known for its multiple biological properties, has been determined, showing a protective effect against cytotoxicity, ROS production and the induction of other oxidative stress markers induced by STE in SH-SY5Y cells.

Finally, the effects of STE on processes such as proliferation, oxidative stress, apoptosis and DNA damage induction have been evaluated in 3D spheroid model of human neuroblastoma SH-SY5Y cells and compared with the effects observed in monolayer SH-SY5Y cell cultures. The results obtained have confirmed the cytotoxicity of STE and its ability to trigger apoptosis, oxidative stress and DNA damage on SH-SY5Y cells in both 2D and 3D cell cultures. However, spheroids have shown more resistance than 2D monolayer cell culture to the toxic effects of STE, as lower concentrations and exposure times were sufficient to cause toxic effects in the 2D system compared to the 3D system.

The results indicate that STE represents a potential health hazard. Therefore, a deeper understanding of the toxic mechanisms of action of STE is needed to prevent adverse health effects on individuals exposed to this or other mycotoxins.



**1.INTRODUCTION**

INTRODUCCIÓN



## 1. INTRODUCTION

### 1.1. Mycotoxins: Generalities

Mycotoxins are toxic low-molecular-weight secondary metabolites produced by filamentous fungi or moulds, mainly belonging to the genera *Aspergillus*, *Fusarium*, *Alternaria* and *Penicillium*. As stable chemical compounds, mycotoxins can be transferred along the whole food chain, during pre-harvest (in the field) or in the post-harvest stages (storage, transport and processing), posing a difficult challenge to food safety and inflicting high economic losses in the agricultural industries worldwide (Marin et al., 2013).

Fungi find ideal conditions for mycotoxin production in a wide variety of food commodities. The foods most commonly contaminated by mycotoxins are the products of the primary sector: cereals and cereal-by-products, fruits and vegetables, coffee, cacao, spices and dried fruits. Moreover, mycotoxins can be found in animal-derived products such as meat, eggs, milk, and milk derivatives due to their carry-over from animals that have consumed contaminated feeds (Habschied et al., 2021).

Contamination by mycotoxins represents an ongoing common concern. Furthermore, global trade of food and feed commodities contributes to the worldwide dispersal of mycotoxins (Smith et al., 2016). During the years 2010 to 2019, the Rapid Alert System for Food and Feed (RASFF) reported 5484 notifications for mycotoxin contamination in food and feed products, with 534 notifications issued only in 2019 (Alshannaq and Yu, 2021; RASFF, 2019). The even more alarming prevalence of mycotoxin-contaminated foods has led to an increased scientific interest in understanding the environmental conditions that favour mycotoxin production, the possible strategies to prevent it, as well as the

effects on human and animal health. However, as natural contaminants, their presence in food commodities is often not completely stoppable and despite numerous efforts have been made, mycotoxins occurrence remains an unavoidable and unpredictable problem (Alshannaq and Yu, 2017).

The importance of mycotoxins is related to their toxicity at low doses. The toxicity caused by mycotoxins can be acute or chronic, being the latter the most frequent. Acute toxicity is characterized by a single exposure to a high dose, with immediate effects. On the other hand, chronic toxicity is characterized by prolonged exposure to low doses, with effects that may occur in the long term (De Ruyck et al., 2015). Human exposure to mycotoxins may occur through the direct consumption of contaminated food or from the consumption of animals fed with mycotoxin-contaminated feed. Other common routes of exposure include skin contact and inhalation (Adegbeye et al., 2020).

What is more, single mycotoxin exposure is not the norm but rather the exception. In fact, the natural co-occurrence of mycotoxins in food and feed is well-known, and can be explained by at least three reasons: (i) one fungal species may produce many different mycotoxins; (ii) food commodities can be contaminated by several fungi simultaneously or in quick succession and (iii) animal diets are usually made up of multiple grain sources. Consequently, in the richly varied modern Western diet, individuals are exposed through their diets to a very wide variety of mycotoxins. On the other hand, third-world nations with relatively consistent diets are no safer, being reliant on cereal crops grown and processed under laxer regulation and prone to significantly higher levels of contamination (Smith et al., 2016).

Mycotoxins exposure can cause damage to the nervous, cardiovascular, respiratory, urinary, digestive or immune system, and at subclinical concentrations may affect animal production and adulterate feed and animal by-products. (Pleadin et al., 2019). Mycotoxicosis is the term used for the toxicological syndromes caused by human exposure to mycotoxins. The symptoms of mycotoxicosis can be different depending on the type of mycotoxin, concentrations, time of exposure, the age, gender and health state of the individual, as well as the interactions with other toxics (Soler and Oswald, 2018). Historically, the oldest food-borne disease known dates to the Middle Ages and was called "ergotism" or St. Anthony's Fire, due to the burning sensation experienced by individual affected. In 1960, the outbreak of another mycotoxicosis in England, the Turkey X disease, culminated in the discovery of aflatoxins and the awareness that low levels of mould metabolites in foods and feed could cause disease in humans and animals. (Stoev, 2015). This gave great impetus to the study of mycotoxins. Since then, various mycotoxins were investigated for individual toxicity and several authors have shown an interest in cellular mechanisms and cellular toxicity in response to mycotoxin exposure. To date, over 500 different classes of mycotoxins have been discovered and various biological effects such as organ toxicity, mutagenicity, carcinogenicity, teratogenicity and modulation of the immune system have been well documented by in vitro and in vivo assays. Although mycotoxins have been investigated in relation to a wide range of adverse human health effects, the full impact on human health of the widespread exposure to mycotoxins remains to be defined (IARC, 2012).

The discovery of the harmful effects of mycotoxin exposure on human and animal health led many national and international public health and

governmental authorities, such as the Food and Drug Administration (FDA), the WHO, the Food Agriculture Organization (FAO), and the European Food Safety Authority (EFSA), to pay serious attention to mycotoxin contamination in food and feed by adopting strict regulatory guidelines for major mycotoxin classes in food and feed. However, all limits must be supported by reliable and extensive research in order to avoid unnecessary restrictions and economic loss. As a rule, there are two main points taken into account in the risk assessment: the toxic effect of particular mycotoxin and an estimate of the consumer's mycotoxin exposure (Stoev, 2013). In this context, *in vitro* studies become embedded in national and international legislation regulating the use of animals in scientific procedures in order to encourage and develop the principles of the 3Rs (Replacement, Reduction, and Refinement) as a framework for humane research on animal (Hampshire and Gilbert, 2019). Noteworthy, the current regulations were established on toxicological data from studies taking into account only one mycotoxin exposure at a time, and do not consider the combined effects of mycotoxins. It is therefore of the utmost importance to assess the toxicological impact of mycotoxins alone and in combinations in order to fully understand the extent of the adverse effects of these common dietary contaminants and to take adequate public health measures.

## 1.2. References

Adegbeye, M.J., Reddy, P.R.K., Chilaka, C.A., Balogun, O.B., Elghandour, M., Rivas-Caceres, R.R., et al., 2020. Mycotoxin toxicity and residue in animal products: Prevalence, consumer exposure and reduction strategies - A review. *Toxicon* 177, 96-108.

Alshannaq, A., Yu, J.H., 2017. Occurrence, Toxicity, and Analysis of Major Mycotoxins in Food. *Int J Environ Res Public Health* 14 (6), 632.

Alshannaq, A., Yu, J.H., 2021. Analysis of E.U. Rapid Alert System (RASFF) Notifications for Aflatoxins in Exported U.S. Food and Feed Products for 2010-2019. *Toxins* 13 (2), 90.

De Ruyck, K., De Boevre, M., Huybrechts, I., De Saeger, S., 2015. Dietary mycotoxins, co-exposure, and carcinogenesis in humans: Short review. *Mutat Res Rev Mutat Res* 766, 32-41.

Habschied, K., Kanizai Saric, G., Krstanovic, V., Mastanjevic, K., 2021. Mycotoxins-Biomonitoring and Human Exposure. *Toxins* 13 (2), 113.

Hampshire, V.A., Gilbert, S.H., 2019. Refinement, Reduction, and Replacement (3R) Strategies in Preclinical Testing of Medical Devices. *Toxicol Pathol* 47, 329-338.

IARC, 2012. Mycotoxins and human health. *IARC Sci Publ*, 87-104.

Marin, S., Ramos, A.J., Cano-Sancho, G., Sanchis, V., 2013. Mycotoxins: occurrence, toxicology, and exposure assessment. *Food Chem Toxicol* 60, 218-237.

Pleadin, J., Frece, J., Markov, K., 2019. Mycotoxins in food and feed. *Adv Food Nutr Res* 89, 297-345.

RASFF, 2019. The Rapid Alert System for Food and Feed — Annual Report 2019; European Commission: Brussels, Belgium.

Smith, M.C., Madec, S., Coton, E., Hymery, N., 2016. Natural Co-Occurrence of Mycotoxins in Foods and Feeds and Their in vitro Combined Toxicological Effects. *Toxins* 8 (4), 94.

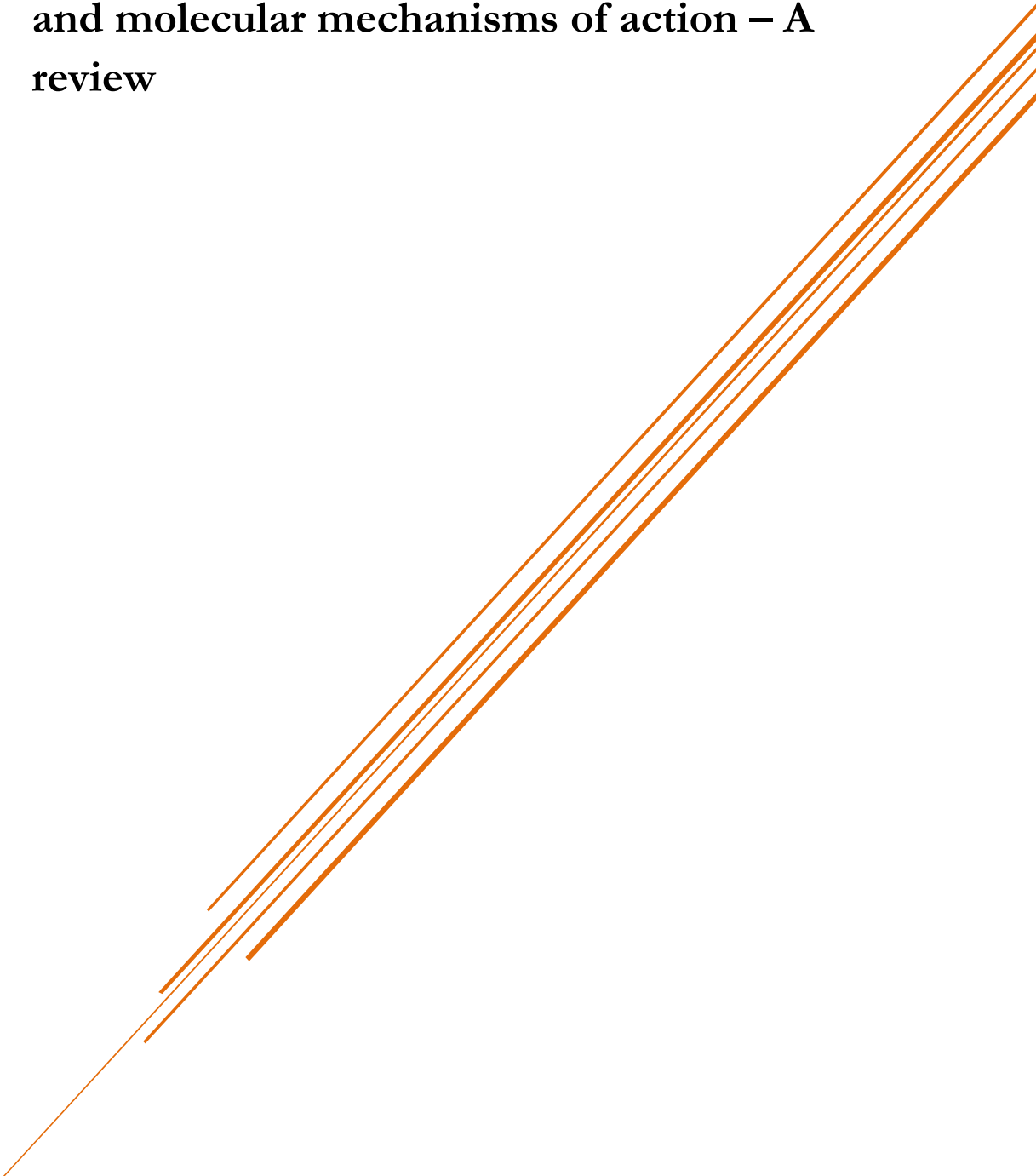
Soler, L., Oswald, I.P., 2018. The importance of accounting for sex in the search of proteomic signatures of mycotoxin exposure. *J Proteomics* 178, 114-122.

Stoev, S.D., 2013. Food safety and increasing hazard of mycotoxin occurrence in foods and feeds. *Crit Rev Food Sci Nutr* 53, 887-901.

Stoev, S.D., 2015. Foodborne mycotoxicoses, risk assessment and underestimated hazard of masked mycotoxins and joint mycotoxin effects or interaction. *Environ Toxicol Pharmacol* 39, 794-809.



### **1.3. Sterigmatocystin: Occurrence, toxicity and molecular mechanisms of action – A review**





Food and Chemical Toxicology

**Sterigmatocystin: Occurrence, toxicity and molecular mechanisms of action – A review**

Veronica Zingales\*, Mónica Fernández-Franzón, Maria-José Ruiz

Laboratory of Food Chemistry and Toxicology, Faculty of Pharmacy, University of

Valencia, Av. Vicent Andrés Estellés s/n, 46100, Valencia, Spain

\*Corresponding author. Laboratory of Toxicology, Faculty of Pharmacy, University of Valencia, Av. Vicent Andrés Estellés, s/n, 46100, Burjassot, Valencia, Spain. *E-mail address:* [vezin@uv.es](mailto:vezin@uv.es) (V. Zingales).

### **Abstract**

The mycotoxin sterigmatocystin (STE) is produced mainly by *Aspergillus* fungi. It has been reported to occur in grains and grain-based products, cheese, coffee, spices and beer. The STE is a known biogenic precursor of aflatoxin B<sub>1</sub>, sharing with it several structural and biological similarities. The STE has been shown to be hepatotoxic and nephrotoxic in animals and it has been classified as possible human carcinogen (group 2B) by IARC. The STE has been reported to cause a marked decrease in cell proliferation in different mammalian cells. Data available on literature suggest that the cellular mechanisms underlying STE-induced toxicity include the induction of oxidative stress, mitochondrial dysfunction, apoptosis, cell cycle arrest, as well as alteration of immune system function and activation of different signalling pathways. Moreover, STE resulted to be genotoxic, being able to form DNA-adducts and induce DNA damage. Despite its strong cytotoxicity, no risk assessments have been still carried out by authorities due to the lack of toxicity data, so research on STE toxicological impact is still going on. This review reports information available regarding STE toxicity and its related mechanisms of action with the aim of updating information regarding last researches on this mycotoxin.

**Keywords:** Sterigmatocystin, Occurrence in food, Biosynthetic and metabolic pathway, Mechanisms of action, Toxicity.

## 1. Generalities

Sterigmatocystin (STE) is a polyketide mycotoxin produced by several fungal species belonging to the genera *Aspergillus*, *Bipolaris*, *Botryotrichum*, *Humicola* and *Penicillium*. The main producers are *Aspergillus* fungi, such as *A. flavus*, *A. parasiticus*, *A. nidulans* and *A. versicolor*, from whose cultures STE was isolated by the first time in 1954 (Gruber-Dorninger et al., 2017; Rank et al., 2011). Fungi capable of producing STE are common food and feed contaminants, with a consequent strong economic impact for the biotechnological, agricultural and food industries (Wagacha and Muthomi, 2008). *Aspergillus flavus* and *A. parasiticus* are among the main species responsible for maize and peanuts contamination (Rank et al., 2011). Moreover, in tropical countries, *A. flavus* seems to be the fungus with the highest contamination rate for rice grains both in field and in post-harvest, probably due to the high temperatures and high relative humidity recorded throughout the year in these countries. On the other hand, *A. versicolor* shows a low but more stable presence during the growing season (Katsurayama et al., 2018; Reddy et al., 2009). Previous studies performed on *A. nidulans* revealed that STE production coincides in time with the sexual development, as demonstrated by the lack of STE production in loss-of-function mutants of sexual development regulators (Bayram and Braus, 2012; Dyer and O’Gorman, 2012). Coupling of these two processes might provide an evolutionary advantage. The mycotoxin production during the sexual development seems to allow the producer organism to defend its sexual structures from fungivores or to successfully compete against other organisms and thereby protect its environmental niche. Furthermore, it has been shown that the interconnection of the sexual development and STE production can be modulated by certain

environmental factors, repressing or activating sexual- or asexual-development and/or secondary metabolism (Amon et al., 2018).

With regards to STE occurrence, in literature limited information is available on the presence of STE in food and feed. During the last 50 years only few surveys on the natural occurrence of STE in food and feed were performed and were partly carried out in the 1970s–1980s with less sophisticated techniques and relatively high limits of detection (LODs), often in the range 20–50 µg/kg. An improvement of the methods was obtained between 1979 and 1985, resulting in a LOD of 10 µg/kg in corn matrix and 2 µg/kg in cheese matrix (Francis et al., 1985; Gorst-Allman and Steyn, 1979). Since the late 1990s more advanced techniques have been employed for the determination of STE in food, up to the development of LC-MS/MS-based methods that have enabled the highly sensitive detection of STE in food, with LODs in the range of 0.05–0.15 µg/kg for grain, cereal products and nuts, and 0.005–0.01 µg/kg for beer (Versilovskis et al., 2007, Versilovskis et al., 2008a). Particularly, using LC-MS/MS-based methods Versilovskis et al., 2008a reported the occurrence of STE in 55 out of 215 grain samples from Latvia, with 24 samples in the range of 25–83 µg/kg. More recently, STE has been included in LC-MS/MS-based multi mycotoxin methods and its determination was measured concurrently with that of other mycotoxins. This resulted in findings in mouldy food (Sulyok et al., 2010), cereal grains (Uhlig et al., 2013), nuts (Varga et al., 2013) and spices (Yogendrarajah et al., 2014).

Overall, STE has been reported to occur in grains and grain-based products (Atalla et al., 2003; Bertuzzi et al., 2019; Uhlig et al., 2013; Versilovskis et al., 2008a; Mo et al., 2015; Yoshinari et al., 2019; Zinedine et al., 2017), coffee

(Garcia-Moraleja et al., 2015; Bokhari and Aly, 2009), spices (Yogendrarajah et al., 2014), nuts (Varga et al., 2013; Youssef et al., 2008), beer (Versilovskis et al., 2008b) and cheese (Versilovskis et al., 2009). In the latter, contamination occurs particularly at the surface, following fungal spoilage during ripening and storage.

Concentrations of STE in grains and grain-based products range from a few  $\mu\text{g}/\text{kg}$  to over  $\text{mg}/\text{kg}$ . The highest STE concentrations were found by Takahashi et al. (1984) in brown rice grains stored in a warehouse for two to three years after harvest. They showed that the concentration of STE in the milled rice plus bran fraction was in the range of 3.8–4.3  $\text{mg}/\text{kg}$ . Lower concentrations were found by Mo et al. (2015). In their study, STE was detected only in 10% of all food products analysed in the survey, exceeding levels of 1.5  $\mu\text{g}/\text{kg}$  only in 1.4% of these.

Among the mycotoxins studied, STE was the most frequently detected mycotoxin in 180 Italian rice samples, with levels detected in the range of 0.16–8.34  $\mu\text{g}/\text{kg}$ , varying with the variety of rice (Bertuzzi et al., 2019). In Japanese cereals and foods collected between 2016 and 2018, Yoshinari et al. (2019) demonstrated the presence of STE in the 19.9% of all samples, with concentrations mainly between 0.05 and 0.5  $\mu\text{g}/\text{kg}$ . No STE contamination was found in beer (Yoshinari et al., 2019). Only in one report STE was detected in 2 out of 26 beer samples, with levels in the range of 4–7.8  $\mu\text{g}/\text{kg}$  (Versilovskis et al., 2008b).

Coffee was found also to be contaminated by STE. Garcia-Moraleja et al. (2015) demonstrated STE occurrence in different coffee beverages with an incidence of 16% and concentrations ranging from 7.65 to 63.19  $\mu\text{g}/\text{kg}$ . Similar

results were obtained by Bokhari and Aly (2009), who detected STE in two of 13 analysed samples of coffee beans, with concentrations of 13 and 11 µg/kg.

Regarding the feedingstuffs, levels of 0.68–2.25 µg/kg of STE were found in 14 naturally incurred feed samples (Biancardi and Dall’Asta, 2015). The STE contamination was detected in the silage and in feed of a commercial maize mill in Burkina Faso (Panasiuk et al., 2019; Warth et al., 2012). However, there are insufficient data to assess the rate of carryover of STE into milk or other animal products, such as meat and eggs, when animals are exposed to contaminated feed (EFSA, 2013).

To ensure animal and public health, as well as agricultural productivity, maximum levels for various mycotoxins were laid down for a number of food commodities and feedingstuffs. However, as regards the occurrence of STE, the maximum levels are not so far regulated by any regulation within the European Union nor are official control/monitoring programmes carried out. Only Czech Republic and Slovakia had set limits of STE at 5 µg/kg for rice, vegetables, potatoes, flour, poultry, meat, milk and 20 µg/kg for other foods (FAO, 2004; Stroka et al., 2004). However, both countries withdrew their legislation on STE when becoming a member of the European Union.

Due to the too limited STE occurrence data in food and feed, no reliable human and animal dietary exposure assessments could be identified, as well as no safe levels in food are known (EFSA, 2013). However, there is an increasing awareness of the importance of establishing a better risk assessment for this mycotoxin. For this reason, the Joint FAO/WHO Expert Committee on Food Additives (JECFA) is currently working on a safety assessment of STE proposed by the Codex Committee on Contaminants in Foods (Joint FAO/WHO, 2015).



Therefore, in light of all this and according to the definition of “emerging mycotoxins” as “mycotoxins, which are neither routinely determined, nor legislatively regulated; however, the evidence of their incidence is rapidly increasing” (Vaclavikova et al., 2013), it may be correct to consider STE as an emerging mycotoxin that needs further research in order to not underestimate the potential risk associated with its exposure.

## **2. Prevention of STE-mediated food contamination**

With becoming increasingly apparent and well known the negative effects of mycotoxins on human and animal health, in the last years several physical, chemical and biological strategies have been developed to reduce and/or eliminate mycotoxigenic fungal growth and mycotoxin biosynthesis in food products, improve food safety and minimize economic losses (Kabak et al., 2006). On the other hand, today’s consumers increasingly demand that their food is minimally processed without the use of synthetic preservatives and additives, because of possible harmful effects on human health. Since the use of natural preservatives to control fungal growth and mycotoxin production is concerning collective interest, in recent years a growing number of *in vitro* and *in vivo* studies have been performed using natural substances to try to counteract the adverse effects associated to mycotoxins exposure (Fernandez-Blanco et al., 2016; Hu et al., 2017; Krishnaswamy et al., 2010). Nevertheless, only few data have been reported about their effects on STE production. Propolis, a natural resinous bee product collected by honeybee workers, has been used to investigate its effect on the growth of *A. versicolor* artificially grown on Ras cheese and STE production during a period of 90 days (Aly and Elewa, 2007). Results revealed that treatment of fungus-inoculated cheese samples with 250 ppm

propolis had a significant effect in decreasing the production of STE but no significant difference in the growth of mould, whereas increased concentrations to 500 and 1000 ppm propolis had a significant inhibitory effect on the growth of mould, which was reduced to zero by treatment at the highest level (Aly and Elewa, 2007). Significant antifungal activity on the mycelial growth of *A. versicolor* and antimycotoxigenic activity on STE production were also demonstrated by onion and garlic essential oils individually, as well as in mixtures (Kocic-Tanackov et al., 2012). Interestingly, the authors observed that the overall effect of the onion essential oil was more potent and lasted longer compared to the garlic essential oil. However, based on the findings, both of the essential oils may be considered a possible natural strategy to help to counteract *A. versicolor* growth and STE production.

### 3. Biosynthetic and metabolic pathway

The STE shares its biosynthetic pathway with the most potent carcinogenic mycotoxins known, the aflatoxins (AFs). Particularly, STE acts as biogenic precursor of aflatoxin B1 (AFB1) and aflatoxin G1 (AFG1) (Fig. 1). In aflatoxigenic species, in which STE is rapidly converted into the direct precursor of AFB1 and AFG1, the *O*-methylsterigmatocystin, STE is rarely accumulated. However, some species, such as *A. nidulans* and *A. versicolor*, are apparently unable to convert STE into *O*-methylsterigmatocystin, probably due the lack of genes encoding the specific methyltransferase required for this conversion (Yabe et al., 1989). Consequently, substrates colonised by these fungi can contain high amounts of STE, while substrates invaded by other species of fungi, such as *A. flavus* and *A. parasiticus*, contain only low amounts of STE, as most of it is converted into AFs (Yabe and Nakajima, 2004).

A variety of biotransformation experiments, cloning strategies and genetic studies were employed to elucidate the stages, identify and clone the genes involved in STE biosynthesis, providing insights into the chemistry of this pathway and making it one of the best characterized pathways of fungal secondary metabolism. What is more, by determining the function of most of the cluster genes involved in STE biosynthesis, it has been shown that they are orthologues of AF cluster genes (Hicks et al., 2002).

Brown et al. (1996) characterized a 60-kb region in the *A. nidulans* genome containing a cluster of 25 genes involved in STE biosynthesis. Based on the polypeptide sequences of regions within the cluster, the genes appear to encode biosynthetic enzymes, including a polyketide synthase, fatty acid synthases (FASs), mono-oxygenases, dehydrogenases, an esterase, *O*-methyltransferases, a desaturase, reductases and oxidases. Furthermore, the authors showed that a loss or a significant reduction of the accumulation of all 25 transcripts is caused by the disruption of a zinc binuclear cluster transcription factor similar to the regulatory gene *affR* required for AFs biosynthesis.

The STE biosynthesis begins with the synthesis of a small fatty acid in a reaction catalysed by a FAS encoded probably by the genes *stcJ* and *stcK*. Thus, the first stable pathway intermediate, norsolonic acid, is assembled from hexanoyl CoA and seven malonates by a polyketide synthetase (PKS) encoded by *stcA*. The next steps involve a series of reactions of dehydration and hydroxylation that lead to the formation of the intermediates averantin, 5'-hydroxyaverantin, averufin, 1-hydroxyversicolorone and versiconal hemiacetal acetate (Anderson, 1992). Four candidate genes encoded putative dehydrogenases have been identified, *stcE*, *stcG*, *stcN* and *stcV*, whereas the

reaction of hydroxylation are likely catalysed by mono-oxygenases encoded by the four unassigned cluster *stcB*, *stcF*, *stcL* and *stcW* (Butchko et al., 1999; Brown et al., 1996). The next step consists in the bioconversion of versiconal hemiacetal acetate into versicolorin A via an esterase, a cyclase and a desaturase. After that, three chemical reactions are required for the conversion of versicolorin A to demethylsterigmatocystin, Baeyer-Villiger oxidation, reduction and decarboxylation (Bhatnagar et al., 1992). As shown by Brown et al. (1996), the gene *stcI* exhibits a high percentage of sequence identity with esterases, suggesting that it could be involved in the formation of versicolorin A, whereas *stcS* and *stcU* seem to be involved in the conversion of versicolorin A to demethylsterigmatocystin, encoding a putative P450 mono-oxygenase and a reductase, respectively. Finally, STE is formed via methylation from demethylsterigmatocystin by a *O*-methyltransferase, presumably encoded by *stcP* (Brown et al., 1996).

As an intermediate in the biosynthesis of AFs, STE shows several similarities in the chemical structure and, thus, in biological activities, especially with AFB1. Dimensions and absolute configuration of the bisdihydrofuran moiety are very similar in both molecules. This suggests a metabolic activation on the same site of AFB1, the C<sub>2</sub>-C<sub>3</sub> double bond (Coulombe, 1993; Essigmann et al., 1979). Particularly, for AFB1 it has been proposed that its mutagenically active form is generated by the epoxidation of the 2,3-vinyl ether double bond in the terminal furan ring (Swenson et al., 1975). Since STE possess the same ring system, a common mechanism concerning their mutagenicity can be reasonably presumed. Strong evidence for the formation of a reactive STE epoxide was obtained when STE was incubated under cell-free conditions with DNA in the presence of rat liver microsomes; subsequent

isolation and degradation of the DNA followed by HPLC analysis revealed the presence of a covalent adduct, which was purified and identified by nuclear magnetic resonance (NMR) spectroscopy and mass spectrometry (MS) as 1,2-dihydro-2-(N<sup>7</sup>-guanyl)-1-hydroxy-STE (Essigmann et al., 1979). The same DNA adduct was obtained in isolated rat liver perfused with STE (Essigmann et al., 1980), further confirming that the mechanism of STE mutagenicity is linked to its covalent binding to the DNA molecule after metabolic activation by liver microsomes P450s and epoxide metabolite formation. However, in contrast to the large literature on AFB1 and other aflatoxins, only little information has been published on the metabolic activation and biochemical effects of STE. Probably due to the structural similarity with AFB1 and following the observation of the DNA adducts, no further efforts have been made to study additional metabolic pathways of STE until recently, when Pfeiffer et al. (2014) reported that hepatic microsomes from humans and rats predominantly form the catechol 9-hydroxy-STE via hydroxylation of the aromatic ring, suggesting a novel pathway in the oxidative metabolism of STE, which may contribute to the toxic and genotoxic effects of this mycotoxin.

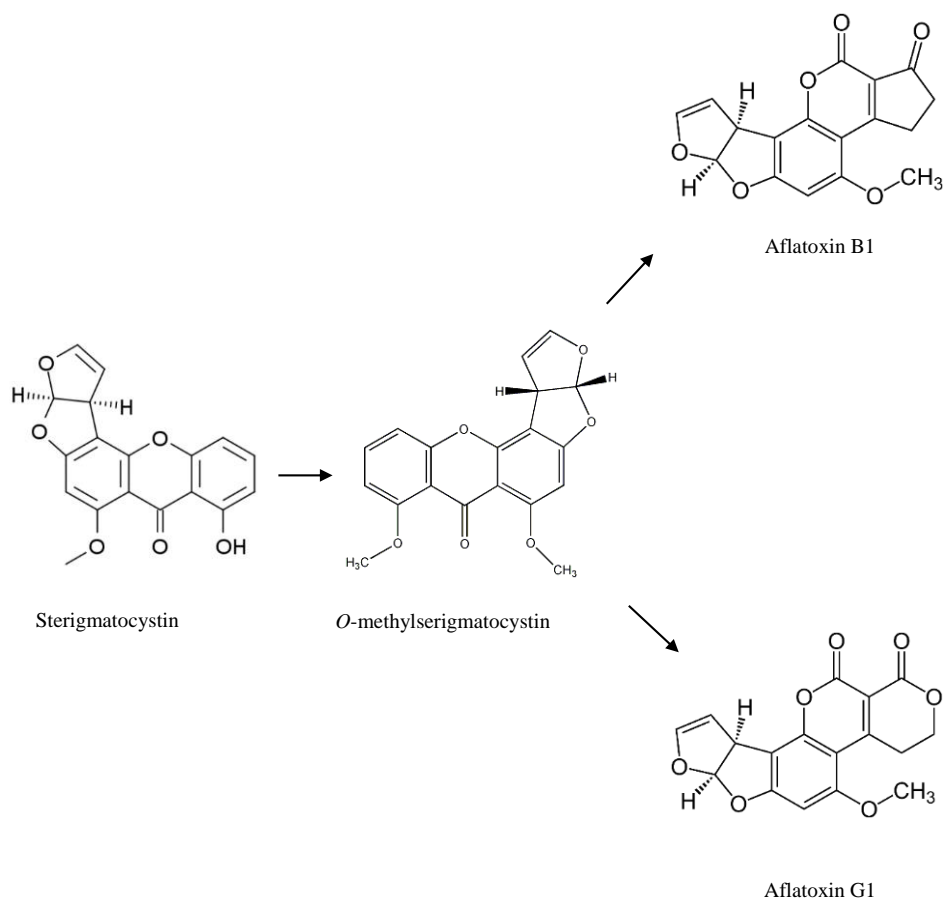


**Fig. 1.** Conversion of sterigmatocystin to aflatoxin B1 and aflatoxin G1.

## 4. Toxicity of STE

### 4.1. *Toxic effects of STE in humans*

Epidemiological evidence highlighted the existence of associations between STE exposure and the risk of cancer development. Epidemiological studies performed in China reveal that STE may be a putative etiological factor for gastric carcinoma, as suggested by the strong positive correlations existing between high levels of STE contamination in foodstuffs and a higher incidence of gastric cancer (Zhang et al., 2003; Lou et al., 1995). What is more, DNA-STE adducts was detected in 4 out of the 13 patients with liver or stomach cancer, with levels of STE in the blood ranging from 65 to 113  $\mu\text{g}/\text{kg}$  body weight (BW) (Tian et al., 1995). Significantly high levels of STE were observed also in patients with hepatocellular carcinoma (HCC). In particular, Hutasanu et al. (2011) detected STE in 26.2% of blood and urine samples collected from patients with liver cirrhosis and HCC, with levels rising to 0.626 ng/ml in blood and 1.053 ng/ml in urine of patients with liver cirrhosis and values rising to 2.02 ng/ml and 9.39 ng/ml in the blood and urine samples of HCC patients (STE mean values in controls were 0.014 ng/ml in blood and 0.005 ng/ml in urine). Similar results were obtained by Cao et al. (2018), who detected STE in the urine samples of 10 of the 30 (33%) patients with HCC, versus 3 of the 30 control patients (10%), whereas, for plasma samples, STE was detected in 12 of the 30 (40%) patients with HCC, versus 4 of the 30 control patients (13%), confirming the hypothesis of a possible role for this mycotoxin in the pathogenesis of the disease.

Despite evidence of its carcinogenicity, only limited data regarding the detection of STE in human blood or urine are available in literature for a dose-

response evaluation and further analysis is needed to state the real hazard STE represents for human health.

### 4.2. *Toxic effects of STE in animal models*

*In vivo* studies demonstrated that STE is able to induce toxic effects in several species of animals, such as mouse, rats, monkeys, chickens, ruminants and fishes by varying the effect with species, route and frequency of administration. Data collected from literature show that the median lethal dose (LD<sub>50</sub>) obtained after STE exposure ranged from 5 µg/egg in 5-day-old chicken embryos to 166 mg/kg BW in rats orally exposed to the mycotoxin (Purchase and van der Watt, 1969; Schroeder and Kelton, 1975). Values of LD<sub>50</sub> equal to 60–85 mg/kg BW and 32 mg/kg BW were obtained respectively in rats and monkeys after intraperitoneal exposures (Purchase and van der Watt, 1969, 1970). Several studies indicate that liver and kidneys represent the main target organs of acute toxicity. Hepatotoxic and nephrotoxic effects were described by Sreemannarayana et al. (1988) in chicks exposed intraperitoneally to STE. Exposure to STE has been shown also to induce oxidative stress-related impairment in rat liver and kidneys (Dubravka et al., 2019; Sivakumar et al., 2001). Similar results were obtained in phylogenetically distant experimental animals, such as the common carp juveniles (Kovesi et al., 2019). disease.

Respect to chronic toxicity, the exposure to STE was associated with clinical conditions of different severity degrees. Bloody diarrhea and reduced milk production, were observed in dairy cows exposed to ≤12 mg STE/kg feed (Vesonder and Horn, 1985). In pig, Kovalenko et al. (2011) revealed decreased feed intake, incidental diarrhea, and necrotic alterations of the liver tissue after exposure to 30 µg STE/kg feed. Negative effects following consumption of STE



contaminated diet were observed in cattle, but not in sheep (Vesonder and Horn, 1985; Böhm and Sayed, 1994).

A number of research groups have described STE also as a potential carcinogenic, mutagenic and teratogenic mycotoxin. The potential carcinogenicity of STE in inducing tumours was documented for the first time in 1970s in experimental animals (Purchase and Van Der Watt, 1970, 1973). In the same years, additional *in vivo* experiments on newborn mice showed that exposure to a single subcutaneous dose of 5 ng STE/kg BW is already capable of generating lung and liver tumours (Fujii et al., 1976). Most recently, the role of STE as putative causal factor of lung adenocarcinoma in mice was further confirmed by Huang et al. (2004). The authors observed the onset of lung adenocarcinoma in 25% and 41.7% of mice exposed to 3 and 30 µg STE/kg BW, respectively, as well as dysplasia of glandular stomach was detected in 50% and 58.3% of mice similarly treated. Also in Mongolian gerbils, a potential role of STE as factor of carcinogenesis has been suggested. Particularly, a significantly higher incidence of gastric carcinogenesis was observed in Mongolian gerbils treated with STE (Kusunoki et al., 2011). Moreover, an enhance of the development of intestinal metaplasia of gastric mucosa has been shown in *Helicobacter pylori*-infected Mongolian gerbils (Ma et al., 2003). The effects of STE on rats with reflux esophagitis indicate that one of the main mechanisms through which STE promotes cancer onset consists in its negative impact on immune function, facilitating the escape of transformed cells from host immune surveillance (Tong et al., 2013). In agreement with these findings, an alteration of the normal immune function following STE exposure was also observed by Liu et al. (2012) and Zhang et al. (2012), providing a further foundation of how STE contributes to its carcinogenesis.

Finally, chromosome aberrations were found in the kidneys of the Nile tilapia fish treated twice a week for 4 weeks with 1.6  $\mu\text{g}$  STE/kg BW and in rat bone marrow cells, when a dose of 31.2 mg STE/kg BW was injected intraperitoneally (Abdel-Wahhab et al., 2005; Ueda et al., 1984).

Accordingly, in light of the animal studies performed to date and of the cases of human cancer analysed, STE has been classified as possibly carcinogenic to humans (Group 2B) by the International Agency for Research on Cancer (IARC, 1987).

### 4.3. *Toxic effects of STE by in vitro methods*

The effects of STE on cell viability have been studied in different cell lines and through different assays. Due to the hepatocarcinogenic property of STE, the HepG2 cells, derived from human hepatocellular carcinoma, are the most used cell model in the studies of STE cytotoxicity. A median inhibitory concentration ( $\text{IC}_{50}$ ) of 3  $\mu\text{M}$  was reported by Gao et al. (2015) on HepG2 cells exposed to STE for 24 h by using the 3-(4,5-dimethylthiazol-2-yl)-2,5-diphenyltetrazolium bromide (MTT) assay. Higher  $\text{IC}_{50}$  values on this cell line were obtained by Bunger et al. (2004) and Liu et al. (2014), whereas no  $\text{IC}_{50}$  values were found at the range of concentrations tested (from 0.78 to 50  $\mu\text{M}$ ) by Zingales et al., 2020a. However, the different values may be explained by the use of different assays conditions. In particular, based on the concentration-response relationship measured by the sulforhodamine B (SRB) method, an  $\text{IC}_{50}$  value equal to 7.3  $\mu\text{M}$  was obtained by Liu et al. (2014), whereas an  $\text{IC}_{50}$  value equal to 286.1  $\mu\text{M}$  was obtained by Bunger et al. (2004) by using the Neutral Red dye assay. Additionally, Bunger et al. (2004) demonstrated that, compared to HepG2 cells, STE exhibited a 7-fold higher toxicity in murine neuroblastoma

Neuro-2a cells ( $IC_{50} = 40.1 \mu\text{M}$ ) and an 80-fold higher toxicity in adenocarcinomic human alveolar basal epithelial A549 cells ( $IC_{50} = 3.7 \mu\text{M}$ ), whereas an  $IC_{50} = 163.3 \mu\text{M}$  was obtained in murine fibroblasts L-929 cells. These findings indicate a higher susceptibility of human pneumocytes to STE than the other cell lines. Moreover, based on these data and in according to the results showed by Palanee et al. (2001), in A549 cells STE seems to produce also a higher cytotoxicity than AFB1 ( $IC_{50} = 10 \mu\text{M}$ ). However, conflicting results were found by Cui et al. (2017), who demonstrated that in A549 and in human bronchial epithelial BEAS-2B cells low concentrations of STE (from 0.06 to 6  $\mu\text{M}$ ) had no effect on cell viability after 24 h treatment, showing a significant concentration-dependent decrease only at concentrations ranging from 12 to 240  $\mu\text{M}$ .

In addition to HepG2 cells, another cell line frequently employed as cellular models for in vitro liver cancer and toxicity studies is represented by the liver cancer Hep3B cells (Qiu et al., 2015). Anninou et al. (2014) evaluated the effects of STE on Hep3B cells by using the MTT assay after 24 and 48 h, obtaining values of  $IC_{50}$  equal to 58  $\mu\text{M}$  and 22  $\mu\text{M}$ , respectively. Further data on the cytotoxicity of STE after more than 24 h of STE exposure are available only in immortalized ovarian CHO-K1 and in human neuroblastoma SH-SY5Y cells, with a time- and concentration-dependent cell proliferation decrease ranging from 92% to 34% and from 91% to 8%, respectively (Zingales et al., 2020b, 2020c; Zouaoui et al., 2016).

Since dietary exposure does not involve a single mycotoxin but rather a complex mixture of mycotoxins that frequently coexist in food, beverage and natural products, it is of great importance to investigate the effects of mycotoxin

mixtures. Furthermore, the toxic effects induced by the combination of two or more mycotoxins cannot always be predicted based upon their individual toxicity but multi-exposure may lead to additive, synergistic or antagonistic toxic effects, with possible adverse effects on consumer health which are riskier than the intake of only one mycotoxin alone (Ruiz et al., 2011; Speijers and Speijers, 2004). However, to the best of our knowledge, studies regarding the effects of STE in combination with other mycotoxins are very limited. Compared to STE alone, higher cytotoxic effects on cell proliferation were induced by the binary and tertiary combinations STE + patulin (PAT), STE + beauvericin (BEA) and STE + PAT + BEA on CHO–K1 cells, as well as by the binary mixture STE + nivalenol (NIV) on HepG2 cells (Zingales et al., 2020a; Zouaoui et al., 2016). Similar results were obtained also by Anninou et al. (2014) on Hep3B cells, in which STE + ochratoxin A (OTA) co-administration caused a significant enhance of cell viability reduction after 24 h at concentrations higher than 0.1 nM and after 48 h at concentrations higher than 1 pM. Less intense effects were observed after co-exposure to STE + citrinin (CTN) and STE + OTA + CTN.

Depending on the assay performed, the concentrations examined, the incubation time and the selected cell line, as well as the different chemical structures and chemical properties among different mycotoxins, discrepancies between the interaction effects may be noted. Properly, whether on one hand mainly additive and synergistic effects were observed for STE in combination with OTA, PAT and/or BEA, on the other hand antagonistic interactions were revealed by STE + CTN and STE + OTA + CTN, highlighting that it is very difficult to predict the type of interaction only on the basis of the effect of individual mycotoxin. For this reason, it is essential to evaluate the cytotoxic

effects induced by mycotoxins exposure both when they are alone and in combinations and the behaviour of each mycotoxin in the mixture.

## 5. Mechanisms of STE-induced toxicity at molecular levels

Toxic effects of mycotoxins are largely attributed to the alteration of the basic metabolic processes in biological systems. In the following sections the main STE cellular effects will be briefly discussed, elucidating the mechanisms and the pathways proposed as the basis of the processes by which STE exerts its toxic effects. A list of studies related to STE-induced toxicity under *in vitro* and *in vivo* conditions is provided in Tables 1 and 2, respectively. 1987).

### 5.1. Oxidative stress

The STE has been found to produce oxidative damage in *in vitro* and *in vivo* studies. In human hepatoma HepG2 cells, it has been shown that reactive oxygen species (ROS) production increased in a concentration-dependent manner after exposure to 0.5–7  $\mu\text{M}$  of STE (Gao et al., 2015; Liu et al., 2014). An increase in early ROS production was also observed after exposure to the binary combination STE + NIV (Zingales et al., 2020a). Additionally, STE has been demonstrated to cause lipid peroxidation. Enhanced malondialdehyde (MDA) levels and reduced glutathione (GSH) content as a consequence of STE-mediated ROS production were obtained in SH-SY5Y cells, which proved unable of counteracting the oxidative stress produced by STE, as suggested by the observed loss of activity of the antioxidant enzymes glutathione peroxidase (GPx), glutathione S-transferase (GST) and superoxide dismutase (SOD) (Zingales et al., 2020c). Signs that STE may induce lipid peroxidation were also reported in *in vivo* studies performed in rats, common carps and chickens

(Balogh et al., 2019; Dubravka et al., 2019; Kovesi et al., 2019; Sivakumar et al., 2001). The doses used in these studies ranged from 0.2 mg STE/kg BW for long-term experiments to 40 mg STE/kg BW for short-term treatment studies. Lipid peroxidation as secondary mechanism of STE toxicity has been hypothesized by Sivakumar et al. (2001), who observed that in rats fed with 0.2 mg STE/kg BW for 30 days STE was able to enhance liver production of ROS and to imbalance the antioxidant defense system, resulting in chain reactions associated with the process of lipid peroxidation. As shown by the authors, the activity of SOD and GPx was enhanced in the STE-treated animals, whereas the activity of catalase (CAT) was severely impaired. Higher SOD activity was observed also in kidneys of rats after short-term oral STE treatment (Dubravka et al., 2019). However, in other studies, opposite results were obtained, with a decrease of GPx activity in chicken and common carp liver and an increase of CAT activity in plasma of rats after exposure to STE (Balogh et al., 2019; Dubravka et al., 2019; Kovesi et al., 2019).

### 5.2. *Antioxidant protection from STE-mediated toxicity*

Several natural and synthetic antioxidant compounds, as well as numerous food components have been shown to be efficacious in containing the toxic effects of mycotoxins (Galvano et al., 2001). However, although most studies were conducted *in vitro* and confined to AFB1, there is a limited knowledge about the efficacy of antioxidants to prevent the toxic effects induced by STE exposure. Cytoprotective effects of N-acetyl-L-cysteine (NAC) pre-treatment were observed in HepG2 and SH-SY5Y cells exposed to STE (Gao et al., 2015; Zingales et al., 2020c). In an *in vivo* study, El-Desouky et al. (2015) demonstrated health benefit effects of an aqueous extract of red pomegranate peels (RPP)

against STE-induced toxicity. In the study, rats fed a STE-contaminated diet showed significant changes in serum biochemical parameters, accompanied by severe histological changes in kidney, liver, intestine and lung tissues. The RRP extract at the two tested concentrations (250 and 500 mg/rat/day) induced significant improvements in all tested parameters and succeeded in overcoming these effects, especially in liver and kidneys, showing a dose-dependent protective effect against STE toxicity. The authors concluded that the aqueous extract of RPP powder could be used as natural antioxidant to enhance the antioxidant properties of functional food (El-Desouky et al., 2015).

### 5.3. *Mechanisms of apoptotic cell death*

It has been demonstrated that induction of apoptosis is one of the most important effects of many carcinogenic mycotoxins (Ayed-Boussema et al., 2008). Apoptosis induced by STE has been demonstrated to represent a common effect in different cell lines. In A549, BEAS-2B and SH-SY5Y cells, STE has been shown to induce apoptosis in a concentration-dependent manner (Cui et al., 2017; Zingales et al., 2020b). The STE has been demonstrated to cause apoptosis also in human gastric epithelial GES-1 cells and in HepG2 cells even at very low concentrations (0.01 and 0.075  $\mu\text{M}$  of STE, respectively) (Liu et al., 2014; Zhang et al., 2013). Focusing on the mechanism of action, it has been suggested that STE-induced apoptosis involves Bcl-2 family proteins. In STE-treated BEAS-2 B cells and A549 cells, the expression of Bax protein was increased, while a marked decrease in Bcl-2 expression was observed. In addition, treatment with STE for 24 h resulted in the activation of caspase-3, confirming that cell apoptosis was executed by caspase-3 (Cui et al., 2017). Increased Bax/Bcl-2 ratio and activated caspase-3 following STE exposure have

been shown also in HepG2 cells by Liu et al. (2014). Furthermore, a possible involvement of p53 in the process of cell apoptosis was indicated by the authors, as suggested by the increase of the expression of the protein with the increase of STE concentrations.

### 5.4. *Damage of DNA and impairment of cell cycle progression*

Genotoxic risk associated with STE has been documented in rat, mouse and human cell lines (Anninou et al., 2014; Curry et al., 1984; Ji et al., 1994; Jiang et al., 2017; Mori et al., 1984; Theumer et al., 2018; Ueda et al., 1984). The STE was shown to induce DNA strand break in human esophageal epithelial Het-1A cells and in human lung A549 and BEAS-2B cancer cells after 24 h of STE exposure at concentrations ranging from 6 to 24  $\mu\text{M}$ , as assessed by comet assay (Huang et al., 2014; Wang et al., 2013). As shown by these studies, even at the lowest concentration of STE, the tail length, tail intensity and olive tail moment obtained were significantly higher in cells exposed to the mycotoxin than in control cells. However, the highest sensitivity to STE was shown by Het-1A cells, suggesting that different cell lines showed different sensitivity to STE.

Damage to DNA was reported also in GES-1 cells exposed to STE by Jiang et al. (2017). In particular, the authors observed a significant time-dependent increase of the number of  $\gamma\text{H2AX}$  foci-positive mitotic cells treated with 12  $\mu\text{M}$  STE, with more serious levels of DNA damage in cells entered in mitosis 48 h after STE treatment, indicating that a longer STE treatment is associated to more serious levels of genotoxicity. Gao et al. (2015) reported that the treatment with STE (1.5, 3 and 6  $\mu\text{M}$ ) for 1 h induced a significant and concentration-related increase in 8-hydroxydeoxyguanosine (8-OHdG) and DNA fragmentation in HepG2 cells. Furthermore, at these concentrations,



elevation of ROS was measured whereas pre-incubation with NAC produced a slight protective effect on STE-induced oxidative DNA damage, suggesting that oxidative stress is implicated in the observed STE genotoxicity.

In primary cultures of human gastric epithelial cells, STE exposure (1  $\mu$ M–0.1 mM) in the presence of S9 microsomal fraction resulted in a significant increase of unscheduled DNA synthesis (Ji et al., 1994). Based on these findings, STE seems to gain the ability to alter DNA synthesis following bioactivation. Similar results were obtained by Stich and Laishes (1975), who reported that STE caused chromosomal aberrations in human fibroblasts and DNA damage, but only in the presence of a microsomal activation system. On the other hand, genotoxic effects were obtained with and without metabolic activation by the SOS Chromotest (Krivobok et al., 1987).

The presence of DNA damage in cells triggers signal transduction pathways that could lead to cell cycle arrest in order to facilitate DNA repair and prevent aberrant mitosis. It has been demonstrated that mycotoxin exposure can disturb cell cycle regulation on several cell types, with an accumulation of cells in one or more specific phases of the cell cycle (Juan-Garcia et al., 2019). The effects of STE on cell cycle progression have been suggested to be cell type- and concentration-dependent. In human acute monocyte leukaemia THP-1 cells, Solhaug et al. (2016) showed that STE induced cell cycle arrest in the S phase. Conversely, STE treatment has been found to lead to G<sub>2</sub>/M phase arrest in mouse embryonic fibroblasts (MEFs) via the loss of the p53-mediated G<sub>1</sub> checkpoint (Xie et al., 2000). Similar results were obtained in GES-1 cells, where STE increased significantly the proportion of cells in G<sub>2</sub>/M phase while decreased that of cells in G<sub>0</sub>/G<sub>1</sub> and S phase (Jiang et al., 2017; Xing et al., 2011).

Furthermore, treatment with relative low concentrations of STE (6 and 12  $\mu\text{M}$ ) was shown to induce S phase arrest in A549 cells and G<sub>2</sub>/M phase arrest in BEAS-2B cells, whereas S and G<sub>2</sub>/M phase arrest was induced in both cell lines following treatment with 24  $\mu\text{M}$  STE (Huang et al., 2014). Although the reduced proliferation is in most cases due to an accumulation of cells in the G<sub>2</sub>/M phase (Jiang et al., 2017; Zhang et al., 2013), accumulation of cells in G<sub>0</sub>/G<sub>1</sub> phase was also reported (Liu et al., 2014). Both phases (G<sub>0</sub>/G<sub>1</sub> and G<sub>2</sub>/M) are considered decision points: at the first one (G<sub>0</sub>/G<sub>1</sub>) cells must choose whether to divide or not, entering in this latter case in a resting stage (G<sub>0</sub>), while the second one (G<sub>2</sub>/M) allows the cells to further check DNA integrity, halting the cell cycle if DNA damage is detected.

### 5.5. *Alteration of cellular signalling pathways*

The STE-induced toxicity appears to involve a series of signalling pathways that are linked to different stress conditions, such as cellular ROS production, DNA damage and cell cycle arrest. Several studies have provided evidences of a direct association between STE-mediated cell cycle arrest at G<sub>2</sub> phase and the activation of the mitogen activated protein kinase (MAPK) signalling pathway. Extracellular signalregulated kinases (ERKs), c-JUN N-terminal kinase (JNK) and mitogen activated protein kinase (p38) are the main MAP kinases controlling many aspects of mammalian cellular physiology. In GES-1 and Het-1 cells, STE was found to increase the phosphorylation and activity of ERK (Cui et al., 2018; Xing et al., 2011). In the same cellular systems, other MAPKs, respectively JNK and p38, were also activated by STE. Moreover, in GES-1 cells, the phosphorylation and activation of JNK and ERK were accompanied with the activation of the PI3K/AKT/mTOR signalling pathway and changes in the

expression levels of Cdc25, Cdc2, CyclinB1–Cdc2 complex, which are all involved in the regulation of the cell cycle progression (Xing et al., 2011). Furthermore, Zhang et al. (2013) indicated that in GES-1 cells the Ataxia Telangiectasia Mutated (ATM) kinase and its downstream molecules, the checkpoint kinase Chk2 and the tumour suppressor protein p53, likely contribute to the STE-induced G<sub>2</sub> arrest.

In Het-1A cells, Wang et al. (2013) and Cui et al. (2018) showed that following the induction of DNA damage by STE, the mismatch repair (MMR) hMLH1 was activated. Subsequently, hMLH1 triggered p38 and ERK MAPK pathway, resulting ultimately in the activation of p53. Eventually, STE induced G<sub>2</sub> phase arrest via hMLH1-ERK/p38-p53 pathway, suggesting that a link between the three signalling pathways (MMR, MAPKs and p53) may be involved in STE-mediated G<sub>2</sub>/M phase arrest (Cui et al., 2018).

In BEAS-2B and A549 cells, STE exposure resulted in a modulation of Cyclin A and CDK1/p-CDK1 protein expression, giving a possible explanation of the observed cell cycle arrest (Huang et al., 2014). Moreover, an increase of the expression of the G<sub>1</sub> phase regulatory proteins CDK4, Cyclin D1, CDK2 and Cyclin E was found by the authors. Considering that CDK4, Cyclin D1, CDK2 and Cyclin E are involved in many types of cancer, it can be assumed that the upregulation of these G<sub>1</sub> phase regulatory proteins may not only accelerate the transmission of BEAS-2B cells and A549 cells from G<sub>1</sub> to S phase, but may also contribute to STE carcinogenicity.

Finally, STE toxicity has been shown to involve other signalling pathways, such as those associated to oxidative stress. In common carp liver, STE treatment resulted in the inhibition of Kelch-like ECH-associated protein 1

(Keap1), and consequently in the activation of the Nuclear factor (erythroid-derived 2)-like 2/Antioxidant Response Element (Nrf2/ARE) pathway (Kovesi et al., 2019). The Nrf2 is considered the housekeeper gene in antioxidant defence systems due to its special ability to bind to antioxidant response elements (ARE) in order to regulate a plethora of antioxidant genes. The activation of the Nrf2/ARE pathway and the induction of the expression of antioxidant enzymes observed by Kovesi et al. (2019) may represent an active response to the increase in ROS production caused by STE treatment, further confirming the ability of STE to induce oxidative stress.

### *5.6. Impairment of mitochondrial function*

In eukaryotic cells, mitochondria play a key role in many physiological process, ensuring the maintenance of cellular homeostasis. In 1984, Kawai and colleagues were the first to suggest that STE toxicity may be related to mitochondrial dysfunction and energy shortage, demonstrating that STE treatment can inhibit mitochondrial respiration in isolated rat liver mitochondria (Kawai et al., 1984). Moreover, Kawai et al. (1986) revealed that STE caused a diminution in the rate of mitochondrial ATP synthesis by acting as proton carrier across mitochondrial inner membranes and, thus, exerting an uncoupling effect on oxidative phosphorylation. Most recently, the abilities of STE to lead to an alteration of the mitochondrial membrane potential and a decrease in the ATP content has been further confirmed in in vitro studies (Liu et al., 2014; Zingales et al., 2020a, Zingales et al., 2020b). Based on the data outlined above, mitochondrial dysfunction may be interpreted as a part of the molecular mechanisms for STE cytotoxicity. However, only few data are available in

literature and further investigations will be necessary to clarify the role of mitochondrial dysfunction in STE toxicity.

### 5.7. *Immune mechanisms*

The current state of knowledge indicates that STE may exert marked immunotoxic effects. If on the one hand Solhaug et al. (2016) showed that exposure to STE (0.625–2.5  $\mu\text{M}$ ) had no effects on the process of differentiation from THP-1 monocytes into macrophages, which prepares the cells to actively participate in the immune responses, on the other hand Huang et al. (2002) and Zhang et al. (2012) proposed that STE leads to the depression of systemic host defense system, as demonstrated by the decreased expression and secretion levels of the pro-inflammatory cytokines tumour necrosis factor (TNF)- $\alpha$ , interleukin-6 (IL-6) and IL-12, detected in human and murine peripheral blood mononuclear cells and in murine peritoneal macrophages after exposure to STE. In addition, STE has been shown to inhibit the expression of human leukocyte antigen (HLA)-I in human peripheral blood mononuclear cells (Xing et al., 2005). The STE exposure resulted also to modulate the expression of a high number of inflammation-associated genes in intratracheally instilled 3-weeks old Swiss Webster mice, suggesting that immunomodulation represents one of the most important biological effects of STE (Miller et al., 2010). In reflux esophagitis rats, the intraperitoneal administration of 30  $\mu\text{g}$  STE/kg BW decreased expression levels of two key regulators of the immune response, the transporter associated with antigen processing 1 (TAP1) and the low molecular weight protein 2 (LMP2). In particular, the rate of TAP-1 positive cells was reduced compared to the control group (20.83% versus 71.17%), as well as the number of LMP2-positive cells (22.50% versus 53.83%), harming significantly

the cell-mediated immune response (Tong et al., 2013). Short-term STE exposure has been shown to alter immune function by affecting the number of immune-regulatory and antigen-presenting cells also in BALB/c mice lymphatic organs (Liu et al., 2012).

Interestingly, the effects of STE on immune function seem to be dose-dependent and tissue-specific. Liu et al. (2012) observed that in mice treated with 3  $\mu\text{g}$  STE/kg BW the proportion of CD8+ T cells was decreased in the thymus, whereas in mice treated with 3 and 30  $\mu\text{g}$  STE/kg BW both proportions of CD4+ and CD8+ T cells were increased in spleen, probably due to a temporary immune response triggered by the STE inhibition.

Although more studies are needed to obtain a clearer view on the effects of STE on the several chain reactions that characterize the immune system, the studies carried out to date allow to define the immunotoxicity as one of the main mechanisms of action through which STE promotes its carcinogenic properties.

**Table 1.** *In vitro* STE toxicity studies.

CELL TYPE	TIME	CONCENTRATIONS	AIM	RESULTS/CONCLUSIONS	REFERENCES
A594, HepG2, L-929, Neuro 2a cells	24 h	STE 3 $\mu\text{M}$ – 3mM (1 – 1000 $\mu\text{g/ml}$ )	Effect of STE on cell proliferation	The STE decreased cell viability in all of the four cell lines studied, exhibiting different cytotoxic effects among them. The A549 cells were found to be the most sensitive cell line to STE, whereas the HepG2 cells were the least sensitive	(Bunger et al., 2004)
ACI rat and C3H mouse hepatocytes	20 h	STE 1 – 10 $\mu\text{M}$ ( $10^{-6}$ – $10^{-5}$ M) for rat hepatocytes STE 2 – 20 $\mu\text{M}$ ( $2 \cdot 10^{-5}$ – $2 \cdot 10^{-6}$ M) for mouse hepatocytes	Genotoxicity assessment of different mycotoxins, including STE, by HPC/DNA Repair Test	The STE showed to be genotoxic	(Mori et al., 1984)
BEAS-2B and A549 cells	24 h	STE 0.06 – 240 $\mu\text{M}$ for MTT assay STE 6, 12, 24 $\mu\text{M}$ for FCM analysis	Effect of STE on cell proliferation, apoptosis and apoptosis related factors	The STE inhibited the proliferation of both cell lines by inducing apoptosis via down-regulation of Bcl-2, up-regulation of Bax and activation of caspase-3	(Cui et al. 2017)

## Introduction

CELL TYPE	TIME	CONCENTRATIONS	AIM	RESULTS/CONCLUSIONS	REFERENCES
	24 h	STE 6, 12, 24 $\mu\text{M}$	Effect of STE on DNA damage and cell cycle progression	The STE induced DNA damage and affected key proteins involved in cell cycle regulation. The effect of STE on cell cycle progression was cell type- and concentration-dependent	(Huang et al., 2014)
CHO-K1	24 h, 48 h and 72 h	STE 1.56 - 50 $\mu\text{M}$ for individual assays STE 0.78 - 6.25 $\mu\text{M}$ for combined assays	Cytotoxicity of STE alone and in combination with BEA and PAT	The STE decreased cell viability in a concentration-dependent manner, resulting less toxic than BEA and PAT. Mainly synergistic and additive interactions were observed.	(Zouaoui et al., 2016)
GES-1 cells	24 h and 48 h	STE 12 $\mu\text{M}$	Role of Chk1 signalling in regulating the checkpoint activation and adaption in cells exposed to STE	The STE treatment for 24 h activated Chk1 and induced G <sub>2</sub> cell cycle, whereas STE treatment for 48 h led to Chk1 inactivation, promoting checkpoint adaptation	(Jiang et al., 2017)



CELL TYPE	TIME	CONCENTRATIONS	AIM	RESULTS/CONCLUSIONS	REFERENCES
	24 h	STE 0.3 – 6 $\mu$ M (100 - 2000 $\mu$ g/l) For signalling pathway assays: STE 3 $\mu$ M (1000 $\mu$ g/l) $\pm$ SP600125 (1 $\mu$ M), PD98059 (50 $\mu$ M) or LY294002 (1 $\mu$ M)	Role of JNK, ERK and PI3K/AKT/mTOR pathways in STE-induced cell cycle arrest	The JNK, ERK and PI3K/AKT/mTOR pathways participated in STE-induced G <sub>2</sub> cell cycle arrest, playing a potential role in gastric carcinogenesis associated to STE exposure	(Xing et al., 2011)
	48 h	STE 0.075, 0.3, 1.5 and 3 $\mu$ M	Molecular mechanisms involved in STE-induced cell cycle arrest	The ATM/p53-related signalling pathway resulted to be involved in STE-induced G <sub>2</sub> cell cycle arrest	(Zhang et al., 2013)
Hep3B cells	24 h and 48 h	STE 1 pM – 0.2 mM ( $10^{-12}$ – $2 \cdot 10^{-4}$ M)	Cytotoxicity and cytogenetic assessment of STE, alone and in combination with OTA and/or CTN	The STE showed toxic effects alone and in combination with OTA and/or CTN, inducing increased sister chromosome exchanges and decreased cell viability and mitotic divisions	(Anninou et al., 2014)

## Introduction

CELL TYPE	TIME	CONCENTRATIONS	AIM	RESULTS/CONCLUSIONS	REFERENCES
HepG2	24 h for MTT assay; 1 h for lysosomal membrane stability, ROS and comet assays; 3 h for 8-OHdG assay	STE 0 – 12 $\mu$ M for MTT assay STE 0 – 6 $\mu$ M for 8-OHdG and ROS assay STE 0 – 6 $\mu$ M $\pm$ pre-treatment with NAC (10 mM) for comet assay STE 0 – 6 $\mu$ M $\pm$ pre-treatment with NH <sub>4</sub> Cl (10 mM)	Genotoxicity assessment of STE	The STE exposure decreased cell viability and lysosomal membrane stability, increased ROS levels and 8-OHdG formation and induced DNA strand breaks	(Gao et al., 2015)
	24 h and 48 h	STE 0.1 – 28 $\mu$ M for SRB assay STE 0.5 – 7 $\mu$ M $\pm$ AFB1 for ROS, MMP, DNA and ATP content assays STE 0.01, 0.1 and 7.5 $\mu$ M for FCM assays	Pro-apoptotic activity of STE and related mechanisms of action	The STE reduced cell viability and decreased the content of both ATP and DNA, while increased ROS and MMP. The STE exposure caused also cell cycle arrest, mitochondrial membrane potential decrease and apoptosis, highlighting that mitochondria is one of the cellular target of STE	(Liu et al., 2014)

CELL TYPE	TIME	CONCENTRATIONS	AIM	RESULTS/CONCLUSIONS	REFERENCES
	24 h, 48 h and 72 h	STE 0.78 - 50 $\mu$ M for individual assays STE 0.78 – 12.5 $\mu$ M for combined assays STE 0.78 – 3.31 $\mu$ M for ROS and mitochondrial membrane potential assays	Cytotoxicity of STE alone and in combination with NIV	The mixture decreased the viability more than STE alone at all time of exposure. No relevant effects on ROS and mitochondrial membrane potential were observed	(Zingales et al., 2020a)
HepG2, ACHN and LS-174T cells	24 h	STE 0.01 $\mu$ M – 0.1 mM ( $10^{-8}$ – $10^{-4}$ M)	Cytotoxicity and genotoxicity potential of different mycotoxins, including STE	The STE resulted to be genotoxic in all the cell lines tested and more genotoxic than the aflatoxin precursors	(Theumer et al., 2018)
Het-1A cells	24 h	STE 6, 12, 24 $\mu$ M	Pathway of STE-induced G <sub>2</sub> cell cycle arrest	Member of MMR signalling pathway, MAPK and p53 pathways were all involved in STE-induced G <sub>2</sub> arrest	(Cui et al. 2018)
	24 h	STE 6, 12 and 24 $\mu$ M	Role of MMR proteins on STE-induced DNA damage and cell cycle arrest	The STE induced DNA damage and triggered hMLH1 protein-mediated G <sub>2</sub> phase cell cycle arrest	(Wang et al., 2013)

## Introduction

CELL TYPE	TIME	CONCENTRATIONS	AIM	RESULTS/CONCLUSIONS	REFERENCES
HPBM cells	24 h	STE 0.3 – 6 $\mu$ M (0.125 - 2 mg/l)	Effect of STE on HLA-I expression	STE inhibited HLA-I expression in a negative dose-dependent manner	(Xing et al., 2005)
	1 h and 64 h	STE 0.09 – 6 $\mu$ M (0.03125 – 2 mg/l)	Effect of STE on human immune function	The STE showed inhibiting effects on the secretion of IL-2	(Huang et al., 2002)
Human gastric epithelial cells	48 h	STE 1 – 100 $\mu$ M ( $10^{-6}$ – $10^{-4}$ M)	Carcinogenic potential of STE on human stomach	Following bioactivation, STE resulted to be able to alter DNA synthesis and induce DNA damage, providing to be a genotoxic mycotoxin	(Ji et al., 1994)
MEFs and HL-60 cells	12 h and 24 h	STE 0.3, 1.5, 3 $\mu$ M (0.1, 0.5 and 1 $\mu$ g/ml) for MEFs cells assays STE 9 $\mu$ M (3 $\mu$ g/ml) for HL-60 cells assays	Cellular responses involved in STE-induced carcinogenesis	The STE-induced failure of p53-mediated cell cycle arrest in G <sub>1</sub> phase, accompanied by induction of MDM2, may represent a possible carcinogenic mechanism of STE	(Xie et al., 2000)

CELL TYPE	TIME	CONCENTRATIONS	AIM	RESULTS/CONCLUSIONS	REFERENCES
SH-SY5Y cells	24h , 48 h and 72 h	STE 0.19 – 25 $\mu$ M for viability assays STE 0.78 – 25 $\mu$ M for mitochondrial toxicity assessment STE 0.78, 1.56 and 3.12 $\mu$ M for ROS, $\Delta\Psi_m$ and apoptosis assays	Pro-apoptotic activity of STE and role of mitochondria in STE-induced toxicity	The STE caused a modulation of mitochondrial function, ATP depletion, oxidative stress and the activation of mitochondrial-related pathway of apoptosis	(Zingales et al., 2020b)
	24 h, 48 h and 72 h	STE 0.19 – 25 $\mu$ M for viability assays STE 0.78, 1.56 and 3.12 $\mu$ M for ROS, LPO, GSH and enzymatic activity assays	The effects of STE on cell viability and its role on the oxidative stress induction	The STE decreased cell viability in a time- and concentration-dependent manner. Oxidative stress played a central role in STE-induced cytotoxicity	(Zingales et al., 2020c)
THP-1 cells	24 h	STE 0 – 20 $\mu$ M for viability and necrosis assays STE 5, 10 and 25 $\mu$ M for cell cycle assay STE 0.625, 1.25 and 2.5 $\mu$ M for differentiation assay	Effects of different mycotoxins, including STE, on the differentiation process from monocytes into macrophages	The STE reduced cell viability and induced necrosis but resulted less potent than other mycotoxins. Cell cycle arrest in S phase was induced by STE. The STE showed no effects in the differentiation process from monocytes into macrophages	(Solhaug et al., 2016)

## Introduction

CELL TYPE	TIME	CONCENTRATIONS	AIM	RESULTS/CONCLUSIONS	REFERENCES
XP-E cells	30 min	STE 1 $\mu\text{M}$ – 1 mM ( $10^{-6}$ – $10^{-3}$ M)	Potential mutagenicity of STE	Activation systems containing the S9 post-mitochondrial fraction, microsomal preparation or supernatant of the livers of various species potentiated the ability of STE to induce DNA repair synthesis and chromatid breakage	(Stich and Laishes, 1975)

Abbreviations: 8-OHdG: 8-hydroxydeoxyguanosine; A549: Adenocarcinomic human alveolar basal epithelial cells; ACHN: Human renal cell adenocarcinoma cells; ACI: August-Copenhagen Irish; AFB1: Aflatoxin B1; ATM/p53: Ataxia Telangiectasia Mutated kinase/tumour protein p53; ATP: Adenosine triphosphate; Bax: Bcl-2-associated X protein; Bcl-2: B-cell lymphoma 2; BEA: Beauvericin; BEAS-2B: Human bronchial epithelial cells; C3H: Inbred mouse strain; Chk1: Checkpoint kinase 1; CHO–K1: Chinese hamster ovary cells; DNA: Deoxyribonucleic acid; ERK: Extracellular signal-regulated kinase; FCM: Flow cytometry; GES-1: Human gastric epithelial cells; GSH: Glutathione; Hep3B: Human hepatocellular carcinoma cells; HepG2: Human hepatocellular carcinoma cells; Het-1A: Human esophageal epithelial cells; HL-60: Human promyelocytic leukaemia cells; HLA-I: Human leukocyte antigen-I; hMLH1: Human mutL homolog 1; HPBM: Human peripheral blood mononuclear cells; IL: Interleukin; JNK: c-JUN N-terminal kinase; L-929: Murine fibroblasts; LPO: Lipid peroxidation; LS-174T: Human epithelial colorectal adenocarcinoma cells; LY294002: PI3K inhibitor; MAPK: Mitogen activated protein kinase; MDM2: murine double minute 2; MEFs: Mouse embryonic fibroblasts; MMP: Mitochondria membrane permeability; MMR: Mismatch repair; MIT: 3-(4,5-dimethylthiazol-2-yl)-2,5-diphenyltetrazolium bromide; NAC: N-acetyl-L-cysteine; Neuro 2a: Murine neuroblastoma cells; NH4Cl: Ammonium chloride; NIV: Nivalenol; p53: Tumour protein p53; PAT: Patulin; PD98059: ERK inhibitor; PI3K/AKT/mTOR: Phosphatidylinositol 3-kinase/protein kinase B/mammalian target of rapamycin; ROS: Reactive oxygen species; SH-SY5Y: Human neuroblastoma cells; SP600125: JNK inhibitor; SRB: Sulforhodamine B; STE: Sterigmatocystin; THP-1: Human acute monocyte leukaemia cells; XP-E cells: Fibroblasts from Xeroderma pigmentosum patient.

**Table 2.** *In vivo* toxicity studies.

<b>ANIMALS</b>	<b>TIME</b>	<b>DOSE</b>	<b>AIM</b>	<b>RESULTS/CONCLUSIONS</b>	<b>REFERENCES</b>
<i>Acute toxicity assays</i>					
BALB/c mice	24 h	STE 3, 30, 300 and 3000 µg/kg BW	Short-term immunotoxic effects of STE	The STE exposure affected the number of pDCs and Treg cells. The effects on CD8 <sup>+</sup> and CD4 <sup>+</sup> T cell proportion resulted tissue-specific and dose dependent	(Liu et al., 2012)
	2, 6, 12 and 24 h	STE 3 mg/kg BW	Effect of STE on immune system	The STE down-regulated the expression of TNF-α, IL-6 and IL-12, showing negative immunomodulatory effects	(Zhang et al., 2012)
Long-Evans rats	0 – 96 h	STE 0.312 µg/kg BW – 312 mg/kg BW (10 <sup>-6</sup> – 1 mM/kg BW)	Cytogenetic toxicity of STE	The STE induced chromosome aberration, reaching the maximum level after 12 h of exposure, whereas a gradual decrease was observed after 96 h	(Ueda et al., 1984)

## Introduction

---

<b>ANIMALS</b>	<b>TIME</b>	<b>DOSE</b>	<b>AIM</b>	<b>RESULTS/CONCLUSIONS</b>	<b>REFERENCES</b>
Male Wistar rats	24 h	STE 10, 20, 40 mg/kg BW	Contribution of oxidative stress in liver and kidneys DNA damage	The STE induced lipid peroxidation and impaired antioxidant defence system. Oxidative stress contributed to STE-induced DNA damage. Kidneys resulted more susceptible to oxidative stress than liver	(Dubravka et al., 2019)
Rats	24 h	STE 10 – 300 mg/kg BW	Acute toxicity of STE	Results showed that the poor solubility of STE and its low absorption may influence on STE LD <sub>50</sub> values estimation. The route of administration affected the site of the liver lesions. Severe and extensive toxic effects were induced in kidneys	(Purchase and van der Watt, 1969)
Swiss albino mice	2 h	STE 0.06, 0.6, 6 mg/kg BW	Genotoxic effects of STE	The STE increased the frequency of sister-chromatid exchange in mouse bone marrow cells at all doses tested and in a dose-dependent manner	(Curry et al., 1984)



ANIMALS	TIME	DOSE	AIM	RESULTS/CONCLUSIONS	REFERENCES
Swiss Webster (CFW) mice	4 – 12 h	STE 12 mg/ kg lung weight ( $4 \cdot 10^{-5}$ mole/kg lung weight)	Inflammatory lung response to different toxins, including STE	Bronchiolar and alveolar spaces and epithelium of STE treated lungs showed signs of inflammation, associated with a high number or significantly changed inflammatory gene transcripts	(Miller et al., 2010)
Common carp ( <i>Cyprinus carpio</i> L.)	24 h	STE 1, 2 and 4 mg/kg feed	Effect of STE-contaminated diet on markers of oxidative stress	Low doses of STE induced earlier oxidative stress and lipid peroxidation, while higher doses showed delayed effects	(Kovesi et al., 2019)
<b><i>Short-, long-term toxicity assays</i></b>					
Broiler chicken	1, 2, 3, 7, and 14 days	STE 1590 µg/kg feed; purified STE 1570.5 µg/kg feed	Effect of mycotoxin diet on lipid peroxidation and glutathione redox parameters	Naturally occurring STE and purified STE induced mild oxidative stress in chicken liver and activated the glutathione redox system	(Balogh et al., 2019)

## Introduction

ANIMALS	TIME	DOSE	AIM	RESULTS/CONCLUSIONS	REFERENCES
CD2F <sub>1</sub> mice	2 weeks 1 year	STE 0.5, 1, 5, 50 and 100 mg/kg BW for the acute toxicity study; STE 0.5, 1 and 5 mg/kg BW for the chronic toxicity study	Tumorigenic effects of STE	In the acute toxicity study, the maximum tolerated dose of STE was 5 µg/g BW. The chronic toxicity study demonstrated that a single s.c. injection of STE at 5, 1 or 0.5 µg/g BW induced mainly tumours of lung and liver.	(Fujii et al., 1976)
Chicken embryos	13 days	STE 1 – 30 µg/egg	Toxicity of STE	Teratogen effects were observed. Doses from 5 to 7 µg killed 50% of the embryos, doses of 10 µg or more killed 90-100% of them. No effects were observed at 1-2 µg.	(Schroeder and Kelton, 1975)
Dairy cattle		Ste 13 – 89 mg/kg feed	To investigate the cause of the bloody diarrhea and death of dairy cattle of a farm in Tennessee	Ingestion of feed contaminated with STE resulted to cause acute clinical symptoms and death in these animals.	(Vesonder and Hornet al., 1985)

ANIMALS	TIME	DOSE	AIM	RESULTS/CONCLUSIONS	REFERENCES
Male Wistar rats	30 days	STE 0.2, 0.3 and 0.4 mg/kg BW	Oxidative stress induced by STE and its effects on liver tissue	The treatment of animals with STE resulted in an enhance of ROS production and lipid peroxidation, a reduction of GSH levels and CAT activity, an increase in SOD and GPx activity and in the activation of the biotransformation process in the liver microsomes	(Sivakumar et al., 2001)
Mongolian gerbils	24 weeks	STE 0.3 – 3 $\mu$ M (100 and 1000 ppb)	Carcinogenetic potential of STE on gastric mucosa	STE induced gastritis, erosion events, polyps and intestinal metaplasia, showing carcinogenic effects in the gastric mucosa	(Kusunoki et al., 2011)
	27 months	STE 0.3 – 3 $\mu$ M (100 or 1000 ppb) + <i>H. pylori</i> (10 ml/kg)	Effect of STE in <i>H. pylori</i> -infected Mongolian gerbils	The co-treatment <i>H. pylori</i> + STE enhanced the development of intestinal metaplasia and increased gastrin level compared to animals infected with <i>H. pylori</i> only	(Ma et al., 2003)

## Introduction

ANIMALS	TIME	DOSE	AIM	RESULTS/CONCLUSIONS	REFERENCES
NIH mice	24 weeks	STE 3 and 30 µg/kg BW STE 3 µg/kg BW + DON 1.5 µg/kg BW STE 30 µg/kg BW + DON 1.5 µg/kg BW	Carcinogenic effects of STE and DON alone and in combination	STE alone induced adenocarcinoma in lung and dysplasia of glandular stomach. The combinations STE+DON showed a synergistic carcinogenic effect	(Huang et al., 2004)
Rats and Piglets	20 days for rats; 10 days for piglets	STE 14.13, 28.25 and 56.50 µg/kg feed for rats; STE 30 µg/ kg feed for piglets	Establishment of the maximum allowable level of STE for animal laboratory and piglets	Concentration of 30 µg/kg feed caused enteritis, diarrhea, liver damage and development of a general toxic reaction	(Kovalenko et al., 2011)
Shaver Starcross 288 chicks	5 injections at 11, 13, 15, 17 and 19 days of age	STE 0.5 and 0.7 mg/kg BW	Effects of STE on the growth pattern of chicks and their organs	The STE treatment affected several organs, such as digestive system, liver, kidneys, pancreas and the immunological system	(Sreemannarayana et al., 1988)
Sheep	6 months	STE 2- 16 mg/kg feed	Toxic effects of STE	No signs of intoxication were observed after STE exposure	(Böhm and Sayed, 1994)

ANIMALS	TIME	DOSE	AIM	RESULTS/CONCLUSIONS	REFERENCES
Sprague-Dawley male rats	4 weeks	STE 18 µg/rat/day + RPP 250 and 500 mg/day	Protective effects of an aqueous extract of RPP against STE toxicity in liver, kidney, intestine and lung	The RPP extract showed a potent antioxidant activity and a dose-dependent protective effect against STE toxicity, especially in liver and kidneys	(El-Desouky et al., 2015)
Wistar rats	52 weeks	STE 0.03, 0.06, 0.3 mM (10, 20 and 100 ppm) for the first 6 months; STE 0.04, 0.09, 0.4 mM (15, 30 and 150 ppm) for the second 6 months	Long-term toxicity of STE	The highest doses of STE induced mortality in the first weeks of treatment. The survived animals developed hepatocarcinoma and, in lower rates, tumours in uterus, ovary, spleen or omentum	(Purchase and Van der Watt, 1970)
	70 weeks	STE (1 mg)	Carcinogenic effects of STE on rat skin	Papillomas and squamous cell carcinomas were induced starting from the 40 <sup>th</sup> week of exposure.	(Purchase and Van der Watt, 1973)

## Introduction

ANIMALS	TIME	DOSE	AIM	RESULTS/CONCLUSIONS	REFERENCES
	7 days	STE (30 µg/kg BW)	Role of STE in esophageal cancer development	The STE negatively impacted the immune function, inhibiting the expression of HLA-I and down-regulating the expression of TAP and LMP genes and, therefore, promoting cancer onset	(Tong et al., 2013)
Nile tilapia fish	4 weeks	STE (1.6 µg/kg BW) + EM (0.5 mg/kg BW)	Protective effect of Egyptian montmorillonite (EM) on STE-induced toxicity and chromosomal aberrations	STE caused a significant decrease of body weight and chromosomal aberrations in the kidney. The administration of EM combined with STE resulted in a reduction of the frequency of chromosomal aberrations.	(Abdel-Wahhab et al., 2005)

Abbreviations: BALB/c mice: Inbred mouse strain; BW: Body weight; CAT: Catalase; CD: Cluster of differentiation; CD2F1 mice: Cross between female BALB/c and male DBA/2; DNA: Deoxyribonucleic acid; DON: Deoxynivalenol; EM: Egyptian montmorillonite; GPx: Glutathione peroxidase; GSH: Glutathione; IL: Interleukin; LD50: Median lethal dose; Long-Evans rats: Outbred rat strain; NIH mice: Inbred mouse strain; pDCs: Plasmacytoid dendritic cells; ROS: Reactive oxygen species; RPP: Red pomegranate peels; s.c.: Subcutaneous; SOD: Superoxide dismutase; Sprague Dawley rat: Outbred rat strain; STE: Sterigmatocystin; Swiss Webster (CFW) mice: Outbred mouse strain; TNF- $\alpha$ : Tumor necrosis factor  $\alpha$ ; Treg: Regulatory T cells; Wistar rat: Outbred rat strain.

## **Concluding remarks**

Data reviewed above suggest that STE is a potent cytotoxic mycotoxin which constitutes a serious risk factor for human and animal health. It has been shown to cause fatal diseases in animals and the incidence of gastric cancer in China has been proposed to be linked to STE exposure. Recently, researchers have focused on elucidating the mechanisms by which STE exerts its toxicity, but only few data are still available. Based on focused studies on *in vitro* models and relatively few *in vivo* studies, the reported metabolic transformation of STE, its ability to form DNA-adducts and cause DNA damage appear to play a critical role in STE-induced carcinogenesis. Moreover, as reviewed previously, STE has been shown to be linked also to reduced immune response and disturbed balance of the adaptive immune system, as well as to the induction of oxidative stress, apoptosis, mitochondrial dysfunction and activation of specific pathways. If on one hand it is obvious that all these mechanisms are related to STE-induced toxicity and carcinogenicity, on the other hand the sensitivities of different types of cells and the sensitivities of same cell types originating from different species, seem to be critical for the outcome of the toxicity. Furthermore, STE seems unlikely to act through a single, well-defined mechanism of action. On the contrary, a network of interacting mechanisms appears to be responsible for STE toxicity (Fig. 2). However, further clarifications in relation to the cellular effects of this mycotoxin are needed. Moreover, a more detailed understanding of the role of ROS in STE-induced toxicity and the use of antioxidants for protecting cells against the action of STE could represent an attractive strategy for the risk assessment of this mycotoxin.

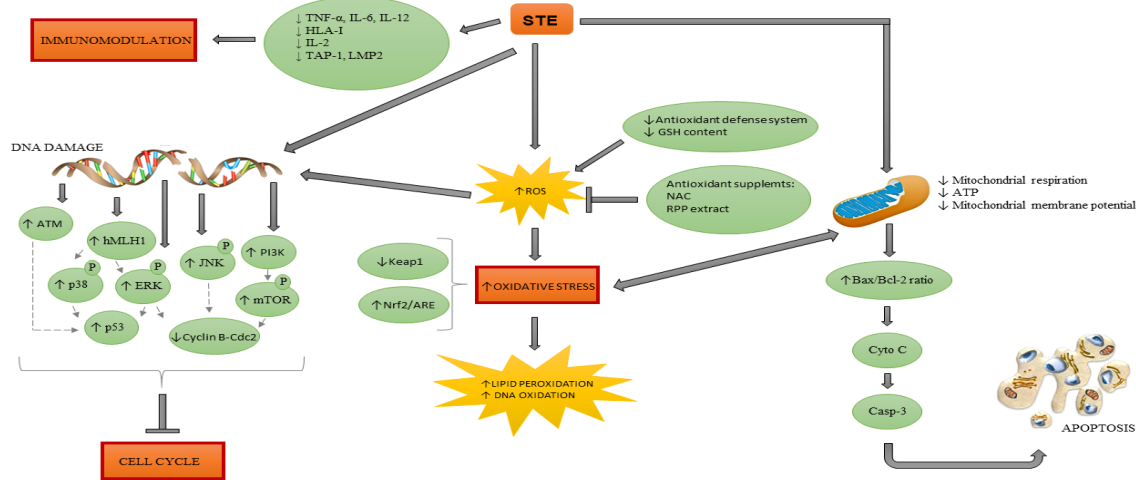


**Fig.2.** Sterigmatocystin-induced molecular mechanisms of action. Abbreviations: ATM: Ataxia Telangiectasia Mutated kinase; ATP: Adenosine triphosphate; Bax: Bcl-2-associated X protein; Bcl-2: B-cell lymphoma 2; Casp-3: Caspase-3; Cdc2: Cell-division cycle 2; Cyto C: Cytochrome C; ERK: Extracellular signal-regulated kinase; GSH: Glutathione; HLA-I: Human leukocyte antigen-I; hMLH1: Human mutL homolog 1; IL: Interleukin; JNK: c-JUN N-terminal kinase; Keap1: Kelch-like ECH-associated protein 1; LMP2: Low molecular weight protein 2; mTOR: Mammalian target of rapamycin; NAC: N-acetyl-L-cysteine; Nrf2/ARE: Nuclear factor (erythroid-derived 2)-like 2/ Antioxidant Response Element; p38: Mitogen activated protein kinase; p53: Tumour protein p53; PI3K: Phosphatidylinositol 3-kinase; ROS: Reactive Oxygen Species; RPP: Red pomegranate peels; STE: Sterigmatocystin; TAP1: Transporter associated with antigen processing 1; TNF- $\alpha$ : Tumor necrosis factor  $\alpha$ .



### **Declaration of competing interest**

The authors declare that they have no known competing financial interests or personal relationships that could have appeared to influence the work reported in this paper.

### **Acknowledgments**

This research has been supported by the Generalitat Valenciana grant (Prometeo 2018/216) and the pre-doctoral research training program “Santiago Grisolia (GRISOLIAP/2018/092) CPI-18-117”.

### **References**

- Abdel-Wahhab, M.A., Hasan, A.M., Aly, S.E., Mahrous, K.F., 2005. Adsorption of sterigmatocystin by montmorillonite and inhibition of its genotoxicity in the Nile tilapia fish (*Oreochromis niloticus*). *Mutat. Res.* 582, 20–27. <https://doi.org/10.1016/j.mrgentox.2004.12.009>.
- Aly, S.A., Elewa, N.A., 2007. The effect of Egyptian honeybee propolis on the growth of *Aspergillus versicolor* and sterigmatocystin biosynthesis in Ras cheese. *J. Dairy Res.* 74, 74–78. <https://doi.org/10.1017/S002202990600207X>.
- Amon, J., Keisham, K., Bokor, E., Kelemen, E., Vagvolgyi, C., Hamari, Z., 2018. Sterigmatocystin production is restricted to hyphae located in the proximity of hulle cells. *J. Basic Microbiol.* 58, 590–596. <https://doi.org/10.1002/jobm.201800020>.
- Anderson, J.A., 1992. Enzymes in aflatoxin biosynthesis. *World J. Microbiol. Biotechnol.* 8, 96–98. <https://doi.org/10.1007/BF02421506>.
- Anninou, N., Chatzaki, E., Papachristou, F., Pitiakoudis, M., Simopoulos, C., 2014. Mycotoxins’ activity at toxic and sub-toxic

concentrations: differential cytotoxic and genotoxic effects of single and combined administration of sterigmatocystin, ochratoxin A and citrinin on the hepatocellular cancer cell line Hep3B. *Int. J. Environ. Res. Publ. Health* 11, 1855–1872. <https://doi.org/10.3390/ijerph110201855>.

Atalla, M.M., Hassanein, N.M., El-Beih, A.A., Youssef, Y.A., 2003. Mycotoxin production in wheat grains by different *Aspergilli* in relation to different relative humidities and storage periods. *Nahrung* 47, 6–10. <https://doi.org/10.1002/food.200390017>.

Ayed-Boussema, I., Bouaziz, C., Rjiba, K., Valenti, K., Laporte, F., Bacha, H., et al., 2008. The mycotoxin Zearalenone induces apoptosis in human hepatocytes (HepG2) via p53-dependent mitochondrial signaling pathway. *Toxicol. In Vitro* 22, 1671–1680. <https://doi.org/10.1016/j.tiv.2008.06.016>.

Balogh, K., Kovesi, B., Zandoki, E., Kulcsar, S., Ancsin, Z., Erdelyi, M., et al., 2019. Effect of sterigmatocystin or aflatoxin contaminated feed on lipid peroxidation and glutathione redox system and expression of glutathione redox system regulatory genes in broiler chicken. *Antioxidants* 8 (7), 201. <https://doi.org/10.3390/antiox8070201>.

Bayram, O., Braus, G.H., 2012. Coordination of secondary metabolism and development in fungi: the velvet family of regulatory proteins. *FEMS Microbiol. Rev.* 36, 1–24. <https://doi.org/10.1111/j.1574-6976.2011.00285.x>.

Bertuzzi, T., Romani, M., Rastelli, S., Giorni, P., 2019. Mycotoxins and related fungi in Italian paddy rice during the growing season and storage. *Toxins* 11 (3), 151. <https://doi.org/10.3390/toxins11030151>.

Bhatnagar, D., Ehrlich, K.C., Cleveland, T.E., 1992. Oxidation-reduction reactions in biosynthesis of secondary metabolites. *Handbook of Applied Mycology* 5, 255–286.

Biancardi, A., Dall'Asta, C., 2015. Determination of sterigmatocystin in feed by LC-MS/MS. *Food Addit. Contam. Part A Chem Anal Control Expo Risk Assess* 32, 2093–2100. <https://doi.org/10.3390/toxins11030151>.

Böhm, J., Sayed, A., 1994. Investigation on toxic effects of sterigmatocystin in sheep. *Wien Tierarztl Monat* 81, 60–64.

Bokhari, F., Aly, M., 2009. Evolution of traditional means of roasting and mycotoxins contaminated coffee beans in Saudi Arabia. *Adv. Biol. Res.* 3, 71–78.

Brown, D.W., Yu, J.H., Kelkar, H.S., Fernandes, M., Nesbitt, T.C., Keller, N.P., et al., 1996. Twenty-five coregulated transcripts define a sterigmatocystin gene cluster in *Aspergillus nidulans*. *Proc. Natl. Acad. Sci. U.S.A.* 93, 1418–1422. <https://doi.org/10.1073/pnas.93.4.1418>.

Bunger, J., Westphal, G., Monnich, A., Hinnendahl, B., Hallier, E., Muller, M., 2004. Cytotoxicity of occupationally and environmentally relevant mycotoxins. *Toxicology* 202, 199–211. <https://doi.org/10.1016/j.tox.2004.05.007>.

Butchko, R.A., Adams, T.H., Keller, N.P., 1999. *Aspergillus nidulans* mutants defective in stc gene cluster regulation. *Genetics* 153, 715–720.

Cao, X., Li, X., Li, J., Niu, Y., Shi, L., Fang, Z., et al., 2018. Quantitative determination of carcinogenic mycotoxins in human and animal biological matrices and animal-derived foods using multi-mycotoxin and analyte-specific high performance liquid chromatography-tandem mass spectrometric methods. *J. Chromatogr. B* 1073, 191–200. <https://doi.org/10.1016/j.jchromb.2017.10.006>.

Coulombe Jr., R.A., 1993. Biological action of mycotoxins. *J. Dairy Sci.* 76, 880–891. [https://doi.org/10.3168/jds.S0022-0302\(93\)77414-7](https://doi.org/10.3168/jds.S0022-0302(93)77414-7).

Cui, J., Wang, J., Huang, S., Jiang, X., Li, Y., Wu, W., et al., 2017. Sterigmatocystin induced apoptosis in human pulmonary cells in vitro. *Exp. Toxicol. Pathol.* 69, 695–699. <https://doi.org/10.1016/j.etp.2017.07.002>.

Cui, J., Wang, J., Huang, S., Jiang, X., Li, Y., Wu, W., et al., 2018. The G2 phase arrest induced by sterigmatocystin is dependent on hMLH1-ERK/p38-p53 pathway in human esophageal epithelium cells in vitro. *Food Chem. Toxicol.* 115, 205–211. <https://doi.org/10.1016/j.fct.2018.03.012>.

Curry, P.T., Reed, R.N., Martino, R.M., Kitchin, R.M., 1984. Induction of sister-chromatid exchanges in vivo in mice by the mycotoxins sterigmatocystin and griseofulvin. *Mutat. Res.* 137, 111–115. [https://doi.org/10.1016/0165-1218\(84\)90099-5](https://doi.org/10.1016/0165-1218(84)90099-5).

Dubravka, R., Daniela, J., Andrea, H.T., Domagoj, K., Nevenka, K., Lada, R., et al., 2019. Sterigmatocystin moderately induces oxidative stress in male Wistar rats after short-term oral treatment. *Mycotoxin Res.* 36, 181–191. <https://doi.org/10.1007/s12550-019-00382-8>.

Dyer, P.S., O’Gorman, C.M., 2012. Sexual development and cryptic sexuality in fungi: insights from *Aspergillus* species. *FEMS Microbiol. Rev.* 36, 165–192. <https://doi.org/10.1111/j.1574-6976.2011.00308.x>.

EFSA, 2013. European food safety authority (EFSA) panel on contaminants in food chain (CONTAM), scientific opinion on the risk for public and animal health related to the presence of sterigmatocystin in food and feed. *EFSA J* 11 (6), 3254. <https://doi.org/10.2903/j.efsa.2013.3254>.

El-Desouky, T.A., Sherif, R.M., Sherif, S.M., Khayria, M.N., 2015. Protective effect of aqueous extract pomegranate peel against sterigmatocystin toxicity in rat. *J. Drug Deliv. Therapeut.* 5, 9–18. <https://doi.org/10.22270/jddt.v5i5.1136>.

Essigmann, J.M., Barker, L.J., Fowler, K.W., Francisco, M.A., Reinhold, V.N., Wogan, G. N., 1979. Sterigmatocystin-DNA interactions: identification of a major adduct formed after metabolic activation in vitro. *Proc. Natl. Acad. Sci. Unit. States Am.* 76, 179–183. <https://doi.org/10.1073/pnas.76.1.179>.

Essigmann, J.M., Donahue, P.R., Story, D.L., Wogan, G.N., Brunengraber, H., 1980. Use of the isolated perfused rat liver to study carcinogen-DNA adduct formation from aflatoxin B1 and sterigmatocystin. *Canc. Res.* 40, 4085–4091.

FAO, 2004. *Worldwide Regulations for Mycotoxins in Food and Feed in 2003*. 1st Ed. Food and Agriculture Organization of the United Nations, Rome, ISBN: 92-5-105162-3.

Fernandez-Blanco, C., Font, G., Ruiz, M.J., 2016. Role of quercetin on Caco-2 cells against cytotoxic effects of alternariol and alternariol monomethyl ether. *Food Chem. Toxicol.* 89, 60–66. <https://doi.org/10.1016/j.fct.2016.01.011>.

Francis Jr., O.J., Ware, G.M., Carman, A.S., Kuan, S.S., 1985. Thin layer chromatographic determination of sterigmatocystin in cheese. *J Assoc Off Anal Chem* 68, 643–645.

Fujii, K., Kurata, H., Odashima, S., Hatsuda, Y., 1976. Tumor induction by a single subcutaneous injection of sterigmatocystin in newborn mice. *Canc. Res.* 36, 1615–1618.

Galvano, F., Piva, A., Ritieni, A., Galvano, G., 2001. Dietary strategies to counteract the effects of mycotoxins: a review. *J. Food Protect.* 64, 120–131. <https://doi.org/10.4315/0362-028x-64.1.120>.

Gao, W., Jiang, L., Ge, L., Chen, M., Geng, C., Yang, G., et al., 2015. Sterigmatocystin-induced oxidative DNA damage in human liver-derived cell

line through lysosomal damage. *Toxicol. In Vitro* 29, 1–7. <https://doi.org/10.1016/j.tiv.2014.08.007>.

Garcia-Moraleja, A., Font, G., Manes, J., Ferrer, E., 2015. Analysis of mycotoxins in coffee and risk assessment in Spanish adolescents and adults. *Food Chem. Toxicol.* 86, 225–233. <https://doi.org/10.1016/j.fct.2015.10.014>.

Gorst-Allman, C.P., Steyn, P.S., 1979. Screening methods for the detection of thirteen common mycotoxins. *J. Chromatogr.* 175, 325–331. [https://doi.org/10.1016/s0021-9673\(00\)89439-x](https://doi.org/10.1016/s0021-9673(00)89439-x).

Gruber-Dorninger, C., Novak, B., Nagl, V., Berthiller, F., 2017. Emerging mycotoxins: beyond traditionally determined food contaminants. *J. Agric. Food Chem.* 65, 7052–7070. <https://doi.org/10.1021/acs.jafc.6b03413>.

Hicks, J., Shimizu, K., Keller, N.P., 2002. Genetics and biosynthesis of aflatoxins and sterigmatocystin. In: Kempken, F., Bennett, J.W. (Eds.), *The Mycota*, XI. Springer-Verlag, Berlin, pp. 55–69.

Hu, Y., Zhang, J., Kong, W., Zhao, G., Yang, M., 2017. Mechanisms of antifungal and anti-aflatoxigenic properties of essential oil derived from turmeric (*Curcuma longa* L.) on *Aspergillus flavus*. *Food Chem.* 220, 1–8. <https://doi.org/10.1016/j.foodchem.2016.09.179>.

Huang, X., Zhang, X., Yan, X., Yin, G., 2002. Effects of sterigmatocystin on interleukin-2 secretion of human peripheral blood mononuclear cells in vitro. *Wei Sheng Yan Jiu* 31, 112–114.

Huang, X.H., Zhang, X.H., Li, Y.H., Wang, J.L., Yan, X., Xing, L.X., et al., 2004.

Carcinogenic effects of sterigmatocystin and deoxynivalenol in NIH mice. *Zhonghua Zhongliu Zazhi* 26, 705–708.

Huang, S., Wang, J., Xing, L., Shen, H., Yan, X., Wang, J., et al., 2014. Impairment of cell cycle progression by sterigmatocystin in human pulmonary cells *in vitro*. *Food Chem. Toxicol.* 66, 89–95. <https://doi.org/10.1016/j.fct.2014.01.024>.

Hutasanu, C., Sfarti, C., Trifan, A., Cojocariu, C., Singeap, A.M., Spac, A., et al., 2011. High levels of sterigmatocystin in patients with chronic liver diseases. *Rev. Med.-Chir. Soc. Med. Nat. Iasi* 115, 33–37.

IARC, 1987. Overall Evaluations of Carcinogenicity: an Updating of IARC Monographs Volumes 1 to 42. France, Supplement 7. Lyon.

Ji, X., Ke, Y., Ning, T., Liang, Y., Wang, D., Shi, G., 1994. Effects of sterigmatocystin and T-2 toxin on the induction of unscheduled DNA synthesis in primary cultures of human gastric epithelial cells. *Nat. Toxins* 2, 115–119. <https://doi.org/10.1002/nt.2620020305>.

Jiang, X., Wang, J., Xing, L., Shen, H., Lian, W., Yi, L., et al., 2017. Sterigmatocystin-induced checkpoint adaptation depends on Chk1 in immortalized human gastric epithelial cells *in vitro*. *Arch. Toxicol.* 91, 259–270. <https://doi.org/10.1007/s00204-016-1682-2>.

Joint FAO/WHO Food Standards Programme Codex Committee on Contaminants, 2015. 9th session.

Juan-Garcia, A., Tolosa, J., Juan, C., Ruiz, M.J., 2019. Cytotoxicity, genotoxicity and disturbance of cell cycle in HepG2 cells exposed to OTA and BEA: single and combined actions. *Toxins* 11 (6), 341. <https://doi.org/10.3390/toxins11060341>.

Kabak, B., Dobson, A.D., Var, I., 2006. Strategies to prevent mycotoxin contamination of food and animal feed: a review. *Crit. Rev. Food Sci. Nutr.* 46, 593–619. <https://doi.org/10.1080/10408390500436185>.

Katsurayama, A.M., Martins, L.M., Iamanaka, B.T., Fungaro, M.H.P., Silva, J.J.,

Frisvad, J.C., et al., 2018. Occurrence of *Aspergillus* section *Flavi* and aflatoxins in Brazilian rice: from field to market. *Int. J. Food Microbiol.* 266, 213–221. <https://doi.org/10.1016/j.ijfoodmicro.2017.12.008>.

Kawai, K., Nakamaru, T., Nozawa, Y., Maebayashi, Y., Yamazaki, M., Natori, S., 1984. Inhibitory effect of sterigmatocystin and 5,6-dimethoxysterigmatocystin on ATP synthesis in mitochondria. *Appl. Environ. Microbiol.* 48, 1001–1003.

Kawai, K., Nakamaru, T., Hisada, K., Nozawa, Y., Mori, H., 1986. The effects of demethylsterigmatocystin and sterigmatin on ATP synthesis system in mitochondria: a comparison with sterigmatocystin. *Mycotoxin Res.* 2, 33–38. <https://doi.org/10.1007/BF03191960>.

Kocic-Tanackov, S., Dimic, G., Levic, J., Tanackov, I., Tepic, A., Vujicic, B., et al., 2012. Effects of onion (*Allium cepa* L.) and garlic (*Allium sativum* L.) essential oils on the *Aspergillus versicolor* growth and sterigmatocystin production. *J. Food Sci.* 77, M278–M284. <https://doi.org/10.1111/j.1750-3841.2012.02662.x>.

Kovalenko, A.V., Soldatenko, N.A., Fetisov, L.N., Streltsov, N.V., 2011. More accurate determination of the minimum allowable level of sterigmatocystin in piglet feed. *Russ. Agric. Sci.* 37, 504–507. <https://doi.org/10.3103/S1068367411060097>.

Kovesi, B., Pelyhe, C., Zandoki, E., Mezes, M., Balogh, K., 2019. Effect of short-term sterigmatocystin exposure on lipid peroxidation and glutathione redox system and expression of glutathione redox system regulatory genes in



common carp liver. *Toxicon* 161, 50–56.  
<https://doi.org/10.1016/j.toxicon.2019.03.001>.

Krishnaswamy, R., Devaraj, S.N., Padma, V.V., 2010. Lutein protects HT-29 cells against Deoxynivalenol-induced oxidative stress and apoptosis: prevention of NF-kappaB nuclear localization and down regulation of NF-kappaB and Cyclo-Oxygenase-2 expression. *Free Radic. Biol. Med.* 49, 50–60.  
<https://doi.org/10.1016/j.freeradbiomed.2010.03.016>.

Krivobok, S., Olivier, P., Marzin, D.R., Seigle-Murandi, F., Steiman, R., 1987. Study of the genotoxic potential of 17 mycotoxins with the SOS Chromotest. *Mutagenesis* 2, 433–439.  
<https://doi.org/10.1093/mutage/2.6.433>.

Kusunoki, M., Misumi, J., Shimada, T., Aoki, K., Matsuo, N., Sumiyoshi, H., et al., 2011. Long-term administration of the fungus toxin, sterigmatocystin, induces intestinal metaplasia and increases the proliferative activity of PCNA, p53, and MDM2 in the gastric mucosa of aged Mongolian gerbils. *Environ. Health Prev. Med.* 16, 224–231. <https://doi.org/10.1007/s12199-010-0190-x>.

Liu, Y., Xing, X., Wang, J., Xing, L., Su, Y., Yao, Z., et al., 2012. Sterigmatocystin alters the number of FoxP3+ regulatory T cells and plasmacytoid dendritic cells in BALB/c mice. *Food Chem. Toxicol.* 50, 1920–1926. <https://doi.org/10.1016/j.fct.2012.03.005>.

Liu, Y., Du, M., Zhang, G., 2014. Proapoptotic activity of aflatoxin B1 and sterigmatocystin in HepG2 cells. *Toxicol Rep* 1, 1076–1086. <https://doi.org/10.1016/j.toxrep.2014.10.016>.

Lou, J.L., Tian, H.J., Meng, Z.H., Gou, Z.Q., 1995. Detection of sterigmatocystin in food/ feed samples from areas with various liver/stomach

cancer incidences by enzyme-linked immunosorbent assay. *Wei Sheng Yan Jiu* 24, 28–31.

Ma, F., Misumi, J., Zhao, W., Aoki, K., Kudo, M., 2003. Long-term treatment with sterigmatocystin, a fungus toxin, enhances the development of intestinal metaplasia of gastric mucosa in *Helicobacter pylori*-infected Mongolian gerbils. *Scand. J. Gastroenterol.* 38, 360–369.

Miller, J.D., Sun, M., Gilyan, A., Roy, J., Rand, T.G., 2010. Inflammation-associated gene transcription and expression in mouse lungs induced by low molecular weight compounds from fungi from the built environment. *Chem. Biol. Interact.* 183, 113–124. <https://doi.org/10.1016/j.cbi.2009.09.023>.

Mo, H.G., Pietri, A., MacDonald, S.J., Anagnostopoulos, C., Spanjere, M., 2015. Survey on sterigmatocystin in food. *EFSA Support Publ* 12, 774E. <https://doi.org/10.2903/sp.efsa.2015.EN-774>.

Mori, H., Kawai, K., Ohbayashi, F., Kuniyasu, T., Yamazaki, M., Hamasaki, T., et al., 1984. Genotoxicity of a variety of mycotoxins in the hepatocyte primary culture/DNA repair test using rat and mouse hepatocytes. *Canc. Res.* 44, 2918–2923.

Palanee, T., Dutton, M.F., Chuturgoon, A.A., 2001. Cytotoxicity of aflatoxin B1 and its chemically synthesised epoxide derivative on the A549 human epithelioid lung cell line. *Mycopathologia* 151, 155–159. <https://doi.org/10.1023/a:1017985924257>.

Panasiuk, L., Jedziniak, P., Pietruszka, K., Piatkowska, M., Bocian, L., 2019. Frequency and levels of regulated and emerging mycotoxins in silage in Poland. *Mycotoxin Res.* 35, 17–25. <https://doi.org/10.1007/s12550-018-0327-0>.

Pfeiffer, E., Fleck, S.C., Metzler, M., 2014. Catechol formation: a novel pathway in the metabolism of sterigmatocystin and 11-methoxysterigmatocystin. *Chem. Res. Toxicol.* 27, 2093–2099. <https://doi.org/10.1021/tx500308k>.

Purchase, I.F., Van Der Watt, J.J., 1970. Carcinogenicity of sterigmatocystin. *Food Chem. Toxicol.* 8, 289–295. [https://doi.org/10.1016/s0015-6264\(70\)80004-9](https://doi.org/10.1016/s0015-6264(70)80004-9).

Purchase, I.F., van der Watt, J.J., 1969. Acute toxicity of sterigmatocystin to rats. *Food Chem. Toxicol.* 7, 135–139. [https://doi.org/10.1016/s0015-6264\(69\)80295-6](https://doi.org/10.1016/s0015-6264(69)80295-6).

Purchase, I.F., Van der Watt, J.J., 1973. Carcinogenicity of sterigmatocystin to rat skin. *Toxicol. Appl. Pharmacol.* 26, 274–281. [https://doi.org/10.1016/0041-008x\(73\)90262-7](https://doi.org/10.1016/0041-008x(73)90262-7).

Qiu, G.H., Xie, X., Xu, F., Shi, X., Wang, Y., Deng, L., 2015. Distinctive pharmacological differences between liver cancer cell lines HepG2 and Hep3B. *Cytotechnology* 67, 1–12. <https://doi.org/10.1007/s10616-014-9761-9>.

Rank, C., Nielsen, K.F., Larsen, T.O., Varga, J., Samson, R.A., Frisvad, J.C., 2011. Distribution of sterigmatocystin in filamentous fungi. *Fungal Biol* 115, 406–420. <https://doi.org/10.1016/j.funbio.2011.02.013>.

Reddy, K.R., Reddy, C.S., Muralidharan, K., 2009. Detection of *Aspergillus* spp. and aflatoxin B1 in rice in India. *Food Microbiol.* 26, 27–31. <https://doi.org/10.1016/j.fm.2008.07.013>.

Ruiz, M.J., Franzova, P., Juan-Garcia, A., Font, G., 2011. Toxicological interactions between the mycotoxins beauvericin, deoxynivalenol and T-2 toxin in CHO-K1 cells in vitro. *Toxicon* 58, 315–326. <https://doi.org/10.1016/j.toxicon.2011.07.015>.

Schroeder, H.W., Kelton, W.H., 1975. Production of sterigmatocystin by some species of the genus *Aspergillus* and its toxicity to chicken embryos. *Appl. Microbiol.* 30, 589–591.

Sivakumar, V., Thanissar, J., Niranjali, S., Devaraj, H., 2001. Lipid peroxidation as a possible secondary mechanism of sterigmatocystin toxicity. *Hum. Exp. Toxicol.* 20, 398–403. <https://doi.org/10.1191/096032701682692955>.

Solhaug, A., Karlsoen, L.M., Holme, J.A., Kristoffersen, A.B., Eriksen, G.S., 2016. Immunomodulatory effects of individual and combined mycotoxins in the THP-1 cell line. *Toxicol. In Vitro* 36, 120–132. <https://doi.org/10.1016/j.tiv.2016.07.012>.

Speijers, G.J., Speijers, M.H., 2004. Combined toxic effects of mycotoxins. *Toxicol. Lett.* 153, 91–98. <https://doi.org/10.1016/j.toxlet.2004.04.046>.

Sreemannarayana, O., Frohlich, A.A., Marquardt, R.R., 1988. Effects of repeated intraabdominal injections of sterigmatocystin on relative organ weights, concentration of serum and liver constituents, and histopathology of certain organs of the chick. *Poultry Sci. J* 67, 502–509. <https://doi.org/10.3382/ps.0670502>.

Stich, H.F., Laishes, B.A., 1975. The response of *Xeroderma pigmentosum* cells and controls to the activated mycotoxins, aflatoxins and sterigmatocystin. *Int. J. Canc.* 16, 266–274. <https://doi.org/10.1002/ijc.2910160209>.

Stroka, J., Dasko, L., Spangenberg, B., Anklam, E., 2004. Determination of the mycotoxin, sterigmatocystin, by thin-layer chromatography and reagent-

free derivatisation. *J Liq Chromatogr R T* 27, 2101–2111. <https://doi.org/10.1081/JLC-120039421>.

Sulyok, M., Krska, R., Schuhmacher, R., 2010. Application of an LC–MS/MS based multi-mycotoxin method for the semi-quantitative determination of mycotoxins occurring in different types of food infected by moulds. *Food Chem.* 119, 408–416. <https://doi.org/10.1016/j.foodchem.2009.07.042>.

Swenson, D.H., Miller, J.A., Miller, E.C., 1975. The reactivity and carcinogenicity of aflatoxin B1-2,3-dichloride, a model for the putative 2,3-oxide metabolite of aflatoxin B1. *Canc. Res.* 35, 3811–3823.

Takahashi, H., Yasaki, H., Nanayama, U., Manabe, M., Matsuura, S., 1984. Distribution of sterigmatocystin and fungal mycelium in individual brown rice kernels naturally infected by *Aspergillus versicolor*. *Cereal Chem.* 61, 48–52.

Theumer, M.G., Henneb, Y., Khoury, L., Snini, S.P., Tadrist, S., Canlet, C., et al., 2018. Genotoxicity of aflatoxins and their precursors in human cells. *Toxicol. Lett.* 287, 100–107. <https://doi.org/10.1016/j.toxlet.2018.02.007>.

Tian, H., Lou, J., Du, C., 1995. Determination of sterigmatocystin in cancerous tissues, blood and urine in patients with liver and stomach cancer. *Zhonghua Yufang Yixue Zazhi* 29, 276–278.

Tong, P.Z., Zhang, G.J., Zhang, X.H., Yan, X., Wang, J.L., 2013. Effects of sterigmatocystin on esophageal epithelium and experimental reflux esophagitis in rats. *Mol. Med. Rep.* 8, 1043–1048. <https://doi.org/10.3892/mmr.2013.1631>.

Ueda, N., Fujie, K., Gotoh-Mimura, K., Chattopadhyay, S.C., Sugiyama, T., 1984. Acute cytogenetic effect of sterigmatocystin on rat bone-marrow cells in vivo. *Mutat. Res.* 139, 203–206. [https://doi.org/10.1016/0165-7992\(84\)90129-5](https://doi.org/10.1016/0165-7992(84)90129-5).

Uhlig, S., Eriksen, G.S., Hofgaard, I.S., Krska, R., Beltran, E., Sulyok, M., 2013. Faces of a changing climate: semi-quantitative multi-mycotoxin analysis of grain grown in exceptional climatic conditions in Norway. *Toxins* 5, 1682–1697. <https://doi.org/10.3390/toxins5101682>.

Vaclavikova, M., Malachova, A., Veprikova, Z., Dzuman, Z., Zachariasova, M., Hajslova, J., 2013. 'Emerging' mycotoxins in cereals processing chains: changes of enniatins during beer and bread making. *Food Chem.* 136, 750–757. <https://doi.org/10.1016/j.foodchem.2012.08.031>.

Varga, E., Glauner, T., Berthiller, F., Krska, R., Schuhmacher, R., Sulyok, M., 2013. Development and validation of a (semi-)quantitative UHPLC-MS/MS method for the determination of 191 mycotoxins and other fungal metabolites in almonds, hazelnuts, peanuts and pistachios. *Anal. Bioanal. Chem.* 405, 5087–5104. <https://doi.org/10.1007/s00216-013-6831-3>.

Versilovskis, A., Bartkevics, V., Mikelsons, V., 2007. Analytical method for the determination of sterigmatocystin in grains using high-performance liquid chromatography-tandem mass spectrometry with electrospray positive ionization. *J. Chromatogr. A* 1157, 467–471. <https://doi.org/10.1016/j.chroma.2007.05.022>.

Versilovskis, A., Bartkevics, V., Mikelsons, V., 2008. Sterigmatocystin presence in typical Latvian grains. *Food Chem.* 109, 243–248. <https://doi.org/10.1016/j.foodchem.2007.12.066>.

Versilovskis, A., De Saeger, S., Mikelsons, V., 2008. Determination of sterigmatocystin in beer by high performance liquid chromatography with

ultraviolet detection. *World Mycotoxin J.* 1, 161–166. <https://doi.org/10.3920/WMJ2008.x012>.

Versilovskis, A., Van Peteghem, C., De Saeger, S., 2009. Determination of sterigmatocystin in cheese by high-performance liquid chromatography-tandem mass spectrometry. *Food Addit. Contam. Part A Chem Anal Control Expo Risk Assess* 26, 127–133. <https://doi.org/10.1080/02652030802342497>.

Vesonder, R.F., Horn, B.W., 1985. Sterigmatocystin in dairy cattle feed contaminated with *Aspergillus versicolor*. *Appl. Environ. Microbiol.* 49, 234–235.

Wagacha, J.M., Muthomi, J.W., 2008. Mycotoxin problem in Africa: current status, implications to food safety and health and possible management strategies. *Int. J. Food Microbiol.* 124, 1–12. <https://doi.org/10.1016/j.ijfoodmicro.2008.01.008>.

Wang, J., Huang, S., Xing, L., Shen, H., Yan, X., Wang, J., et al., 2013. Role of hMLH1 in sterigmatocystin-induced G(2) phase arrest in human esophageal epithelial Het-1A cells in vitro. *Toxicol. Lett.* 217, 226–234. <https://doi.org/10.1016/j.toxlet.2012.12.020>.

Warth, B., Parich, A., Atehnkeng, J., Bandyopadhyay, R., Schuhmacher, R., Sulyok, M., et al., 2012. Quantitation of mycotoxins in food and feed from Burkina Faso and Mozambique using a modern LC-MS/MS multitoxin method. *J. Agric. Food Chem.* 60, 9352–9363. <https://doi.org/10.1021/jf302003n>.

Xie, T.X., Misumi, J., Aoki, K., Zhao, W.Y., Liu, S.Y., 2000. Absence of p53-mediated G1 arrest with induction of MDM2 in sterigmatocystin-treated cells. *Int. J. Oncol.* 17, 737–742. <https://doi.org/10.3892/ijo.17.4.737>.

Xing, X., Wang, J., Xing, L.X., Li, Y.H., Yan, X., Zhang, X.H., 2011. Involvement of MAPK and PI3K signaling pathway in sterigmatocystin-induced

G2 phase arrest in human gastric epithelium cells. *Mol. Nutr. Food Res.* 55, 749–760. <https://doi.org/10.1002/mnfr.201000344>.

Yabe, K., Nakajima, H., 2004. Enzyme reactions and genes in aflatoxin biosynthesis. *Appl. Microbiol. Biotechnol.* 64, 745–755. <https://doi.org/10.1007/s00253-004-1566-x>.

Xing, L.X., Zhang, X.H., Li, Y.H., Yan, X., Wang, J., Wang, F.R., 2005. Effects of sterigmatocystin on HLA-I expression of human peripheral blood mononuclear cells in vitro. *Wei Sheng Yan Jiu* 34, 454–456.

Yabe, K., Ando, Y., Hashimoto, J., Hamasaki, T., 1989. Two distinct O-methyltransferases in aflatoxin biosynthesis. *Appl. Environ. Microbiol.* 55, 2172–2177. <https://doi.org/10.1128/AEM.55.9.2172-2177.1989>.

Yogendrarajah, P., Jacxsens, L., De Saeger, S., De Meulenaer, B., 2014. Co-occurrence of multiple mycotoxins in dry chilli (*Capsicum annum* L.) samples from the markets of Sri Lanka and Belgium. *Food Contr.* 46, 26–34. <https://doi.org/10.1016/j.foodcont.2014.04.043>.

Yoshinari, T., Takeuchi, H., Kosugi, M., Taniguchi, M., Waki, M., Hashiguchi, S., et al., 2019. Determination of sterigmatocystin in foods in Japan: method validation and occurrence data. *Food Addit. Contam. Part A Chem Anal Control Expo Risk Assess* 36, 1404–1410. <https://doi.org/10.1080/19440049.2019.1628359>.

Youssef, M.S., El-Maghraby, O.M.O., Ibrahim, Y.M., 2008. Mycobiota and mycotoxins of Egyptian peanut (*Arachis hypogaeae* L.) seeds. *Int. J. Bot.* 4, 349–360. <https://doi.org/10.3923/ijb.2008.349.360>.

Zhang, X., Wang, F., Wang, J., Yan, X., Huang, X., Xie, T., et al., 2003. Experimental lung carcinoma induced by fungi and mycotoxins—a review. *Beijing Da Xue Xue Bao Yi Xue Ban* 35, 4–6.



Zhang, Y., Yao, Z.G., Wang, J., Xing, L.X., Xia, Y., Zhang, X.H., 2012. Effects of sterigmatocystin on TNF- $\alpha$ , IL-6 and IL-12 expression in murine peripheral blood mononuclear cells and peritoneal macrophages in vivo. *Mol. Med. Rep.* 5, 1318–1322. <https://doi.org/10.3892/mmr.2012.788>.

Zhang, D., Cui, Y., Shen, H., Xing, L., Cui, J., Wang, J., et al., 2013. Sterigmatocystin-induced DNA damage triggers G2 arrest via an ATM/p53-related pathway in human gastric epithelium GES-1 cells in vitro. *PLoS One* 8, e65044. <https://doi.org/10.1371/journal.pone.0065044>.

Zinedine, A., Fernandez-Franzon, M., Manes, J., Manyes, L., 2017. Multi-mycotoxin contamination of couscous semolina commercialized in Morocco. *Food Chem.* 214, 440–446. <https://doi.org/10.1016/j.foodchem.2016.07.098>.

Zingales, V., Fedeli, C., Fernandez-Franzon, M., Ruiz, M.J., 2020. Cytotoxic effects of individual and combined sterigmatocystin and nivalenol on liver hepatocellular carcinoma cells. *Food Chem. Toxicol.* 143, 111473. <https://doi.org/10.1016/j.fct.2020.111473>.

Zingales, V., Fernández-Franzón, M., Ruiz, M.J., 2020. Sterigmatocystin-induced cytotoxicity via oxidative stress induction in human neuroblastoma cells. *Food Chem. Toxicol.* 136, 110956. <https://doi.org/10.1016/j.fct.2019.110956>.

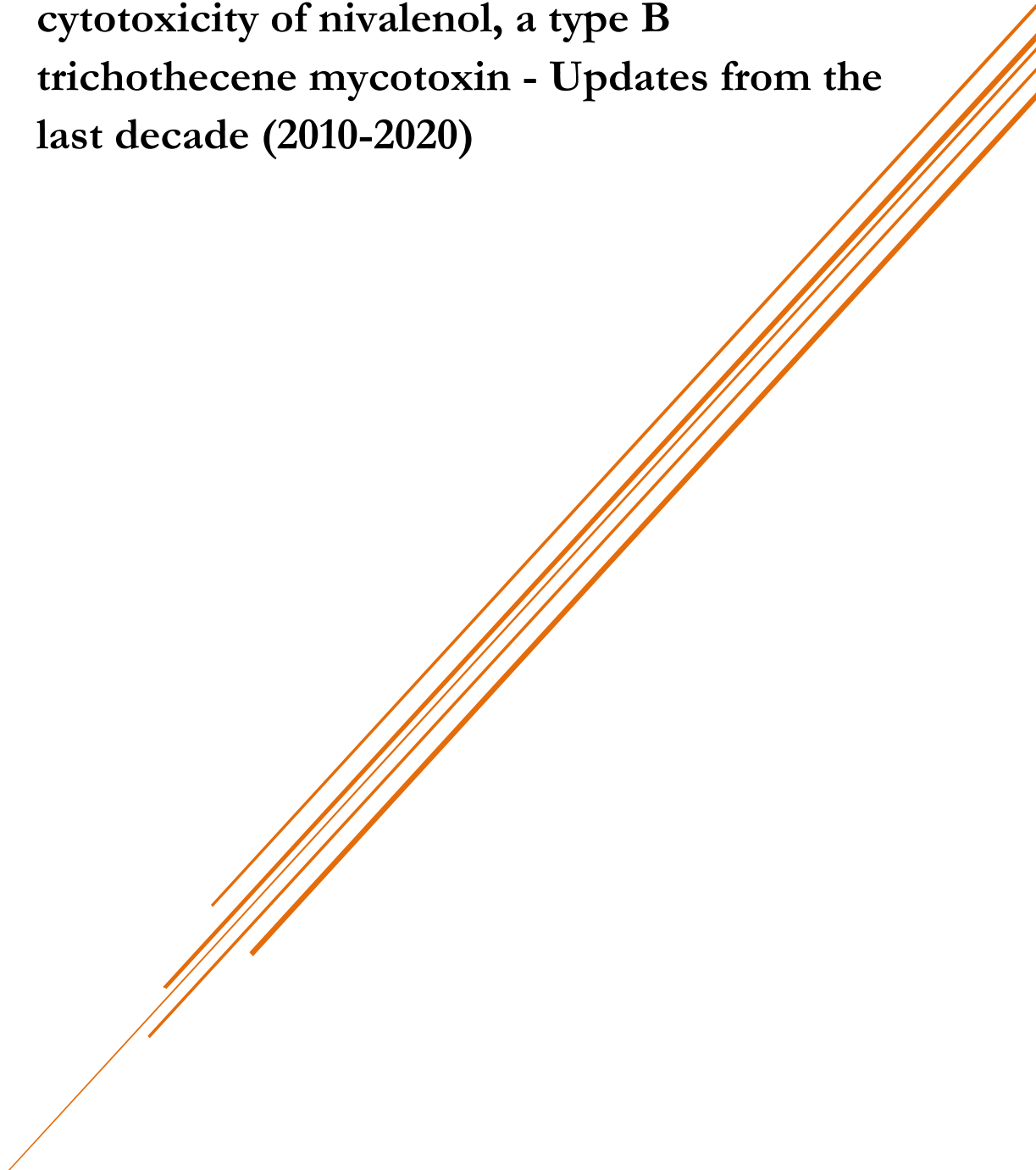
Zingales, V., Fernández-Franzón, M., Ruiz, M.J., 2020. The role of mitochondria in sterigmatocystin-induced apoptosis on SH-SY5Y cells. *Food Chem. Toxicol.* 142, 111493. <https://doi.org/10.1016/j.fct.2020.111493>.

Zouaoui, N., Mallebrera, B., Berrada, H., Abid-Essefi, S., Bacha, H., Ruiz, M.J., 2016. Cytotoxic effects induced by patulin, sterigmatocystin and

beauvericin on CHO-K1 cells. Food Chem. Toxicol. 89, 92–103.

<https://doi.org/10.1016/j.fct.2016.01.010>.

**1.4. Occurrence, mitigation and in vitro cytotoxicity of nivalenol, a type B trichothecene mycotoxin - Updates from the last decade (2010-2020)**

A decorative graphic consisting of several parallel orange lines of varying thicknesses, extending diagonally from the bottom left towards the top right of the page.



Food and Chemical Toxicology

**Occurrence, mitigation and in vitro cytotoxicity of  
nivalenol, a type B trichothecene mycotoxin - Updates from  
the last decade (2010-2020)**

Veronica Zingales\*, Mónica Fernández-Franzón, Maria-José Ruiz

Laboratory of Food Chemistry and Toxicology, Faculty of Pharmacy, University of

Valencia, Av. Vicent Andrés Estellés s/n, 46100, Valencia, Spain

\*Corresponding author. Laboratory of Toxicology, Faculty of Pharmacy, University of Valencia, Av. Vicent Andrés Estellés, s/n, 46100, Burjassot, Valencia, Spain. *E-mail address:* [vezin@uv.es](mailto:vezin@uv.es) (V. Zingales).

### **Abstract**

The present review aims to give an overview of the literature of the last decade (2010–2020) concerning the occurrence of the type B trichothecene mycotoxin nivalenol (NIV) and its *in vitro* toxicity, with the purpose of updating information regarding last researches on this mycotoxin. The most recent studies on the possible methods for preventing *Fusarium* spp. growth and NIV production are also discussed. Recently, various environmental factors have been shown to influence strongly NIV occurrence. However, *Fusarium* spp. of the NIV genotype have been found almost worldwide. With regard to NIV cytotoxicity, NIV has been reported to cause a marked decrease in cell proliferation in different mammalian cells. In particular, the recent data suggest that organs containing actively proliferating cells represent the main targets of NIV. Moreover, NIV resulted to cause immunosuppression, gastrointestinal toxicity and genotoxicity. However, sufficient evidence of carcinogenicity in humans is currently lacking, and the International Agency for Research on Cancer (IARC) classifies it as a group 3 carcinogen. Further researches and the discovery of effective treatment strategies to prevent NIV contamination and to counteract its toxicity are urgently required against this common food-borne threat to human health and livestock.

**Keywords:** Nivalenol, Trichothecene mycotoxin, Occurrence, Mitigation, *In vitro* toxicity.

## 1. Introduction

Mycotoxins are toxic secondary metabolites produced by different types of fungi, belonging mainly to the *Aspergillus*, *Penicillium* and *Fusarium* genera. Several *Fusarium* species are known to be the causal agents of *Fusarium* head blight (FHB) and *Fusarium* crown rot (FCR; also known as foot and root rot), two of the most devastating diseases that affect small grain cereal production worldwide. During the infection process, *Fusarium* spp. biosynthesize different mycotoxins that can compromise food safety, including trichothecenes, zearalenone (ZEA) and fumonisins (Mesterhazy, 2020).

Trichothecenes family is divided into four subgroups (A-D), depending on the chemical structure (Krska et al., 2001). Whereas type C and D trichothecenes occur rarely in food and feed, type A and B trichothecenes are toxicologically the most important and extensively studied groups, being frequently found as contaminants in various commodities. Type A trichothecenes include T-2 toxin (T-2), its acetylated derivative HT-2 toxin (HT-2) and their precursors, such as diacetoxyscirpenol (DAS) and neosolaniol (NEO); whereas type B trichothecenes include nivalenol (NIV), deoxynivalenol (DON) and their acetylated derivatives, 4-acetylnivalenol (fusarenone X or 4-ANIV), 3-acetyldeoxynivalenol (3-ADON), and 15-acetyldeoxynivalenol (15-ADON) (McCormick et al., 2011). In general, in Europe, type B trichothecenes are mainly produced by *F. culmorum* and *F. graminearum*, while *F. poae* is a well-known species for the biosynthesis of NIV, DAS, T-2 and HT-2 toxins (Edwards et al., 2012).

The NIV is a member of type B trichothecenes produced by several *Fusarium* species. The NIV has frequently been observed in agricultural products.

Compared to DON, another type B trichothecene from which it differs only by an additional hydroxyl group at the C-4 position, NIV ingested orally by animals is more toxic. However, although dietary exposure to NIV has been associated with an increased incidence of oesophageal and gastric carcinomas (Hsia et al., 2004), the International Agency for Research on Cancer (IARC) has classified NIV as Group 3 (unclassifiable as to carcinogenicity in humans), due to its inadequate evidence of carcinogenicity in experimental animals (IARC, 1993). Nevertheless, NIV warrants particular attention because of its frequency of contamination and its immunotoxicity and haematotoxicity in mammals (SCF, 2000).

## 2. Occurrence and distribution of NIV

### 2.1. Influence of environmental factors

The NIV contamination is largely influenced by a variety of environmental factors ranging from climatic conditions and farm practice, handling and storage to processing and distribution of food (Magan et al., 2010). Determining how ecological conditions affect *Fusarium* spp. behaviour and mycotoxin production is important for modelling the risk of mycotoxin in crops. Based on the results provided by Nazari et al. (2018), the optimum temperature for the production of NIV in durum wheat heads inoculated with *F. poae* was between 25°C and 35°C (with estimated optimal temperature ( $T_{opt}$ ) equal to 27.5°C), whereas the fungus failed to produce NIV at temperatures  $\leq 10^\circ\text{C}$ . Furthermore, the authors demonstrated that the  $T_{opt}$  for NIV production by *F. poae* was higher than the  $T_{opt}$  for colony growth (24.7°C), suggesting that NIV is produced when the fungus is experiencing stress, such as elevated temperatures. In agreement with these results, Shen et al. (2012) confirmed that climatic conditions are one of the



predominant factors that may influence the geographic distribution of *Fusarium* spp. and trichothecene chemotype diversity in China, with a significantly higher prevalence of *F. asiaticum* NIV chemotype in the southern warmer regions of China. The conclusion that NIV strains are mostly distributed in warmer regions was supported also by Zhou et al. (2018). Conversely, Schöneberg et al. (2019) observed higher NIV production by *F. poae* in cereal grains after inoculation at 10°C than after inoculation at warmer temperatures (15–20°C). It could be hypothesized that this disparity is due to a diverse adaptation to climatic conditions of *Fusarium* spp. isolated from different countries. Finally, if on the one hand Covarelli et al. (2015) suggested that climatic conditions have a strong impact on the occurrence of 3-ADON and 15-ADON, on the other hand, the authors concluded that NIV contamination occurred irrespective of climatic conditions, showing a constant presence in the analysed grain samples with a similar average contamination during different years.

## 2.2. *Nivalenol genotype distribution*

In the last years, molecular surveillance using polymerase chain reaction (PCR) assay for the genotyping of *Fusarium* species from DNA extracted from contaminated grains along with multi-toxin analyses using high performance liquid chromatography/mass spectrometry (HPLC/MS) technology for precise quantification of the toxins are contributing noticeably to a better understanding of the distribution of *Fusarium* population and, in particular, of the NIV chemotype around the world. Such knowledge is determinant for the prediction of the risk of contamination by NIV and for the elaboration of disease management strategies in the surveyed areas. In fact, the presence of a certain toxigenic *Fusarium* species is not always predictive of NIV contamination. As

shown by Pasquali et al. (2010), the presence in grains of *F. poae*, a known NIV producer, was not predictive of NIV accumulation, but *F. culmorum* with NIV chemotype was mostly responsible for accumulation of this toxin in contaminated wheat in Luxemburg. Additionally, *F. culmorum* strains with NIV chemotype were found in 31 of 191 isolates from wheat fields in northern Algeria (Laraba et al., 2017). Both *F. culmorum* and *F. graminearum* were significantly correlated with high concentrations of NIV detected in harvested maize plants intended for silage in the north-western European region of Flanders (Vandicke et al., 2019). However, NIV chemotypes in *F. culmorum* were rarely found in eastern locations of Europe, suggesting that the presence of a specific chemotype might depend on distinct cropping practices or distinct climatic conditions (Pasquali et al., 2016). With regard to the overall distribution of chemotypes by species for *F. cortaderiae*, the NIV genotype was found in the rice-growing regions of Brazil (Gomes et al., 2015), in the wheat-growing areas of eastern Uruguay, where was the major responsible for FHB in wheat, along with *F. asiaticum* (Umpierrez-Failache et al., 2013), and in the corn stubble of southern Brazil, where the NIV genotype also accounted for the vast majority of *F. meridionale* isolates (Del Ponte et al., 2015). In particular, the authors documented significant regional differences in the frequency of *F. meridionale* with the NIV genotype. Moreover, in eastern China and in Brazil isolates of *F. asiaticum* producing NIV in the rice substrate were found (Qiu and Shi, 2014; Gomes et al., 2015). However, the percentage of NIV genotype for *F. asiaticum* strains shows an important disparity. Ndoye et al. (2012) reported that almost all *F. asiaticum* were of the NIV genotype, most of which were derived from the warmer regions in southern China. Lower frequency was obtained by Shen et al. (2012). In Brazil, only three *F. asiaticum* strains were isolated from FHB-infected

wheat heads, all of the NIV genotype (Del Ponte et al., 2015). Similarly, Zhou et al. (2018) isolated only three *F. asiaticum* strains from maize ears and kernel rot samples in China, all of the NIV genotype but none of them produced the toxin NIV in the toxin assay.

A list of studies related to the distribution of the *Fusarium* species of the NIV genotype is provided in Table 1.

### 2.3. Occurrence of nivalenol in food and feed

In the last decade, NIV has been reported to occur in wheat (Del Ponte et al., 2015; Lindblad et al., 2013; Umpierrez-Failache et al., 2013), groundnuts (Oyedele et al., 2017), barley (Beccari et al., 2018; Garmendia et al., 2018) and maize (Duan et al., 2016; Reisinger et al., 2019; Schollenberger et al., 2012; Vandicke et al., 2019). Concentrations of NIV ranged from a few  $\mu\text{g}/\text{kg}$  to over  $\text{mg}/\text{kg}$ . The highest NIV concentration was found by Schollenberger et al. (2012) in maize rudimentary ears, with a mean at  $27,209 \mu\text{g}/\text{kg}$  and a maximum at  $125,315 \mu\text{g}/\text{kg}$ . High NIV levels were also observed in dairy maize silage samples collected in Europe from 2014 to 2018 (Reisinger et al., 2019). In this study, 59.5% of samples resulted to be contaminated by NIV, with a mean concentration equal to  $113 \mu\text{g}/\text{kg}$ . Despite moderate median values, maximum NIV levels reached  $5770 \mu\text{g}/\text{kg}$  in a maize silage sample from Denmark, collected in 2015. Notably, another sample from the Netherlands and collected in 2018 contained  $2260 \mu\text{g}/\text{kg}$  of NIV, implying that prominent NIV levels were not limited to one country or season. Among the mycotoxins studied, NIV was the most frequently detected mycotoxin in harvested maize fields from the north-western European region of Flanders, being present in 99.2% of 257 samples between 2016 and 2018, with a mean concentration rising from  $650.7$

$\mu\text{g}/\text{kg}$  in 2016, to 719.0  $\mu\text{g}/\text{kg}$  in 2017 and 881.9  $\mu\text{g}/\text{kg}$  in 2018 (Vandicke et al., 2019).

In Italian durum and soft wheat collected between 2009 and 2010, Covarelli et al. (2015) demonstrated that the presence of NIV was almost always 100%, with mean concentrations between 347.6 and 651.6  $\mu\text{g}/\text{kg}$ . In wheat collected from Sweden between 2009 and 2011, lower NIV levels were reported, with maximum concentrations ranging from 39 to 111  $\mu\text{g}/\text{kg}$  (Lindblad et al., 2013). Low concentrations were found also by Chala et al. (2014) in grain samples collected from Ethiopia. In their study, NIV was detected only in 5.7% of sorghum samples and in 12.1% of finger millet samples, with a mean concentration equals to 23.9  $\mu\text{g}/\text{kg}$  and 6.25  $\mu\text{g}/\text{kg}$ , respectively. Moreover, low incidence (3.6%) and low concentrations of NIV (from 4.5 to 13.4  $\mu\text{g}/\text{kg}$ ) were found in groundnut samples from Nigeria (Oyedele et al., 2017).

In 506 Korean marked food samples, 12% were positive for NIV, with higher amounts detected more in raw materials or slightly processes foods, compared to highly processed foods (Lee et al., 2020). In particular, cereal and cereal-based products exhibited the highest contamination levels (107.2  $\mu\text{g}/\text{kg}$ ), followed by legumes and legume-based products (31.7  $\mu\text{g}/\text{kg}$ ). Lower contamination levels were detected in cereal-based baby foods (17.1  $\mu\text{g}/\text{kg}$ ), whereas NIV was no detected in alcoholic beverage.

Malting barley samples were found also to be contaminated by NIV. Beccari et al. (2018) demonstrated NIV occurrence in malting barley samples cultivated in the central Italy during the season 2013–2014, being the most frequent mycotoxin detected (83%), with a maximum value of 66.2  $\mu\text{g}/\text{kg}$ .

To ensure animal and public health, as well as agricultural productivity, maximum levels for various mycotoxins were laid down for a number of food commodities and feeding stuffs. However, as regards the occurrence of NIV, the maximum levels are not so far regulated by any regulation within the European Union. In 2000 a scientific opinion on NIV was issued by the Scientific Committee on Food (SCF), establishing a temporary tolerable daily intake (t-TDI) of 0–0.7 µg/kg BW per day, based on the evaluation of the general toxicity of NIV. In 2010 the Japanese Food Safety Commission (FSCJ) issued a t-TDI of 0.4 µg/kg BW per day. More recently, taking into account data on NIV occurrence collected in 18 European countries between 2001 and 2011, the European Food Safety Authority established a tolerable daily intake (TDI) of 1.2 µg/kg BW per day (EFSA, 2013).

**Table 1.** Reports on the occurrence of NIV genotypes since last decade

Country	<i>Fusarium</i> spp.	Year	Sample	NIV genotype percentage	Reference
Algeria	<i>F. culmorum</i>	2014-2015	Wheat	16.2 %	(Laraba et al., 2017)
Arkansas	<i>F. graminearum</i>	2001-2007	Wheat	12 %	(Gale et al., 2011)
Brazil	<i>F. asiaticum</i>	2008-2012	Kernels	100 %	(Gomes et al., 2015)
Brazil	<i>F. asiaticum</i>	2009-2011	Wheat	100 %	(Del Ponte et al., 2015)
Brazil	<i>F. austroamericanum</i>	2009-2011	Wheat	25 %	(Del Ponte et al., 2015)
Brazil	<i>F. cortaderiae</i>	2008-2012	Kernels	100 %	(Gomes et al., 2015)
Brazil	<i>F. cortaderiae</i>	2009-2011	Wheat	82.4 %	(Del Ponte et al., 2015)
Brazil	<i>F. graminearum</i>	2008-2009	Barley	29.3 %	(Astolfi et al., 2011)
Brazil	<i>F. meridionale</i>	2008-2012	Kernels	100 %	(Gomes et al., 2015)
China	<i>F. asiaticum</i>	2008-2010	Wheat	14 %	(Shen et al., 2012)
China	<i>F. asiaticum</i>	2009	Maize	97 %	(Ndoye et al., 2012)
China	<i>F. asiaticum</i>	2013	Rice	23 %	(Qiu and Shi, 2014)
China	<i>F. asiaticum</i>	2013	Maize	9 %	(Qiu and Shi, 2014)

Country	<i>Fusarium</i> spp.	Year	Sample	NIV genotype percentage	Reference
China	<i>F. asiaticum</i>	2013	Wheat	23 %	(Qiu and Shi, 2014)
China	<i>F. asiaticum</i>	2014-2015	Maize	100 %	(Zhou et al., 2018)
China	<i>F. meridionale</i>	2009-2014	Maize	76.2 %	(Duan et al., 2016)
China	<i>F. meridionale</i>	2014-2015	Maize	100 %	(Zhou et al., 2018)
Flanders	<i>F. culmorum</i>	2016-2018	Maize	NQ	(Vandicke et al., 2019)
Flanders	<i>F. graminearum</i>	2016-2018	Maize	NQ	(Vandicke et al., 2019)
Gulf Coast of USA	<i>F. graminearum</i>	2001-2007	Wheat	25 %	(Gale et al., 2011)
Luxembourg	<i>F. culmorum</i>	2007-2008	Wheat	46.8 %	(Pasquali et al., 2010)
Luxembourg	<i>F. graminearum</i>	2007-2008	Wheat	5.8 %	(Pasquali et al., 2010)
Missouri	<i>F. graminearum</i>	2001-2007	Wheat	2 %	(Gale et al., 2011)
North Carolina	<i>F. graminearum</i>	2001-2007	Wheat	40 %	(Gale et al., 2011)
Paraná (Brazil)	<i>F. meridionale</i>	2009-2011	Wheat	29.2 %	(Del Ponte et al., 2015)

## Resultados

---

Country	<i>Fusarium</i> spp.	Year	Sample	NIV genotype percentage	Reference
Rio Grande do Sul (Brazil)	<i>F. meridionale</i>	2009-2011	Wheat	9 %	(Del Ponte et al., 2015)
Southern Louisiana	<i>F. asiaticum</i>	2001-2007	Wheat	100 %	(Gale et al., 2011)
Southern Louisiana	<i>F. graminearum</i>	2001-2007	Wheat	93.6 %	(Gale et al., 2011)
Uruguay	<i>F. asiaticum</i>	2002, 2009, 2011, 2012	Wheat	NQ	(Umpierrez-Failache et al., 2013)
Uruguay	<i>F. brasiliicum</i>	2002, 2009, 2011, 2012	Wheat	NQ	(Umpierrez-Failache et al., 2013)
Uruguay	<i>F. cortaderiae</i>	2002, 2009, 2011, 2012	Wheat	NQ	(Umpierrez-Failache et al., 2013)

NQ: not quantified



### 3. Mitigation of NIV-mediated food contamination

The growing consumer demand for food minimally processed without the use of synthetic fungicides is increasingly motivating the search for economically and environmentally attractive options for manage fungal incidence and mitigate mycotoxicological contamination. Among the different strategies that may be adopted to reduce *Fusarium* mycotoxin contamination in cereals, the use of biological control agents (BCAs), antioxidant natural compounds and good agricultural practices (GAP) are some of the most widely studied.

Bemvenuti et al. (2019) investigated the effect of  $\gamma$ -oryzanol, a mixture of lipid and ferulic acid abundant in rice bran, on the growth of *F. graminearum* and NIV production *in vitro*. Results revealed that  $\gamma$ -oryzanol (1.0 g/kg) had a significant effect in decreasing the mycelium growth, which was reduced to zero by treatment at the highest concentration (1.2 g/kg). Decrease in NIV production was observed at concentrations equal to 0.8 and 1.0 g/kg. Significant antifungal activity on the *F. graminearum* mycelial growth and antimycotoxigenic activity on NIV production were demonstrated also by the phenolic acids extracted from microalgae *Spirulina* sp. and *Nannochloropsis* sp. (Scaglioni et al., 2019). Interestingly, the authors observed that the treatments with phenolic extracts were more efficient in preventing the production of trichothecenes than the fungicide tebuconazole.

Furthermore, yeasts obtained from winter wheat grain have been shown to inhibit the development of *Fusarium* pathogens through antibiosis and competition and decrease trichothecene concentrations in the grain of bread wheat and durum wheat. Notably, the isolate *Debaryomyces hansenii* Dh53 resulted to reduce NIV concentration by 18.12- fold in the grain of non-inoculated bread

wheat (Wachowska et al., 2020). Antagonistic ability against mycotoxigenic *F. avenaceum*, *F. cerealis*, *F. culmorum*, *F. graminearum* and *F. temperatum* species was also demonstrated by *Trichoderma* spp., with the best capacity for reducing NIV showed by the *Trichoderma* strains AN240 and AN255 (Blaszczyk et al., 2017). In corn silage stored at 28 °C, treatment with *Pediococcus pentosaceus* 17604 (PP) and *Lactobacillus plantarum* KR107070 (LP) decreased NIV levels. However, increased NIV content or no significant differences were observed at different temperature of storage (20°C and 37°C) (Wang et al., 2018).

Alcoholic fermentation with *Saccharomyces cerevisiae* has been highlighted to be also a promising method for mitigate mycotoxins in cereals, since, throughout fermentation, contaminants may be transformed into less toxic compounds by the activity of specific molecules yielded by the microorganism. In this regard, Boeira et al. (2021) showed that after 96 h of alcoholic fermentation, NIV was mitigated by 56.5%.

If on one hand the use of yeast-delivered preparations for minimalizing mycotoxin contamination is an area of present research with promising results, on the other hand Li et al. (2017) showed that it is possible confer increased ability to detoxify NIV and increased resistance to NIV producing *Fusarium* strains also by inducing stable transgenic events. Properly, the authors demonstrated that with constitutive overexpression, transgenic wheat expressing the barley UDP-glucosyltransferase HvUGT13248 gene provides resistance to both DON and NIV, proposing this gene as excellent candidate for FHB control.

---

#### 4. *In vitro* toxicity

##### 4.1. *Cytotoxicity*

The effects of NIV on cell viability have been studied in different cell lines and through different assays. Table 2 summarizes the types of cells, the time of exposure and the median inhibitory concentration ( $IC_{50}$ ) determined by *in vitro* methods.

Considering that trichothecenes have been displayed to alter cell proliferation especially in tissue with high rates of cell turnover, such as intestinal epithelial cell, the porcine jejuna epithelial (IPEC-J2) cells and human colorectal adenocarcinoma (Caco-2) cells are the most used cell model in the studies of NIV cytotoxicity. Similar  $IC_{50}$  values were obtained by Wan et al. (2013a) and Alassane-Kpembé et al. (2013) on IPEC-J2 and Caco-2 cells, respectively, using the 3-(4,5-dimethylthiazol-2-yl)-2,5-diphenyltetrazolium bromide (MTT) assay after 48 h of exposure to NIV. Further data on the cytotoxicity of NIV after 48 h of exposure are available on calf small intestinal epithelial cells B (CIEB) and human monocytic leukemia cells (THP-1) (Reisinger et al., 2019; Smith et al., 2018). On the other hand, the effects of 24 h of exposure resulted in very different  $IC_{50}$  values on human hepatocellular carcinoma (HepG2) cells, on the C2BBel cell clone of Caco-2 cells and on rat non-tumorigenic intestinal epithelial cells (IEC-6), with a higher  $IC_{50}$  value obtained on the latest (Bianco et al., 2012; Vejdovszky et al., 2016; Zingales et al., 2020). Based on these data, and in accordance with the results obtained by Taranu et al. (2010), which showed that human lymphocytes reacted more sensitively to NIV than porcine cells, it may be concluded that cells of human origin are more sensitive to 24 h of exposure to NIV than those of different origin.

Since most food commodities present the co-occurrence of different mycotoxins, as most of fungal species may produce a number of mycotoxins simultaneously and, additionally, several fungal species may be present in a given food product, it is of great importance to investigate the effects of mycotoxin mixtures. Mycotoxin multi-exposure can lead to additive, synergistic, or antagonistic effects; furthermore, the toxicity of the mixture cannot always be predicted based on the individual toxicity of each mycotoxin from the mixture. Thus, investigations of commonly observed toxin mixtures are needed to enable more accurate and effective risk assessments. Compared to NIV alone, higher cytotoxic effects on cell proliferation were induced by the binary (NIV + fumonisin B1 (FB1), NIV + ZEA), tertiary (NIV + DON + ZEA, NIV + DON + FB1, NIV + ZEA + FB1) and quaternary (NIV + DON + ZEA + FB1) combinations on the Caco-2/human colon carcinoma (HT29-MTX) 70/30 co-culture (Wan et al., 2014). On the contrary, compared to the individual mycotoxin NIV, no increases in overall cytotoxicity of binary, tertiary and quaternary mixtures of NIV with DON, ZEA and FB1 were observed by Wan et al. (2013a) on IPC-J2 cells. In line with these results, the study performed by Vejdovszky et al. (2016) on the combinatory effects of NIV, DON and ZEA showed no-additive effects for mixtures containing NIV. Finally, no-additive effects on cell viability were observed even by Bianco et al. (2012) on IEC-6 cells co-exposed to NIV and DON. Interestingly, in Caco-2 cells and in IPEC-1 cells the combination of DON and NIV was described as being synergistic (Alassane-Kpembi et al., 2013, 2015). Mainly additive/synergistic effects were observed in HepG2 cells exposed to the binary combination NIV + sterigmatocystin (STE). However, as evidenced by the Combenefit method, while NIV was found to enhance the cytotoxic effect of STE, vice versa, STE was not able to increase

the cytotoxicity of NIV (Zingales et al., 2020). Furthermore, Smith et al. (2018) observed additivity on THP-1 cells exposed to the lowest concentrations of NIV (0.01 and 0.3  $\mu\text{M}$ ) in combination with T-2 toxin, whereas antagonism was observed in the presence of higher concentrations of NIV (0.8, 3, and 10  $\mu\text{M}$ ), highlighting that it is very difficult to predict the type of interaction only on the basis of the effect of individual mycotoxin. Depending on the assay performed, the concentrations examined, the incubation time and the selected cell line, as well as the different chemical structures and chemical properties among different mycotoxins, discrepancies between the interaction effects may be noted. Despite the active experimental efforts, so far data describing the possible effects of NIV combined with other mycotoxins are very sparse and not sufficient to establish the real health risk from exposure to the combination of NIV with other mycotoxins.

**Table 2.** Comparative IC<sub>50</sub> values of NIV in different cell lines.

CELL LINE	TIME OF EXPOSURE	ASSAY	IC <sub>50</sub>	REFERENCE	CELL LINE
Caco-2 cells	24 h	WST-1	6.9 µM	(Vejdovszky et al., 2016)	Caco-2 cells
Caco-2 cells	48 h	MTT	0.9 µM	(Alassane-Kpembé et al., 2013)	Caco-2 cells
Caco-2 cells	48 h	NR	0.69 µM	(Alassane-Kpembé et al., 2013)	Caco-2 cells
CIEB cells	48 h	NR	0.8 µM	(Reisinger et al., 2019)	CIEB cells
CIEB cells	48 h	SRB	1 µM	(Reisinger et al., 2019)	CIEB cells
CIEB cells	48 h	WST-1	0.8 µM	(Reisinger et al., 2019)	CIEB cells
HepG2 cells	24 h	MTT	0.96 µM	(Zingales et al., 2020)	HepG2 cells
HepG2 cells	48 h	MTT	0.76 µM	(Zingales et al., 2020)	HepG2 cells
HepG2 cells	72 h	MTT	0.66 µM	(Zingales et al., 2020)	HepG2 cells
Human PBMC	72 h	[methyl- <sup>3</sup> H]-thymidine	0.25 µM (0.079 µg/ml)	(Taranu et al., 2010)	Human PBMC
IEC-6 cells	24 h	MTT	17.75 µM	(Bianco et al., 2012)	IEC-6 cells

CELL LINE	TIME OF EXPOSURE	ASSAY	IC <sub>50</sub>	REFERENCE	CELL LINE
IPEC-J2 cells	48 h	MTT	0.94 $\mu$ M	(Wan et al., 2013a)	IPEC-J2 cells
Porcine PBMC	72 h	[methyl- <sup>3</sup> H]-thymidine	0.29 $\mu$ M (0.091 $\mu$ g/ml)	(Taranu et al., 2010)	Porcine PBMC
Porcine splenocytes	72 h	[methyl- <sup>3</sup> H]-thymidine	0.15 $\mu$ M (0.049 $\mu$ g/ml)	(Taranu et al., 2010)	Porcine splenocytes
THP-1 cells	48 h	MTS	0.77 $\mu$ M	(Smith et al., 2018)	THP-1 cells
CIEB cells	48 h	NR	0.8 $\mu$ M	(Reisinger et al., 2019)	CIEB cells
CIEB cells	48 h	SRB	1 $\mu$ M	(Reisinger et al., 2019)	CIEB cells
CIEB cells	48 h	WST-1	0.8 $\mu$ M	(Reisinger et al., 2019)	CIEB cells

Abbreviations: Caco-2: human colorectal adenocarcinoma cells; CIEB: calf small intestinal epithelial cells B; HepG2: human hepatocellular carcinoma cells; IEC-6: rat non-tumorigenic intestinal epithelial cells; IPEC-J2: porcine jejuna epithelial cells; MTS: 3-(4,5-Dimethylthiazol-2-yl)-5-(3-carboxymethoxyphenyl)-2-(4-sulphophenyl)-2H-tetrazolium; MTT: 3-(4,5-dimethylthiazol-2-yl)-2,5-diphenyltetrazolium bromide; NR: Neutral Red; PBMC: Peripheral blood mononuclear cells; SRB: sulforhodamine B; THP-1: human monocytic leukemia cells; WST-1: Water Soluble Tetrazolium Salts-1.

### 4.2. Immunotoxicity

The current state of knowledge indicates that NIV may exert marked immunomodulatory activity. The NIV has been shown to influence the lipopolysaccharide (LPS)-induced maturation process of murine bone marrow-derived dendritic cells (DCs). Properly, Luongo et al. (2010) demonstrated that *in vitro* pre-treatment of DCs with NIV 3  $\mu$ M resulted in a reduction of the expression of major histocompatibility complex (MHC) class II molecules. Furthermore, an almost completely inhibition of nitric oxide production, that normally occurs in response to LPS-induced maturation, as well as a significant decrease of the percentage of CD11c and CD86 double positive cells, representing the population of mature DCs, were observed after exposure to NIV 2  $\mu$ M. Similarly, in THP-1 cells, NIV affected monocyte function, as demonstrated by the induction of a significant down-regulation of the expression of the CD14 and CD7 cell surface markers, with a total inhibition after 48 h of exposure to NIV in combination with T-2 toxin (Smith et al., 2018). At molecular level, the NIV exposure resulted also to modulate the expression of a high number of inflammation-associated genes. In human chondrocytes, NIV has been shown to increase the relative mRNA expression of tumour necrosis factor (TNF)- $\alpha$  and interleukin (IL)-1 $\beta$  (Cao et al., 2010). Furthermore, Wan et al. (2013b) found that NIV was a potent inducer of IL-1 $\alpha$ , IL-1 $\beta$ , IL-6, IL-8, TNF- $\alpha$  and monocyte chemoattractant protein (MCP)-1 mRNA expression in porcine IPEC-J2 cells, with the induction of a stronger pro-inflammatory response when NIV was combined with DON, ZEA and/or FB1. Interestingly, NIV seems to be more immunotoxic than DON, as demonstrated by the inhibition of a higher extent of secretion of the anti-inflammatory IL-10 and the induction of significantly higher TNF- $\alpha$  amounts compared to DON in



DCs (Luongo et al., 2010). In addition, in human promyelocytic leukemia (HL60) cells, NIV was shown to significantly elicited the secretion of the pro-inflammatory IL-8 (Nagashima et al., 2011a, 2011b). What is more, Nagashima et al. (2011a) concluded that NF- $\kappa$ B is important for NIV-induced IL-8 secretion, as suggested by the lower secretion of IL-8 (183.1%) in cells concomitantly treated with NIV and the NF- $\kappa$ B inhibitor dexamethasone compared to cells treated with NIV alone (241.5%). Although more studies are needed to obtain a clearer view on the effects of NIV on the several chain reactions that characterize the immune system, the studies carried out in the last decade allow to hypothesize the immunotoxicity as one of the main mechanisms of action of NIV.

#### 4.3. *Genotoxicity and cell death mechanisms*

In IEC-6 cells, the exposure to NIV 10  $\mu$ M for 24 h caused hypodiploid nuclei formation and alteration of cell cycle distribution, leading to apoptosis, as demonstrated by the induction of the pro-apoptotic protein Bax, the inhibition of the anti-apoptotic protein Bcl-2 and the induction of caspase-3 activation (Bianco et al., 2012). Conversely, caspase-3 was not activated by NIV (1–3  $\mu$ M) in DCs, suggesting that the observed concentration-dependent decrease of cell viability was essentially associated with necrosis, but not with apoptosis induction (Luongo et al., 2010). Similar results were obtained by Smith et al. (2018), which observed that mainly cell necrosis was induced in THP-1 cells after 12 h of exposure to 0.8  $\mu$ M NIV + 0.006  $\mu$ M T-2 toxin.

### 4.4. *Intestinal cell bioavailability, transport and permeability*

In humans, there is a body of evidence suggesting that exposure to trichothecenes frequently results in outbreaks of gastroenteritis (Pestka, 2010). The intestine is the first barrier to food contaminants, such as mycotoxins, and therefore, following ingestion of contaminated food or feed, the intestine and intestinal mucosa can be exposed to high concentrations of them. Cheat et al. (2015) revealed high intestinal mucosal changes after acute exposure to NIV (1–10  $\mu\text{M}$ ). In particular, a concentration-dependent decrease of the histological scores of the pig jejunal explant cultures was induced after 4 h of exposure to NIV from concentrations of 1  $\mu\text{M}$ . Interestingly, NIV showed the greatest toxicity when compared with the acute DON-induced impacts. In IEC-6 cells, NIV exposure caused significant pro-oxidant effects and, once more, to a greater extent than those caused by DON (Adesso et al., 2017; Del Regno et al., 2015). At molecular level, NIV (2  $\mu\text{M}$ ) was shown to induce the downregulation of the mRNA expression of mucin genes MUC5AC and MUC5B on Caco-2/HT29-MTX co-cultures, a well-characterized standard model for intestinal absorption, transport and permeability studies. Decreases in total mucin-like glycoprotein secretion were also observed, which suggest mucus depletion in response to mycotoxin exposure. Additionally, additive effects were noted in most of the mixtures of NIV with the other *Fusarium* toxins DON, ZEA and FB1, suggesting that these combinations of toxins may influence bacterial translocation and susceptibility to mucosal infections in IECs (Wan et al., 2014). In IPEC-J2 cells, Wan et al. (2013c) showed that NIV treatment, individually and in combination with DON, ZEA and/or FB1, significantly affected the mRNA expression of porcine  $\beta$ -defensin ( $\text{p}\beta\text{D}$ )-1 and -2, potentially leading to the disruption of microbial homeostasis and to the development of chronic enteric diseases. What

is more, NIV exposure, alone and in combination, resulted in a significant reduction in antibacterial activity of cells against *Escherichia coli*, confirming a dysregulated activity of the IECs induced by NIV.

#### 4.5. *Other nivalenol cytotoxic effects*

It has been hypothesized that the mycotoxin NIV may be involved in the development of Kashin-Beck Disease (KBD), an age-related endemic degenerative osteoarthropathy mainly affecting adolescents of the mainland of China. Li et al. (2014) showed that exposure of bovine chondrocytes to NIV (0.32–1.6  $\mu\text{M}$ ) decreased matrix deposition, enhancing the production of catabolic enzymes (metalloproteinases-2, -3 and -9 and A disintegrin and metalloproteinase with thrombospondin motifs-4 and -5). In addition, an extensive remodelling of F-actin and vimentin filaments distributions was observed, likely contributing to the characteristic catabolic phenotype of KBD. Similar pro-catabolic effects of NIV were demonstrated by Lu et al. (2012) in an engineered cartilage model, obtained using chondrocytes seeded on bone marrow gelatin. In particular, although no effects on chondrocyte morphology or engineered cartilage formation were observed, exposure to NIV (320 nM) resulted in the inhibition of the expression of extracellular matrix (ECM) components, such as aggrecan and collagen type II, and increased levels of metalloproteinases, leading to an excess of catabolism in the ECM, which is consistent with the pathological changes of KBD.

## 5. Conclusion

The NIV is a potent cytotoxic mycotoxin and constitutes a serious risk factor for public and animal health, being a natural contaminant of several food and feed commodities worldwide. Numerous efforts have been made to minimize the risk of NIV contamination and related economic losses. However, most of the strategies studied to counteract the FHB pathogens have been performed under controlled laboratory conditions and very few evidence has been provided under field conditions. In *in vitro* studies, NIV cytotoxicity has been found to be stronger than that reported for other members of the same trichothecenes type B family and the occurrence in combination could also increase its toxicity. However, so far NIV carcinogenicity in humans is not classifiable. This toxin has been shown to impact primarily organs containing actively dividing cells. As has been reviewed previously, the immune system is sensitive to NIV, as well as the intestinal epithelial cells. In this regard, it can be hypothesized that the production of ROS might be associated with the gastrointestinal toxicity induced by NIV. Further investigations are needed on ROS generation and oxidative stress to assess whether it could be an important pathway in NIV-induced toxicity. Moreover, NIV has been linked to genotoxic activity and induction of cell death *via* apoptosis or necrosis. Interestingly, as emerged by this review, the sensitivities of different types of cells, as well as the sensitivities of the same cell types originating from different species, seem to be critical for the outcome of NIV cytotoxicity. Thus, more emphasis on studying the cellular effects of this mycotoxin and the effective measures to counteract its cytotoxicity should be the goal for future investigations.

### **CRedit authorship contribution statement**

**Veronica Zingales:** Writing – original draft, Writing – review & editing.

**Mónica Fernández-Franzón:** Supervision. **Maria-José Ruiz:** Conceptualization, Supervision, Funding acquisition.

### **Declaration of competing interest**

The authors declare that they have no known competing financial interests or personal relationships that could have appeared to influence the work reported in this paper.

### **Acknowledgments**

This research has been supported by the Generalitat Valenciana grant (Prometeo 2018/216) and the pre-doctoral research training program “Santiago Grisolia (GRISOLIAP/2018/092) CPI-18-117”.

### **References**

Adesso, S., Autore, G., Quaroni, A., Popolo, A., Severino, L., Marzocco, S., 2017. The food contaminants nivalenol and deoxynivalenol induce inflammation in intestinal epithelial cells by regulating reactive oxygen species release. *Nutrients* 9 (12), 1343. <https://doi.org/10.3390/nu9121343>.

Alassane-Kpembi, I., Kolf-Clauw, M., Gauthier, T., Abrami, R., Abiola, F.A., Oswald, I.P., et al., 2013. New insights into mycotoxin mixtures: the toxicity of low doses of Type B trichothecenes on intestinal epithelial cells is synergistic. *Toxicol. Appl. Pharmacol.* 272, 191–198. <https://doi.org/10.1016/j.taap.2013.05.023>.

Alassane-Kpembé, I., Puel, O., Oswald, I.P., 2015. Toxicological interactions between the mycotoxins deoxynivalenol, nivalenol and their acetylated derivatives in intestinal epithelial cells. *Arch. Toxicol.* 89, 1337–1346. <https://doi.org/10.1007/s00204-014-1309-4>.

Astolfi, P., dos Santos, J., Schneider, L., Gomes, L.B., Silva, C.N., Tessmann, D.J., et al., 2011. Molecular survey of trichothecene genotypes of *Fusarium graminearum* species complex from barley in southern Brazil. *Int. J. Food Microbiol.* 148, 197–201. <https://doi.org/10.1016/j.ijfoodmicro.2011.05.019>.

Beccari, G., Senatore, M.T., Tini, F., Sulyok, M., Covarelli, L., 2018. Fungal community, *Fusarium* head blight complex and secondary metabolites associated with malting barley grains harvested in Umbria, central Italy. *Int. J. Food Microbiol.* 273, 33–42. <https://doi.org/10.1016/j.ijfoodmicro.2018.03.005>.

Bemvenuti, R., Rodrigues, M.H., Furlong, E., 2019. Efficiency of  $\gamma$ -oryzanol against the complex *Fusarium graminearum* growth and mycotoxins production. *Food Sci. Technol. Int.* 39, 240–246. <https://doi.org/10.1590/fst.01818>.

Bianco, G., Fontanella, B., Severino, L., Quaroni, A., Autore, G., Marzocco, S., 2012. Nivalenol and deoxynivalenol affect rat intestinal epithelial cells: a concentration related study. *PloS One* 7, e52051. <https://doi.org/10.1371/journal.pone.0052051>.

Błaszczak, L., Basinska-Barczak, A., Cwiek-Kupczynska, H., Gromadzka, K., Popiel, D., Stepień, L., 2017. Suppressing effect of *Trichoderma* spp. on toxigenic *Fusarium* species. *Pol. J. Microbiol.* 66, 85–100. <https://doi.org/10.5604/17331331.1234996>.

---

Boeira, C.Z., Silvello, M.A.C., Remedi, R.D., Feltrin, A.C.P., Santos, L.O., Garda- Buffon, J., 2021. Mitigation of nivalenol using alcoholic fermentation and magnetic field application. *Food Chem.* 340, 127935. <https://doi.org/10.1016/j.foodchem.2020.127935>.

Cao, P.H., Cao, J.L., Cao, L.M., Yang, Y.J., Li, W.B., 2010. Effect of Nivalenol and selenium on IL-1beta and TNF-alpha secretion in cultured chondrocytes, 26, 313–315. *Xi Bao Yu Fen Zi Mian Yi Xue Za Zhi*.

Chala, A., Taye, W., Ayalew, A., Krska, R., Sulyok, M., Logrieco, A., 2014. Multimycotoxin analysis of sorghum (*Sorghum bicolor* L. Moench) and finger millet (*Eleusine coracana* L. Garten) from Ethiopia. *Food Contr.* 45, 29–35. <https://doi.org/10.1016/j.foodcont.2014.04.018>.

Cheat, S., Gerez, J.R., Cognie, J., Alassane-Kpembé, I., Bracarense, A.P., Raymond- Letron, I., et al., 2015. Nivalenol has a greater impact than deoxynivalenol on pig jejunum mucosa in vitro on explants and in vivo on intestinal loops. *Toxins* 7, 1945–1961. <https://doi.org/10.3390/toxins7061945>.

Covarelli, L., Beccari, G., Prodi, A., Generotti, S., Etruschi, F., Juan, C., et al., 2015. Fusarium species, chemotype characterisation and trichothecene contamination of durum and soft wheat in an area of central Italy. *J. Sci. Food Agric.* 95, 540–551. <https://doi.org/10.1002/jsfa.6772>.

Del Ponte, E.M., Spolti, P., Ward, T.J., Gomes, L.B., Nicolli, C.P., Kuhnem, P.R., et al., 2015. Regional and field-specific factors affect the composition of fusarium head blight pathogens in subtropical no-till wheat agroecosystem of Brazil. *Phytopathology* 105, 246–254. <https://doi.org/10.1094/PHYTO-04-14-0102-R>.

Del Regno, M., Adesso, S., Popolo, A., Quaroni, A., Autore, G., Severino, L., et al., 2015. Nivalenol induces oxidative stress and increases

deoxynivalenol pro-oxidant effect in intestinal epithelial cells. *Toxicol. Appl. Pharmacol.* 285, 118–127. <https://doi.org/10.1016/j.taap.2015.04.002>.

Duan, C., Qin, Z., Yang, Z., Li, W., Sun, S., Zhu, Z., et al., 2016. Identification of pathogenic *Fusarium* spp. causing maize ear rot and potential mycotoxin production in China. *Toxins* 8 (6), 186. <https://doi.org/10.3390/toxins8060186>.

Edwards, S.G., Imathiu, S.M., Ray, R.V., Back, M., Hare, M.C., 2012. Molecular studies to identify the *Fusarium* species responsible for HT-2 and T-2 mycotoxins in UK oats. *Int. J. Food Microbiol.* 156, 168–175. <https://doi.org/10.1016/j.ijfoodmicro.2012.03.020>.

EFSA, 2013. Scientific Opinion on risks for animal and public health related to the presence of nivalenol in food and feed. *EFSA J* 11 (6), 3262.

Gale, L.R., Harrison, S.A., Ward, T.J., O'Donnell, K., Milus, E.A., Gale, et al., 2011. Nivalenol-type populations of *Fusarium graminearum* and *F. asiaticum* are prevalent on wheat in southern Louisiana. *Phytopathology* 101, 124–134. <https://doi.org/10.1094/PHYTO-03-10-0067>.

Garmendia, G., Pattarino, L., Negrin, C., Martinez-Silveira, A., Pereyra, S., Ward, T.J., et al., 2018. Species composition, toxigenic potential and aggressiveness of *Fusarium* isolates causing Head Blight of barley in Uruguay. *Food Microbiol.* 76, 426–433. <https://doi.org/10.1016/j.fm.2018.07.005>.

Gomes, L.B., Ward, T.J., Badiale-Furlong, E., Del Ponte, E.M., 2015. Species composition, toxigenic potential and pathogenicity of *Fusarium graminearum* species complex isolates from Southern Brazilian rice. *Plant Pathol.* 64, 980–987. <https://doi.org/10.1111/ppa.12332>.

Hsia, C.C., Wu, Z.Y., Li, Y.S., Zhang, F., Sun, Z.T., 2004. Nivalenol, a main *Fusarium* toxin in dietary foods from high-risk areas of cancer of



---

esophagus and gastric cardia in China, induced benign and malignant tumors in mice. *Oncol. Rep.* 12, 449–456.

IARC, 1993. *Mycotoxins*. IARC Monogr. Eval. Carcinog. Risk Chem. Humans 56, 489.

Krska, R., Baumgartner, S., Josephs, R., 2001. The state-of-the-art in the analysis of type- A and -B trichothecene mycotoxins in cereals. *Fresenius' J. Anal. Chem.* 371, 285–299. <https://doi.org/10.1007/s002160100992>.

Laraba, I., Bouregghda, H., Abdallah, N., Bouaicha, O., Obonor, F., Moretti, A., et al., 2017. Population genetic structure and mycotoxin potential of the wheat crown rot and head blight pathogen *Fusarium culmorum* in Algeria. *Fungal Genet. Biol.* 103, 34–41. <https://doi.org/10.1016/j.fgb.2017.04.001>.

Lee, S.Y., Woo, S.Y., Tian, F., Song, J., Michlmayr, H., Kim, J.B., Chun, H.S., 2020. Occurrence of deoxynivalenol, nivalenol, and their glucosides in Korean market foods and estimation of their population exposure through food consumption. *Toxins* 12 (2), 89. <https://doi.org/10.3390/toxins12020089>.

Li, S., Blain, E.J., Cao, J., Caterson, B., Duance, V.C., 2014. Effects of the mycotoxin nivalenol on bovine articular chondrocyte metabolism in vitro. *PloS One* 9, e109536. <https://doi.org/10.1371/journal.pone.0109536>.

Li, X., Michlmayr, H., Schweiger, W., Malachova, A., Shin, S., Huang, Y., et al., 2017. A barley UDP-glucosyltransferase inactivates nivalenol and provides *Fusarium* Head Blight resistance in transgenic wheat. *J. Exp. Bot.* 68, 2187–2197. <https://doi.org/10.1093/jxb/erx109>.

Lindblad, M., Gidlund, A., Sulyok, M., Borjesson, T., Krska, R., Olsen, M., et al., 2013. Deoxynivalenol and other selected *Fusarium* toxins in Swedish wheat—occurrence and correlation to specific *Fusarium* species. *Int. J. Food Microbiol.* 167, 284–291. <https://doi.org/10.1016/j.ijfoodmicro.2013.07.002>.

Lu, M., Cao, J., Liu, F., Li, S., Chen, J., Fu, Q., et al., 2012. The effects of mycotoxins and selenium deficiency on tissue-engineered cartilage. *Cells Tissues Organs* 196, 241–250. <https://doi.org/10.1159/000335046>.

Luongo, D., Severino, L., Bergamo, P., D'Arienzo, R., Rossi, M., 2010. Trichothecenes NIV and DON modulate the maturation of murine dendritic cells. *Toxicol* 55, 73–80. <https://doi.org/10.1016/j.toxicol.2009.06.039>.

Magan, N., Aldred, D., Mylona, K., Lambert, R.J., 2010. Limiting mycotoxins in stored wheat. *Food Addit. Contam. Part A Chem Anal Control Expo Risk Assess* 27, 644–650. <https://doi.org/10.1080/19440040903514523>.

McCormick, S.P., Stanley, A.M., Stover, N.A., Alexander, N.J., 2011. Trichothecenes: from simple to complex mycotoxins. *Toxins* 3, 802–814. <https://doi.org/10.3390/toxins3070802>.

Mesterhazy, A., 2020. Updating the breeding philosophy of wheat to Fusarium Head Blight (FHB): resistance components, QTL identification, and phenotyping-a review. *Plants* 9 (12). <https://doi.org/10.3390/plants9121702>.

Nagashima, H., Kushiro, M., Nakagawa, H., 2011a. Nuclear factor-kappaB inhibitors alleviate nivalenol-induced cytotoxicity in HL60 cells. *Environ. Toxicol. Pharmacol.* 31, 258–261. <https://doi.org/10.1016/j.etap.2010.09.014>.

Nagashima, H., Nakagawa, H., Kushiro, M., 2011b. Geldanamycin, an inhibitor of heat shock protein 90, mitigates nivalenol caused changes in cytokine secretion in HL60 cells. *Jpn. Agric. Res. Q.* 45, 441–444. <https://doi.org/10.6090/jarq.45.441>.

Nazari, L., Patteri, E., Manstretta, V., Terzi, V., Morcia, C., Somma, S., et al., 2018. Effect of temperature on growth, wheat head infection, and

---

nivalenol production by *Fusarium poae*. *Food Microbiol.* 76, 83–90. <https://doi.org/10.1016/j.fm.2018.04.015>.

Ndoye, M., Zhang, J.B., Wang, J.H., Gong, A.D., Li, H.P., Qu, B., et al., 2012. Nivalenol and 15-acetyldeoxynivalenol chemotypes of *Fusarium graminearum* clade species are prevalent on Maize throughout China. *J. Phytopathol.* 160, 519–524. <https://doi.org/10.1111/j.1439-0434.2012.01944.x>.

Oyedele, O.A., Ezekiel, C.N., Sulyok, M., Adetunji, M.C., Warth, B., Atanda, O.O., et al., 2017. Mycotoxin risk assessment for consumers of groundnut in domestic markets in Nigeria. *Int. J. Food Microbiol.* 251, 24–32. <https://doi.org/10.1016/j.ijfoodmicro.2017.03.020>.

Pasquali, M., Beyer, M., Logrieco, A., Audenaert, K., Balmas, V., Basler, R., et al., 2016. A European database of *Fusarium graminearum* and *F. Culmorum* trichothecene genotypes. *Front. Microbiol.* 7, 406. <https://doi.org/10.3389/fmicb.2016.00406>.

Pasquali, M., Giraud, F., Brochot, C., Cocco, E., Hoffmann, L., Bohn, T., 2010. Genetic *Fusarium* chemotyping as a useful tool for predicting nivalenol contamination in winter wheat. *Int. J. Food Microbiol.* 137, 246–253. <https://doi.org/10.1016/j.ijfoodmicro.2009.11.009>.

Pestka, J.J., 2010. Deoxynivalenol: mechanisms of action, human exposure, and toxicological relevance. *Arch. Toxicol.* 84, 663–679. <https://doi.org/10.1007/s00204-010-0579-8>.

Qiu, J., Shi, J., 2014. Genetic relationships, carbendazim sensitivity and mycotoxin production of the *Fusarium graminearum* populations from maize, wheat and rice in eastern China. *Toxins* 6, 2291–2309. <https://doi.org/10.3390/toxins6082291>.

Reisinger, N., Schurer-Waldheim, S., Mayer, E., Debevere, S., Antonissen, G., Sulyok, et al., 2019. Mycotoxin occurrence in maize silage-A neglected risk for bovine gut health? *Toxins* 11 (10), 577. <https://doi.org/10.3390/toxins11100577>.

Scaglioni, P.T., de Oliveira Garcia, S., Badiale-Furlong, E., 2019. Inhibition of in vitro trichothecenes production by microalgae phenolic extracts. *Food Res. Int.* 124, 175–180. <https://doi.org/10.1016/j.foodres.2018.07.008>.

SCF, 2000. Opinion of the scientific committee on food on Fusarium toxins – Part 4: nivalenol, adopted on 19 october 2000. (SCF/CS/CNTM/MYC/26 final). [https://ec.europa.eu/food/sites/food/files/safety/docs/sci-com\\_scf\\_out74\\_en.pdf](https://ec.europa.eu/food/sites/food/files/safety/docs/sci-com_scf_out74_en.pdf).

Schollenberger, M., Muller, H.M., Ernst, K., Sondermann, S., Liebscher, M., Schlecker, C., et al., 2012. Occurrence and distribution of 13 trichothecene toxins in naturally contaminated maize plants in Germany. *Toxins* 4, 778–787. <https://doi.org/10.3390/toxins4100778>.

Schöneberg, T., Kibler, K., Wettstein, F.E., Bucheli, T.D., Forrer, H.R., Musa, T., et al., 2019. Influence of temperature, humidity duration and growth stage on the infection and mycotoxin production by *Fusarium langsethiae* and *Fusarium poae* in oats. *Plant Pathol.* 68 (1), 173–184. <https://doi.org/10.1111/ppa.12922>.

Shen, C.M., Hu, Y.C., Sun, H.Y., Li, W., Guo, J.H., Chen, H.G., 2012. Geographic distribution of trichothecene chemotypes of the *Fusarium graminearum* species complex in major winter wheat production areas of China. *Plant Dis.* 96, 1172–1178. <https://doi.org/10.1094/PDIS-11-11-0974-RE>.

Smith, M.C., Madec, S., Troadec, S., Coton, E., Hymery, N., 2018. Effects of fusariotoxin co-exposure on THP-1 human immune cells. *Cell Biol. Toxicol.* 34, 191–205. <https://doi.org/10.1007/s10565-017-9408-7>.

Taranu, I., Marina, D.E., Burlacu, R., Pinton, P., Damian, V., Oswald, I.P., 2010. Comparative aspects of in vitro proliferation of human and porcine lymphocytes exposed to mycotoxins. *Arch. Anim. Nutr.* 64, 383–393. <https://doi.org/10.1080/1745039X.2010.492140>.

Umpierrez-Failache, M., Garmendia, G., Pereyra, S., Rodriguez-Haralambides, A., Ward, T.J., Vero, S., 2013. Regional differences in species composition and toxigenic potential among *Fusarium* head blight isolates from Uruguay indicate a risk of nivalenol contamination in new wheat production areas. *Int. J. Food Microbiol.* 166, 135–140. <https://doi.org/10.1016/j.ijfoodmicro.2013.06.029>.

Vandicke, J., De Visschere, K., Croubels, S., De Saeger, S., Audenaert, K., Haesaert, G., 2019. Mycotoxins in Flanders' fields: occurrence and correlations with *Fusarium* species in whole-plant harvested maize. *Microorganisms* 7 (11), 571. <https://doi.org/10.3390/microorganisms7110571>.

Vejdovszky, K., Warth, B., Sulyok, M., Marko, D., 2016. Non-synergistic cytotoxic effects of *Fusarium* and *Alternaria* toxin combinations in Caco-2 cells. *Toxicol. Lett.* 241, 1–8. <https://doi.org/10.1016/j.toxlet.2015.10.024>.

Wachowska, U., Stuper-Szablewska, K., Perkowski, J., 2020. Yeasts isolated from wheat grain can suppress fusarium head blight and decrease trichothecene concentrations in bread wheat and durum wheat grain. *Pol. J. Environ. Stud.* 29, 4345–4360. <https://doi.org/10.15244/pjoes/118427>.

Wan, L.Y., Allen, K.J., Turner, P.C., El-Nezami, H., 2014. Modulation of mucin mRNA (MUC5AC and MUC5B) expression and protein production

and secretion in Caco-2/ HT29-MTX co-cultures following exposure to individual and combined *Fusarium* mycotoxins. *Toxicol. Sci.* 139, 83–98. <https://doi.org/10.1093/toxsci/kfu019>.

Wan, L.Y., Turner, P.C., El-Nezami, H., 2013a. Individual and combined cytotoxic effects of *Fusarium* toxins (deoxynivalenol, nivalenol, zearalenone and fumonisins B1) on swine jejunal epithelial cells. *Food Chem. Toxicol.* 57, 276–283. <https://doi.org/10.1016/j.fct.2013.03.034>.

Wan, L.Y., Woo, C.S., Turner, P.C., Wan, J.M., El-Nezami, H., 2013b. Individual and combined effects of *Fusarium* toxins on the mRNA expression of pro-inflammatory cytokines in swine jejunal epithelial cells. *Toxicol. Lett.* 220, 238–246. <https://doi.org/10.1016/j.toxlet.2013.05.003>.

Wan, M.L., Woo, C.S., Allen, K.J., Turner, P.C., El-Nezami, H., 2013c. Modulation of porcine beta-defensins 1 and 2 upon individual and combined *Fusarium* toxin exposure in a swine jejunal epithelial cell line. *Appl. Environ. Microbiol.* 79, 2225–2232. <https://doi.org/10.1128/AEM.03277-12>.

Wang, M., Xu, S., Wang, T., Jia, T., Xu, Z., Wang, X., et al., 2018. Effect of inoculants and storage temperature on the microbial, chemical and mycotoxin composition of corn silage. *Asian-Australas. J. Anim. Sci.* 31, 1903–1912. <https://doi.org/10.5713/ajas.17.0801>.

Zhou, D., Wang, X., Chen, G., Sun, S., Yang, Y., Zhu, Z., et al., 2018. The major *Fusarium* species causing maize ear and kernel rot and their toxigenicity in chongqing, China. *Toxins* 10 (2), 90. <https://doi.org/10.3390/toxins10020090>.

Zingales, V., Fedeli, C., Fernandez-Franzon, M., Ruiz, M.J., 2020. Cytotoxic effects of individual and combined sterigmatocystin and nivalenol on

liver hepatocellular carcinoma cells. Food Chem. Toxicol. 143, 111473.  
<https://doi.org/10.1016/j.fct.2020.111473>.





## **2.OBJECTIVES**

OBJETIVOS



## 2. OBJETIVOS

El objetivo general de la presente Tesis Doctoral es profundizar en el conocimiento de los efectos tóxicos y los mecanismos de acción de la micotoxina esterigmatocistina mediante métodos *in vitro*.

Para lograr este propósito, se han planteado los siguientes objetivos específicos:

1. Realizar una revisión bibliográfica de la información toxicológica disponible sobre las micotoxinas esterigmatocistina y nivalenol.
2. Determinar la citotoxicidad de la esterigmatocistina de forma individual y en combinación con el nivalenol en células de carcinoma hepatocelular humano (HepG2).
3. Determinar la citotoxicidad de la esterigmatocistina de forma individual en células de neuroblastoma humano (SH-SY5Y).
4. Evaluar el estrés oxidativo mediante la determinación de la producción de especies reactivas de oxígeno (citoplasmáticas y mitocondriales) y peroxidación lipídica tras la exposición de esterigmatocistina en células SH-SY5Y.
5. Estudiar la influencia de los sistemas de defensa antioxidante endógenos (enzimáticos y no enzimáticos) y exógenos (quercetina) frente al daño oxidativo producido por la esterigmatocistina en células SH-SY5Y.
6. Estudiar el papel de las mitocondrias en la toxicidad inducida por la esterigmatocistina mediante la evaluación de la proliferación celular en células SH-SY5Y sujetas a un cambio de metabolismo energético.

## Objetivos

---

7. Determinar el potencial de membrana mitocondrial, muerte celular, daño al ADN y ciclo celular tras la exposición a esterigmatocistina en células SH-SY5Y.
8. Evaluar la respuesta inflamatoria mediante la determinación de la expresión de citoquinas pro-inflamatorias tras la exposición a esterigmatocistina en células SH-SY5Y.
9. Evaluar los efectos de la esterigmatocistina sobre procesos como proliferación, estrés oxidativo, apoptosis y daño al ADN en modelos de cultivo celular tridimensionales (3D) de neuroblastoma (esferoides) de células SH-SY5Y y compararlos con el efecto inducido en los cultivos de las células SH-SY5Y en monocapa (2D).

## 2. OBJECTIVES

The overall objective of the present PhD Thesis consists in evaluating the toxic effects and the mechanisms of action of the mycotoxin sterigmatocystin by *in vitro* methods.

To achieve this aim, the following specific objectives were proposed:

1. To review the available toxicological information on sterigmatocystin and nivalenol mycotoxins.
2. To determine the cytotoxicity of sterigmatocystin and nivalenol individually and in combination in human hepatocellular carcinoma cells (HepG2).
3. To determine individual cytotoxicity of sterigmatocystin in human neuroblastoma cells (SH-SY5Y).
4. To evaluate the oxidative stress by determination of the production of reactive oxygen species (cytoplasmic and mitochondrial) and lipid peroxidation in SH-SY5Y cells exposed to sterigmatocystin.
5. To determine the effect of the influence of endogenous (enzymatic and non-enzymatic) and exogenous (quercetin) antioxidant defence systems against the oxidative damage produced by sterigmatocystin in SH-SY5Y cells.
6. To evaluate the role of mitochondria on sterigmatocystin-induced toxicity by evaluating cell proliferation in SH-SY5Y cells subject to an energy metabolism change.
7. To determine the mitochondrial membrane potential, cell death, DNA damage and cell cycle in SH-SY5Y cells exposed to sterigmatocystin.

## Objetivos

---

8. To evaluate the inflammatory response by determining the expression levels of pro-inflammatory cytokines in SH-SY5Y cells exposed to sterigmatocystin.
9. To evaluate the effects of sterigmatocystin on processes such as cell proliferation, oxidative stress, apoptosis and DNA damage on the three-dimensional (3D) spheroid model of human neuroblastoma SH-SY5Y and compare them with the effect induced on the SH-SY5Y monolayer cell culture.

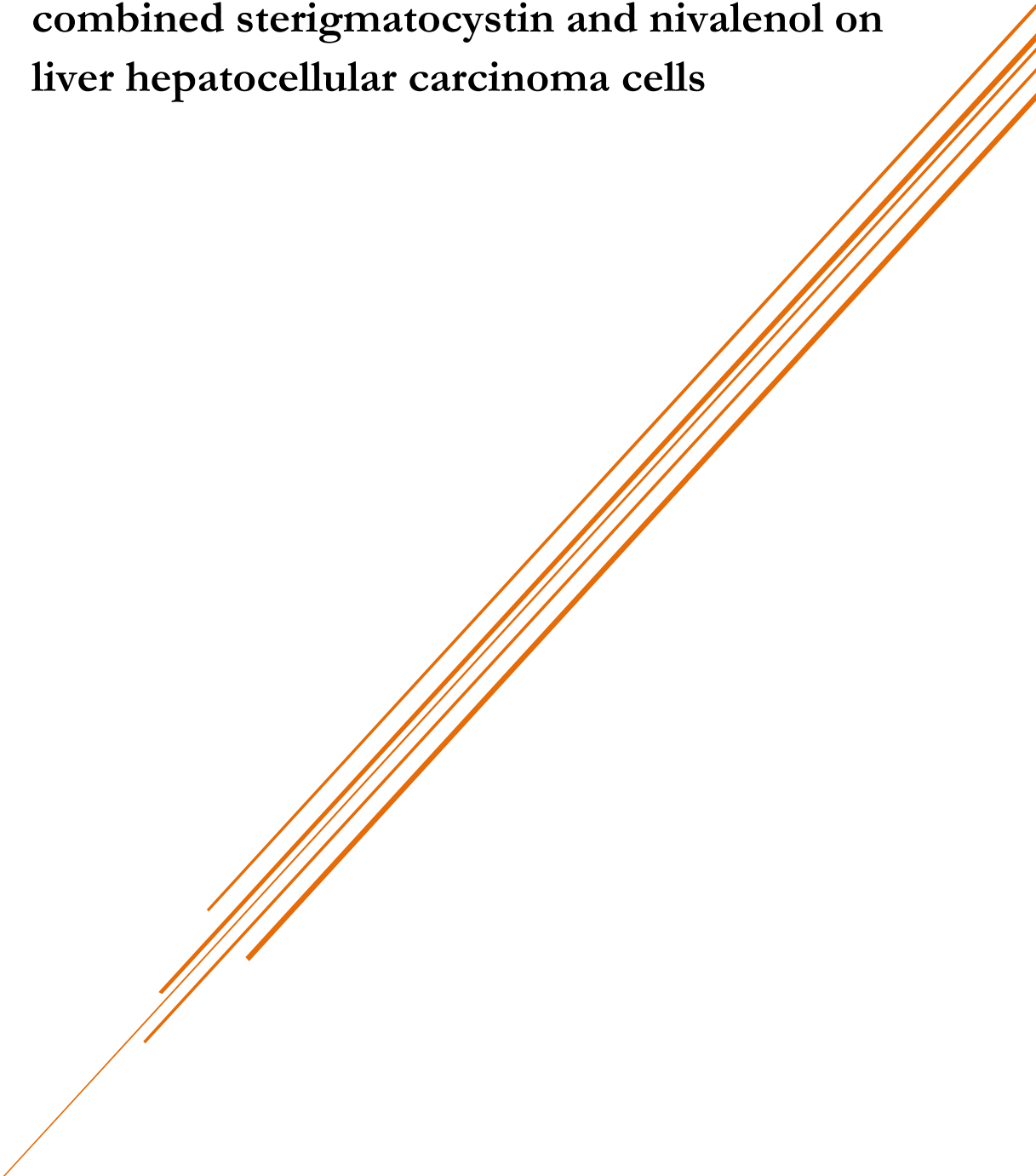
## **3.RESULTS**

## RESULTADOS





### **3.1. Cytotoxic effects of individual and combined sterigmatocystin and nivalenol on liver hepatocellular carcinoma cells**





Food and Chemical Toxicology

**Cytotoxic effects of individual and combined  
sterigmatocystin and nivalenol on liver hepatocellular  
carcinoma cells**

Veronica Zingales<sup>\*1</sup>, Clarissa Fedeli<sup>1</sup>, Mónica Fernández-Franzón,  
Maria-José Ruiz

Laboratory of Food Chemistry and Toxicology, Faculty of Pharmacy, University of  
Valencia, Av. Vicent Andrés Estellés s/n, 46100, Valencia, Spain

\*Corresponding author. Laboratory of Toxicology, Faculty of Pharmacy,  
University of Valencia, Av. Vicent Andrés Estellés, s/n, 46100, Burjassot,  
Valencia, Spain. *E-mail address:* [vezin@uv.es](mailto:vezin@uv.es) (V. Zingales).

<sup>1</sup> These authors have contributed equally to the study, and thus may be regarded  
as the first author.

### **Abstract**

Since humans are exposed to different mycotoxins through daily intake, there is increasing concern about the adverse effects of the interactions between them. Cytotoxicity of sterigmatocystin (STE) and nivalenol (NIV) alone and in combination in human hepatocarcinoma (HepG2) cells was evaluated by MTT assay. Furthermore, ROS production and alteration of  $\Delta\Psi_m$  as mechanisms of action were assessed. Cells were treated with concentrations ranging from 0.15 to 5  $\mu\text{M}$  for NIV and from 0.78 to 50  $\mu\text{M}$  for STE individually and in binary combinations. The combination ratio between the mixture STE + NIV was 10:1. The  $\text{IC}_{50}$  values of NIV ranged from 0.96 to 0.66  $\mu\text{M}$ , whereas no  $\text{IC}_{50}$  values were obtained for STE at any time tested. For the combinations studied, synergistic, antagonistic and additive effects were obtained with the two type of analyses performed, the isobologram analysis and the Combeneft method. No relevant effects on ROS and  $\Delta\Psi_m$  were observed. In conclusion, predictive models based on combination data could help to better understand the interactions between mycotoxins and their implications in food safety assessment. However, a further analysis of the molecular mechanism underlying these interactive effects is required.

**Keywords:** Mycotoxins, Cytotoxicity, Interactions, Isobolograms, Combeneft.

## 1. Introduction

Mycotoxins are secondary toxic metabolites produced by filamentous fungi. They are widespread in food and feed and their presence could be considered a significant global concern for human health (Luongo et al., 2006). In fact, the natural co-occurrence of different mycotoxins has been detected in several commodities. However, data on combined toxic effects of mycotoxins are limited and health risk assessments are usually based on one single mycotoxin exposure (Liu et al., 2014; Wan et al., 2013; Yang et al., 2017).

Nivalenol (NIV), a mycotoxin produced by various species of *Fusarium* fungi, belongs to the trichothecenes group, a family with a common tetracyclic, sesquiterpenoid 12,13 epoxytrichothec-9-ene ring system. *Fusarium* fungi are, probably, the most prevalent toxin-producing fungi commonly found on cereals grown in temperate regions of America, Europe and Asia (Luongo et al., 2006). In Europe the highest concentrations of NIV in food, feed and unprocessed grains were found in oats, maize, barley, wheat and their products (EFSA, 2013a).

Sterigmatocystin (STE) has been found in cereal grains and grain commodities following the fungal contamination at the storage stage (EFSA, 2013b). However, in the literature, there is a relatively little information on the occurrence of STE in food and feed.

Based on current evidence, NIV and STE individually can produce different toxic effects. The NIV is able to induce cytotoxicity, oxidative stress, genotoxicity and apoptosis in human and animal cells (Nagashima, 2018). Moreover, this trichothecene showed several inhibitory effects on primary

metabolism of eukaryotic cells, including inhibition of DNA and protein synthesis as well as mitochondrial function (Arunachalam and Doohan, 2013; Rocha et al., 2005). The NIV could be also associated to many other chronic effects in humans, such as gastrointestinal, hepatic, respiratory, dermal alterations and immunosuppression (Berek et al., 2001; Ferreira Lopes et al., 2017; Smith et al., 2017, 2018; Yang et al., 2017).

With regard to STE mycotoxin, it showed cytotoxic as well as oxidant activities (Liu et al., 2014; Zingales et al., 2019; Zouaoui et al., 2016). Furthermore, it has been shown to be able to inhibit ATP synthesis and impair cell cycle (Huang et al., 2014; Kawai et al., 1984). The STE is a carcinogenic mycotoxin produced mainly by *Aspergillus* and *Penicillium* species of fungi (Anninou et al., 2014; Liu et al., 2014). The International Agency for Research on Cancer (IARC, 1987) has classified STE as a possible human carcinogen (group 2B).

Since a complete and balanced diet normally contains a variety of different foods, the consequent possibility of exposure to more than one mycotoxin is high (EFSA, 2013a, 2013b). The growing research effort of the effects derived from mycotoxins combination has led to demonstrate the existence of complex interactions due to chronic co-exposure to multiple mycotoxins (Bensassi et al., 2014; Grenier and Oswald, 2011). Indeed, the toxic effects induced by the combination of two or more mycotoxins cannot always be predicted based upon their individual toxicity but multi-exposure may lead to additive, synergistic or antagonistic toxic effects (Speijers and Speijers, 2004). The implications of co-occurrence of mycotoxins in food safety assessment are generally not well-know, as well as only limited information is available on the type of interaction between

concomitant occurring mycotoxins and its consequent toxic effect (Bouaziz et al., 2013; Bouslimi et al., 2008; Fernandez-Blanco et al., 2016; Liu et al., 2014; Ruiz et al., 2011a; Zouaoui et al., 2016).

One of the main effects that can be attributed to acute exposure to mycotoxins is the alteration of liver function (Bennett and Klich, 2003). The liver and, thus, the hepatocytes represent the principal site for drug metabolism. In fact, liver parenchymal cells contain the majority of the enzymes required for drug metabolism and therefore are considered a relevant *in vitro* toxicology standard model for xenobiotic metabolism and toxicity studies (LeCluyse, 2001). Since over 50% of the drugs that induce liver injury in human clinical trials are not hepatotoxic to animals, human hepatocytes are needed for more accurate *in vitro* screening of drug toxicity (Olson et al., 2000). In particular, the HepG2 cell line, derived from human hepatocellular carcinoma, seems to be a good surrogate to primary human hepatocytes for toxicology studies, since these cells are characterized by owning a high number of mitochondria and being strong ATP producers (Gomez-Lechon et al., 2014).

Thus, in light of all this, the aim of the present study consisted in investigating the cytotoxic effects associated with the individual exposure to NIV and STE as well as the possible mechanisms undergoing their toxicity on HepG2 cells. Then, the effects of NIV and STE were assessed in binary combination.

### 2. Material and methods

#### 2.1. Reagents

Human hepatocellular carcinoma (HepG2) cell line was obtained from American Type Culture Collection (ATCC HB-8065, Manassas, VA, USA). The reagent grade chemicals and cell culture compounds used, namely Dulbecco's Modified Eagle Medium (DMEM), New Born Calf Serum (NBCS), antibiotics, trypsin/EDTA solutions, Phosphate Buffer Saline (PBS), 3–4,5-dimethylthiazol-2yl-2,5-diphenyltetrazolium bromide (MTT), dimethyl sulfoxide (DMSO), 2',7'-dichlorodihydrofluorescein diacetate (H2-DCFDA), Rhodamine 123 dye (Rh123) were purchased from Sigma-Aldrich (St. Luis. USA). Standard of selected mycotoxins, NIV (purity  $\geq 98\%$ ; MW 312.32 g/mol) and STE (purity  $\geq 98\%$ ; MW 324.28 g/mol) were purchased from Sigma-Aldrich (St. Luis. USA). Chemical structures of NIV and STE are shown in Fig. 1. Stock solutions of the mycotoxins were prepared in methanol and maintained at  $-20\text{ }^{\circ}\text{C}$ . The final mycotoxin concentrations were achieved by adding NIV or STE solutions to the culture medium with a final methanol concentration  $\leq 1\%$  (v/v). Appropriate controls containing the same amount of solvent were included in each experiment.

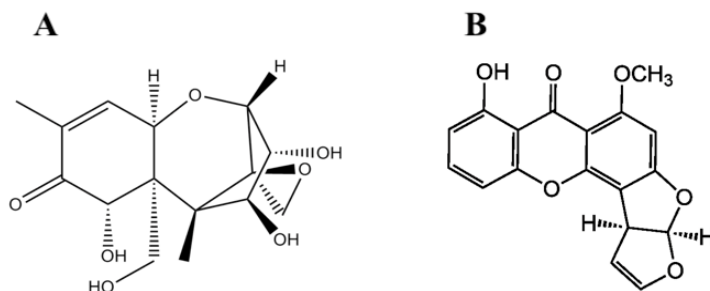
#### 2.2. Cell culture

The HepG2 cells were cultured in DMEM medium supplemented with 10% NBCS, 100 U/ml penicillin and 100 mg/ml streptomycin in monolayer culture flasks. The incubation conditions were pH 7.4, 5%  $\text{CO}_2$  at  $37\text{ }^{\circ}\text{C}$  and 95% air atmosphere at constant humidity. Twice a week, the monolayer of HepG2 cells was subcultured ( $< 40$  subcultures to maintain genetic homogeneity) after



treatment with trypsin-EDTA for 3 min at 37 °C in a 1:3 split ratio. Absence of mycoplasma was checked routinely using the Mycoplasma Stain kit (Sigma-Aldrich, St. Louis, MO, USA).

**Fig. 1.** Chemical structures of Nivalenol (A) and Sterigmatocystin (B).



### 2.3. *In vitro* cytotoxicity

The cell viability was evaluated by MTT assay as described by Ruiz et al., (2006) with some modifications. Briefly, HepG2 cells were seeded in 96-well microplates at a density of  $2 \times 10^4$  cells/well. After 24 h, when the cells reached 70–80% of confluence, the culture medium was replaced with fresh medium containing different serial dilutions (serial dilution factor = 2) concentrations ranging from 0.15 to 5  $\mu$ M for NIV and from 0.78 to 50  $\mu$ M for STE. The mycotoxins were exposed during 24, 48 and 72 h. During the exposure time, neither the medium nor the mycotoxins were replenished. For the MTT assay, after the time of exposure, the medium containing the mycotoxin was replaced with fresh medium containing 50  $\mu$ l (5 mg/ml PBS) of MTT salt. After 4 h of incubation at 37 °C under darkness, the resulting formazan crystals were solubilized in DMSO. The absorbance was measured at 540 nm using an

automatic ELISA plate reader (MultiSkanEX, LabSystem, Helsinki, Finland). Cell viability was expressed as a percentage relative to the solvent control (1% MeOH). Two independent experiments for each time of exposure were performed. The mean 50% inhibition concentration (IC<sub>50</sub>) values were calculated using SigmaPlot version 11 (Systat Software Inc., GmbH, Germany).

### *2.4. Assessment of effect of mycotoxin combination*

#### *2.4.1. Experimental design*

The most relevant aspect in the study of mixtures of mycotoxins consists in the analysis of the dose-response data resulting from the interaction in terms of synergistic or antagonistic effects, depending on the ability of this interaction to potentiate or diminish the toxic effects of the individual mycotoxins, respectively. If the mycotoxins do not interact with each other, their effects can be added and described as additives.

For the study of the type of interaction among NIV and STE in their binary combination, the range of concentrations tested was selected taking into consideration the concentrations found in cereals, as previously reported in literature, and considering the average European consumption of cereals. In particular, according to the international report on the presence of mycotoxins in cereals and cereal products from the Mediterranean area, NIV, together with beauvericin (BEA), are the most predominant mycotoxins (Serrano et al., 2012), with a concentration that varies from 2 to 2120 µg/kg (EFSA, 2013a). On the other hand, in the literature only limited information is available on the occurrence of STE in food and feed. However, according to the data reported by the European Food Safety Authority (EFSA, 2013b), levels in the range of 0.7–4300 µg/kg of STE have been determined in grains. Considering that the

consumption of cereals in Europe is 132 kg/year (FAOSTAT, 2013), the estimated total intake of NIV and STE is ranging from 2.3 nM to 2.44  $\mu\text{M}/\text{day}$  and from 0.77 nM to 4.78  $\mu\text{M}/\text{day}$ , respectively. The concentrations selected (from 0.08 to 1.26  $\mu\text{M}$  for NIV and from 0.78 to 12.5  $\mu\text{M}$  for STE, with five serial dilutions for each mycotoxin) are included in these ranges. In addition, higher concentrations (up to 12.5  $\mu\text{M}$  for STE) have been tested since the mycotoxin concentration in food depends on dietary food variety. The mixtures STE + NIV were prepared at constant 10:1 ratio. All the concentrations in the combinations tested were chosen to obtain equipotent toxicity for each mycotoxin in a mixture. The identification of the type of interaction between the mixtures was performed using two methods, the isobologram analysis and the Combenefit method.

#### 2.4.2. *Isobologram analysis*

The type of interaction that occurs when NIV and STE are in binary combination was described by the median-effect/combination index (CI)-isobologram equation by Chou and Talalay (1984) and Chou (2006). The isobologram analysis involves plotting the dose–effect curves for each compound and its combinations in multiple diluted concentrations using the median-effect equation:

$$fa/fu = (D/D_m)^m$$

where  $D$  is the concentration of a product,  $D_m$  is the medium-effect dose (e.g.,  $\text{IC}_{50}$ ,  $\text{EC}_{50}$  or  $\text{LC}_{50}$ ) that inhibits the cells under study by 50%,  $fa$  is the fraction affected by concentration  $D$  (e.g. percentage of inhibition/100),  $fu$  is the unaffected fraction (therefore  $fa = 1 - fu$ ) and  $m$  is the coefficient signifying the

shape of the dose-effect relationship, where  $m = 1$ ,  $m > 1$ , and  $m < 1$  indicate hyperbolic, sigmoidal, and negative sigmoidal dose-effect curve, respectively (Chou and Talalay, 1984). Therefore, the method takes into account both the potency ( $D_m$ ) and shape ( $m$ ) parameters.

The medium-effect equation for a single compound can be extended to multiple mycotoxins, becoming:

$$[(f\hat{a})_{1,2}/(\hat{a})_{1,2}]^{1/m} = D_1/(D_m)_1 + D_2/(D_m)_2 + (D)_1(D)_2/(D_m)_1(D_m)_2$$

Chou and Talalay (1984) introduced the term combination index  $(CI)_x$  for quantification of synergism or antagonism between two compounds:

$$CI = D_1/(D_x)_1 + D_2/(D_x)_2$$

$$D_x = D_m[f\hat{a}/(1-f\hat{a})]^{1/m}$$

$$CI = (D)_1/(D_m)_1[f\hat{a}/(1-f\hat{a})]^{1/m_1} + (D)_2/(D_m)_2[f\hat{a}/(1-f\hat{a})]^{1/m_2}$$

where in the denominator  $(D_x)_1$  is for  $D_1$  “alone” that inhibits a system  $x\%$ , and  $(D_x)_2$  is for  $D_2$  “alone” that inhibits a system  $x\%$ . Finally, the general equation for  $n$ -compound combination at  $x\%$  inhibition becomes:

$$(CI)_x^n = \sum_{j=1}^n (D)_j/(D_x)_j = \frac{(D_x)_{1-n}\{[D]_j \sum_{j=1}^n [D]\}}{(D_m)_j\{(f\hat{a}x)_j/[1 - (f\hat{a}x)_j]\}^{1/m_j}}$$

where  $(CI)_x^n$  is the combination index for  $n$  compounds (e.g., mycotoxins) at  $x\%$  inhibition (e.g., proliferation inhibition);  $(D_x)_{1-n}$  is the sum of the concentration of  $n$  compounds that exerts  $x\%$  inhibition in combination,  $\{[D]_j/\sum_{j=1}^n [D]\}$  is the proportionality of the concentration of each

of  $n$  compounds that exerts  $x\%$  inhibition in combination; and  $(D_m)_i \{ (f_{ax})_i / [1 - (f_{ax})_i] \}^{1/m_i}$  is the concentration of each compound alone that exerts  $x\%$  inhibition. The CI  $< 1$ ,  $= 1$ , and  $> 1$  indicates synergism, additive and antagonism effect of the combination, respectively. The type of interaction produced by NIV and STE combination was evaluated by isobologram analysis using CalcuSyn software version 2.1. (Biosoft, Cambridge, UK, 1996-2007).

### 2.4.3. *Combeneft analysis*

Combeneft is a software tool that enables the visualization, analysis and quantification of substance combination effects (Di Veroli et al., 2016). Data from combination exposures were processed using three synergy reference models: highest single agent (HSA) model, Loewe additivity model and Bliss independence model.

Combeneft implements a surface approach, allowing model-based quantification of substance combinations by comparing data obtained to mathematical models of dose-responses for non-synergistic combinations. To quantify the interaction between substances, the observed combination response is compared to the expected effect ( $y_e$ ) under the assumption of non-interaction predicted by a reference model. Consider that substance 1 at concentration  $x_1$  produces an effect  $y_1$  and substance 2 at the concentration  $x_2$  produces an effect  $y_2$ , while when combined they produce an effect  $y_c$ . Namely, a substance interaction will be classified as synergistic when  $y_c$  is greater than  $y_e$ . Otherwise, antagonism is concluded when the combination produces less than what is expected.

The HAS model states that the expected combination effect equals to the higher effect of individual substances:

$$y_{e(HSA)} = \max(y_1, y_2)$$

Therefore, any additional effect over the higher single substance will be considered as HAS synergy.

The Loewe additivity model states that must satisfy:

$$\frac{x_1}{X_{LOEWE}^1} + \frac{x_2}{X_{LOEWE}^2} = 1$$

where  $X_{LOEWE}^1$  and  $X_{LOEWE}^2$  are the doses of substance 1 and 2 alone that produce  $y_{e(LOEWE)}$ .

$$y_{e(LOEWE)} = \frac{E_{min} + E_{max} \left( \frac{x_1 + x_2}{m} \right)^\lambda}{1 + \left( \frac{x_1 + x_2}{m} \right)^\lambda}$$

here,  $E_{min}$  and  $E_{max}$  are the minimal and maximal effects of the substance;  $m$  is the dose that produces the midpoint effect of  $E_{min} + E_{max}$ , also known as relative  $EC_{50}$ , and  $\lambda$  is the shape parameter indicating the sigmoidicity or slope of the curve. Definitely, the equation shows that  $y_{e(LOEWE)}$  is equal to the single substance response at dose  $x_1 + x_2$ .

The Bliss independence model assumes a stochastic process in which two substances acts independently. Thus,  $y_{e(BLISS)}$  can be calculated based on the probability of independent events as

$$y_{e(BLISS)} = y_1 + y_2 - y_1 y_2$$

Using the Combenefit tool, the differences between the model-based  $y_e$  and the actual effect of the mycotoxin combination were determined in the context of the model used. The values obtained were defined as synergy score ( $S$ ):

$$S_{HSA} = y_e - y_{e(HSA)}$$

$$S_{LOEWE} = y_e - y_{e(LOEWE)}$$

$$S_{BLISS} = y_e - y_{e(BLISS)}$$

If the actual effect of the mycotoxin combination is greater than the expected effect,  $S$  is greater than zero. Otherwise, it is less than zero. A higher  $S$  denotes greater synergy of the corresponding substance combination.

### 2.5. Measurement of intracellular ROS

Early intracellular reactive oxygen species (ROS) production was measured in HepG2 cells exposed to STE and NIV, both individually and in mixtures, by using H<sub>2</sub>-DCFDA. The H<sub>2</sub>-DCFDA is taken up by cells and then deacetylated by intracellular esterases; the resulting non-fluorescent 2,7-dichlorofluorescein (H<sub>2</sub>-DCF) is switched to highly fluorescent dichlorofluorescein (DCF) when oxidized by ROS. The ROS generation was evaluated according to Ruiz-Leal and George (2004). Briefly, a number of  $4 \times 10^4$  cells/well were seeded in a 96-well black culture microplate. Once cells reached 100% of confluence, the culture medium was replaced with fresh medium containing 20  $\mu$ M H<sub>2</sub>-DCFDA. After incubation for 20 min in the dark, H<sub>2</sub>-DCFDA was removed and cells were washed twice with PBS before adding fresh medium containing 1% of methanol (control), the serial dilutions of each mycotoxin or the binary combinations

between them. Individual treatments were assayed at a concentration range of 0.08–0.31  $\mu\text{M}$  for NIV, and at a range of 0.78–3.31  $\mu\text{M}$  for STE with three serial dilutions for each mycotoxin. Concentrations assayed for binary combinations (STE + NIV) were prepared at constant 10:1 ratio. All the concentrations in the combinations tested were chosen to obtain equipotent toxicity for each mycotoxin in a mixture. Increases in fluorescence were measured on a Wallace Victor2, model 1420 multilabel counter (Perkin Elmer, Turku, Finland), at intervals up to 2 h at excitation/emission wavelengths of 485/535 nm. Determinations were performed in two independent experiments (mean  $\pm$  SEM;  $n = 2$ ). Results were expressed as increase in fluorescence respect to the control.

### 2.6. *Measurement of mitochondrial membrane potential ( $\Delta\Psi_m$ )*

The alteration of  $\Delta\Psi_m$  was determined on HepG2 cells using Rh123 as described by Baracca et al. (2003). Briefly, HepG2 cells were seeded in a 96-well black culture microplate at a density of  $4 \times 10^4$  cells/well. Once cells reached 100% of confluence, they were exposed to NIV (0.31, 0.16 and 0.08  $\mu\text{M}$ ) and STE (3.13, 1.56 and 0.78  $\mu\text{M}$ ) individually and in combination. For the STE + NIV mixtures, three different concentrations of each mycotoxin (3.13, 1.56 and 0.78  $\mu\text{M}$  for STE and 0.31, 0.16 and 0.08  $\mu\text{M}$  for NIV) were set, with a constant 10:1 ratio. All the concentrations in the combinations tested were chosen to obtain equipotent toxicity for each mycotoxin in a mixture. After 24 h of exposure, the medium was removed and the cells were incubated with 5  $\mu\text{M}$  Rh123 in fresh medium for 15 min at 37 °C in the dark. The fluorescence was measured on a Wallace Victor2, model 1420 multilabel counter (Perkin Elmer, Turku, Finland) at excitation/emission wavelengths of 485/535 nm. Determinations were performed in two independent experiments (mean  $\pm$  SEM;



n = 2). Results were expressed as percentages of the fluorescence values obtained with respect to the control.

### 2.7. *Statistical analysis of data*

Statistical analysis of data was carried out using SPSS version 22 (SPSS, Chicago, IL, USA), statistical software package. Data were expressed as mean  $\pm$  SEM of different independent experiments. The statistical analysis of the results was performed by Student's *t*-test for paired samples. Differences between groups were analysed statistically with one-way ANOVA followed by the Tukey HDS *post-hoc* test for multiple comparisons. The level of  $p \leq 0.05$  was considered statistically significant.

## 3. Results

### 3.1. *Cytotoxicity of individual mycotoxins*

The cytotoxic effects of NIV and STE were evaluated on HepG2 cells by MTT assay after 24, 48 and 72 h of exposure in order to determine the molar concentration of individual mycotoxins able to reach the IC<sub>50</sub> values. The viability decreased significantly in cells exposed to NIV in a time- and concentration-dependent manner. Particularly, cell viability decreased until 77% after 24 h of NIV exposure, and until 81% after 48 h, achieving a 100% of cell mortality when cells were exposed to the highest concentration tested of NIV for 72 h (data not shown). No significant reduction in cell viability after 24, 48 and 72 h of STE exposure was observed; only a cell viability reduction equal to 10%, 20% and 24% for these time of exposure, respectively, was induced by the highest concentration of STE (50  $\mu$ M; data not shown).

Table 1 shows the  $IC_{50}$  ( $\mu\text{M}$ )  $\pm$  SEM (n=2) values of NIV and STE in HepG2 cells after 24, 48 and 72 h of exposure. As observed in Table 1,  $IC_{50}$  values were obtained in HepG2 cells exposed to NIV at the three times of exposure, whereas STE did not show any  $IC_{50}$  value at the range of concentrations tested at all time of exposure, being the less cytotoxic.

### 3.2. *Cytotoxicity of binary mixture of mycotoxins*

The binary combination of mycotoxins NIV + STE was evaluated using the MTT assay after 24, 48 and 72 h of exposure (Fig. 2). The mixture led to a significant decrease of HepG2 cell viability. Significant differences between the binary combination and STE taken individually can be observed at all exposure time, with a cell viability reduction induced by the mixture NIV + STE much higher than that induced by STE alone. In particular, as shown in Fig. 2a, the binary combination decreased cell viability from 6% to 62% more than STE alone after 24 h of exposure, as well as, a reduction ranging from 18% to 85% and from 8% to 86% respect to STE assayed individually was observed after 48 and 72 h, respectively (Fig. 2b and c). On the other hand, no differences were obtained between the highest concentration of NIV and the mixture after 24, 48 and 72 h of exposure. In fact, after 24 and 48 h of exposure significant differences can be observed between the mixture and NIV alone only at the lower concentrations, with a decrease induced by the first one ranging from 5% to 15% compared to NIV assayed individually (Fig. 2a and b). No significant differences were obtained after 72 h respect to NIV at all concentrations tested.

**Table 1.** The  $IC_{50}$  ( $\mu M$ )  $\pm$  SEM (n=2) values of NIV and STE in HepG2 cells determined by MTT assay after 24, 48 and 72 h of exposure.

Mycotoxin	$IC_{50}$ ( $\mu M$ ) $\pm$ SEM		
	24 h	48 h	72 h
NIV	$0.96 \pm 0.08$	$0.76 \pm 0.1$	$0.66 \pm 0.032$
STE	> 50 *	>50 *	> 50 *

\* Highest concentration tested

### 3.3. *Interaction of mycotoxin combination by isobologram analysis*

In order to determine the type of interaction among NIV and STE in their combination, the isobologram analysis was performed. The dose-effect relationship parameters ( $Dm$ ,  $m$  and  $r$ ) of the two mycotoxins tested individually and their binary combination, as well as mean combination index (CI) values of mycotoxin combinations are detailed in Table 2. The Fig. 3 shows the CI versus fractional effect ( $f_a$ ) plots of mycotoxin interactions after 24, 48 and 72 h of exposure. As assessed by CI-isobologram equation, mainly additive effects have been produced by the binary mixture NIV + STE, whereas synergism was evidenced only at the lowest fraction affected ( $IC_{25}$ ) after 24 and 48 h of exposure (CI values equal to  $0.614 \pm 0.15$  and  $0.58 \pm 0.18$ , respectively).

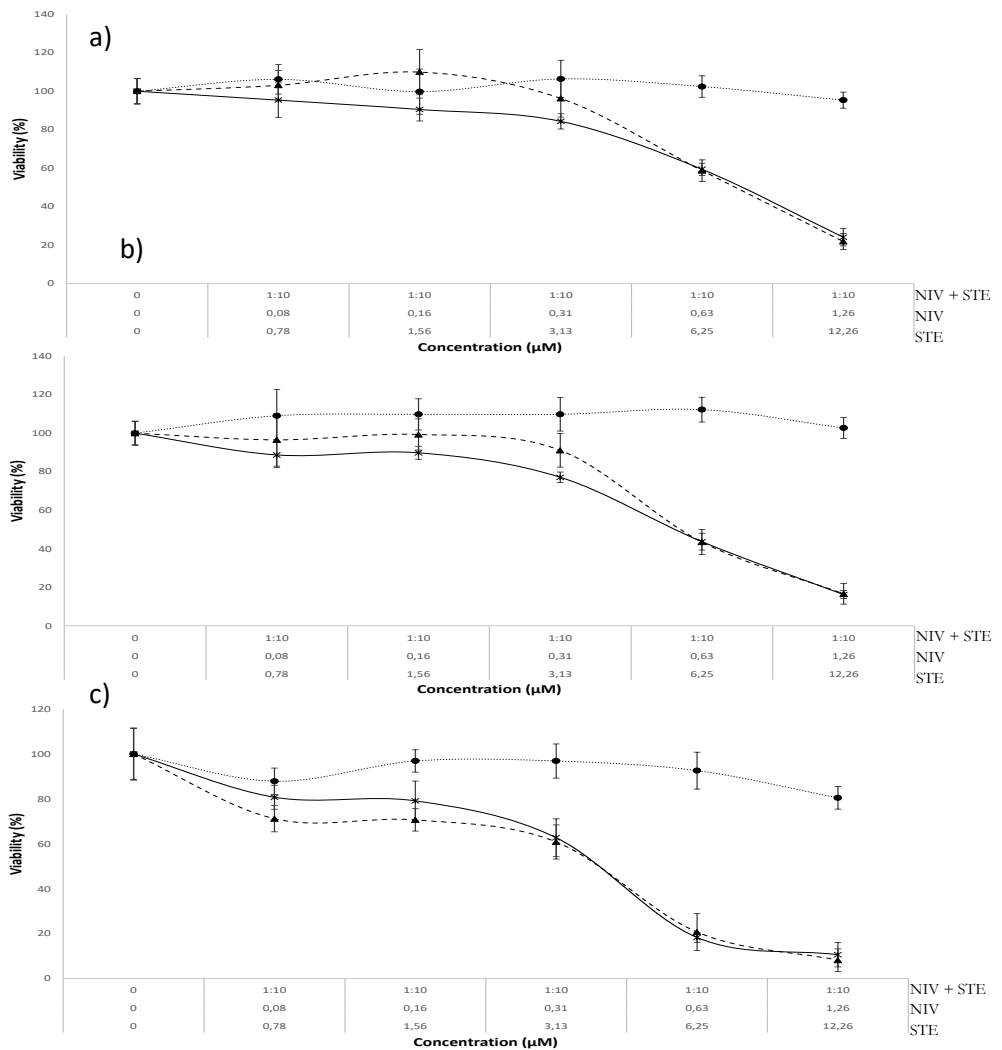


**Fig. 2.** Cytotoxic effects of individual and binary combination of NIV and STE in HepG2 cells performed by MTT assay after 24 h (a), 48 h (b) and 72 h (c) of exposure; NIV (---▲---), STE (·····) and NIV+STE (---\*---). (\*)  $p \leq 0.05$  indicates significant difference between the mixture and STE assayed individually. (#)  $p \leq 0.05$  indicates significant difference between the mixture and NIV assayed individually.

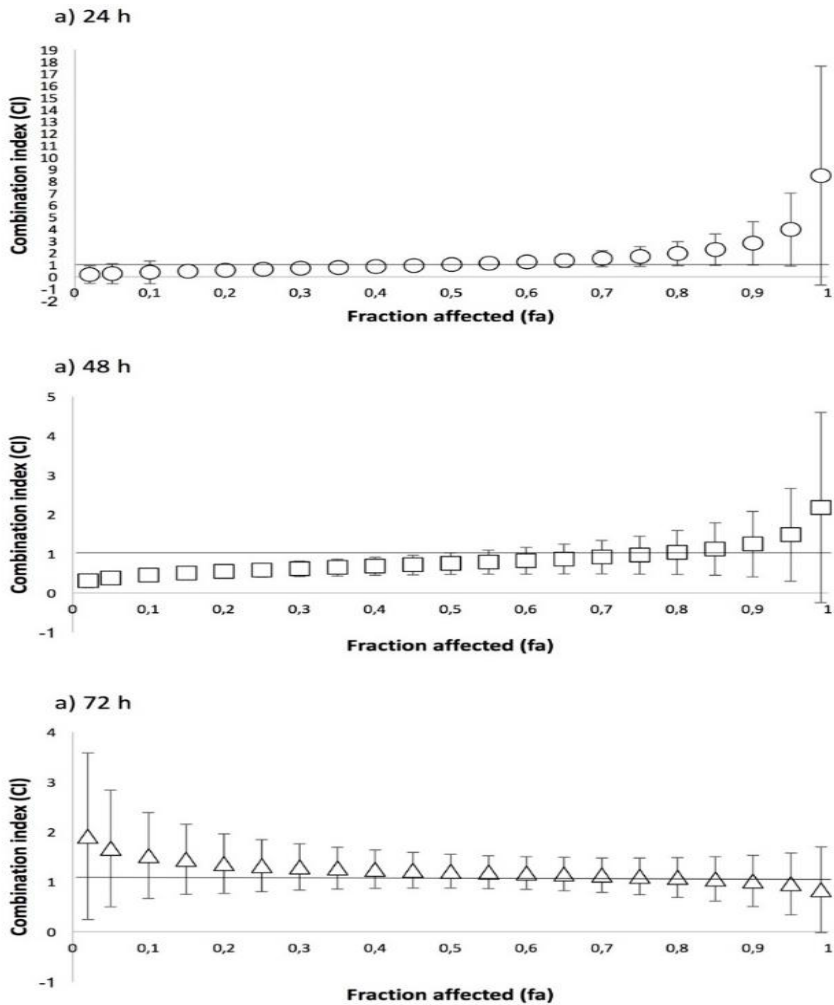


**Fig. 3.** Fractional effect ( $fa$ )/combination index (CI) curve as described by Chou and Talalay model on HepG2 cells exposed to 24 h (a), 48 h (b) and 72 h (c). Each point represents the CI  $\pm$  SD at  $fa$  by computer simulation (from  $fa = 0.25$  to  $0.90$ ) as determined in our experiments. The dotted line indicates additive, the area under the dotted line synergism, and the area above of the dotted line antagonism.

**Table 2.** Dose–effect relationship parameters and mean combination index (CI) values (as a function of fractional inhibition of proliferation) of binary mixture of NIV and STE on HepG-2 cells.

Mycotoxin	Time (h)	$D_m$ ( $\mu\text{M}$ )	$m$	$r$	CI Values at following effect levels			
					IC <sub>25</sub>	IC <sub>50</sub>	IC <sub>75</sub>	IC <sub>90</sub>
NIV	24	0.94	3.16	0.9736				
	48	0.69	2.17	0.9199				
	72	0.25	1.29	0.9371				
STE	24	$\geq 50$	0.39	0.9871				
	48	$\geq 50$	0.39	0.9871				
	72	$\geq 50$	0.73	0.8716				
NIV + STE	24	0.96	1.28	0.9514	$0.614 \pm 0.15$ Syn	$1.019 \pm 0.34$ Add	$1.690 \pm 0.81$ Add	$2.802 \pm 1.81$ Add
	48	0.52	1.44	0.9539	$0.580 \pm 0.18$ Syn	$0.749 \pm 0.27$ Add	$0.966 \pm 0.48$ Add	$1.246 \pm 0.83$ Add
	72	0.30	1.44	0.9567	$1.327 \pm 0.52$ Add	$1.215 \pm 0.34$ Add	$1.114 \pm 0.33$ Add	$1.021 \pm 0.51$ Add

The parameters  $m$ ,  $D_m$  and  $r$  are the antilog of  $x$ -intercept, the slope and the linear correlation coefficient of the median-effect plot, which signifies the shape of the dose–effect curve, the potency (IC<sub>50</sub>), and conformity of the data to the mass–action law, respectively (Chou, 2006; Chou and Talalay, 1984).  $D_m$  and  $m$  values are used for calculating the CI values (CI < 1, =1, and >1 indicate synergism (Syn), additive effect (Add), and antagonism (Ant), respectively. IC<sub>25</sub>, IC<sub>50</sub>, IC<sub>75</sub> and IC<sub>90</sub>, are the doses required to inhibit proliferation 25%, 50%, 75% and 90%, respectively. IC<sub>25</sub>, IC<sub>50</sub>, IC<sub>75</sub>, IC<sub>90</sub> and the dose–effect parameters were calculated by using Computer software CalcuSyn.

### 3.4. Interaction of mycotoxin combination by Combeneft analysis

A dose-matrix approach was used to determine the combination response (additivity, synergy, or antagonism) using the software Combeneft. The program predicts the response surface of no-interaction based on single agent responses using each of the different models (HSA model, Loewe additivity model and Bliss independence model) and compares this with the measured response. The Fig. 4a shows a dose-response matrix between 5 concentrations of NIV and 5 concentrations of STE in a 2-fold dilution scheme. The cytotoxicity induced by the single mycotoxins and their combination on HepG2 cells is shown in Fig. 4b. As it can be shown in Fig. 4b, NIV significantly enhanced the cytotoxic effect of STE on HepG2 cells. Conversely, STE has not been able to enhance the cytotoxicity of NIV. The binary combination responses at various concentration levels were quantified by computational methods. The Fig. 4c–e represents the surface response of NIV and STE on HepG2 cells in a  $5 \times 5$  checkerboard design. The coloured areas denote the degree of synergism. As the Loewe synergy and antagonism surface map shows (Fig. 4c), the interaction between NIV and STE was almost likely additive/synergistic over the whole dose-response matrix, with the strongest synergistic effect centred at the concentration of 12.5  $\mu\text{M}$  of STE and 0.31  $\mu\text{M}$  of NIV. However, the plot also revealed some antagonistic combinations. In particular, antagonistic interactions between NIV and STE seem to occur in the region in which the concentration of NIV is fixed at 1.26  $\mu\text{M}$ . In general, a very good concordance between the Loewe additive method and the other two methods used was observed (Fig. 4-e), supporting the overall conclusions for each combination.



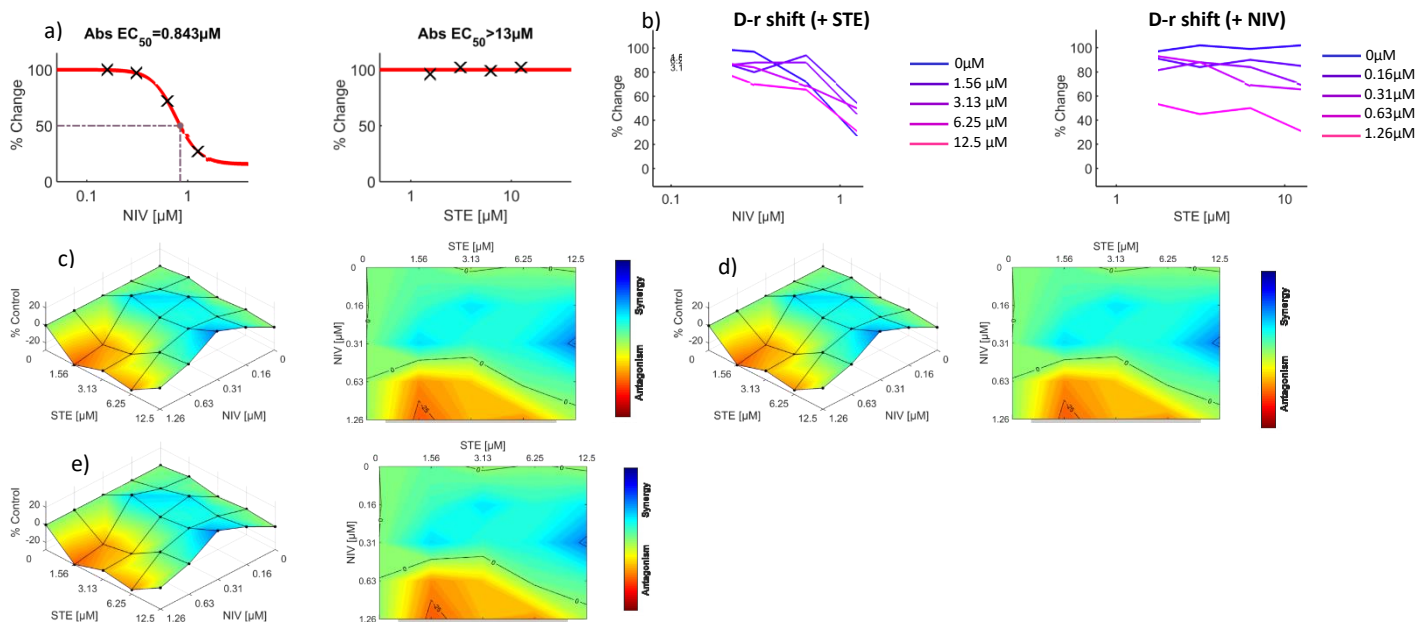


**Fig. 4.** Effect of the binary combination NIV + STE on HepG2 cells. a) Single agent dose response curves induced by NIV or STE on HepG2 cells. b) Single-agent and combination dose-response shift. c-e) Surface plots of HepG2 cells treated with NIV, STE or combined NIV + STE shown in 2D and 3D. Each point represents the mean of two independent measurements. Plots were generated using Combenefit program by applying three methods for combined treatments: Loewe additivity model (c), HSA model (d) and Bliss independence model (e). Level of antagonism or synergism is represented by color scale bar.

### 3.5. *Intracellular reactive oxygen species*

Changes in the redox status in HepG2 cells in response to NIV (0.08, 0.16 and 0.31  $\mu\text{M}$ ), STE (0.78, 1.56 and 3.31  $\mu\text{M}$ ) and different mixtures NIV + STE (0.08  $\mu\text{M}$  NIV+ 0.78  $\mu\text{M}$  STE; 0.16  $\mu\text{M}$  NIV + 1.56  $\mu\text{M}$  STE; 0.31  $\mu\text{M}$  NIV + 3.13  $\mu\text{M}$  STE) was determined. The production of ROS was determined during a period of time ranging from 0 to 120 min. Results obtained demonstrate that HepG2 cells treated with NIV or STE individually did not show any significant concentration-dependent variation in the production of oxidizing species when compared to the basal rate (Fig. 5). However, a significant increase in ROS production was observed in control cells and in both mycotoxins at all concentrations tested during the period of exposure from 5 to 120 min respect to respect to the time 0 min were observed in cells exposed to the binary mixture 0.08  $\mu\text{M}$  NIV +0.78  $\mu\text{M}$  STE and 0.31  $\mu\text{M}$  NIV +3.13  $\mu\text{M}$  STE at the time of exposure 5 and 60 min, respectively. Additionally, at 45 min the mixture 0.08  $\mu\text{M}$  NIV +0.78  $\mu\text{M}$  STE increased significantly ROS production respect to the control.

### 3.6. *Measurement of mitochondrial membrane potential ( $\Delta\Psi_m$ )*

The alteration of  $\Delta\Psi_m$  was determined in HepG2 cells exposed to NIV (0.08, 0.16 and 0.31  $\mu\text{M}$ ), STE (0.78, 1.56 and 3.13  $\mu\text{M}$ ) and the mixtures NIV + STE (0.08  $\mu\text{M}$  NIV+ 0.78  $\mu\text{M}$  STE; 0.16  $\mu\text{M}$  NIV + 1.56  $\mu\text{M}$  STE; 0.31  $\mu\text{M}$  NIV + 3.13  $\mu\text{M}$  STE) by using the fluorescent probe Rh123. As shown in Fig. 6, exposure of HepG2 cells for 24 h to increasing concentrations of NIV resulted in no alteration of the  $\Delta\Psi_m$ , as demonstrated by no significant variation in the Rh123 fluorescence intensity observed with respect to the control cells. No changes in  $\Delta\Psi_m$  were also obtained in cells exposed to the mixtures NIV +

STE. Contrarily, a significant alteration of the  $\Delta\Psi_m$  was observed when HepG2 cells was exposed to the highest concentration of STE (3.13  $\mu\text{M}$ ).

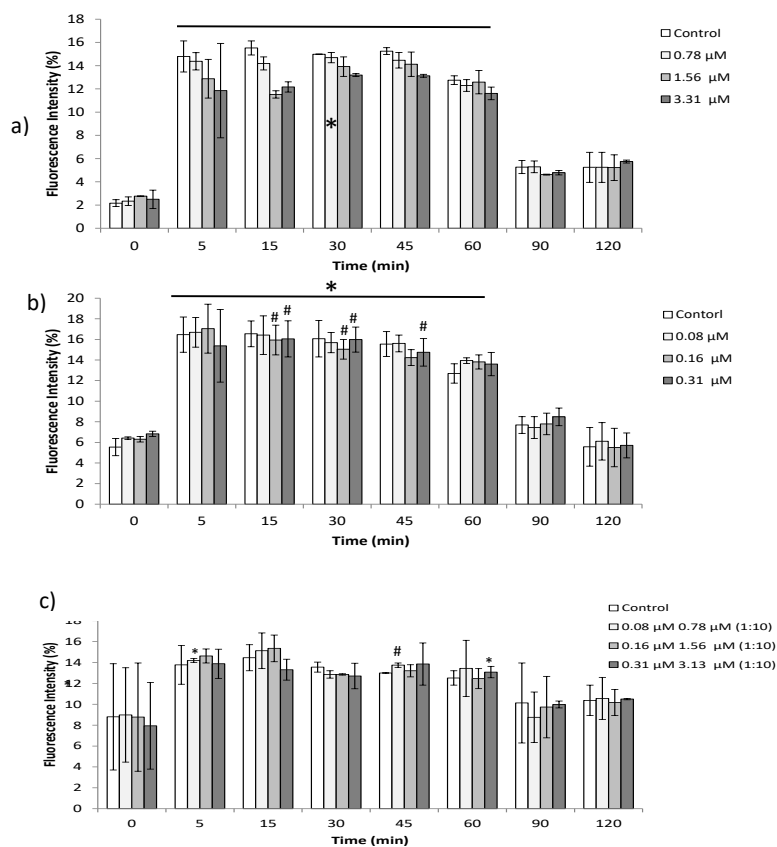


**Fig. 5.** Time dependence of ROS-induced fluorescence in HepG2 cells exposed to NIV (a), STE (b) and NIV + STE (c). Results are expressed as mean  $\pm$  SEM (n=2). (\*)  $p \leq 0.05$  indicates significant difference from the time 0 minutes; (#)  $p \leq 0.05$  indicates significant difference from the control.

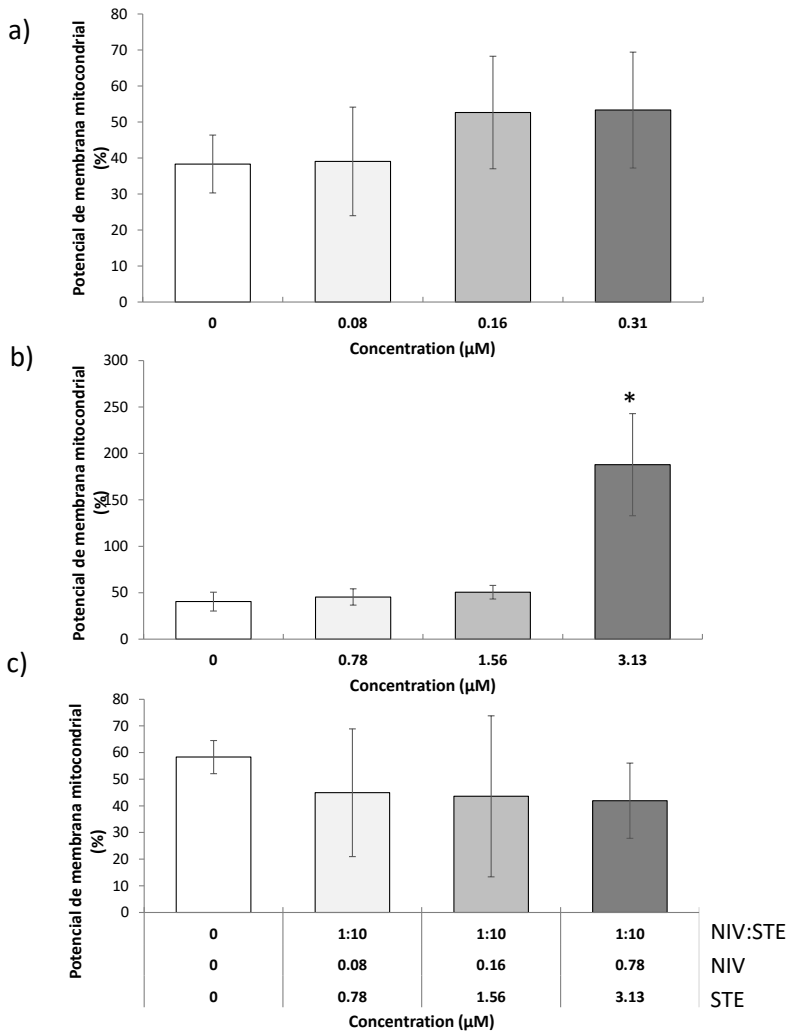


**Fig. 6.** Measurement of mitochondrial membrane potential ( $\Delta\Psi_m$ ) in HepG2 cells after 24 h of exposure to different concentrations of NIV (a), STE (b) and NIV + STE (c). Results are expressed as mean  $\pm$  SEM (n=2). (\*)  $p \leq 0.05$  indicates significant difference from the control.

#### 4. Discussion

In the present study it has been explored the individual and combined cytotoxic effects of NIV and STE on HepG2 cells. Literature data repeatedly report the substantial cytotoxicity associated with exposure to NIV or STE to different cell lines (Alassane-Kpembi et al., 2013; Anninou et al., 2014; Bunger et al., 2004; Smith et al., 2017). Regarding NIV mycotoxin, in our study the IC<sub>50</sub> values obtained measuring the reduction of formazan by mitochondrial dehydrogenases of living cells through the MTT assay ranged from  $0.96 \pm 0.08$  to  $0.66 \pm 0.032$   $\mu$ M (24, 48 and 72 h of exposure). On the other hand, with regard to STE mycotoxin, no significant reduction in cell viability after 24, 48 and 72 h of exposure was observed, suggesting that HepG2 cells are more sensitive to NIV than STE. Since dietary exposure do not involve a single mycotoxin but rather a complex mixture of mycotoxins that is frequently found in food, beverage and natural products, the study of the toxic effects of mycotoxins alone may not predict their effects in natural environment. In fact, simultaneously or sequentially exposure to multiple mycotoxins may alter the toxicological impact of an individual mycotoxin, leading to possible adverse effects on consumer health which are riskier than the intake of only one mycotoxin alone, depending on the nature of their possible interactions (antagonistic, synergistic or additive) (Ruiz et al., 2011a, 2011b). Therefore, if on one hand the studies based on single mycotoxin exposure allow to improve the knowledge on the mechanisms of toxicity under controlled conditions, on the other hand, for mimicking the real-life exposure situation and characterize adequately the risk associated with daily intake, it is of high importance to analyse the response of the cells exposed to mixture of mycotoxins in different combinations. Furthermore, data from literature highlight the existence of

striking differences on the cytotoxic effects of mycotoxin mixtures according to the type of cells exposed and, mainly, on the method for analysing the dose-effect relationship in cell culture. For these reasons, in the present study mycotoxin interactions have been assessed by applying two different mathematical models to the recorded data.

To the best of our knowledge, there are no studies about the cytotoxicity of NIV and STE in combination, as well as the occurrence of NIV+STE mixtures in food commodities has not been demonstrated so far. However, considering that NIV and STE are both mycotoxins produced by two species of fungi predominant in warm, humid climates, it can be assumed that these two mycotoxins may be present simultaneously in food products (Chidambaram et al., 2017).

Results obtained in the present study highlight that the binary mixture led to a significant decrease of HepG2 cell viability. Particularly, the mixture decreased the viability more than STE alone at all time of exposure (Fig. 2a–c), showing a lower toxicity of STE respect to the binary combination. The same behaviour has been observed in CHO-K1 cells exposed to STE in combination with patulin (PAT) or BEA (Zouaoui et al., 2016). Regarding NIV mycotoxin, the mixture NIV + STE resulted to be more cytotoxic respect to the lowest concentrations of NIV after 24 and 48 h, whereas no differences were observed compared to the highest concentrations, as well as, compared to all concentrations tested after 72 h of exposure. Similar results were reported by Smith et al. (2017) when the mixture NIV+T-2 toxin (T-2) was studied in HepaRG cells.

Over the last few years, researchers developed predictive models for mycotoxin based on combination data in order to estimate the true risk of harmfulness (Segvic Klaric, 2012). The isobologram method has been widely used to carry out many studies of mycotoxin interactions (Luongo et al., 2008; Prosperini et al., 2014; Ruiz et al., 2011a, 2011b). In the present study, as determined by this method, the nature of the interactions produced by the binary combinations NIV +STE was quite uniform along the fraction affected (Fig. 3; Table 2). In general, additive effects predominated but at the lowest values of  $f_a$  (IC<sub>25</sub>) the interaction became synergistic at the time of exposure 24 and 48 h. The CI-isobologram method provides an accurate prediction of the interaction between mycotoxins in combination. It combines a qualitative assessment of interactions via an isobolographic analysis and a quantification of synergy or antagonism by calculating a combination index and dose reduction index at different effect levels. However, it cannot elucidate the mechanisms by which these types of interactions are produced. Therefore, it is difficult to give an explanation to the behavior observed. Nevertheless, tentatively, it could be hypothesized that at the lowest concentrations each mycotoxin facilitates and enhances the activity of the other mycotoxin in the mixture, by increasing its absorption or by decreasing its metabolic degradation (Cavaliere et al., 2005), whereas, at higher concentrations, NIV and STE bind their receptors and the resulting effect is the sum of their individual effects (additive). The same behaviour was observed in Caco-2 cells exposed to NIV in combination with deoxynivalenol (DON), where synergy effects at low cytotoxicity levels turned into an additive effect with the increase of the fraction affected (Alassane-Kpembi et al., 2013). The studies regarding DON and NIV mixture effects were the most numerous among the mycotoxin interaction studies because of the

frequent co-occurrence of DON and NIV in the diet. From all of the studies, a synergistic toxicity effect was often observed (Alassane-Kpembé et al., 2015, 2017; Tajima et al., 2002; Yang et al., 2017). The NIV has been combined also with other mycotoxins, such as zearalenone (ZEA), Fusarenon-X (FX) and 5-acetyl-deoxynivalenol (15-ADON), showing synergistic, additive and antagonistic effects, respectively (Alassane-Kpembé et al., 2013; Tajima et al., 2002; Yang et al., 2017). With regard to STE mycotoxin, in literature fewer interaction studies have been described with this mycotoxin. Results similar to those observed in our study were obtained by Zouaoui et al. (2016) in CHO-K1 cells exposed to STE + PAT and STE + BEA. In fact, both binary combinations produced synergism at low concentration affected followed by additive effects at higher concentrations. Nevertheless, antagonistic interactions were revealed in Hep3B cells exposed to the mixtures STE + citrinin (CTN) and STE + ochratoxin A (OTA) at concentrations ranging from  $10^{-8}$  to  $10^{-6}$  M (Anninou et al., 2014). As it can be noted, a great variety of results can be found in literature. A plausible explanation for these discrepancies could be that as individual toxins show large different effects depending on the incubation time, the selected cell line and the range of concentrations, also the differences in the interaction effects can be influenced by the same factors. Furthermore, the differences between mycotoxin interactions could be due to the different chemical structures, chemical properties and the competition or not for the same cell receptor. Thus, in light of all this, it can be concluded that it is difficult to predict the type of interaction only on the basis of the effect of individual mycotoxin. So, it is essential to study the mycotoxin mechanisms of action when they are alone and in combinations.



In the present study, a further analysis of the types of interactions occurred in the binary combinations NIV + STE was performed by using the Combenefit software. It implemented a surface plot approach, to visualize the map of interaction over all the tested dose pairs in a serially diluted manner. The two selected mathematical models revealed different effects when the mycotoxins were incubated in HepG2 cells. However, as data from literature demonstrate, differences between the nature of interactions in mycotoxin mixtures can be due not only to the type of cells exposed but, mainly, to the approach and the method for analysing the dose-response relationship in cell culture (Smith et al., 2017; Tammer et al., 2007). All the models that can be used present some advantages and limitations that were discussed in the recent review from Fouquier and Guedj (2015). Therefore, since there is still no reference methodology to characterize mycotoxin interactions, the analysis of their combinations may be facilitated by the collective use of different approaches (Fouquier and Guedj, 2015). Results obtained by using Combenefit software confirmed that HepG2 cell viability in the presence of STE is modulated by the presence of NIV; conversely, for mixtures containing STE there were no increases in overall cytotoxicity of such mixtures, compared to NIV alone (Fig. 4b). Furthermore, according to the Combenefit method, the nature of interactions produced by the binary combination NIV + STE tested was mainly additive/synergistic over the whole dose-response matrix, with the strongest synergistic effect showed by the combination  $0.31 \mu\text{M}$  NIV +  $12.5 \mu\text{M}$  STE. Although the isobologram method established the existence of additive and synergistic interactions, antagonism effects were revealed by all the three models incorporated in the Combenefit software (HSA, Loewe additive model and Bliss independence model). Antagonism, that is the predominant interaction produced when NIV is fixed at

the concentration of 1.26  $\mu\text{M}$ , may be due to a competition of the two mycotoxins for the same receptor, resulting in a lower effect than the expected. Similar results were obtained by Smith et al. (2017) in HepaRG cells exposed to the mixture NIV + T-2. More specifically, Smith et al. (2017) showed that the combination 0.6  $\mu\text{M}$  NIV + 0.04  $\mu\text{M}$  T-2 led to synergistic effects with the three models performed (response additivity model (RA), independent joint action model (IJA) and CI-isobologram model), whereas the two highest combinations (4  $\mu\text{M}$  NIV + 0.27  $\mu\text{M}$  T-2 and 10  $\mu\text{M}$  NIV + 0.67  $\mu\text{M}$  T-2) led to antagonistic, additive and synergistic effects on cell viability reduction according to the RA, IJA and CI-isobologram approaches, respectively, confirming the high impact of the concentrations tested as well as the relevance of the selected model when studying mycotoxin interactions.

Some studies have indicated that the cytotoxic effects of mycotoxins are related to the induction of oxidative stress (Ferrer et al., 2009). However, in the present study, following the exposure to NIV or STE individually, no significant differences in ROS production (Fig. 5a and b), as well as no alterations of  $\Delta\Psi\text{m}$  (Fig. 6a and b), were observed respect to control cells, with the exception for cells exposed to the highest STE concentration (3.13  $\mu\text{M}$ ), in which a significant increase of  $\Delta\Psi\text{m}$  was obtained. Although only limited reports about the ability of STE and NIV to alter  $\Delta\Psi\text{m}$  are available in literature, as regards the ability to induce oxidative stress, our findings are consistent with our previous study carried out on human neuroblastoma SH-SY5Y cells, in which STE exposure did not induce significant changes in early ROS production. However, a significant increase in the production of oxidizing species was observed after a longer exposure time (24 h) (Zingales et al., 2019). On the other hand, Gao et al. (2015) suggested that oxidative stress plays an important role in STE

cytotoxicity in HepG2 cells. However, they observed a significant increase only after the exposure at 3 and 6  $\mu\text{M}$  STE, concentrations higher than those tested in our study. Cellular stress responses have been shown to be caused by mixtures of NIV and DON in IEC-6 cells. In particular, a significant release of ROS was obtained by Del Regno et al. (2015) in IEC-6 cells after 20 h of NIV (0.5–5  $\mu\text{M}$ ) exposure, with a further increase following the simultaneous addition of DON. Instead, based on our results, a significant generation of ROS respect to control cells was induced only by the mixture containing the lowest concentrations of both mycotoxins NIV and STE after 45 min of exposure. The differences observed in ROS production respect to data reported by literature could be explained by the different mixture of mycotoxins tested and, mainly, by the different exposure time. In this study, ROS production was determined at short intervals of time and, in general, no changes were detected. However, in most of the similar studies mentioned before, assays have been performed after longer exposure times.

In conclusion, the present study confirms that the toxicity of a mixture of mycotoxins cannot be predicted solely on the basis of the effect of the individual compounds. The additive/synergistic behavior observed after the exposure of HepG2 cells to some of the mixtures may indicate a potential risk associated to the co-occurrence of these mycotoxins in food, which also indicates that the evaluation of the data from a single mycotoxin can lead to an underestimation of its toxicity. The development of predictive models for mycotoxin based on combination data is a valuable tool to estimate the true risk of harmfulness and establish regulatory standards about mixtures in food and feed. However, considering the wide presence of mycotoxins and other xenobiotics in food, this study focused on binary mixtures of NIV and STE does not reflect the real life

scenario, where more complex mixtures are found. Therefore, similar studies are required to evaluate the responses after the exposure of *in vitro* cell cultures to more complex mixtures. Furthermore, to understand the molecular mechanism underlying the interactive effects, a molecular-level investigation of mycotoxin-mycotoxin interaction is required in the future in order to develop more effective detoxification and remediation strategies aiming at understanding mycotoxin impact on human and animal health.

### **CRedit authorship contribution statement**

**Veronica Zingales:** Investigation, Validation, Formal analysis, Writing - original draft, Writing - review & editing. **Clarissa Fedeli:** Investigation, Validation, Formal analysis, Writing - original draft. **Mónica Fernández-Franzón:** Supervision. **Maria-José Ruiz:** Conceptualization, Supervision, Project administration, Funding acquisition.

### **Declaration of competing interest**

The authors declare that they have no known competing financial interests or personal relationships that could have appeared to influence the work reported in this paper.

### **Acknowledgments**

This research has been supported by the Spanish Ministry of Economy and Competitiveness (AGL2016-77610-R), the Generalitat Valenciana grant (Prometeo 2018/216) and the pre-doctoral research training program “Santiago Grisolia (GRISOLIAP/2018/092) CPI-18-117”.

---

## References

Alassane-Kpembi, I., Kolf-Clauw, M., Gauthier, T., Abrami, R., Abiola, F.A., Oswald, I.P., Puel, O., 2013. New insights into mycotoxin mixtures: the toxicity of low doses of Type B trichothecenes on intestinal epithelial cells is synergistic. *Toxicol. Appl. Pharmacol.* 272, 191–198.

Alassane-Kpembi, I., Puel, O., Oswald, I.P., 2015. Toxicological interactions between the mycotoxins deoxynivalenol, nivalenol and their acetylated derivatives in intestinal epithelial cells. *Arch. Toxicol.* 89, 1337–1346.

Alassane-Kpembi, I., Puel, O., Pinton, P., Cossalter, A.M., Chou, T.C., Oswald, I.P., 2017. Co-exposure to low doses of the food contaminants deoxynivalenol and nivalenol has a synergistic inflammatory effect on intestinal explants. *Arch. Toxicol.* 91, 2677–2687.

Anninou, N., Chatzaki, E., Papachristou, F., Pitiakoudis, M., Simopoulos, C., 2014. Mycotoxins' activity at toxic and sub-toxic concentrations: differential cytotoxic and genotoxic effects of single and combined administration of sterigmatocystin, ochratoxin A and citrinin on the hepatocellular cancer cell line Hep3B. *Int. J. Environ. Res. Publ. Health* 11, 1855–1872.

Arunachalam, C., Doohan, F.M., 2013. Trichothecene toxicity in eukaryotes: cellular and molecular mechanisms in plants and animals. *Toxicol. Lett.* 217, 149–158.

Baracca, A., Sgarbi, G., Solaini, G., Lenaz, G., 2003. Rhodamine 123 as a probe of mitochondrial membrane potential: evaluation of proton flux through F<sub>0</sub> during ATP synthesis. *Biochim. Biophys. Acta* 1606, 137–146.

Bennett, J.W., Klich, M., 2003. Mycotoxins. *Clin. Microbiol. Rev.* 16, 497–516.

Bensassi, F., Gallerne, C., Sharaf el Dein, O., Hajlaoui, M.R., Lemaire, C., Bacha, H., 2014. In vitro investigation of toxicological interactions between the fusariotoxins deoxynivalenol and zearalenone. *Toxicon* 84, 1–6.

Berek, L., Petri, I.B., Mesterhazy, A., Teren, J., Molnar, J., 2001. Effects of mycotoxins on human immune functions in vitro. *Toxicol. Vitro* 15, 25–30.

Bouaziz, C., Bouslimi, A., Kadri, R., Zaied, C., Bacha, H., Abid-Essefi, S., 2013. The in vitro effects of zearalenone and T-2 toxins on Vero cells. *Exp. Toxicol. Pathol.* 65, 497–501.

Bouslimi, A., Bouaziz, C., Ayed-Boussema, I., Hassen, W., Bacha, H., 2008. Individual and combined effects of ochratoxin A and citrinin on viability and DNA fragmentation in cultured Vero cells and on chromosome aberrations in mice bone marrow cells. *Toxicology* 251, 1–7.

Bunger, J., Westphal, G., Monnich, A., Hinnendahl, B., Hallier, E., Muller, M., 2004. Cytotoxicity of occupationally and environmentally relevant mycotoxins. *Toxicology* 202, 199–211.

Cavaliere, C., Foglia, P., Pastorini, E., Samperi, R., Lagana, A., 2005. Development of a multiresidue method for analysis of major *Fusarium* mycotoxins in corn meal using liquid chromatography/tandem mass spectrometry. *Rapid Commun. Mass Spectrom.* 19, 2085–2093.

Chidambaram, J.D., Prajna, N.V., Larke, N., Macleod, D., Srikanthi, P., Lanjewar, S., Shah, M., Lalitha, P., Elakkiya, S., Burton, M.J., 2017. In vivo confocal microscopy appearance of *Fusarium* and *Aspergillus* species in fungal keratitis. *Br. J. Ophthalmol.* 101, 1119–1123.

Chou, T.C., 2006. Theoretical basis, experimental design, and computerized simulation of synergism and antagonism in drug combination studies. *Pharmacol. Rev.* 58, 621–681.

Chou, T.C., Talalay, P., 1984. Quantitative analysis of dose-effect relationships: the combined effects of multiple drugs or enzyme inhibitors. *Adv. Enzym. Regul.* 22, 27–55.

Del Regno, M., Adesso, S., Popolo, A., Quaroni, A., Autore, G., Severino, L., Marzocco, S., 2015. Nivalenol induces oxidative stress and increases deoxynivalenol pro-oxidant effect in intestinal epithelial cells. *Toxicol. Appl. Pharmacol.* 285, 118–127.

Di Veroli, G.Y., Fornari, C., Wang, D., Mollard, S., Bramhall, J.L., Richards, F.M., Jodrell, D.I., 2016. Combenefit: an interactive platform for the analysis and visualization of drug combinations. *Bioinformatics* 32, 2866–2868.

EFSA, 2013a. European food safety authority (efsa) panel on contaminants in food chain (CONTAM), scientific opinion on risks for animal and public health related to the presence of nivalenol in food and feed. *EFSA J.* 11 (6), 3262.

EFSA, 2013b. European food safety authority (efsa) panel on contaminants in food chain (CONTAM), scientific opinion on the risk for public and animal health related to the presence of sterigmatocystin in food and feed. *EFSA J.* 11 (6), 3254.

FAOSTAT, 2013. Food Balance Sheet. <http://faostat.fao.org>.

Fernandez-Blanco, C., Font, G., Ruiz, M.J., 2016. Interaction effects of enniatin B, deoxinivalenol and alternariol in Caco-2 cells. *Toxicol. Lett.* 241, 38–48.

Ferreira Lopes, S., Vacher, G., Ciarlo, E., Savova-Bianchi, D., Roger, T., Niculita-Hirzel, H., 2017. Primary and immortalized human respiratory cells display different patterns of cytotoxicity and cytokine release upon exposure to deoxynivalenol, nivalenol and Fusarenon-X. *Toxins (Basel)* 9.

Ferrer, E., Juan-Garcia, A., Font, G., Ruiz, M.J., 2009. Reactive oxygen species induced by beauvericin, patulin and zearalenone in CHO-K1 cells. *Toxicol. Vitro* 23, 1504–1509.

Fouquier, J., Guedj, M., 2015. Analysis of drug combinations: current methodological landscape. *Pharmacol. Res. Perspect* 3, e00149.

Gao, W., Jiang, L., Ge, L., Chen, M., Geng, C., Yang, G., Li, Q., Ji, F., Yan, Q., Zou, Y., Zhong, L., Liu, X., 2015. Sterigmatocystin-induced oxidative DNA damage in human liver-derived cell line through lysosomal damage. *Toxicol. Vitro* 29, 1–7.

Gomez-Lechon, M.J., Tolosa, L., Conde, I., Donato, M.T., 2014. Competency of different cell models to predict human hepatotoxic drugs. *Expet Opin. Drug Metabol. Toxicol.* 10, 1553–1568.

Grenier, B., Oswald, I., 2011. Mycotoxin co-contamination of food and feed: meta-analysis of publications describing toxicological interactions. *World Mycotoxin J.* 4, 285–313.

Huang, S., Wang, J., Xing, L., Shen, H., Yan, X., Wang, J., Zhang, X., 2014. Impairment of cell cycle progression by sterigmatocystin in human pulmonary cells in vitro. *Food Chem. Toxicol.* 66, 89–95.

IARC, 1987. Overall Evaluations of Carcinogenicity: an Updating of IARC Monographs Volumes 1 to 42. Supplement 7. Lyon, France.

Kawai, K., Nakamaru, T., Nozawa, Y., Maebayashi, Y., Yamazaki, M., Natori, S., 1984. Inhibitory effect of sterigmatocystin and 5,6-dimethoxysterigmatocystin on ATP synthesis in mitochondria. *Appl. Environ. Microbiol.* 48, 1001–1003.



LeCluyse, E.L., 2001. Human hepatocyte culture systems for the in vitro evaluation of cytochrome P450 expression and regulation. *Eur. J. Pharmaceut. Sci.* 13, 343–368.

Liu, Y., Du, M., Zhang, G., 2014. Proapoptotic activity of aflatoxin B1 and sterigmatocystin in HepG2 cells. *Toxicol. Rep.* 1, 1076–1086.

Luongo, D., De Luna, R., Russo, R., Severino, L., 2008. Effects of four *Fusarium* toxins (fumonisin B(1), alpha-zearalenol, nivalenol and deoxynivalenol) on porcine whole- blood cellular proliferation. *Toxicon* 52, 156–162.

Luongo, D., Severino, L., Bergamo, P., De Luna, R., Lucisano, A., Rossi, M., 2006. Interactive effects of fumonisin B1 and alpha-zearalenol on proliferation and cytokine expression in Jurkat T cells. *Toxicol. Vitro* 20, 1403–1410.

Nagashima, H., 2018. Deoxynivalenol and nivalenol toxicities in cultured cells: a review of comparative studies. *Food Saf. (Tokyo)* 6, 51–57.

Olson, H., Betton, G., Robinson, D., Thomas, K., Monro, A., Kolaja, G., Lilly, P., Sanders, J., Sipes, G., Bracken, W., Dorato, M., Van Deun, K., Smith, P., Berger, B., Heller, A., 2000. Concordance of the toxicity of pharmaceuticals in humans and in animals. *Regul. Toxicol. Pharmacol.* 32, 56–67.

Prosperini, A., Font, G., Ruiz, M.J., 2014. Interaction effects of *Fusarium* enniatins (A, A1, B and B1) combinations on in vitro cytotoxicity of Caco-2 cells. *Toxicol. Vitro* 28, 88–94.

Rocha, O., Ansari, K., Doohan, F.M., 2005. Effects of trichothecene mycotoxins on eukaryotic cells: a review. *Food Addit. Contam.* 22, 369–378.

Ruiz-Leal, M., George, S., 2004. An in vitro procedure for evaluation of early stage oxidative stress in an established fish cell line applied to investigation of PHAH and pesticide toxicity. *Mar. Environ. Res.* 58, 631–635.

Ruiz, M.J., Festila, L.E., Fernández, M., 2006. Comparison of basal cytotoxicity of seven carbamates in CHO-K1 cells. *Environ. Toxicol. Chem.* 88, 345–354.

Ruiz, M.J., Franzova, P., Juan-Garcia, A., Font, G., 2011a. Toxicological interactions between the mycotoxins beauvericin, deoxynivalenol and T-2 toxin in CHO-K1 cells in vitro. *Toxicol.* 58, 315–326.

Ruiz, M.J., Macakova, P., Juan-Garcia, A., Font, G., 2011b. Cytotoxic effects of mycotoxin combinations in mammalian kidney cells. *Food Chem. Toxicol.* 49, 2718–2724.

Segvic Klaric, M., 2012. Adverse effects of combined mycotoxins. *Arh. Hig. Rada. Toksikol.* 63, 519–530.

Serrano, A.B., Font, G., Ruiz, M.J., Ferrer, E., 2012. Co-occurrence and risk assessment of mycotoxins in food and diet from Mediterranean area. *Food Chem.* 135, 423–429.

Smith, M.C., Hymery, N., Troadec, S., Pawtowski, A., Coton, E., Madec, S., 2017. Hepatotoxicity of fusariotoxins, alone and in combination, towards the HepaRG human hepatocyte cell line. *Food Chem. Toxicol.* 109, 439–451.

Smith, M.C., Madec, S., Troadec, S., Coton, E., Hymery, N., 2018. Effects of fusariotoxin co-exposure on THP-1 human immune cells. *Cell Biol. Toxicol.* 34, 191–205.

Speijers, G.J., Speijers, M.H., 2004. Combined toxic effects of mycotoxins. *Toxicol. Lett.* 153, 91–98.

Tajima, O., Schoen, E.D., Feron, V.J., Groten, J.P., 2002. Statistically designed experiments in a tiered approach to screen mixtures of *Fusarium* mycotoxins for possible interactions. *Food Chem. Toxicol.* 40, 685–695.

Tammer, B., Lehmann, I., Nieber, K., Altenburger, R., 2007. Combined effects of mycotoxin mixtures on human T cell function. *Toxicol. Lett.* 170, 124–133.

Wan, L.Y., Turner, P.C., El-Nezami, H., 2013. Individual and combined cytotoxic effects of *Fusarium* toxins (deoxynivalenol, nivalenol, zearalenone and fumonisins B1) on swine jejunal epithelial cells. *Food Chem. Toxicol.* 57, 276–283.

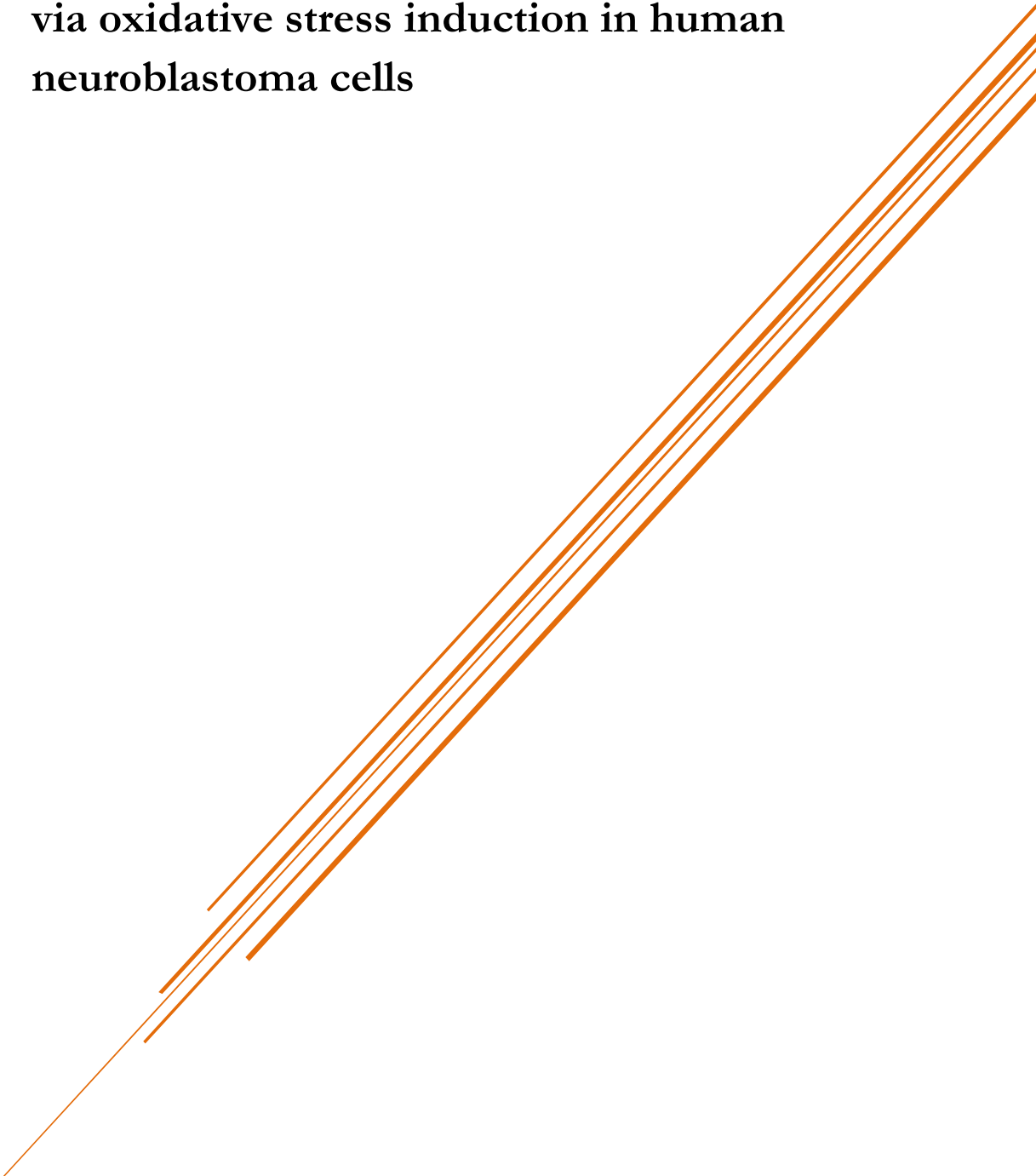
Yang, Y., Yu, S., Tan, Y., Liu, N., Wu, A., 2017. Individual and combined cytotoxic effects of Co-occurring deoxynivalenol family mycotoxins on human gastric epithelial cells. *Toxins (Basel)* 9.

Zingales, V., Fernandez-Franzon, M., Ruiz, M.J., 2019. Sterigmatocystin-induced cytotoxicity via oxidative stress induction in human neuroblastoma cells. *Food Chem. Toxicol.* 136, 110956.

Zouaoui, N., Mallebrera, B., Berrada, H., Abid-Essefi, S., Bacha, H., Ruiz, M.J., 2016. Cytotoxic effects induced by patulin, sterigmatocystin and beauvericin on CHO-K1 cells. *Food Chem. Toxicol.* 89, 92–103.



## **3.2. Sterigmatocystin-induced cytotoxicity via oxidative stress induction in human neuroblastoma cells**





Food and Chemical Toxicology

**Sterigmatocystin-induced cytotoxicity via oxidative stress induction in human neuroblastoma cells**

Veronica Zingales\*, Mónica Fernández-Franzón, Maria-José Ruiz

Laboratory of Food Chemistry and Toxicology, Faculty of Pharmacy, University of

Valencia, Av. Vicent Andrés Estellés s/n, 46100, Valencia, Spain

\*Corresponding author. Laboratory of Toxicology, Faculty of Pharmacy, University of Valencia, Av. Vicent Andrés Estellés, s/n, 46100, Burjassot, Valencia, Spain. *E-mail address:* [vezin@uv.es](mailto:vezin@uv.es) (V. Zingales).

### **Abstract**

Sterigmatocystin (STE) is a mycotoxin produced by fungi of the genus *Aspergillus*. Considering that the effect of STE on neuronal system has not been well studied, the aim of the present study consists to investigate the cytotoxic effects of STE in human neuroblastoma (SH-SY5Y) cells. Moreover, the role of oxidative stress and intracellular defense systems was assessed by evaluating reactive oxygen species (ROS) generation, lipid peroxidation (LPO) and antioxidant no-enzymatic (GSH) levels and enzymatic (GPx, GST, CAT and SOD) activity. Our results revealed that STE decreased cell viability in a dose and time-dependent manner. Furthermore, after 24 h of exposure, STE induced an increase in ROS generation and LPO at all concentrations tested (0.78, 1.56 and 3.12  $\mu\text{M}$ ), as well as a depletion of GSH levels, an increase in GSSG content and a decrease in GSH/GSSG ratio at the highest concentrations. The activity of all antioxidant enzymes resulted to be also decreased. Additionally, an enhance of the oxidative damage was caused by BSO, a GSH depletor, while NAC, a GSH precursor, showed a scavenger activity. Our findings suggest that STE could injure SH-SY5Y cells via oxidative stress and highlight the antioxidant role of the glutathione system.

**Keywords:** Sterigmatocystin, Cytotoxicity, Oxidative stress, Glutathione, SH-SY5Y cells.



## 1. Introduction

Mycotoxins are toxic secondary metabolites of low-molecular-weight produced by filamentous fungi. They are characterized by their potential to cause adverse health effects in humans and animals following consumption of contaminated foods or feedstuffs (Bennett and Klich, 2003; Hussein and Brasel, 2001). The high prevalence of mycotoxin-contaminated food has led to focus the scientific attention on the study of mycotoxins (Marin et al., 2013; Murugesan et al., 2015). In addition to the serious public health problems produced by these fungal toxins, significant economic losses are also associated with mycotoxin contamination due to decreased market value of contaminated food (Wu, 2006). Sterigmatocystin (STE) is a mycotoxin produced mainly by fungi belonging to the genus *Aspergillus*. It was isolated by the first time in 1954 from *A. vesicolor* cultures (Diaz Nieto et al., 2018). Although in the literature only limited information is available on the occurrence of STE in food and feed, it has been reported to occur in grains and grain-based products following fungal contamination during the post-harvest stage (Versilovskis et al., 2007). Sterigmatocystin has been occasionally reported to occur also in cheese, green coffee beans, spices, nuts and beer (EFSA, 2013; Versilovskis and De Saeger, 2010; Versilovskis et al., 2009). Acute toxicity, cytotoxicity, mutagenicity and carcinogenicity have been associated with STE exposure. Many studies showed that STE is able to induce tumours in animal models (Huang et al., 2004; Xing et al., 2007). In Mongolian gerbils it has been demonstrated that long-term administration of STE can induce intestinal metaplasia in the gastric mucosa (Kusunoki et al., 2011; Ma et al., 2003). Recently, STE was detected also in urine and plasma of patients with documented hepatocellular carcinoma (Cao et al., 2018). In light of all this, STE has been classified in the Group 2B (possible

human carcinogen) by the International Agency for Research on Cancer (IARC, 1987; Pitt et al., 2012). In vitro studies demonstrated that STE exerts its cytotoxic effects through different mechanisms of action. Cell cycle arrest and DNA damage may represent two of the common toxic effects of STE (Anninou et al., 2014; Huang et al., 2014; Liu et al., 2014). Gao et al. (2015) suggested that oxidative stress plays a crucial role in STE-induced DNA damage in HepG2 cells. Oxidative stress occurs when the production of reactive oxygen species (ROS) exceeds the antioxidant capacity of cells to scavenge ROS. As consequent effect, lipid peroxidation, DNA fragmentation, protein oxidation and, in presence of elevated ROS levels, genome changes are induced (Cooke et al., 2003; Devasagayam et al., 2004). However, mammalian cells are equipped with a protective endogenous antioxidant system formed by non-enzymatic antioxidant such as the glutathione (GSH) and enzymatic protective systems such as glutathione peroxidase (GPx), glutathione S-transferase (GST), superoxide dismutase (SOD) and catalase (CAT). The GSH together with its coupled antioxidant enzyme system represent the first line of defense against the damaging effects of oxidative stress. The GSH can act non-enzymatically, as a radical scavenger, or as co-substrate for enzymatic degradation of toxic substances. In each case, GSH is oxidized to glutathione disulphide (GSSG). The ratio GSH/GSSG in mitochondria is approximately 10:1 under normal condition (Meredith and Reed, 1982). The relationship between the reduced and oxidized status of GSH is considered an index of cellular redox status and a biomarker of oxidative damage. In fact, during oxidative stress an increase in GSSG and a decrease in the reduced form are observed. The GSH depletion to about 15–20% of total GSH levels can impair the cellular defense system and lead to cell injury and death (Reed, 1990). An important role is also played by

the GSH-related enzymes. The GPx catalyses the conversion of GSH to GSSG and competes with CAT in the reduction of hydrogen peroxide (H<sub>2</sub>O<sub>2</sub>) to H<sub>2</sub>O. Working in concert with these H<sub>2</sub>O<sub>2</sub>-removing enzymes, SOD is involved in the dismutation of superoxide radicals to O<sub>2</sub> and H<sub>2</sub>O<sub>2</sub>. Finally, GSH also works as the substrate for GST, a detoxifying enzyme that removes toxic compounds by binding with GSH.

The role of GSH can be evaluated in in vitro system by addition of chemical compounds able to increase or decrease the rate of its synthesis. In particular, N-acetyl-cysteine (NAC) represents a GSH precursor because it is a source of sulfhydryl groups. On the other hand, D-L-buthionine-(S,R)-sulfoximine (BSO) causes GSH depletion, acting as a specific inhibitor of the enzyme that catalyses the synthesis of GSH in the cytosol, the  $\gamma$ -glutamylcysteine synthetase (GLC).

Considering the role of oxidative stress and lipid peroxidation in the development of neurodegenerative disorders, like Alzheimer's disease and Parkinson's disease (Burchell et al., 2010; Butterfield and Lauderback, 2002; Mancuso et al., 2007), environmental and dietary factors that might be implicated in oxidative stress and neurodegeneration are of great interest.

In light of this, the aim of the present study was to investigate the effects of STE on cell viability and its role on the oxidative stress in human neuroblastoma cells using the SH-SY5Y cell line. The choice of the cell line was based on the evidence that they represent one of the most common in vitro model used for assessing the neurological effects of toxic substances, including mycotoxins (Axelsson et al., 2006; Hayashi et al., 2018; Stockmann-Juvala et al., 2006). In fact, these cells of human origin can contribute to understand the

molecular mechanisms of toxicity in cellular levels similarly as in experimental animal models. Additionally, the effect of the pre-treatments with NAC or BSO on the antioxidant system was also evaluated.

## 2. Material and methods

### 2.1. Reagents

The reagent grade chemicals and cell culture compounds used, namely culture medium DMEM Ham's-F12, penicillin, streptomycin, trypsin/EDTA solutions, phosphate buffer saline (PBS), fetal bovine serum (FBS), neutral red (NR) dye, dimethyl sulfoxide (DMSO), thiobarbituric acid (TBA), deferoxamine mesylate salt (DFA), di-ter-butylmethylphenol (BHT), 1,1,3,3-tetramethoxypropan, 2',7'-dichlorodihydrofluorescein diacetate (H<sub>2</sub>-DCFDA),  $\beta$ -nicotinamide adenine dinucleotide phosphate ( $\beta$ -NADPH), sodium azide (NaN<sub>3</sub>), GSH, GSSG, glutathione reductase (GR), NAC, BSO, o-phthaldialdehyde (OPT), N-ethylmaleimide (NEM), t-octylphenoxypolyethoxyethanol (Triton-X 100), 1-chloro-2,4-dinitrobenzene (CDNB), ethylenediaminetetraacetic acid (EDTA), tris hydroxymethyl aminomethane (Tris), 4',6-diamidine-2'-phenylindole dihydrochloride (DAPI) and H<sub>2</sub>O<sub>2</sub> were from Sigma-Aldrich (St. Louis Mo. USA). Methanol (MeOH) was from VWR International (LLC, Pennsylvania, USA). Standard of the selected mycotoxin STE (MW: 324.28 g/mol) was purchased from Sigma-Aldrich (St. Louis Mo. USA). Chemical structure of STE is shown in Fig. 1. Stock solutions of the mycotoxin was prepared in methanol and maintained at -20°C.

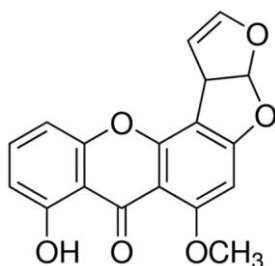


**Fig. 1.** Chemical structure of sterigmatocystin.

## 2.2. Cell culture and treatment

Human neuroblastoma (SH-SY5Y) cells were cultured in DMEM Ham's-F12 medium supplemented with 10% FBS, 100 U/mL penicillin and 100 mg/mL streptomycin. The incubation conditions were pH 7.4, 5% CO<sub>2</sub> at 37 °C and 95% air atmosphere at constant humidity. The medium was changed every 2–3 days. The final STE concentrations tested were achieved by adding STE solutions to the culture medium with a final methanol concentration  $\leq 1\%$  (v/v). Appropriate controls containing the same amount of solvents were included in each experiment.

## 2.3. In vitro cytotoxicity

The neutral red (NR) assay was performed to determine cell proliferation. The NR assay is based on the capability of the viable cells to incorporate and retain the NR dye into their lysosomes. It was performed as described by Ruiz et al. (2006). For this endpoint bioassay, the SH-SY5Y cells were plated in 96-well microplates at a density of  $3 \times 10^4$  cells/well. After 48 h, when the cells reached 80% of confluence, the culture medium was replaced with fresh medium

containing eight serial dilutions (serial dilution factor=2) of the mycotoxin ranging from 25 to 0.19  $\mu\text{M}$ . The STE was exposed during 24, 48 and 72 h. During the exposure time, neither the medium nor the mycotoxin were replenished.

For NR assay, the NR solution was pre-incubated overnight at 37 °C and filtered prior to use through a 0.22  $\mu\text{m}$  membrane filter, in order to remove the precipitates of dye crystals. After 24, 48 and 72 h of exposure to STE, the medium was removed and 200  $\mu\text{l}$  of freshly prepared NR solution (50  $\mu\text{g}/\text{ml}$ ) was added to each well and the plates returned to the incubator at 37 °C, 5%  $\text{CO}_2$ . After 3 h of incubation, the NR solution was removed and cells were fixed with formaldehyde –  $\text{CaCl}_2$  solution, and then extracted by adding acetic acid – ethanol solution. Plates were gently shaken for 5 min to achieve the complete dissolution.

The absorbance was measured at 540 nm using an automatic ELISA plate reader (MultiSkanEX, Labsystem, Helsinki, Finland). Cell viability was expressed as a percentage relative to the solvent control (1% MeOH). Two independent experiments for each time of exposure were conducted. The mean 50% inhibitory concentration (IC50) values were calculated using SigmaPlot version 11 (Systat Software Inc., GmbH, Germany).

#### 2.4. *Intracellular ROS generation*

Early intracellular ROS production was monitored in SH-SY5Y cells by adding  $\text{H}_2\text{-DCFDA}$ . The  $\text{H}_2\text{-DCFDA}$  is taken up by cells and then deacetylated by intracellular esterases; the resulting non-fluorescent 2',7'-dichlorodihydrofluorescein ( $\text{H}_2\text{-DCF}$ ) is switched to highly fluorescent

dichlorofluorescein (DCF) when oxidized by ROS. The generation of ROS was monitored according to Ruiz-Leal and George (2004). Briefly,  $3 \times 10^4$  cells/well were seeded in a 96-well black culture microplate. Once the cells reach 90% confluence, the culture medium was replaced and cells were loaded with  $20 \mu\text{M}$   $\text{H}_2\text{-DCFDA}$  in fresh medium for 20 min. Subsequently  $\text{H}_2\text{-DCFDA}$  was removed and  $200 \mu\text{l}$ /well of fresh medium, 1% MeOH (control) or medium with STE (0.78, 1.56 and  $3.12 \mu\text{M}$ ) was added. The selection of the three different concentrations assayed is correlated with those found in food and were selected according to the previous cytotoxic assays carried out. All of these concentrations resulted to be no toxic to SH-SY5Y and below the  $\text{IC}_{50}$  values obtained. Increases in fluorescence were measured on a Wallace Victor2, model 1420 multilabel counter (PerkinElmer, Turku, Finland), at intervals up to 2 h at excitation/emission wavelengths of 485/535 nm. Results are expressed as increase in fluorescence respect to solvent control. Determinations were performed in two independent experiments with 24 replicates each.

Additionally, ROS generation after 24 h of STE exposure was evaluated by using CellROX™ Deep Red Reagent (C10422, Life Technologies), a fluorogenic probe designed to reliably measure ROS in living cells. In a reduced state, the cell-permeable CellROX Deep Red dye is no fluorescent and, upon oxidation, exhibits excitation/emission maxima at 640/665 nm. The assay was performed as described by Lin et al. (2012), with some modifications. Briefly, a number of  $7 \times 10^5$  cells/well were seeded in six-well plates. After 24 h of exposure at STE (0.78, 1.56 and  $3.12 \mu\text{M}$ ), SH-SY5Y cells were trypsinized and CellROX Deep Red Reagent was added at a final concentration of  $5 \mu\text{M}$  in fresh medium to the cells. After incubation for 30 min at  $37^\circ\text{C}$  in the dark, the medium was removed and the cells were washed three times with PBS. Three independent

experiments were carried out and 10,000 live cells were acquired and analysed by a BD LSRFortessa (BD Biosciences) flow cytometry. Dead cells were not considered by staining with DAPI (20 ng/ml).

### 2.5. *Lipid peroxidation assay*

Lipid peroxidation (LPO) assay was carried out by determining the formation of reactive thiobarbituric acid reactive substances (TBARS), according to Ferrer et al. (2009). The TBARS allows to determine the production of a red adduct between TBA and malondialdehyde (MDA), which is a biomarker used to prove that the LPO process has occurred. Briefly,  $7 \times 10^5$  cells/well were seeded in six-well plates. Once the cells reached 90% confluence, cells were exposed to 0.78, 1.56 and 3.12  $\mu\text{M}$  STE for 24 h. Then, the medium was removed and cells were washed with PBS, homogenized in 150mM sodium phosphate buffer ( $\text{NaH}_2\text{PO}_4$ ) pH 7.4 and lysate with the Ultra-Turrax T8 IKA®-WERKE. Immediately, cells were boiled at 100 °C in water bath for 20 min under acid condition in the presence of 0.5% TBA, 1.5mM DFA and 3.75% BHT. After that, the samples were placed on ice for 5 min and centrifuged at 2880 g for 15 min. The absorbance was measured at 532 nm. Two independent experiments were conducted. Results were expressed as ng of MDA/mg of protein measured by the Lowry method.

### 2.6. *GSH determination*

Determination of GSH and GSSG was assayed according to Maran et al. (2009). Briefly,  $7 \times 10^5$  cells/well were seeded in six-well plates. The cells were exposed to different treatments: (a) fresh medium (medium DMEM Ham's-F12 with 10% FBS), (b) BSO pre-treatment (medium DMEM Ham's-F12 with 10%



FBS plus 60  $\mu\text{M}$  BSO) and (c) NAC pre-treatment (medium DMEM Ham's-F12 with 10% FBS plus 1mM NAC). Once the cells reached 90% confluence, the culture medium was replaced with fresh medium containing different concentrations of STE (0.78, 1.56 and 3.12  $\mu\text{M}$ ) for 24 h of incubation. Afterwards, the medium was removed and cells were washed with PBS and then homogenized in 0.25 ml of 20mM Tris and 0.1% Triton.

Concentrations of GSH and GSSG were determined using the microplate reader Wallace Victor2, model 1420 multilabel counter (PerkinElmer, Turku, Finland) with excitation and emission wavelength of 345 and 424 nm, respectively. The GSH and GSSG levels were expressed in  $\mu\text{g}/\text{mg}$  proteins. Determinations were performed in two independent experiments with 4 replicates each.

### 2.7. *Determination of enzymatic activities*

To determine the scavenging procedures in SH-SY5Y cells exposed to STE, the GPx, GST, CAT and SOD activities were determined at the concentrations previously selected (0.78, 1.56 and 3.12  $\mu\text{M}$ ). For these assays,  $7 \times 10^5$  cells/well were seeded in six-well plates. The cells were exposed to different treatments: (a) fresh medium (medium DMEM Ham's-F12 with 10% FBS), (b) BSO pre-treatment (medium DMEM Ham's-F12 with 10% FBS plus 60  $\mu\text{M}$  BSO) and (c) NAC pre-treatment (medium DMEM Ham's-F12 with 10% FBS plus 1mM NAC). After cells achieved the 90% confluence, cells were treated with STE for 24 h. Then, the medium was removed and cells were homogenized in 0.1M phosphate buffer pH 7.5 containing 2mM EDTA.

The GPx activity was assayed spectrophotometrically using H<sub>2</sub>O<sub>2</sub> as substrate for Se-dependent peroxidase activity of GPx by following oxidation of NADPH during the first 5 min in a coupled reaction with GR, as described by Maran et al. (2009). In 1ml final volume, the reaction mixture contained 500 µl of 0.1M phosphate buffer, pH 7.5 with 4mM NaN<sub>3</sub> and 2mM EDTA, 100 µl of 20mM GSH, 250 µl of ultrapure water, 2 U freshly prepared GR, 20 µl of 10mM NADPH and 50 µl of 5mM H<sub>2</sub>O<sub>2</sub>. Fifty microliter of homogenized cell sample was added to the reaction mixture. One unit of GPx will reduce 1 µmol of GSSG per min at pH 7.5. The GPx enzymatic activity was calculated by using a molar absorptivity of NADPH (6.22mM<sup>-1</sup> cm<sup>-1</sup>) and expressed as µmol of NADPH oxidized/min/mg of protein. Assays were conducted at 25 °C in a thermocirculator of PerkinElmer UV/vis spectrometer Lambda 2 version 5.1. The absorbance was measured at 340 nm.

The GST activity was determined by following the conjugation of GSH with CDNB during 5 min, according to the method of Maran et al. (2009). The reaction mixture contained in a final volume of 1 ml: 825 µl of 0.1M Na/K phosphate buffer at pH 6.5, 100 µl of 20mM GSH, 25 µl of 50mM CDNB dissolved in ethanol and 50 µl of homogenized cell sample. The GST activity was expressed as mol of product formed/min/mg of protein using a molar absorptivity of CDNB (9.6mM<sup>-1</sup> cm<sup>-1</sup>). Enzymatic activity was assayed in a thermocirculator of PerkinElmer UV/vis spectrometer Lambda 2 version 5.1. The absorbance was measured at 340 nm.

The CAT activity was measured according to Ueda et al. (1990). Briefly, 100 µl of homogenized cell sample was mixed with 500 µl of 0.5M potassium phosphate buffer at pH 7.2 and 400 µl of 40mM H<sub>2</sub>O<sub>2</sub>. The rate of enzymatic

decomposition of H<sub>2</sub>O<sub>2</sub> was determined as absorbance decrements at 240 nm for 3 min at 30 °C with a spectrophotometer (Super Aquarius CECIL 9500 CE). The CAT activity was calculated by using the molar absorptivity of H<sub>2</sub>O<sub>2</sub> (43.6mM<sup>-1</sup> cm<sup>-1</sup>) and expressed as μmol H<sub>2</sub>O<sub>2</sub>/min/mg of protein.

The SOD activity was determined using the Ransod kit (Randox Laboratories, United Kingdom) adapted for 1.5 ml cuvettes. The SOD destroys the free radical superoxide by converting it to peroxide. The SOD activity was monitored at 505 nm during 3 min at 37 °C with a spectrophotometer (PerkinElmer UV/Vis Lambda 2 version 5.1). The SOD results were expressed as units of SOD per mg protein. All the enzyme determinations were performed in triplicate.

#### 2.8. *Pre-treatment with BSO or NAC*

To study the effects of BSO and NAC on the reduction of the intracellular GSH content and on the enzymatic activities, cells were pretreated with BSO or NAC prior to STE exposure. Approximately, 7×10<sup>5</sup> cells/well were exposed to 60 μM BSO or 1mM NAC dissolved in medium for 48 h followed by exposure to freshly prepared medium containing STE at the designated concentrations (0.78, 1.56 and 3.12 μM) for 24 h. Cells containing 1% MeOH in the medium were used as control. After 24 h of exposure, the GSH content and enzymatic activities were determined as previously described. Comparison between cells exposed to different concentration of STE in fresh medium and BSO or NAC pre-treatment were performed.

### 2.9. *Determination of total protein*

The protein content was determined by the Bio-Rad DC Protein Assay, catalogue number 5000116. Protein concentration ( $\mu\text{g}/\text{ml}$ ) was measured at 690 nm.

### 2.10. *Statistical analysis*

Statistical analysis of data was carried out using GraphPad Prism version 7 (GraphPad Software, California, USA), statistical software package. Data were expressed as mean  $\pm$  SEM of different independent experiments. The statistical analysis of the results was performed by Student's t - test for paired samples. Difference between groups were analysed statistically with one-way ANOVA followed by the Tukey HDS post-hoc test for multiple comparisons. The difference level of  $p \leq 0.05$  was considered statistically significant.

## 3. Results

### 3.1. *In vitro cytotoxicity*

The cytotoxic effect of STE on SH-SY5Y cells was evaluated by NR assay over 24, 48 and 72 h in order to determine the molar concentration of mycotoxin able to reach the  $\text{IC}_{50}$ . Cells exposed to STE mycotoxin revealed a decrease in cell viability in a time and concentration- dependent manner (data not shown). Our results indicate that cells treated with STE showed at 24 h an  $\text{IC}_{50} = 19.26 \pm 39.53 \mu\text{M}$ ; at 48 h an  $\text{IC}_{50} = 2.41 \pm 1.47 \mu\text{M}$  and at 72 h an  $\text{IC}_{50} = 0.48 \pm 0.09 \mu\text{M}$ . Sterigmatocystin decreases cell proliferation from 8% to 67%, from 18% to 72% and from 20% to 91% after 24, 48 and 72 h respectively. These results allowed setting the concentrations for the following assays.

---

### 3.2. Intracellular ROS generation

Considering the results of cytotoxicity, the role of oxidative stress was decided to investigate. First of all, production of ROS in response to 0.78, 1.56 and 3.12  $\mu\text{M}$  STE was studied. The SH-SY5Y cells were exposed to STE from 0 to 120 min and the production of ROS was determined by DCFH-DA assay (Fig. 2). Results obtained demonstrated that SH-SY5Y cells treated with STE did not show any significant variation in the early production of ROS depending on the time or concentrations of exposure when compared to the basal rate. However, a significant ( $p \leq 0.05$ ) increase of oxidizing species production was observed after 24 h of STE exposure using the fluorogenic probe CellROX Deep Red Reagent starting from the lowest concentration (Fig. 3a). Taken together, our results showed that generation of ROS was dependent on concentration of STE only when SH-SY5Y cells were exposed to STE for 24 h. An example of the dot plots representative of the control and the cells exposed to the highest concentration tested (3.12  $\mu\text{M}$ ) of STE can be observed in Fig. 3b–c.

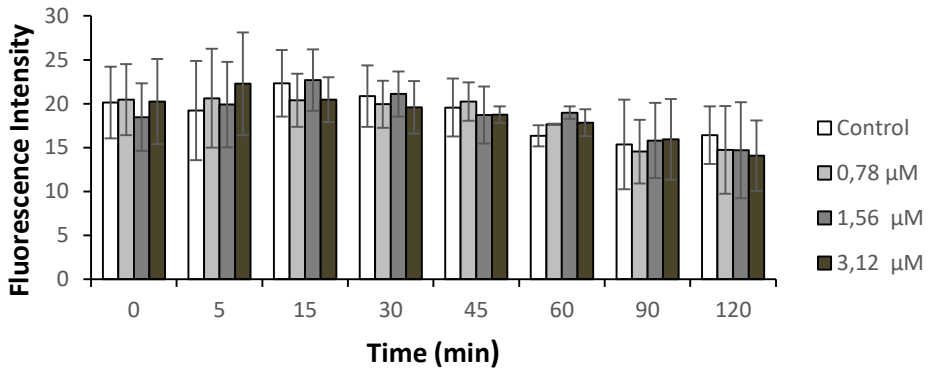


**Fig. 2.** Time dependence of ROS-induced fluorescence in SH-SY5Y cells exposed to STE at 0.78, 1.56 and 3.12  $\mu\text{M}$ . The H2-DCFDA was added to SH-SY5Y cells and left for 20 min previously to STE addition from 0 to 120 min. Results are expressed as mean  $\pm$  SEM (n=2). There were no significant differences between the concentrations and the control.

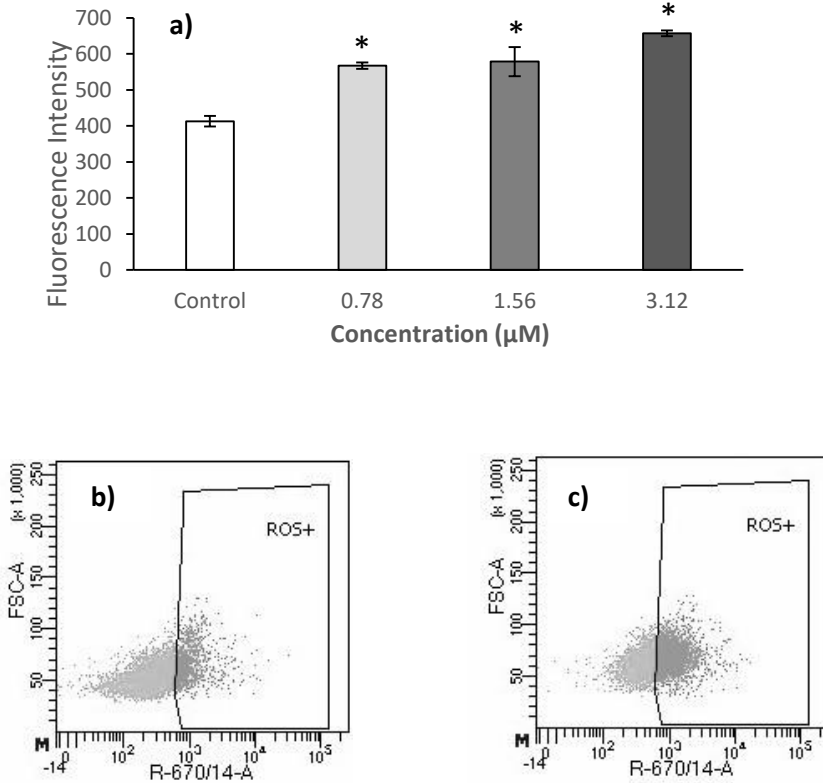


**Fig. 3.** The ROS-induced fluorescence in SH-SY5Y cells exposed to STE at 0.78, 1.56 and 3.12 μM during 24 h. Cells were stained with CellROX Deep Red Reagent and subjected to ROS analysis by flow cytometry. a) Data are expressed as mean ± SEM (n=3). (\*)  $p \leq 0.005$  indicates a significant difference from the control. b) Dot plot representative of control SH-SY5Y cells and c) Dot plot representative of SH-SY5Y cells exposed to 3.12 μM of STE.

### 3.3. Lipid peroxidation assay

The LPO on SH-SY5Y was determined by the TBARS method in the presence of STE (0.78, 1.56 and 3.12  $\mu\text{M}$ ). Results obtained show that after 24 h of exposure, STE increases significantly the production of MDA starting from the lowest concentration (Fig. 4). In particular, significant difference between 0.78 and 1.56  $\mu\text{M}$  and between 0.78 and 3.12  $\mu\text{M}$  of STE were observed related to MDA production. No difference between 1.56 and 3.12  $\mu\text{M}$  of STE were obtained.

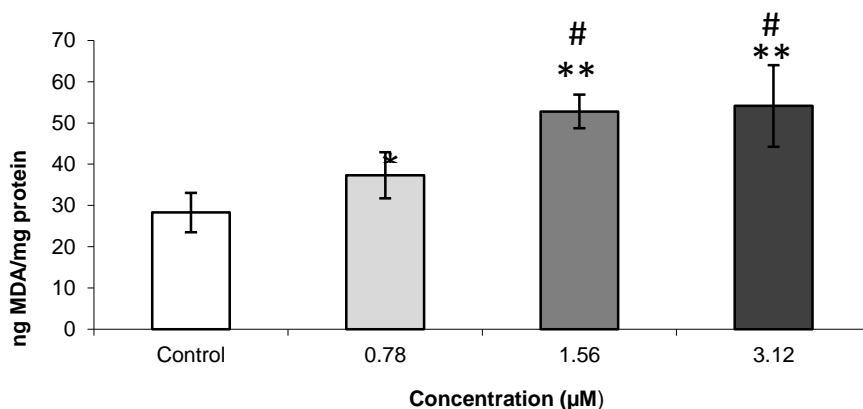


**Fig. 4.** The LPO as measured by MDA production in SH-SY5Y cells incubated for 24h with 0.78, 1.56 and 3.12  $\mu\text{M}$  of STE. Results are expressed as mean  $\pm$  SEM (n=2) in ng of MDA/mg of protein measured by Lowry method. (\*)  $p \leq 0.005$ , (\*\*)  $p \leq 0.000$  indicates a significant difference from solvent control. (#)  $p \leq 0.01$  indicates a significant difference from 0.78  $\mu\text{M}$  of STE.



### 3.4. GSH determination

The alteration on GSH, GSSG and GSH/GSSG ratio was measured after 24 h of STE exposure at 0.78, 1.56 and 3.12  $\mu\text{M}$  in SH-SY5Y cells grown in fresh medium or pre-treated with NAC or BSO (Fig. 5).

In fresh medium, the GSH and GSSG levels were not affected by 0.78  $\mu\text{M}$  STE. However, after 1.56 and 3.12  $\mu\text{M}$  of STE exposure the GSH levels significantly ( $p \leq 0.05$ ) decreased (respectively, by 61% and 47%; Fig. 5a) while the GSSG content significantly ( $p \leq 0.05$ ) increased (respectively, by 167% and 113%; Fig. 5b) compared to the control cells. As shown in Fig. 5c, in accordance with the previous results, GSH/GSSG ratio significantly decreased in cells exposed to 1.56 and 3.12  $\mu\text{M}$  of STE in fresh medium (by 85% and 75%, respectively) compared to control cells.

Concerning the pre-treatment effects, NAC and BSO resulted efficient modulators of the GSH.

The BSO pre-treatment produced a 45% decrease of GSH levels in controls (cells not exposed to STE) compared to the controls without BSO, while no significant changes were observed in GSSG content. Additionally, a significant ( $p \leq 0.05$ ) decrease on GSH levels by 84% and 80% (Fig. 5a) and a significant ( $p \leq 0.05$ ) increase on GSSG content by 93% and 60% (Fig. 5b) were also obtained after 1.56 and 3.12  $\mu\text{M}$  of STE exposure compared to their own controls. The depletion of GSH induced by BSO in cells exposed to STE ranged between 41% and 79% compared to the assay without BSO pre-treatment. Finally, the ratio GSH/GSSG was significantly decreased in control cells after BSO pre-treatment (by 43%) comparing to control cells in medium (Fig. 5c). In

cells pre-treated with BSO, at the highest STE concentrations (1.56 and 3.12  $\mu\text{M}$ ) a significant decrease was also observed respect to the control cells pre-treated with BSO (by 93% and 88%, respectively) and respect to the corresponding cells grown in medium (by 72% and 73%, respectively). Instead, at the lowest concentration of STE a significant increase was observed in cells pre-treated with BSO (by 62%) compared to their own control cells.

On the other hand, regarding the effects of NAC pre-treatment, in control cells was observed a significant increase on GSH and GSSG levels (by 16% and 111%, respectively) respect to controls without NAC, while the ratio GSH/GSSG was significantly decreased by 48% (Fig. 5). In addition, in cells exposed to 0.78 and 1.56  $\mu\text{M}$  STE, the pre-treatment with NAC induced an increase of GSH (by 25% and 51%, respectively) respect to cells in fresh medium, showing a protective effect of NAC on SH-SY5Y cells at these concentrations. However, with the increase of STE concentrations, this cytoprotective effect of NAC decreases, until to show no effects when cells are exposed to 3.12  $\mu\text{M}$  of STE (Fig. 5a). In NAC pre-treatment, a significant increase of GSSG was only observed in cells exposed at the lowest concentration of STE respect to the corresponding cells in medium, while at 1.56 and 3.12  $\mu\text{M}$  of STE no change was obtained (Fig. 5b). As well as in BSO pre-treatment, in cells pretreated with NAC and exposed to the highest STE concentrations the ratio GSH/GSSG significantly decreased (by 46% and 41%, respectively) compared to their own control cells, while, if compared to the corresponding cells in medium, the ratio resulted to be significantly increased (by 84% and 25%, respectively). Conversely, at the lowest STE concentration, the ratio significantly decreased by 94%.

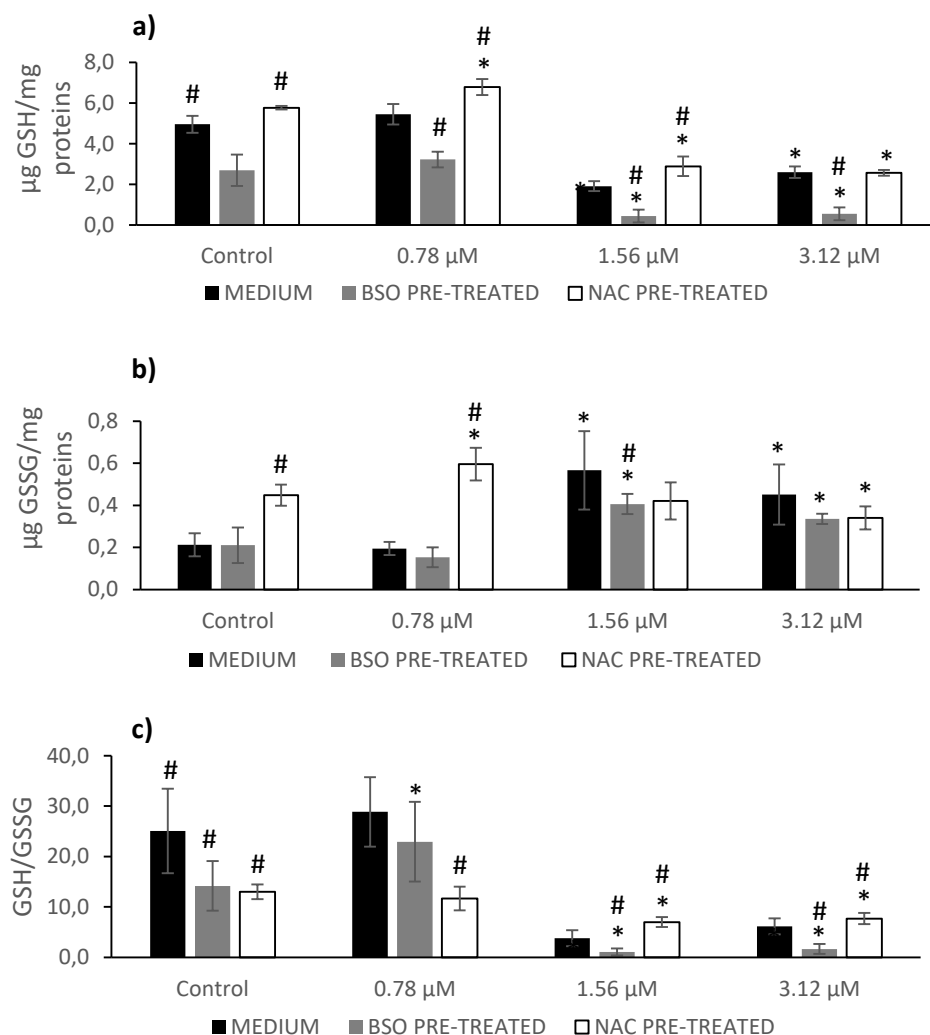


**Fig. 5.** Effect of STE (0.78, 1.56 and 3.12  $\mu\text{M}$ ) with and without NAC or BSO pre-treatment on GSH levels (a), GSSG levels (b), and on the GSH/GSSG ratio (c) after 24 h of exposure. Data are expressed as mean values  $\pm$  SEM of two independent experiments with 4 replicates each. \*  $p \leq 0.05$  indicates a significant difference from the respective control (fresh medium, BSO pre-treatment and NAC pre-treatment); #  $p \leq 0.05$  indicates a significant difference respect to the fresh medium

### 3.5. *Enzymatic activity*

The GPx, GST, CAT and SOD activities were measured in SH-SY5Y cells after 24 h of incubation with 0.78, 1.56 and 3.12  $\mu\text{M}$  STE. As shown in Fig. 6, the GPx activity decreased significantly in SH-SY5Y cells exposed to 0.78 and 1.56  $\mu\text{M}$  of STE in fresh medium (by 45% and 47%, respectively), while at the highest concentration an increase was observed (by 18%). A significant decrease was also observed at all concentrations tested in cells pre-treated with BSO respect to their own control cells (ranged from 27% to 58%) and also to the corresponding cells in fresh medium (ranged from 24% to 89%). After 0.78 and 1.56  $\mu\text{M}$  of STE exposure in NAC pre - treatment, the GPx activity resulted increased respect to the cells in fresh medium (respectively, by 24% and 49%) and decreased respect to their own control cells (respectively, by 37% and 27%).

The GST activity decreased significantly in cells exposed to 1.56 and 3.12  $\mu\text{M}$  of STE in fresh medium (by 23% and 27%, respectively), while at the lowest STE concentration, no changes were observed (Fig. 7). In BSO pre-treatment, a significant decrease was observed in cells exposed to 0.78 and 1.56  $\mu\text{M}$  STE respect to the corresponding cells in medium (by 76% and 48%, respectively). Respect to the corresponding cells grown in medium, in NAC pre-treatment a significant decrease was observed at the lowest STE concentration (42%), while a significant increase was obtained at the highest concentration by 57%. Additionally, after 0.78 and 1.56  $\mu\text{M}$  of STE exposure the decrease of GST activity was significant also compared to the control cells pre-treated with NAC (Fig. 7).

As can be observed in Fig. 8, no changes on CAT activity were obtained in cells exposed to STE at all concentrations tested respect to the control cells

in fresh medium, except for the cells exposed to 3.12  $\mu\text{M}$  STE, where the CAT activity resulted lightly decreased (8%). Similarly, in BSO pre-treatment condition, CAT activity no changes at all concentrations studied of STE compared to the control cells pre-treated with BSO. However, an increase was observed respect to the corresponding cells in fresh medium. Conversely, after NAC pre – treatment CAT activity significantly decreased at all STE concentrations and in control cells respect to the corresponding cells in medium. In addition, at the lowest STE concentration a little decrease was obtained (8%) respect to the control cells pre-treated with NAC, while a little increase was observed at the highest STE concentration (11%).

Finally, no changes on SOD activity were observed except for cells grown in medium exposed to 1.56 and 3.12  $\mu\text{M}$  respect to their own control cells, with a 15% and 30% decrease, respectively (Fig. 9). However, the SOD activity increased in a STE concentration-dependent manner in BSO pre-treated cells respect to the corresponding cells in medium, with an increase ranged from 16% to 77%. An increase was observed also in NAC pre-treated cells exposed to 3.12  $\mu\text{M}$  respect the corresponding cells in medium (46%).

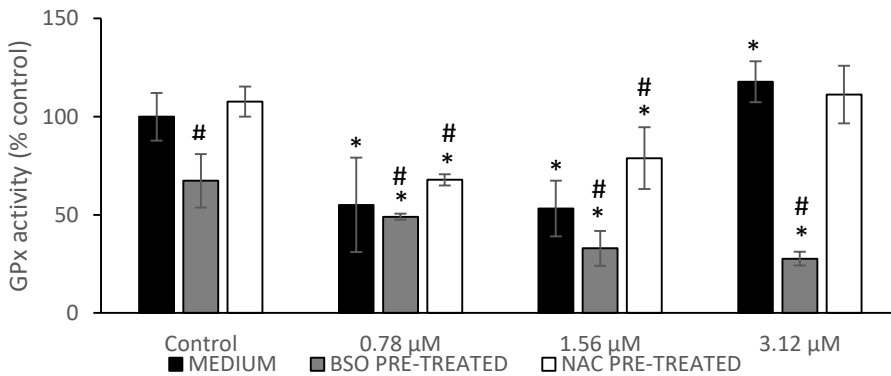


**Fig. 6.** Effect of STE (0.78, 1.56 and 3.12 μM) with and without NAC or BSO pre-treatment on glutathione peroxidase activity after 24 h of exposure. Data are expressed in % of the unexposed control. GPx activity is expressed as μmol of NADPH oxidized/min/mg of protein; mean ± SEM ( $n = 3$ ). \*  $p \leq 0.05$  indicates a significant difference from the respective solvent control; #  $p \leq 0.05$  indicates a significant difference respect to the medium.

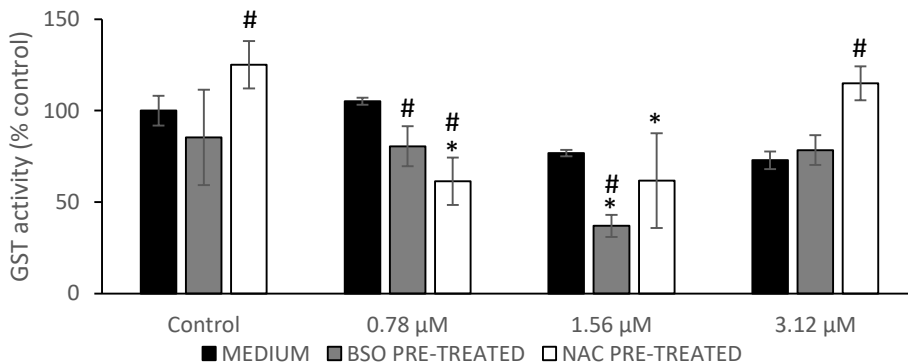


**Fig. 7.** Effect of STE (0.78, 1.56 and 3.12 μM) with and without NAC or BSO pre-treatment on glutathione S-transferase activity after 24 h of exposure. Data are expressed in % of the unexposed control. GST activity is expressed as mol of product formed/min/mg of protein; mean ± SEM ( $n = 3$ ). \*  $p \leq 0.05$  indicates a significant difference from the respective solvent control; #  $p \leq 0.05$  indicates a significant difference respect to the medium.

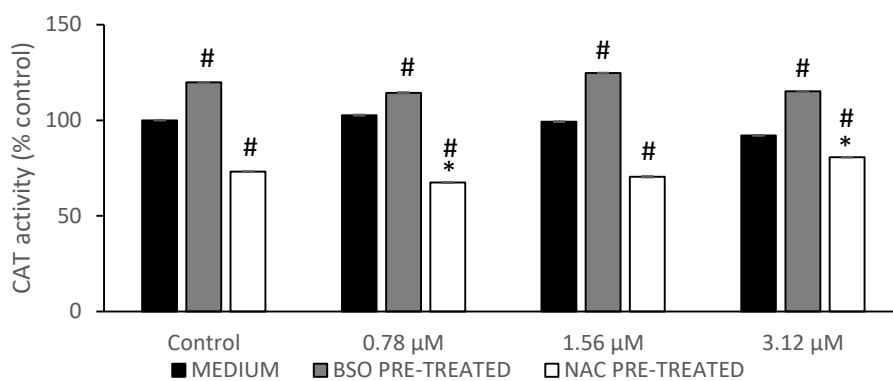


**Fig. 8.** Effect of STE (0.78, 1.56 and 3.12 μM) with and without NAC or BSO pre-treatment on catalase activity after 24 h of exposure. Data are expressed in % of the unexposed control. CAT activity is expressed as μmol H<sub>2</sub>O<sub>2</sub>/min/mg of protein; mean ± SEM (*n* = 3). \* *p* ≤ 0.05 indicates a significant difference from the respective solvent control; # *p* ≤ 0.05 indicates a significant difference respect to the medium.

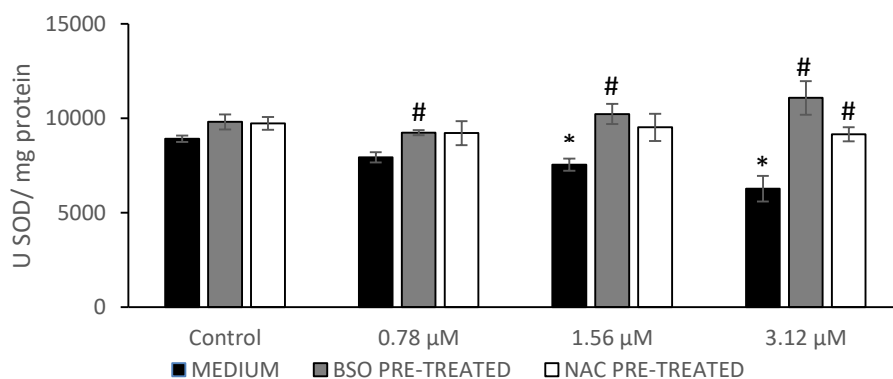


**Fig. 9.** Effect of STE (0.78, 1.56 and 3.12 μM) with and without NAC or BSO pre-treatment on superoxide dismutase activity after 24 h of exposure. The SOD activity is expressed as units of SOD/mg of protein; mean ± SEM (*n* = 3). \* *p* ≤ 0.05 indicates a significant difference from the respective solvent control; # *p* ≤ 0.05 indicates a significant difference respect to the medium.

#### 4. Discussion

The STE is a noteworthy mycotoxin with mutagenic and carcinogenic effects (Purchase and Van Der Watt, 1970). Several authors have demonstrated the ability of STE to decrease cell viability in different cell lines, including HepG2 cells (Bunger et al., 2004; Gao et al., 2015; Liu et al., 2014), CHO–K1 cells (Zouaoui et al., 2016), Hep3B cells (Anninou et al., 2014) and in human pulmonary cells (Cui et al., 2017). However, the number of study about the effect of STE on neuronal system is limited (Bunger et al., 2004). The present study is conducted to investigate the cytotoxic effect of STE and the role played by oxidative stress on human neuroblastoma SH-SY5Y cells. The IC<sub>50</sub> values obtained, revealed that STE reduces cell viability in a dose and time-dependent manner by increasing lysosomal damage as assessed by the NR assay. Our results show that STE inhibits SH-SY5Y proliferation at high micromolar concentrations after 24 h of exposure, similar to ones obtained in CHO–K1 (IC<sub>50</sub>=25.0 μM), Hep3B (IC<sub>50</sub>=58.0 μM) and Neuro-2a (IC<sub>50</sub>=40.1 μM) cells (Anninou et al., 2014; Zouaoui et al., 2016). In according with our results that show a lightly decrease of cell viability after 24 h of exposure at the lowest concentrations tested, Cui et al. (2017) demonstrated that concentrations of STE ranging from 0.06 to 6 μM have no effect on cell viability in A549 and BEAS-2B cells. Nevertheless at higher concentrations (from 12 to 240 μM), a significant concentration-dependent decrease was observed in both cell lines. In contrast, lower IC<sub>50</sub> values were obtained by Bunger et al. (2004) in A-549 cells (IC<sub>50</sub>=3.7 μM) and by Gao et al. (2015) in HepG2 cells (IC<sub>50</sub>=3μM) after 24 h of exposure. Differences between IC<sub>50</sub> values obtained for STE could be caused by different cell sensitivity of each type of cell line and, among the same cell line, by different supplements in the medium and cytotoxic assay conditions. Data for IC<sub>50</sub> values



after 48 h of STE exposure is available only in CHO–K1 ( $IC_{50}=17.5 \mu\text{M}$ ) and Hep3B ( $IC_{50}=22 \mu\text{M}$ ) cells (Anninou et al., 2014; Zouaoui et al., 2016). Instead, the  $IC_{50}$  value after 72 h of exposure is available only in CHO–K1 cells ( $IC_{50}=12.5 \mu\text{M}$ ), as reported by Zouaoui et al. (2016). In both cell lines, and in accordance with our results, the  $IC_{50}$  values obtained after 48 and 72 h of STE exposure are lower than the corresponding  $IC_{50}$  values obtained after 24 h, demonstrating that STE cytotoxicity increases with the time of exposure. However, in both cases the  $IC_{50}$  values obtained are higher than those found in our study, suggesting that STE is more cytotoxic towards human neuronal cells than other cell lines.

For the other assays, three concentrations of STE were chosen. Concentrations used in the present study were selected taking into account the concentrations found previously in food commodities and the average consumption of cereals in Europe. In particular, according to the data reported by the European Food Safety Authority (EFSA, 2013), levels in the range of 0.7–4300  $\mu\text{g}/\text{kg}$  of STE have been determined in grains. Considering that the consumption of cereals in Europe is 132  $\text{kg}/\text{year}$  (FAOSTAT, 2013), the estimated total intake of STE is ranging from 0.77  $\text{nM}$  to 4.78  $\mu\text{M}/\text{day}$ . The three concentrations selected (0.78, 1.56 and 3.12  $\mu\text{M}$ ) are included in this range. Moreover, the selection of these three concentrations was due to the fact that they showed cytotoxic effects to SH-SY5Y cells, but all of them were lower than the  $IC_{50}$  obtained by NR assay. Our study showed that in SH-SY5Y cells, STE triggered a concentration - dependent enhancement of intracellular ROS levels after 24 h of exposure (Fig. 3), demonstrating its implication in cell toxicity. These findings are consistent with those of Gao et al. (2015) in HepG2 cells. In particular, they observed an increase of oxidizing species with the increase of

STE concentrations (1.5, 3 and 6  $\mu\text{M}$ ). Nevertheless, a significant increase was obtained only after the exposure at 3 and 6  $\mu\text{M}$  STE. Moreover, cytotoxicity of STE via ROS production has been evidenced by Liu et al. (2014) in HepG2 cells, who observed a ROS increase along the treatment concentrations (from 0.5 to 7  $\mu\text{M}$ ). However, only limited reports about the ability of STE to induce oxidative stress are available. According to Ferrer et al. (2009), excessive ROS production can cause macromolecules oxidation, such as membrane lipids, leading to the process of lipid peroxidation. In the present study, enhanced LPO is indicated by the observed increase in MDA levels, highlighting the ability of STE to interact with membrane lipids (Fig. 4). These results suppose that ROS generation is involved in STE cytotoxicity and LPO has been produced as a consequence of ROS production in SH-SY5Y cells. Several mycotoxins were reported to be able to increase LPO. Deoxynivalenol (DON) was observed increase MDA levels in human peripheral blood lymphocytes after 6, 12 and 24 h of exposure (Yang et al., 2014). Aflatoxin B1 (AFB1) and fumonisin B1 (FB1) were shown to produce MDA increase after 48 h of exposure in spleen mononuclear cells (SMC). Kouadio et al. (2007) suggested that FB1, DON and zearalenone (ZEA) exposure induced LPO and, consequently, affected the functionality of the mitochondria in Caco-2 cells. In fact, MDA increase in association with ROS generation plays a crucial role in the molecular events which result in cell damage. In common crap and in male Wistar albino rats treated with STE-contaminated diet, higher levels of TBARS were observed, resulting in a slightly effect on GSH redox system in the first case and in a reduction of GSH levels and an increase of the activity of the antioxidant enzymes (SOD and GPx) in the second one (Kovesi et al., 2019; Sivakumar et al., 2001). The GSH is involved in a variety of cellular function such as DNA

---

repair, cell cycle, regulation of cell signalling and transcriptional factors (Dalton et al., 2004). Considering that the levels of GSH determine the balance in the antioxidant defence system, the impact on cellular GSH and GSSG content was evaluated after 24 h of STE exposure. A significant decrease of intracellular GSH and a significant increase of GSSG levels at high concentrations of STE were found in SH-SY5Y cells as a response to oxidative damage. Analogous effects were observed with beauvericin (BEA) in CHO-K1 cells (Mallebrera et al., 2014), ZEA and its metabolites in CHO-K1 and HepG2 cells (Tatay et al., 2016, 2017), OTA in HepG2 cells (Ramya et al., 2014) and DON in HT-29 cells (Krishnaswamy et al., 2010). To understand the role of GSH in the detoxification mechanisms of STE, the protective effects of the antioxidant enzymes (GPx, GST, CAT and SOD) against the damage produced by oxidant substances generation were determined. The noted drop in GSH levels seems to be not related to its utilization through the activity of GPx and GST enzymes, as suggested by the decreased activities obtained. Therefore, it is proposed a direct utilization of GSH as an antioxidant in no-enzymatic reaction with ROS. Grosicka-Maciag et al. (2008) affirmed that GPx is itself susceptible to the oxidation by the oxidative reactive molecules and lipid peroxides and could be inactivated in oxidative stress conditions. Thus, the decrease of GPx activity observed in our study could be associated to the inactivation by ROS which were increased as time of exposure and STE concentrations increased. Furthermore, the decreased GPx activity could be due also to the reduced availability of GPx substrate, the GSH, which were depleted until about 60% after 24 h of exposure, as speculated by Dinu et al. (2011). Our results are in accordance with these observations, since when intracellular GSH levels were increased in cells pre-treated with NAC, the cells were more resistant to STE cytotoxic effects, as

demonstrated by the increase in GPx activity. However, while at the highest concentration of STE the protective effect of NAC seems to be partially inhibited, in cells grown in medium a significant increase in GPx activity was obtained, suggesting that this enzyme defense system was stimulated to detoxify STE exposure.

The GSTs are a family of isoenzymes that catalyze the conjugation of GSH with electrophilic compounds. These enzymes are involved in the detoxification of a multitude of xenobiotics and in the protective mechanisms against cellular damage. No increases or almost unchanged GST activity indicate that this enzyme was not implicated in STE detoxification.

The STE also resulted no activate SOD and CAT activities. They represent another source of defense against oxidative stress. The SOD enzyme catalyses the transformation of the superoxide anion radical into  $H_2O_2$  and  $O_2$ . The CAT and GPx work in tandem to scavenge excess of  $H_2O_2$  but, while CAT directly catalyses the transformation of  $H_2O_2$  to  $H_2O$  and  $O_2$ , GPx uses GSH as a substrate to transformate  $H_2O_2$  to  $H_2O$ . In our study, SOD activity significantly decreased in a dose-dependent manner in SH-SY5Y cells exposed to STE as well as CAT activity resulted slightly decreased or almost unchanged. In light of all this, it can be assumed that SH-SY5Y cells are unable to counteract the oxidative stress produced by STE, as suggested by the observed loss of activity of all antioxidant enzymes, leading to a further intensification and a predisposition of cells to oxidative damage.

No data about the effects of STE on the non-enzymatic and enzymatic antioxidant protective systems is available in the literature. Nevertheless, the effects of various mycotoxins on the cellular antioxidant defense system have

been very well studied by different authors. Results similar to those found in our study were obtained by Ramyaa et al. (2014) in HepG2 cells exposed to 10  $\mu\text{M}$  OTA. Additionally, Dinu et al. (2011) showed that SOD and CAT were up-regulated in Hek-293 cells after 6–12 h of 2.5  $\mu\text{M}$  DON exposure, whereas, the activity of both enzymes tended to the control levels after 24 h of exposure. In the same ways, after a temporal activation of GPx, also the activity of this enzyme resulted decreased after 24 h of DON exposure, suggesting that the intense oxidative stress produced after 24 h of exposure induced a failure of the antioxidant enzymatic activity. On the other hand, opposite results were observed in HT-29 cells, where the exposure to 250 ng/ml and 500 ng/ml DON for 24 h produced an increase of the activity of CAT, SOD and GPx enzymes (Krishnaswamy et al., 2010). Similar results were obtained by Mallebrera et al. (2014). They observed an increase in GPx activity in CHO–K1 cells exposed to different concentrations of BEA (0.1, 1 and 5  $\mu\text{M}$ ), whereas a stimulation of GST enzymatic activity was obtained only at low concentrations, may be due to a saturation process when the substrate concentration increases. Furthermore, in HepG2 and CHO–K1 cells exposed to ZEA and its metabolites ( $\alpha$ -zearalenol;  $\alpha$ -ZOL;  $\beta$ -zearalenol;  $\beta$ -ZOL), an upregulation of the antioxidant defense system by increasing the activity of GPx and SOD was reported, suggesting that these enzymes play a crucial role in providing protection against oxidative damage induced by these mycotoxins. However, a reduction in CAT activity was found, which could be due to the high concentrations of  $\text{H}_2\text{O}_2$  produced under mycotoxin exposure (Tatay et al., 2016, 2017). In fact, in a situation of overdone of  $\text{H}_2\text{O}_2$  production, a depression of CAT activity may occur, and it can be even inactivated (Mates, 2000). Anyway, the different response in enzyme activity among our results and those obtained by other authors are due to the different

mycotoxins and the different concentrations assayed in each test, the employment of different experimental conditions as well as the type of cell lines studied.

The aim of the present study was to investigate the impact of intracellular GSH and its coupled antioxidant enzyme system. Moreover, the role of radicals scavenging, by cell pre-treatment with BSO or NAC, a GSH depletor and GSH promoter, respectively, was also studied. For this reason, BSO and NAC were applied in combination with the mycotoxin in subsequent experiments. In our study, BSO showed a harmful effect in the GSH/GSSG assay, decreasing significantly GSH levels in cells exposed to STE at all concentrations tested. Similar depletions of GSH via BSO treatment have already been described on other cell lines (Maran et al., 2010; Woelflingseder et al., 2018). Probably because of this higher GSH depletion, when SH-SY5Y cells were exposed to BSO pre-treatment, after STE exposure, GPx and GST activities decreased further than in cells without BSO pre-treatment. On the other hand, an increase of SOD and CAT activity respect to the cells grown in fresh medium was observed, suggesting that in presence of BSO an additional generation of H<sub>2</sub>O<sub>2</sub> occurs. Subsequently, CAT activity is stimulated instead of GPx, probably because of the greater depletion of its substrate, namely GSH, achieved by BSO pre-treatment. If BSO pre-treatment enhanced the predisposition of cells to oxidant damage induced by STE, NAC pre-treatment seems to help to detoxify the mycotoxin in SH-SY5Y cells. It has been shown that the presence of NAC is able to block ROS production induced by STE in HepG2 cells (Gao et al., 2015). In fact, NAC is known to react directly with oxidative metabolites and prevent oxidative stress (Fishbane et al., 2004). In our study, the GSH levels and the enzymatic activities related to GSH (GPx and GST) resulted to be increased in

NAC pre-treated cells. In particular, although the increase of GPx activity was observed at 0.78 and 1.56  $\mu\text{M}$ , the GST activity increased in cells exposed to 3.12  $\mu\text{M}$ , suggesting that at the highest STE concentration NAC pre-treatment stimulated GST enzymatic activity to detoxify the mycotoxin. Thus, cytoprotection provided by NAC is unlikely to be a result of increasing GSH levels but also to the direct radical scavenging properties of NAC, highlighting the ability of this precursor to help to detoxify STE in SH-SY5Y cells.

Overall, our results support the hypothesis that STE exposure decreases the cell viability and increases the LPO and free radical formation, leading to the activation of the GSH redox system in SH-SY5Y cells. These findings suggest that oxidative stress plays a central role in STE-induced cytotoxicity. Further studies are still needed to investigate other intracellular mechanisms of action potentially involved in the toxicity induced by STE exposure.

### **Declaration of competing interest**

The authors declare that they have no known competing financial interests or personal relationships that could have appeared to influence the work reported in this paper.

### **Acknowledgments**

This research has been supported by the Spanish Ministry of Economy and Competitiveness (AGL 2016-77610-R) and the pre-doctoral research training program "Santiago Grisolia (GRISOLIAP/2018/ 092) CPI-18-117".

### References

Anninou, N., Chatzaki, E., Papachristou, F., Pitiakoudis, M., Simopoulos, C., 2014. Mycotoxins' activity at toxic and sub-toxic concentrations: differential cytotoxic and genotoxic effects of single and combined administration of sterigmatocystin, ochratoxin A and citrinin on the hepatocellular cancer cell line Hep3B. *Int. J. Environ. Res. Public Health* 11, 1855–1872.

Axelsson, V., Holback, S., Sjogren, M., Gustafsson, H., Forsby, A., 2006. Gliotoxin induces caspase-dependent neurite degeneration and calpain-mediated general cytotoxicity in differentiated human neuroblastoma SH-SY5Y cells. *Biochem. Biophys. Res. Commun.* 345, 1068–1074.

Bennett, J.W., Klich, M., 2003. Mycotoxins. *Clin. Microbiol. Rev.* 16, 497–516.

Bunger, J., Westphal, G., Monnich, A., Hinnendahl, B., Hallier, E., Muller, M., 2004. Cytotoxicity of occupationally and environmentally relevant mycotoxins. *Toxicology* 202, 199–211.

Burchell, V.S., Gandhi, S., Deas, E., Wood, N.W., Abramov, A.Y., Plun-Favreau, H., 2010. Targeting mitochondrial dysfunction in neurodegenerative disease: Part I. *Expert Opin. Ther. Targets* 14, 369–385.

Butterfield, D.A., Lauderback, C.M., 2002. Lipid peroxidation and protein oxidation in Alzheimer's disease brain: potential causes and consequences involving amyloid betapeptide-associated free radical oxidative stress. *Free Radic. Biol. Med.* 32, 1050–1060.

Cao, X., Li, X., Li, J., Niu, Y., Shi, L., Fang, Z., Zhang, T., Ding, H., 2018. Quantitative determination of carcinogenic mycotoxins in human and animal biological matrices and animal-derived foods using multi-mycotoxin and



---

analyte-specific high performance liquid chromatography-tandem mass spectrometric methods. *J. Chromatogr. B* 1073, 191–200.

Cooke, M.S., Evans, M.D., Dizdaroglu, M., Lunec, J., 2003. Oxidative DNA damage: mechanisms, mutation, and disease. *FASEB J.* 17, 1195–1214.

Cui, J., Wang, J., Huang, S., Jiang, X., Li, Y., Wu, W., Zhang, X., 2017. Sterigmatocystin induced apoptosis in human pulmonary cells in vitro. *Exp. Toxicol. Pathol.* 69, 695–699.

Dalton, T.P., Chen, Y., Schneider, S.N., Nebert, D.W., Shertzer, H.G., 2004. Genetically altered mice to evaluate glutathione homeostasis in health and disease. *Free Radic. Biol. Med.* 37, 1511–1526.

Devasagayam, T.P., Tilak, J.C., Bloor, K.K., Sane, K.S., Ghaskadbi, S.S., Lele, R.D., 2004. Free radicals and antioxidants in human health: current status and future prospects. *J. Assoc. Phys. India* 52, 794–804.

Diaz Nieto, C.H., Granero, A.M., Zon, M.A., Fernandez, H., 2018. Sterigmatocystin: a mycotoxin to be seriously considered. *Food Chem. Toxicol.* 118, 460–470.

Dinu, D., Bodea, G.O., Ceapa, C.D., Munteanu, M.C., Roming, F.I., Serban, A.I., Hermenean, A., Costache, M., Zarnescu, O., Dinischiotu, A., 2011. Adapted response of the antioxidant defense system to oxidative stress induced by deoxynivalenol in Hek-293 cells. *Toxicon* 57, 1023–1032.

EFSA, 2013. European food safety authority (efsa) panel on contaminants in food chain (CONTAM), scientific opinion on the risk for public and animal health related to the presence of sterigmatocystin in food and feed. *EFSA J* 11 (6), 3254.

FAOSTAT, 2013. Food Balance Sheet. <http://faostat.fao.org>.

Ferrer, E., Juan-Garcia, A., Font, G., Ruiz, M.J., 2009. Reactive oxygen species induced by beauvericin, patulin and zearalenone in CHO-K1 cells. *Toxicol. In Vitro* 23, 1504–1509.

Fishbane, S., Durham, J.H., Marzo, K., Rudnick, M., 2004. N-acetylcysteine in the prevention of radiocontrast-induced nephropathy. *J. Am. Soc. Nephrol.* 15, 251–260.

Gao, W., Jiang, L., Ge, L., Chen, M., Geng, C., Yang, G., Li, Q., Ji, F., Yan, Q., Zou, Y., Zhong, L., Liu, X., 2015. Sterigmatocystin-induced oxidative DNA damage in human liver-derived cell line through lysosomal damage. *Toxicol. In Vitro* 29, 1–7.

Grosicka-Maciag, E., Kurpios, D., Czczot, H., Szumilo, M., Skrzycki, M., Suchocki, P., Rahden-Staron, I., 2008. Changes in antioxidant defense systems induced by thiram in V79 Chinese hamster fibroblasts. *Toxicol. In Vitro* 22, 28–35.

Hayashi, A., Jose Dorantes-Aranda, J., Bowman, J.P., Hallegraeff, G., 2018. Combined cytotoxicity of the phycotoxin okadaic acid and mycotoxins on intestinal and neuroblastoma human cell models. *Toxins* 10 (12), 526.

Huang, S., Wang, J., Xing, L., Shen, H., Yan, X., Wang, J., Zhang, X., 2014. Impairment of cell cycle progression by sterigmatocystin in human pulmonary cells in vitro. *Food Chem. Toxicol.* 66, 89–95.

Huang, X.H., Zhang, X.H., Li, Y.H., Wang, J.L., Yan, X., Xing, L.X., Wang, F.R., 2004. Carcinogenic effects of sterigmatocystin and deoxynivalenol in NIH mice. *Zhonghua Zhongliu Zazhi* 26, 705–708.

Hussein, H.S., Brasel, J.M., 2001. Toxicity, metabolism, and impact of mycotoxins on humans and animals. *Toxicology* 167, 101–134.

---

IARC, 1987. Overall Evaluations of Carcinogenicity: an Updating of IARC Monographs Volumes 1 to 42. Supplement 7. Lyon, France.

Kouadio, J.H., Dano, S.D., Moukha, S., Mobio, T.A., Creppy, E.E., 2007. Effects of combinations of Fusarium mycotoxins on the inhibition of macromolecular synthesis, malondialdehyde levels, DNA methylation and fragmentation, and viability in Caco-2 cells. *Toxicol* 49, 306–317.

Kovesi, B., Pelyhe, C., Zandoki, E., Mezes, M., Balogh, K., 2019. Effect of short-term sterigmatocystin exposure on lipid peroxidation and glutathione redox system and expression of glutathione redox system regulatory genes in common carp liver. *Toxicol* 161, 50–56.

Krishnaswamy, R., Devaraj, S.N., Padma, V.V., 2010. Lutein protects HT-29 cells against Deoxynivalenol-induced oxidative stress and apoptosis: prevention of NF-kappaB nuclear localization and down regulation of NF-kappaB and Cyclo-Oxygenase-2 expression. *Free Radic. Biol. Med.* 49, 50–60.

Kusunoki, M., Misumi, J., Shimada, T., Aoki, K., Matsuo, N., Sumiyoshi, H., Yamaguchi, T., Yoshioka, H., 2011. Long-term administration of the fungus toxin, sterigmatocystin, induces intestinal metaplasia and increases the proliferative activity of PCNA, p53, and MDM2 in the gastric mucosa of aged Mongolian gerbils. *Environ. Health Prev. Med.* 16, 224–231.

Lin, C.C., Lee, I.T., Wu, W.L., Lin, W.N., Yang, C.M., 2012. Adenosine triphosphate regulates NADPH oxidase activity leading to hydrogen peroxide production and COX-2/PGE2 expression in A549 cells. *Am. J. Physiol. Lung Cell Mol. Physiol.* 303, L401–L412.

Liu, Y., Du, M., Zhang, G., 2014. Proapoptotic activity of aflatoxin B1 and sterigmatocystin in HepG2 cells. *Toxicol. Rep.* 1, 1076–1086.

Ma, F., Misumi, J., Zhao, W., Aoki, K., Kudo, M., 2003. Long-term treatment with sterigmatocystin, a fungus toxin, enhances the development of intestinal metaplasia of gastric mucosa in *Helicobacter pylori*-infected Mongolian gerbils. *Scand. J. Gastroenterol.* 38, 360–369.

Mallebrera, B., Font, G., Ruiz, M.J., 2014. Disturbance of antioxidant capacity produced by beauvericin in CHO-K1 cells. *Toxicol. Lett.* 226, 337–342.

Mancuso, C., Scapagini, G., Curro, D., Giuffrida Stella, A.M., De Marco, C., Butterfield, D.A., Calabrese, V., 2007. Mitochondrial dysfunction, free radical generation and cellular stress response in neurodegenerative disorders. *Front. Biosci.* 12, 1107–1123.

Maran, E., Fernandez-Franzon, M., Font, G., Ruiz, M.J., 2010. Effects of aldicarb and propoxur on cytotoxicity and lipid peroxidation in CHO-K1 cells. *Food Chem. Toxicol.* 48, 1592–1596.

Maran, E., Fernandez, M., Barbieri, P., Font, G., Ruiz, M.J., 2009. Effects of four carbamate compounds on antioxidant parameters. *Ecotoxicol. Environ. Saf.* 72, 922–930.

Marin, S., Ramos, A.J., Cano-Sancho, G., Sanchis, V., 2013. Mycotoxins: occurrence, toxicology, and exposure assessment. *Food Chem. Toxicol.* 60, 218–237.

Mates, J.M., 2000. Effects of antioxidant enzymes in the molecular control of reactive oxygen species toxicology. *Toxicology* 153, 83–104.

Meredith, M.J., Reed, D.J., 1982. Status of the mitochondrial pool of glutathione in the isolated hepatocyte. *J. Biol. Chem.* 257, 3747–3753.

Murugesan, G.R., Ledoux, D.R., Naeherer, K., Berthiller, F., Applegate, T.J., Grenier, B., Phillips, T.D., Schatzmayr, G., 2015. Prevalence and effects of

---

mycotoxins on poultry health and performance, and recent development in mycotoxin counteracting strategies. *Poult. Sci.* 94, 1298–1315.

Pitt, J.I., Wild, C.P., Baan, R.A., Gelderblom, W.C.A., Miller, J.D., Riley, R.T., Wu, F., 2012. Improving Public Health through Mycotoxin Control. International Agency for Research on Cancer (IARC Scientific Publications Series, No. 158), Lyon, France.

Purchase, I.F., Van Der Watt, J.J., 1970. Carcinogenicity of sterigmatocystin. *Food Cosmet. Toxicol.* 8, 289–295.

Ramyaa, P., Krishnaswamy, R., Padma, V.V., 2014. Quercetin modulates OTA-induced oxidative stress and redox signalling in HepG2 cells - up regulation of Nrf2 expression and down regulation of NF-kappaB and COX-2. *Biochim. Biophys. Acta* 1840, 681–692.

Reed, D.J., 1990. Glutathione: toxicological implications. *Annu. Rev. Pharmacol. Toxicol.* 30, 603–631.

Ruiz-Leal, M., George, S., 2004. An in vitro procedure for evaluation of early stage oxidative stress in an established fish cell line applied to investigation of PHAH and pesticide toxicity. *Mar. Environ. Res.* 58, 631–635.

Ruiz, M.J., Festila, L.E., Fernández, M., 2006. Comparison of basal cytotoxicity of seven carbamates in CHO-K1 cells. *Environ. Toxicol. Chem.* 88, 345–354.

Sivakumar, V., Thanislass, J., Niranjali, S., Devaraj, H., 2001. Lipid peroxidation as a possible secondary mechanism of sterigmatocystin toxicity. *Hum. Exp. Toxicol.* 20, 398–403.

Stockmann-Juvala, H., Naarala, J., Loikkanen, J., Vahakangas, K., Savolainen, K., 2006. Fumonisin B1-induced apoptosis in neuroblastoma, glioblastoma and hypothalamic cell lines. *Toxicology* 225, 234–241.

Tatay, E., Espin, S., Garcia-Fernandez, A.J., Ruiz, M.J., 2017. Oxidative damage and disturbance of antioxidant capacity by zearalenone and its metabolites in human cells. *Toxicol. In Vitro* 45, 334–339.

Tatay, E., Font, G., Ruiz, M.J., 2016. Cytotoxic effects of zearalenone and its metabolites and antioxidant cell defense in CHO-K1 cells. *Food Chem. Toxicol.* 96, 43–49.

Ueda, M., Mozaffar, S., Tanaka, A., 1990. Catalase from *Candida boidinii* 2201. *Methods Enzymol.* 188, 463–467.

Versilovskis, A., Bartkevics, V., Mikelsone, V., 2007. Analytical method for the determination of sterigmatocystin in grains using high-performance liquid chromatography-tandem mass spectrometry with electrospray positive ionization. *J. Chromatogr. A* 1157, 467–471.

Versilovskis, A., De Saeger, S., 2010. Sterigmatocystin: occurrence in foodstuffs and analytical methods—an overview. *Mol. Nutr. Food Res.* 54, 136–147.

Versilovskis, A., Van Peteghem, C., De Saeger, S., 2009. Determination of sterigmatocystin in cheese by high-performance liquid chromatography-tandem mass spectrometry. *Food Addit. Contam. A* 26, 127–133.

Woelflingseder, L., Del Favero, G., Blazevic, T., Heiss, E.H., Haider, M., Warth, B., Adam, G., Marko, D., 2018. Impact of glutathione modulation on the toxicity of the *Fusarium* mycotoxins deoxynivalenol (DON), NX-3 and butenolide in human liver cells. *Toxicol. Lett.* 299, 104–117.

Wu, F., 2006. Mycotoxin reduction in Bt corn: potential economic, health, and regulatory impacts. *Transgenic Res.* 15, 277–289.

Xing, L.X., Zhang, X.H., Shen, H.T., Li, Y.H., Liu, J., Xing, X., Zhou, B.J., Yan, X., Wang, J.L., 2007. Experimental study on the carcinogenic effects

of sterigmatocystin in new born BALB/c mice. *Zhonghua Bing Li Xue Za Zhi* 36, 265–266.

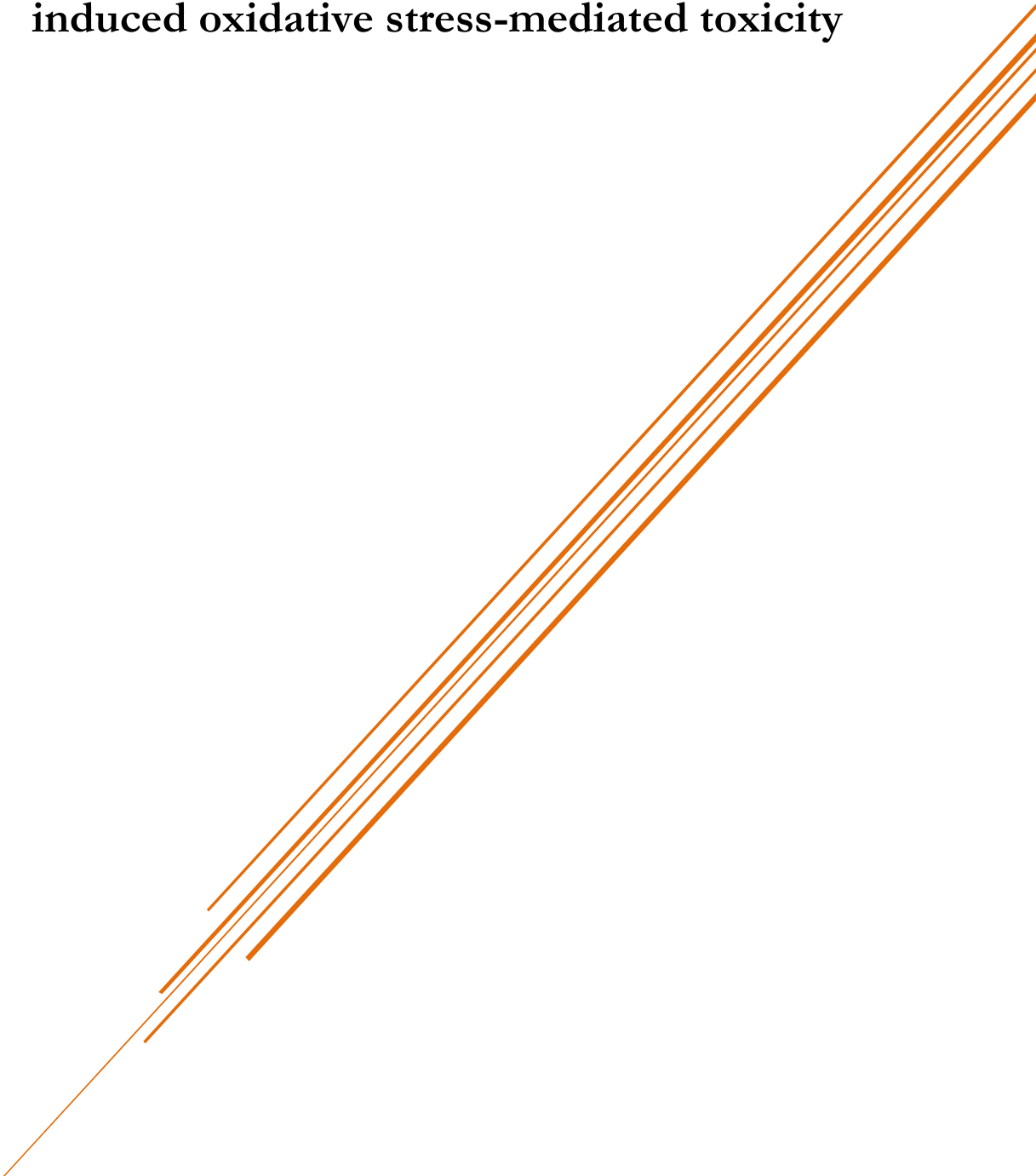
Yang, W., Yu, M., Fu, J., Bao, W., Wang, D., Hao, L., Yao, P., Nussler, A.K., Yan, H., Liu, L., 2014. Deoxynivalenol induced oxidative stress and genotoxicity in human peripheral blood lymphocytes. *Food Chem. Toxicol.* 64, 383–396.

Zouaoui, N., Mallebrera, B., Berrada, H., Abid-Essefi, S., Bacha, H., Ruiz, M.J., 2016. Cytotoxic effects induced by patulin, sterigmatocystin and beauvericin on CHO-K1 cells. *Food Chem. Toxicol.* 89, 92–103.





### **3.3. Role of quercetin on sterigmatocystin-induced oxidative stress-mediated toxicity**





Food and Chemical Toxicology

(Under Review)

**Role of quercetin on sterigmatocystin-induced oxidative stress-mediated toxicity**

Veronica Zingales<sup>1\*</sup>, M. Salome Sirerol-Piquer<sup>2</sup>, Mónica Fernández-Franzón<sup>1</sup>, Maria-José Ruiz<sup>1</sup>

<sup>1</sup>Laboratory of Food Chemistry and Toxicology, Faculty of Pharmacy, University of Valencia, Av. Vicent Andrés Estellés s/n, 46100, Valencia, Spain

<sup>2</sup>Department of Cell Biology, Functional Biology and Physical Anthropology, University of Valencia, Av. Vicent Andrés Estellés s/n, 46100, Valencia, Spain.

\*Corresponding author. Laboratory of Toxicology, Faculty of Pharmacy, University of Valencia, Av. Vicent Andrés Estellés, s/n, 46100, Burjassot, Valencia, Spain. *E-mail address:* [vezin@uv.es](mailto:vezin@uv.es) (V. Zingales).

### Abstract

Oxidative stress appears to be a common trigger for many of the effects associated with the exposure to various mycotoxins, including sterigmatocystin (STE). However, studies to alleviate STE toxicity through the use of natural antioxidant are sparsely reported in literature. In the present study, the cytoprotective effect of quercetin (QUE) was tested in SH-SY5Y cells against STE-induced oxidative stress and cytotoxicity. The MTT assay revealed that STE decreased cell viability, whereas pre-treatment of cells with QUE restored it. The QUE was also found to counteract STE-induced ROS generation and decrease STE-induced up-regulation of the expression of the stress-inducible enzymes HO-1 and NOS-2. Pre-treatment with QUE also prevented STE-induced nuclear translocation of NF- $\kappa$ B, as measured by immunofluorescence. Finally, considering the key role played by NF- $\kappa$ B in the regulation of inflammation, the effect of STE on the pro-inflammatory cytokines TNF- $\alpha$  and IL-6 expression was evaluated. Our results showed the down-regulation of TNF- $\alpha$  and IL-6 following STE exposure, suggesting a negative immunomodulatory effect of STE. In QUE pre-treated samples, TNF- $\alpha$  and IL-6 were significantly further reduced, indicating the anti-inflammatory role of QUE. The results of the present study demonstrate for the first time that QUE exerts a cytoprotective role in STE-induced toxicity.

**Keywords:** Sterigmatocystin; Quercetin; Oxidative stress; Inflammation; NF- $\kappa$ B; SH-SY5Y cells.

## 1. Introduction

Oxidative stress is reported to play a key role in the onset of numerous human clinical conditions, such as cardiovascular diseases, liver diseases, lung diseases, gastrointestinal disorders, chronic inflammation as well as aging and a number of neurodegenerative diseases (Alfadda and Sallam, 2012; Salim, 2014). In toxicological syndromes caused by exposure to environmental and food toxins, the involvement of reactive oxygen species (ROS) has been well documented (Mavrommatis et al., 2021). It has been shown that several mycotoxins, including sterigmatocystin (STE), generate free radicals that induce lipid peroxidation and changes in the antioxidant cellular status (Balogh et al., 2019; Sivakumar et al., 2001; Zingales et al., 2020a).

The STE is a polyketide mycotoxin mainly produced by fungi belonging to the genus *Aspergillus*. In the last few years a global growing attention is grabbed by STE as it causes genotoxicity, hepatotoxicity and nephrotoxicity in animals and high incidence of liver and stomach cancer has been reported in areas with high levels of STE contamination (Abdel-Wahhab et al., 2005; Hutanasu et al., 2011; Kovesi et al., 2019; Tian et al., 1995). A network of interacting mechanisms has been associated to STE toxicity (Zingales et al., 2020b). Among these, oxidative stress appears to be of particular interest (Klaunig and Kamendulis, 2004). Thus, therapeutic strategies aimed at preventing or delaying ROS might be a reasonable choice against STE-induced toxicity. However, attempts to alleviate STE-induced toxicity through the use of natural substances are poorly reported in literature (Aly and Elewa, 2007; El-Desouky et al., 2015; Kocic-Tanackov et al., 2012).

In recent years, dietary antioxidants have been received increasing attention by researchers for their anti-carcinogenic, anti-inflammatory and anti-mutagenic properties (Vina et al., 2006). Numerous studies have consistently shown that the consumption of natural products in the form of beverages as well as diets rich in fruits and vegetables, have a cytoprotective effect, since many antioxidants may act as free radical scavengers resulting in an augmentation and fortification of the endogenous defence system (Devore et al., 2013; Mandel et al., 2006; Vanella et al., 2017).

Quercetin (QUE; 3,3',4',5,7-pentahydroxyflavone), a naturally occurring dietary flavonol compound belonging to the polyphenolic flavonoid substances, has shown great beneficial effects in a broad spectrum of areas relevant to human health. Several studies have presented different health or pharmacological actions of QUE, including anti-cancer, anti-inflammatory, anti-diabetic, anti-allergic and cardio-protective activities (Barcelos et al., 2011; Bischoff, 2008; Chen et al., 2010; Larson et al., 2010; Mendoza and Burd, 2011; Russo et al., 2012). Moreover, QUE has been introduced as an anti-neurodegeneration agent (Sharma et al., 2016; Zaplatic et al., 2019). The beneficial properties of QUE have been attributed mainly to its strong antioxidant and chelating capacity as well as to its property to interact and modulate antioxidant enzyme activities. A number of beneficial health effects of QUE acting via modulating signalling pathways and gene expressions have been also demonstrated in cell and animal models (Xiao et al., 2018).

The deep interest of the scientific community in the study of QUE is mainly due to its widespread availability among dietary sources, contributing approximately 75% to the total flavonols intake. Major dietary sources include

lettuce, chili pepper, cranberry, onion, tomato, broccoli and apple, and it is also present in a wide variety of plant-derived infusions (Babaei et al., 2018; Nemeth and Piskula, 2007; Silvester et al., 2019).

Although several studies in literature have provide the cytoprotective effects of QUE against various oxidative insults, this is the first study where the efficacy of QUE as an antioxidant and potent free radical scavenger was evaluated on STE-induced toxicity in human SH-SY5Y neuroblastoma cells. In particular, we present here for the first time the sequence of some underlying molecular mechanism for STE-induced toxicity in presence and absence of QUE pre-treatment, with specific reference to oxidative stress and nuclear localization of the transcription factor NF- $\kappa$ B p65 (NF- $\kappa$ B). In addition, expression of inflammatory markers was studied.

## 2. Material and methods

### 2.1. Reagents

The reagent grade chemicals and cell culture compounds used, namely culture medium DMEM Ham's-F12, penicillin, streptomycin, trypsin/EDTA solutions, phosphate buffer saline (PBS), fetal bovin serum (FBS), quercetin (QUE), tetrazolium bromide (MTT), 2',7'-dichlorodihydrofluorescein diacetate (H2-DCFDA) and paraformaldehyde were from Sigma Chemical Co (St. Louis, MO, USA). Dimethyl sulfoxide (DMSO) was obtained from Fisher Scientific (Geel, Belgium). Methanol (MeOH) was from VWR International (LLC, Pennsylvania, USA). The primary monoclonal antibody rabbit anti-human NF- $\kappa$ B p65 was purchased from Cell Signaling Technology (Danvers, MA, USA).

Standard of the selected mycotoxin STE (MW: 324.28 g/mol) was purchased from Sigma-Aldrich (St. Louis Mo. USA). Stock solutions of the mycotoxin were prepared in methanol and maintained at -20°C.

### 2.2. *Cell culture and treatment*

Human neuroblastoma SH-SY5Y cells were cultured in DMEM Ham's-F12 medium supplemented with 10% FBS, 100 U/mL penicillin and 100 mg/mL streptomycin. The incubation conditions were pH 7.4, 5% CO<sub>2</sub> at 37°C and 95% air atmosphere at constant humidity. The medium was changed every 2-3 days. The final STE concentrations tested were achieved by adding STE solutions to the culture medium with a final methanol concentration  $\leq 1\%$  (v/v). Appropriate controls containing the same amount of solvent were included in each experiment.

### 2.3. *Cytotoxicity assay by MTT test*

Cell viability was determined by the MTT assay, as described by Ruiz et al. (2006). Cells were seeded in 96 well plate at a density of  $3 \times 10^4$  cells/well. After 48 h, when the cells reached 80% of confluence, cells were exposed to increasing concentrations of STE (0.19 – 25  $\mu\text{M}$ ) for 24 h. The concentrations of STE were chosen based on our previous reports (Zingales et al., 2020a, 2020c). The QUE dissolved in DMSO was added to the cells to reach a final concentration of 10  $\mu\text{M}$  (final solvent concentration did not exceed 0.1% v/v) to determine the efficacy of 2 h pre-treatment. The concentration of QUE was based on serum concentrations of patients given a non-cytotoxic oral dose of the flavonoid (Lakhanpal and Rai, 2007). After the exposure time, the medium containing STE was replaced with fresh medium containing 50  $\mu\text{l}$  of MTT salt (5 mg/ml PBS).



After 4 h of incubation at 37 °C under darkness, the resulting formazan crystals were solubilized in DMSO. The absorbance was measured at 540 nm using an automatic ELISA plate reader (MultiSkanEX, Labsystem, Helsinki, Finland). Cell viability was expressed as a percentage relative to the solvent control (1% MeOH). Two independent experiments for each time of exposure were conducted with 4 replicates each.

#### 2.4. Measurement of ROS

The generation of intracellular ROS was measured according to Sanchez-Carranza et al. (2018). Briefly,  $3 \times 10^4$  cells/well were seeded in a 96-well black culture microplate. Once the cells reach 90% confluence, the culture medium was replaced with fresh medium containing STE (0.78, 1.56 and 3.12  $\mu\text{M}$ ). The selection of the three concentrations assayed is correlated with those found in food and were selected according to the previous cytotoxic assays carried out. All of these concentrations resulted to be no toxic to SH-SY5Y and below the  $\text{IC}_{50}$  values obtained in our previous studies (Zingales et al., 2020a, 2020c). In the QUE pre-treatment groups, cells were pre-treated with QUE for 2 h and then exposed to STE (0.78, 1.56 and 3.12  $\mu\text{M}$ ) for 24 h. After the exposure time, cells were washed with PBS and incubated with 20  $\mu\text{M}$   $\text{H}_2\text{-DCFDA}$  in fresh medium for 30 min. The  $\text{H}_2\text{-DCFDA}$  in the cell is cleaved by intracellular esterases, producing the non-fluorescent 2',7'-dichlorodihydrofluorescein ( $\text{H}_2\text{-DCF}$ ), which accumulates into the cell. When oxidized by intracellular ROS,  $\text{H}_2\text{-DCF}$  give the fluorescent product DCF. The resulting fluorescence was then measured on a Wallace Victor2, model 1420 multilabel counter (PerkinElmer, Turku, Finland), at excitation/emission wavelengths of 485/535 nm. Results are expressed as increase in fluorescence respect to solvent control. Determinations

were performed in two independent experiments with 24 replicates each different concentrations assayed is correlated with those found in food and were selected according to the previous cytotoxic assays carried out. All of these concentrations resulted to be no toxic to SH-SY5Y and below the IC<sub>50</sub> values obtained. Increases in fluorescence were measured on a Wallace Victor2, model 1420 multilabel counter (PerkinElmer, Turku, Finland), at intervals up to 2 h at excitation/emission wavelengths of 485/535 nm. Results are expressed as increase in fluorescence respect to solvent control. Determinations were performed in two independent experiments with 24 replicates each.

### 2.5. *Immunofluorescence*

Nuclear localization of NF- $\kappa$ B was detected by immunofluorescence, as described previously by Na et al. (2006). Cells ( $9 \times 10^4$  cells/well) were seeded in 48-well plates and exposed to 0.78, 1.56 and 3.12  $\mu$ M of STE. To determine the time of optimum translocation, cells were exposed to STE for different time intervals (15, 30, 60 min, 3, 6 and 24 h). Pre-treatment with QUE was carried out for 2 h, followed by exposure to STE (0.78, 1.56 and 3.12  $\mu$ M) for 24 h, which was the time point of maximum translocation. Following treatments, cells were washed in PBS, fixed with 4% paraformaldehyde for 20 min, washed three times with 0.1 M phosphate buffer (PB) and incubated in blocking solution (0.1% Triton X-100 and 10% FBS in 0.1 M PB) for 1 h at room temperature. Subsequently, cells were incubated with primary antibody anti- NF-  $\kappa$ B (1:400 dilution in blocking solution) at 4°C overnight. The cells were then washed three times with 0.1 M PB and incubated with appropriated Alexa Fluor<sup>®</sup> 488 affinity conjugated secondary antibody (1:800 dilution in blocking solution) for 1 h at room temperature. Nuclei were stained with DAPI for 10 min. The images were

---

captured and analyzed using IN Cell Analyzer 2000 (GE Healthcare). For quantification, 30 fields for well were observed at a magnification of 40x. Three independent experiments were performed and at least 300 cells per field were counted; a cell was verified by the presence of a DAPI-stained nucleus. The results were expressed as nuclei/cytoplasm ratio fluorescence intensity of cells positive for the antibody under study.

### 2.6. RNA extraction and quantification

For the evaluation of inflammatory genes expression, cells were seeded at a density of  $7 \times 10^5$  cells/well in a 6 well plate, treated with STE and QUE as mentioned in measurement of ROS experiment. Then, total RNA of cells was isolated using ReliaPrep™ RNA Cell Miniprep System kit and treated with RNase free DNase (Promega) to remove genomic DNA contamination, according to the manufacturer's instructions. The extracted RNA of each sample was firstly checked for quantity and quality using Nanodrop2000 (Thermo Scientific), showing concentrations between 419.9 and 141.4 ng/μl and appropriate 260/280 and 260/230 ratios both  $\geq 2$ . The RNA samples were stored at  $-20$  °C until their dilution to 100 ng/μl with pure Milli-Q H<sub>2</sub>O until their reverse transcription to complementary DNA (cDNA).

### 2.7. Reverse transcription and qPCR reaction

First, synthesis of cDNA was carried out using 5 μl of total RNA (500 ng) according to the instructions of TaqMan™ MicroRNA Reverse Transcription Kit protocol (Thermo Fisher Scientific, Madrid, Spain). The qPCR was performed for all primer pairs and a single amplification product was obtained for each gene by the melting curve assay. Primer pairs for each gene were designed based on

the entire coding region of the candidate genes using Primer-BLAST (Ye et al., 2012), according to the following parameters: primer length of about 20 bases, GC content of 45–60%, melting temperature ( $T_m$  value) between 58 and 60 °C, and amplicon product size ranging from 50 to 150 base pair. Primer amplification efficiency was determined from standard curve generated by cDNA serial dilution (serial dilution factor = 2) for each gene in triplicate. The gene-specific primers used in the present study are listed in Table 1. Real-time amplification reactions were performed in 96 well plates using SYBR Green detection reactive and run with the StepOne Plus Real-time PCR instrument (Applied Biosystems). Reactions were prepared in a total volume of 10  $\mu$ l containing: 3  $\mu$ l of 1:2 diluted template, 2  $\mu$ l of amplification primer mix (forward/reverse of each gene; 2.5  $\mu$ M) and 5  $\mu$ l of SYBR Green (Applied Biosystems). Non-template controls (NTC) were also included for each primer pair, replacing the template by DNase and RNase free water. Determinations were performed in two independent experiments with 3 replicates each. The cycling conditions were set as default: initial denaturation step of 95 °C for 5 min to activate the Taq DNA polymerase, followed by 40 cycles of denaturation at 95 °C for 15 s, annealing temperatures ranging from 58 to 60 °C (depending on the primers) for 15 s and elongation at 72 °C for 45 s. The melting curve was generated by heating the amplicon from 60 to 90 °C. Baseline, threshold cycles (Ct) and primer parameters analysis were automatically determined using the StepOne Plus Software version 2.3 (Applied Biosystems).

### 2.8. *Statistical analysis*

Statistical analysis of data was carried out using GraphPad Prism version 7 (GraphPad Software, San Diego, California, USA), statistical software package.

Data were expressed as mean  $\pm$  SEM of different independent experiments. The statistical analysis of the results was performed by Student's t-test for paired samples. Differences between groups were analyzed statistically with one-way ANOVA followed by the Tukey HSD post-hoc test for multiple comparisons. The difference level of  $p \leq 0.05$  was considered statistically significant.

## Resultados

---

**Table 1.** Gene-specific primers for *q*PCR experiments.

Gene Symbol	Gene Name	Optimum Temp. (C°)	Forward primer/Reverse primer
<i>NOS-2</i>	Nitric Oxide Synthase-2	60	ACAGCACATTTCAGATCCCCA/ GCCGAGATTTGAGCCTCATG
<i>HO-1</i>	Heme Oxygenase-1	60	AAGACTGCGTTCCTGCTCAAC/ AAAGCCCTACAGCAACTGTCTG
<i>TNF-<math>\alpha</math></i>	Tumour Necrosis Factor- $\alpha$	60	GTCAACCTCCTCTCTGCCAT/ CCAAAGTAGACCTGCCAGA
<i>IL-6</i>	Interleukin-6	58	TCATTCCCTCAACTTGGTGTG/ AGCCTTCTCTTTTGAAGTGG
<i>18S rRNA</i>	18S ribosomal RNA	58	CGGCTACCACATCCAAGGAA/ GCTGGAATTACCGCGGCT

### 3. Results

#### 3.1. *Cytotoxicity assay*

In order to determine cell viability and standardize STE concentrations, an MTT test was performed. The results of the concentration-response study revealed a concentration-dependent decrease in cell viability caused by exposure to STE (0.19 – 25  $\mu\text{M}$ ), while treatment with QUE alone resulted in a higher cell viability compared to control cells. (Fig. 1). Furthermore, QUE pre-treatment at 10  $\mu\text{M}$  for 2 h followed by STE exposure for 24 h showed a statistically significant cytoprotective effect against STE-induced cytotoxicity at all tested mycotoxin concentrations, restoring cell viability at a rate between 126% and 80%.

#### 3.2. *Quercetin alleviates STE-induced ROS generation*

In order to test the extent of QUE antioxidant property in cytoprotection, protective effect of QUE against STE-induced oxidative stress was determined. Considering the results obtained from the cytotoxicity assay and keeping in mind our previous studies on STE toxicity (Zingales et al., 2020a, 2020c), three concentrations of STE (0.78, 1.56 and 3.12  $\mu\text{M}$ ) were shortlisted.

Exposure to STE at all concentrations tested for 24 h significantly increased ROS generation (Fig. 2). The value of ROS was expressed as relative fluorescence compared to control cells. Pre-treatment of cells with QUE 10  $\mu\text{M}$  for 2 h followed by STE exposure for 24 h significantly prevented STE-induced ROS generation, up to not being significantly different from control cells. Pre-treatment with QUE 10  $\mu\text{M}$  alone resulted in a statistically significant decrease in ROS levels when compared to control cells. concentration of STE only when

SH-SY5Y cells were exposed to STE for 24 h. An example of the dot plots representative of the control and the cells exposed to the highest concentration tested ( $3.12 \mu\text{M}$ ) of STE can be observed in Fig. 3b–c.

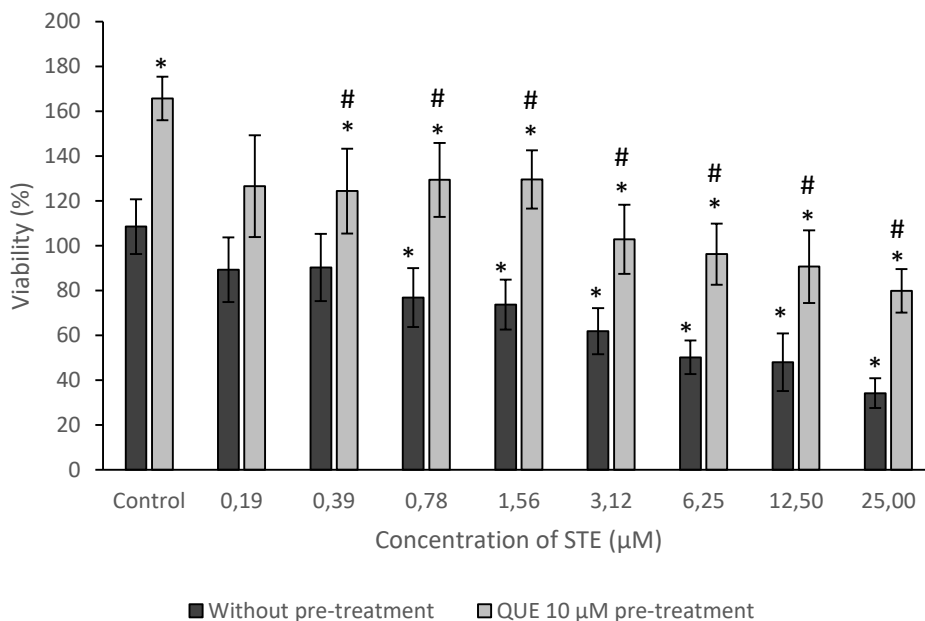


**Fig. 1.** Effect of QUE on STE-induced loss of cell viability in SH-SY5Y cell line. Cells were treated with STE ( $0.19 - 25 \mu\text{M}$ ) for 24 h in the presence or absence of QUE pre-treatment ( $10 \mu\text{M}$ ) for 2 h. Cell viability was assessed by MTT assay. Data are expressed as mean  $\pm$  SEM of two independent experiments ( $n = 2$ ) with 4 replicates each. (\*)  $p \leq 0.05$  indicates a significant difference compared to the corresponding solvent control. (#)  $p \leq 0.05$  indicates a significant difference respect to the corresponding STE treated cells.



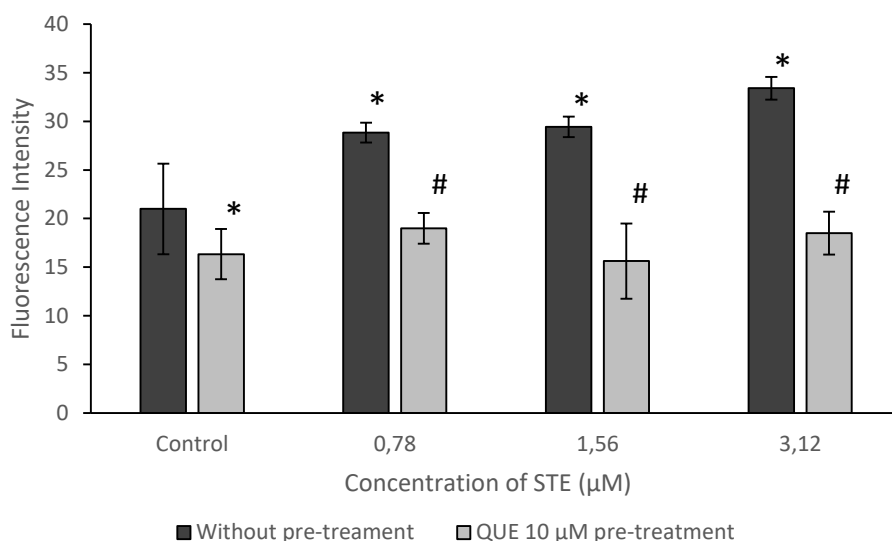


**Fig. 2.** Effect of QUE on STE-induced oxidative stress in SH-SY5Y cell line. Cells were treated with STE (0.78, 1.56 and 3.12 µM) for 24 h in the presence or absence of QUE pre-treatment (10 µM) for 2 h. The ROS generation was assessed by H2-DCFDA assay. Data are expressed as mean  $\pm$  SEM of two independent experiments (n = 2) with 24 replicates each. (\*)  $p \leq 0.05$  indicates a significant difference compared to the corresponding solvent control. (#)  $p \leq 0.05$  indicates a significant difference respect to the corresponding STE treated cells.

### 3.3. Effect of QUE and STE on other oxidative stress parameters

#### 3.3.1. Quercetin suppress STE-induced NOS-2 and HO-1 expression

Nitric oxide synthase-2 (NOS-2) and heme oxygenase-1 (HO-1) are stress-inducible enzymes, both implicated in mediating the oxidative stress damage. In the present study, the effect of QUE and STE on NOS-2 and HO-1 expression was investigated by real-time PCR. Our results indicated that NOS-2 and HO-1 expression was induced by 24 h of exposure to STE at all concentrations tested

(0.78, 1.56 and 3.12  $\mu\text{M}$ ), with a fold increase ranging from 1.6 to 1.8 and from 2 to 2.9, respectively (Fig. 3). Pre-treatment of cells with QUE 10  $\mu\text{M}$  for 2 h followed by STE for 24 h resulted in no changes in NOS-2 expression levels compared to the corresponding control cells and in a significant decrease when compared to cells exposed to STE 0.78 and 1.56  $\mu\text{M}$  alone. On the other hand, pre-treatment with QUE did not completely prevent HO-1 from being expressed, but slightly lowered its induced expression which was a statistically significant decrease only in cells exposed to the highest STE concentration.

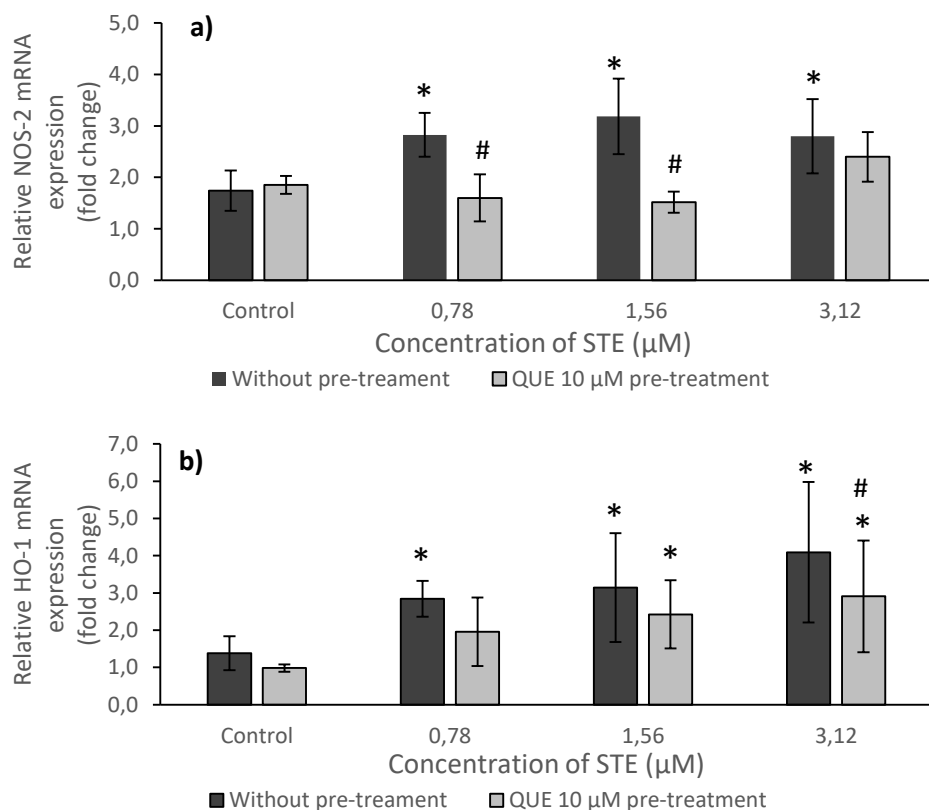
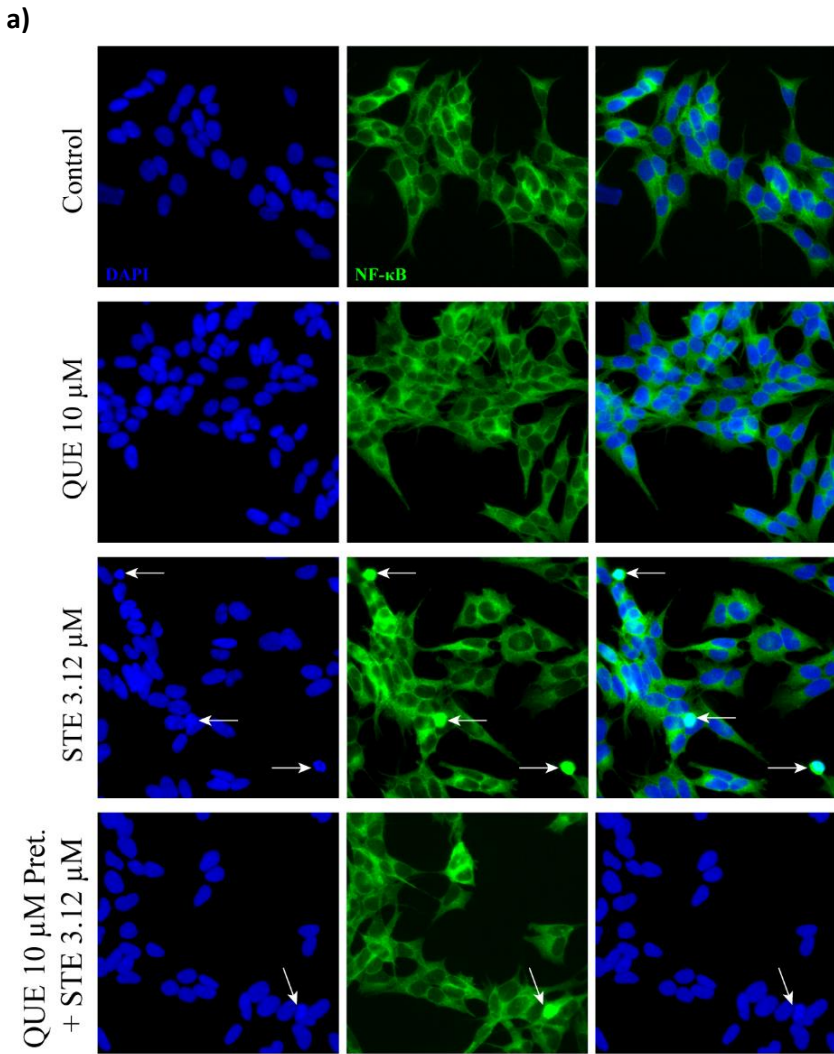


**Fig. 3.** Effect of STE and QUE on NOS-2 (a) and HO-1 (b) expression in SH-SY5Y cell line. Cells were treated with STE (0.78, 1.56 and 3.12 μM) for 24 h in the presence or absence of QUE pre-treatment (10 μM) for 2 h. The relative mRNA expression levels were measured by real-time PCR. The average of the target gene values was normalized to the corresponding 18S rRNA value and expressed as fold change compared with the solvent control. Data are expressed as mean ± SEM of three independent experiments ( $n = 3$ ) with 3 replicates each. (\*)  $p \leq 0.05$  indicates a significant difference compared to the corresponding solvent control. (#)  $p \leq 0.05$  indicates a significant difference respect to the corresponding STE treated cells. indicates a significant difference from solvent control. (#)  $p \leq 0.01$  indicates a significant difference from 0.78 μM of STE.

### 3.3.2. *Quercetin prevents STE-induced nuclear localization of NF- $\kappa$ B*

Under normal physiological conditions, the transcription factor NF- $\kappa$ B is maintained as an inactive form in the cytoplasm of cells by binding with its inhibitory protein I- $\kappa$ B. Various extracellular stimuli including oxidative stress induce the activation of I- $\kappa$ B kinase (IKK) that phosphorylates I- $\kappa$ B, leading to its ubiquitinylation and degradation by proteasomes. Unmasking the nuclear localization signal of NF- $\kappa$ B results in a rapid activation and translocation of NF- $\kappa$ B into the nucleus, where it up-regulates the expression of genes involved in inflammatory response.

To better understand the underlying molecular mechanism of STE-induced toxicity, the effect on nuclear translocation of the transcription factor NF- $\kappa$ B was studied through indirect immunofluorescence, with the primary antibody directed against NF- $\kappa$ B, FITC conjugated secondary antibody and nucleus stained with DAPI. Co-localization of FITC and DAPI results in a characteristic turquoise blue color. To determine NF- $\kappa$ B translocation, cells were exposed to STE treatment (0.78, 1.56 and 3.12  $\mu$ M) for different time intervals (15, 30, 60 min, 3, 6 and 24 h). Our findings indicated that NF- $\kappa$ B migrates into the nucleus following 24 h of STE exposure (Fig. 4c). Pre-treatment of cells with QUE 10  $\mu$ M for 2 h followed by STE for 24 h resulted in a major retention of NF- $\kappa$ B in the cytoplasm compared to STE treated groups alone (Fig.4d). The bar graph of the nuclei/cytoplasm ratio fluorescence intensity of cells positive for the antibody under study is shown in Fig. 4e.



(Caption of the figure on the next page)

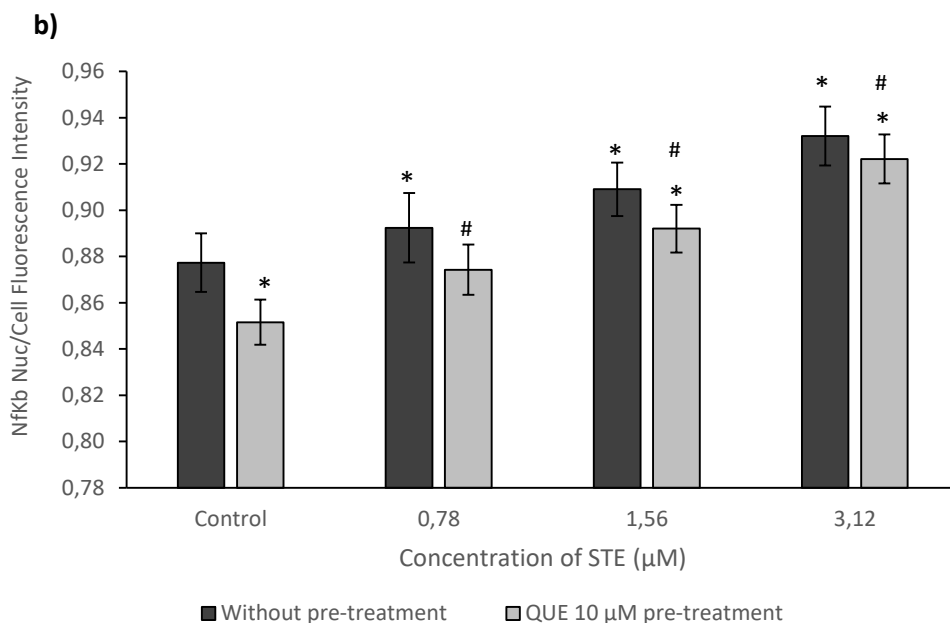


**Fig. 4.** Effect of STE and QUE on NF- $\kappa$ B translocation. a) The SH-SY5Y cells were exposed to STE (0.78, 1.56 and 3.12  $\mu\text{M}$ ) for 24 h in presence or absence of QUE 10  $\mu\text{M}$  pre-treatment, fixed and studied for localization of NF- $\kappa$ B through indirect immunofluorescence using FITC conjugated secondary antibody (green). The nucleus was stained with DAPI (blue). Figures show DAPI staining, FITC staining and overlay. Images were obtained by using the automated microscope IN Cell Analyzer 2000 (40x magnification). The data shown are representative of three independent experiments. b) Quantification of the nuclei/cytoplasm ratio fluorescence intensity. Data are expressed as mean  $\pm$  SEM ( $n = 3$ ). (\*)  $p \leq 0.05$  indicates a significant difference compared to the corresponding solvent control. (#)  $p \leq 0.05$  indicates a significant difference respect to the corresponding STE treated cells.

---

### 3.4. Effect of QUE and STE on inflammatory markers

As NF- $\kappa$ B is a pleiotropic regulator of numerous genes involved in the immune and inflammatory response, we continued to explore the effect of STE and QUE on the expression of the pro-inflammatory cytokines tumor necrosis factor- $\alpha$  (TNF- $\alpha$ ) and interleukin-6 (IL-6). The analysis of the relative mRNA expression levels of TNF- $\alpha$  in the various samples indicated that no statistically significant changes were induced by 24 h of STE exposure at all concentration tested (Fig. 5a). On the other hand, IL-6 mRNA was down-regulated in a concentration-dependent manner by STE (Fig. 5b). Compared to cells exposed to the mycotoxin alone, pre-treatment of cells with QUE 10  $\mu$ M for 2 h followed by STE for 24 h resulted in a further lower expression of both inflammatory genes in cells exposed to STE 0.78 and 1.56  $\mu$ M. As concerning the highest STE concentration, a down-regulation of TNF- $\alpha$  mRNA was obtained compared to STE treated group alone, whereas for IL-6 expression no differences were observed between cells exposed to STE 3.12  $\mu$ M in presence or absence of QUE pre-treatment. For both genes, QUE treatment alone significantly lowered the mRNA expression levels compared to control cells.

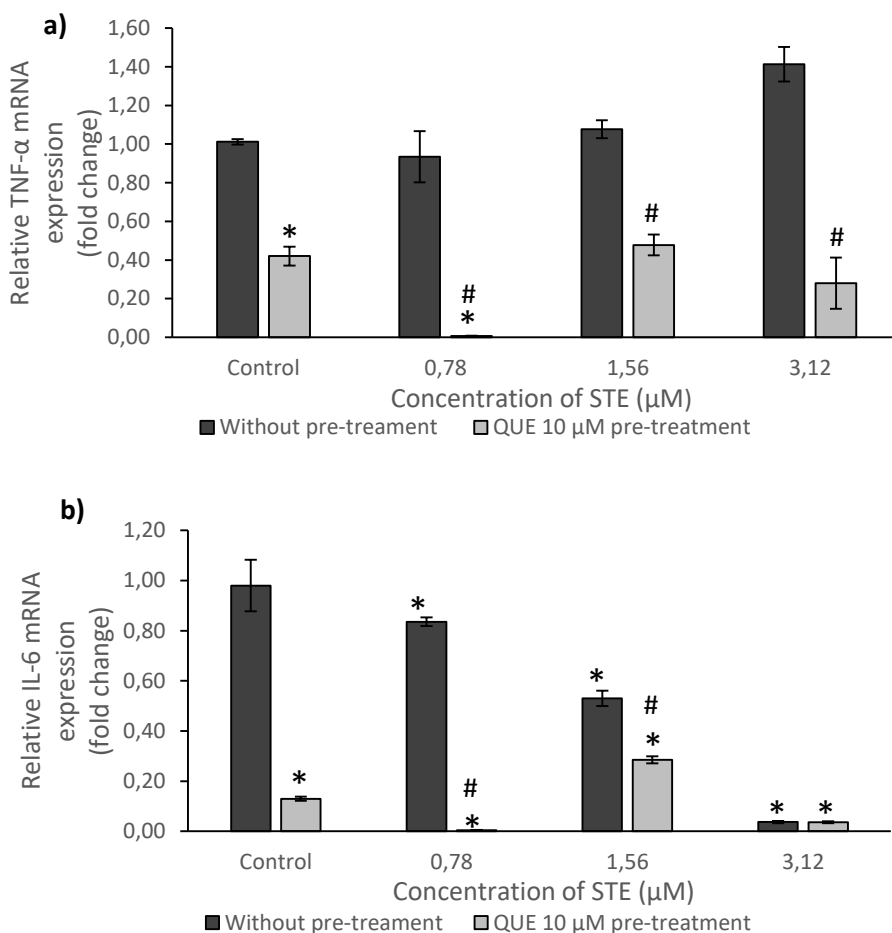


**Fig. 5.** Effect of STE and QUE on TNF- $\alpha$  (a) and IL-6 (b) expression in SH-SY5Y cell line. Cells were treated with STE (0,78, 1,56 and 3,12  $\mu\text{M}$ ) for 24 h in the presence or absence of QUE pre-treatment (10  $\mu\text{M}$ ) for 2 h. The relative mRNA expression levels were measured by real-time PCR. The average of the target gene values was normalized to the corresponding 18S rRNA value and expressed as fold change compared with the solvent control. Data are expressed as mean  $\pm$  SEM of three independent experiments ( $n = 3$ ) with 3 replicates each. (\*)  $p \leq 0,05$  indicates a significant difference compared to the corresponding solvent control. (#)  $p \leq 0,05$  indicates a significant difference respect to the corresponding STE treated cells.



#### 4. Discussion

It is now well known that excessive ROS generation from both endogenous and exogenous insults causes an imbalance of the normal cell reduction-oxidation (redox) state, which can trigger cell damage by oxidizing macromolecular structures, such as DNA, proteins, lipids, and all the other cell components, as well as disrupting normal cellular signaling (Bergamini et al., 2004). To counteract the detrimental effects of free radicals, cells normally contain a battery of endogenous protective systems; however, it is possible that ROS production supersedes the cell ability to counter it (Thannickal and Fanburg, 2000). Dietary intake of antioxidants is a plausible and effective way to augment and fortify endogenous antioxidant defense systems, since many antioxidants act as free radical scavengers and immunomodulators, resulting in cytoprotection (Kuchi Bhotla et al., 2021).

Oxidative stress appears to be a common trigger for many of the effects associated to STE exposure (Balogh et al., 2019; Dubravka et al., 2019; Gao et al., 2015; Kovesi et al., 2019; Zingales et al., 2020a). Nevertheless, effective antioxidants against its toxicity are sparsely reported in literature (El-Desouky et al., 2015; Gao et al., 2015; Zingales et al., 2020a). The present study attempts to explore the *in vitro* cytoprotective effect of the flavonol QUE on STE-induced oxidative stress as well as some molecular redox signaling molecules using human neuroblastoma SH-SY5Y cells. In our study, the pre-treatment with QUE (10  $\mu$ M) significantly was found to restore the STE-mediated impairment of cell viability. Cytoprotective effect of QUE against STE-induced toxicity is attributable to its ability to perform as a powerful antioxidant and free radical scavenger. Results showed that pre-treatment of cells with QUE (10  $\mu$ M) for 2

h followed by STE exposure significantly reduced STE-induced ROS up to the levels of untreated control cells. This agrees well with the existing literature showing QUE as a powerful antioxidant capable to reduce mycotoxin-induced oxidative stress-mediated cell death by inhibiting the increase in intracellular ROS (Boussabbeh et al., 2016; Ghadiri et al., 2019; Gitika et al., 2006; Periasamy et al., 2016; Ramyaa and Padma, 2013).

In addition, our present study provided further indication of the involvement of oxidative stress in STE-induced cytotoxicity, as evidenced by the induction of other indicators of oxidative stress, such as HO-1 and NOS-2. An overwhelming body of evidence indicates that both antioxidant enzymes are induced by a wide range of stress-related stimuli (Chen et al., 2017; Consoli et al., 2021; Farghali et al., 2009). While the first one catalyzes the first and rate-limiting step in heme degradation, playing a major role in the defense against oxidative tissue injury, the last one encodes inducible-NOS (iNOS) and generates nitric oxide (NO) by oxidative deamination of arginine. In the present study, we found that STE exposure induced a concentration-dependent up-regulation of the HO-1 and NOS-2 mRNA levels. If on one hand increased HO-1 expression levels has been shown to represent an adaptive response to increased oxidative stress, on the other hand, it has been demonstrated that alteration in NO signaling through increased NOS-2 expression leads to mitochondrial enzymes, nucleic acids and proteins damages and cell death (Allen and Bayraktutan, 2009; Lee et al., 2005). Therefore, our results further confirm the ability of STE to induce oxidative stress. However, QUE pre-treatment substantially decreased the expression of both genes. In particular, the STE-induced up-regulation of NOS-2 was reduced until NOS-2 expression was not significantly different compared to control cells at all concentrations of STE. On

---

the contrary, as regards the antioxidant enzyme HO-1, QUE pre-treatment did not completely prevent its expression, reducing it only in cells exposed to the lowest STE concentration. However, the increase in HO-1 expression induced by QUE at the highest STE concentrations may be interpreted as an enhancement of the cellular antioxidant defense system.

It has been reported that for the transcriptional activation of the NOS-2 promoter is required the redox signaling molecule NF- $\kappa$ B. The NF- $\kappa$ B transcription factor is a central regulator of immune and inflammatory response and is known to be induced by ROS. Therefore, we decided to evaluate the effect of STE on NF- $\kappa$ B nuclear translocation in the presence and absence of QUE pre-treatment. Our results showed that STE induced nuclear translocation of NF- $\kappa$ B after 24 h of exposure. Pre-treatment of cells with QUE followed by STE exposure resulted in reduced activation of NF- $\kappa$ B compared to cells treated only with STE, indicating that QUE modulates the transcription factor NF- $\kappa$ B. The ability of QUE to reduce NF- $\kappa$ B nuclear translocation may be related to its antioxidant capacity, possibly through inhibition of ROS generation. However, in cells pre-treated with QUE and exposed to the highest concentrations of STE, significant activation of the transcription factor NF- $\kappa$ B was observed compared to control cells, suggesting that other mycotoxin-induced stimuli might be involved in NF- $\kappa$ B nuclear translocation. Similar results were obtained in HepG2 human hepatocellular carcinoma cells (Ramya et al., 2014) and in Vero normal African green monkey kidney cells (Ramya and Padma, 2013) exposed to ochratoxin A (OTA).

Finally, considering the key role played by NF- $\kappa$ B in the regulation of the inflammatory response, we evaluated the putative effect of STE in the presence and absence of QUE pre-treatment on the expression levels of the pro-inflammatory cytokines TNF- $\alpha$  and IL-6 in SH-SY5Y cells. Our results showed no changes in TNF- $\alpha$  expression levels and a down-regulation of IL-6 mRNA following STE exposure. Likewise, Zhang et al. (2012) found that STE significantly down-regulated the expression of TNF- $\alpha$  and IL-6 mRNA levels in murine peripheral blood mononuclear cells (mPBMCs) and peritoneal macrophages, as well as decreased serum TNF- $\alpha$  and IL-6 levels in BALB/c mice, suggesting a negative immunomodulatory effect of STE. Furthermore, several mycotoxins have been shown to down-regulate cytokines production and have a negative immunomodulatory effects. In swine alveolar macrophages TNF- $\alpha$  mRNA levels resulted to be decreased after Fumonisin B1 incubation (Liu et al., 2002). The production of IL-6 was inhibited by deoxynivalenol (DON) in human lymphocytes, as well as citrinin (CIN) has been shown to significantly reduce IL-6 levels in the A549 human alveolar epithelial carcinoma cells (Johannessen et al., 2007). Accordingly, the results of our study, despite their preliminary character, confirm that similarly to other mycotoxins, STE has negative immunomodulatory effects, which can lead to depression of the systemic host defence system. As regards to QUE pre-treatment, it resulted in reduced TNF- $\alpha$  and IL-6 mRNA expression levels compared to cells treated only with STE, maybe due to the attenuation of NF- $\kappa$ B activation. Similar to our results, QUE was reported to inhibit the release of inflammatory markers during lipopolysaccharide exposure, due to reduced activation of the nuclear factor NF- $\kappa$ B (Lee et al., 2016; Nair et al., 2006; Periasamy et al., 2016).

In conclusion, in the present study it has been demonstrated for the first time the sequence of some of the molecular mechanisms implicated in STE-induced toxicity, highlighting the firm involvement of oxidative stress. In addition, the results of this study revealed the protective role of QUE in STE-induced oxidative damage through its antioxidant and immunomodulatory properties. Taking together, our results make QUE an attractive dietary flavonol for protection against STE toxicity. Since there is an increasing awareness of the importance of establishing the potential risk associated with STE exposure, a thorough knowledge on the cellular effects of this mycotoxin and effective measures to combat its toxicity represent important aspects to be considered from the angle of food safety. Overall, further investigations are needed to better explore the good potential of QUE as a cytoprotective agent for STE-induced mycotoxicosis, as well as to verify its ability *in vivo* to reduce STE-toxicity.

### **Acknowledgments**

We would like to thank the cell culture and microscopy service from the SCSIE of the University of Valencia for their technical support. This research has been supported by the Generalitat Valenciana pre-doctoral grant "Santiago Grisolia (GRISOLIAP/2018/092) CPI-18-117" and by the Spanish Ministry of Science and Innovation project (PID2020-115871RB-I00-ALJ).

### **Conflict of interest statement**

The authors declare that there are no conflicts of interest.

## References

- Abdel-Wahhab, M.A., Hasan, A.M., Aly, S.E., Mahrous, K.F., 2005. Adsorption of sterigmatocystin by montmorillonite and inhibition of its genotoxicity in the Nile tilapia fish (*Oreochromis niloticus*). *Mutat Res* 582, 20-27. doi: 10.1016/j.mrgentox.2004.12.009
- Alfadda, A.A., Sallam, R.M., 2012. Reactive oxygen species in health and disease. *J Biomed Biotechnol* 2012, 936486. doi: 10.1155/2012/936486
- Allen, C.L., Bayraktutan, U., 2009. Oxidative stress and its role in the pathogenesis of ischaemic stroke. *Int J Stroke* 4, 461-470. doi: 10.1111/j.1747-4949.2009.00387.x
- Aly, S.A., Elewa, N.A., 2007. The effect of Egyptian honeybee propolis on the growth of *Aspergillus versicolor* and sterigmatocystin biosynthesis in Ras cheese. *J Dairy Res* 74, 74-78. doi: 10.1017/S002202990600207X
- Babaei, F., Mirzababaei, M., Nassiri-Asl, M., 2018. Quercetin in Food: Possible Mechanisms of Its Effect on Memory. *J Food Sci* 83, 2280-2287. doi: 10.1111/1750-3841.14317
- Balogh, K., Kovesi, B., Zandoki, E., Kulcsar, S., Ancsin, Z., Erdelyi, M., et al., 2019. Effect of Sterigmatocystin or Aflatoxin Contaminated Feed on Lipid Peroxidation and Glutathione Redox System and Expression of Glutathione Redox System Regulatory Genes in Broiler Chicken. *Antioxidants* 8 (7): 201. doi: 10.3390/antiox8070201
- Barcelos, G.R., Grotto, D., Angeli, J.P., Serpeloni, J.M., Rocha, B.A., Bastos, J.K., et al., 2011. Evaluation of antigenotoxic effects of plant flavonoids quercetin and rutin on HepG2 cells. *Phytother Res* 25, 1381-1388. doi: 10.1002/ptr.3436

---

Bergamini, C.M., Gambetti, S., Dondi, A., Cervellati, C., 2004. Oxygen, reactive oxygen species and tissue damage. *Curr Pharm Des* 10, 1611-1626. doi: 10.2174/1381612043384664

Bischoff, S.C., 2008. Quercetin: potentials in the prevention and therapy of disease. *Curr Opin Clin Nutr Metab Care* 11, 733-740. doi: 10.1097/MCO.0b013e32831394b8

Boussabbeh, M., Prola, A., Ben Salem, I., Guilbert, A., Bacha, H., Lemaire, C., et al., 2016. Crocin and quercetin prevent PAT-induced apoptosis in mammalian cells: Involvement of ROS-mediated ER stress pathway. *Environ Toxicol* 31, 1851-1858. doi: 10.1002/tox.22185

Chen, C., Zhou, J., Ji, C., 2010. Quercetin: a potential drug to reverse multidrug resistance. *Life Sci* 87, 333-338. doi: 10.1016/j.lfs.2010.07.004

Chen, Z.Q., Mou, R.T., Feng, D.X., Wang, Z., Chen, G., 2017. The role of nitric oxide in stroke. *Med Gas Res* 7, 194-203. doi: 10.4103/2045-9912.215750

Consoli, V., Sorrenti, V., Grosso, S., Vanella, L., 2021. Heme Oxygenase-1 Signaling and Redox Homeostasis in Physiopathological Conditions. *Biomolecules* 11. doi: 10.3390/biom11040589

Devore, E.E., Kang, J.H., Stampfer, M.J., Grodstein, F., 2013. The association of antioxidants and cognition in the Nurses' Health Study. *Am J Epidemiol* 177, 33-41. doi: 10.1093/aje/kws202

Dubravka, R., Daniela, J., Andrea, H.T., Domagoj, K., Nevenka, K., Lada, R., et al., 2019. Sterigmatocystin moderately induces oxidative stress in male Wistar rats after short-term oral treatment. *Mycotoxin Res* 36, 181-191. doi: 10.1007/s12550-019-00382-8

El-Desouky, T.A., Sherif, R.M., Sherif, S.M., Khayria, M.N., 2015. Protective effect of aqueous extract pomegranate peel against sterigmatocystin toxicity in rat. *J. Drug Deliv. Therapeut.* 5, 9–18. <https://doi.org/10.22270/jddt.v5i5.1136>.

Farghali, H., Cerny, D., Kamenikova, L., Martinek, J., Horinek, A., Kmonickova, E., et al., 2009. Resveratrol attenuates lipopolysaccharide-induced hepatitis in D-galactosamine sensitized rats: role of nitric oxide synthase 2 and heme oxygenase-1. *Nitric Oxide* 21, 216-225. doi: 10.1016/j.niox.2009.09.004

Gao, W., Jiang, L., Ge, L., Chen, M., Geng, C., Yang, G., et al., 2015. Sterigmatocystin-induced oxidative DNA damage in human liver-derived cell line through lysosomal damage. *Toxicol In Vitro* 29, 1-7. doi: 10.1016/j.tiv.2014.08.007

Ghadiri, S., Spalenza, V., Dellaflora, L., Badino, P., Barbarossa, A., Dall'Asta, C., et al., 2019. Modulation of aflatoxin B1 cytotoxicity and aflatoxin M1 synthesis by natural antioxidants in a bovine mammary epithelial cell line. *Toxicol In Vitro* 57, 174-183. doi: 10.1016/j.tiv.2019.03.002

Gitika, B., Sai Ram, M., Sharma, S.K., Ilavazhagan, G., Banerjee, P.K., 2006. Quercetin protects C6 glial cells from oxidative stress induced by tertiary-butylhydroperoxide. *Free Radic Res* 40, 95-102. doi: 10.1080/10715760500335447

Hutanasu, C., Sfarti, C., Trifan, A., Cojocariu, C., Singeap, A.M., Spac, A., Stanciu, C., 2011. High levels of sterigmatocystin in patients with chronic liver diseases. *Rev Med Chir Soc Med Nat Iasi* 115, 33-37.

Johannessen, L.N., Nilsen, A.M., Lovik, M., 2007. Mycotoxin-induced depletion of intracellular glutathione and altered cytokine production in the



---

human alveolar epithelial cell line A549. *Toxicol Lett* 168, 103-112. doi: 10.1016/j.toxlet.2006.11.002

Klaunig, J.E., Kamendulis, L.M., 2004. The role of oxidative stress in carcinogenesis. *Annu Rev Pharmacol Toxicol* 44, 239-267. doi: 10.1146/annurev.pharmtox.44.101802.121851

Kocic-Tanackov, S., Dimic, G., Levic, J., Tanackov, I., Tepic, A., Vujicic, B., et al., 2012. Effects of onion (*Allium cepa* L.) and garlic (*Allium sativum* L.) essential oils on the *Aspergillus versicolor* growth and sterigmatocystin production. *J Food Sci* 77, M278-284. doi: 10.1111/j.1750-3841.2012.02662.x

Kovesi, B., Pelyhe, C., Zandoki, E., Mezes, M., Balogh, K., 2019. Effect of short-term sterigmatocystin exposure on lipid peroxidation and glutathione redox system and expression of glutathione redox system regulatory genes in common carp liver. *Toxicon* 161, 50-56. doi: 10.1016/j.toxicon.2019.03.001

Kuchi Bhotla, H., Meyyazhagan, A., Pappusamy, M., Park, S., Arumugam, V.A., Pushparaj, K., et al., 2021. Dietary nutrients and their control of the redox bioenergetic networks as therapeutics in redox dysfunctions sustained pathologies. *Pharmacol Res* 170, 105709. doi: 10.1016/j.phrs.2021.105709

Lakhanpal, P., Rai, D.K., 2007. Quercetin: a versatile flavonoid. *Internet J. Med.* 2, 22–37. doi: 10.4314/ijmu.v2i2.39851

Larson, A.J., Symons, J.D., Jalili, T., 2010. Quercetin: A Treatment for Hypertension?-A Review of Efficacy and Mechanisms. *Pharmaceuticals* 3, 237-250. doi: 10.3390/ph3010237

Lee, M., McGeer, E.G., McGeer, P.L., 2016. Quercetin, not caffeine, is a major neuroprotective component in coffee. *Neurobiol Aging* 46, 113-123. doi: 10.1016/j.neurobiolaging.2016.06.015

Lee, Y.M., Cheng, P.Y., Hong, S.F., Chen, S.Y., Lam, K.K., Sheu, J.R., et al., 2005. Oxidative stress induces vascular heme oxygenase-1 expression in ovariectomized rats. *Free Radic Biol Med* 39, 108-117. doi: 10.1016/j.freeradbiomed.2005.02.033

Liu, B.H., Yu, F.Y., Chan, M.H., Yang, Y.L., 2002. The effects of mycotoxins, fumonisin B1 and aflatoxin B1, on primary swine alveolar macrophages. *Toxicol Appl Pharmacol* 180, 197-204. doi: 10.1006/taap.2002.9406

Mandel, S., Amit, T., Reznichenko, L., Weinreb, O., Youdim, M.B., 2006. Green tea catechins as brain-permeable, natural iron chelators-antioxidants for the treatment of neurodegenerative disorders. *Mol Nutr Food Res* 50, 229-234. doi: 10.1002/mnfr.200500156

Mavrommatis, A., Giamouri, E., Tavrizelou, S., Zacharioudaki, M., Danezis, G., Simitzis, P.E., et al., 2021. Impact of Mycotoxins on Animals' Oxidative Status. *Antioxidants* 10 (2), 214. doi: 10.3390/antiox10020214

Mendoza, E.E., Burd, R., 2011. Quercetin as a systemic chemopreventative agent: structural and functional mechanisms. *Mini Rev Med Chem* 11, 1216-1221. doi: 10.2174/13895575111091216

Na, H.J., Lee, G., Oh, H.Y., Jeon, K.S., Kwon, H.J., Ha, K.S., et al., 2006. 4-O-Methylgallic acid suppresses inflammation-associated gene expression by inhibition of redox-based NF-kappaB activation. *Int Immunopharmacol* 6, 1597-1608. doi: 10.1016/j.intimp.2006.06.004

Nair, M.P., Mahajan, S., Reynolds, J.L., Aalinkeel, R., Nair, H., Schwartz, S.A., et al., 2006. The flavonoid quercetin inhibits proinflammatory cytokine (tumor necrosis factor alpha) gene expression in normal peripheral blood

---

mononuclear cells via modulation of the NF-kappa beta system. *Clin Vaccine Immunol* 13, 319-328. doi: 10.1128/CVI.13.3.319-328.2006

Nemeth, K., Piskula, M.K., 2007. Food content, processing, absorption and metabolism of onion flavonoids. *Crit Rev Food Sci Nutr* 47, 397-409. doi: 10.1080/10408390600846291

Periasamy, R., Kalal, I.G., Krishnaswamy, R., Viswanadha, V., 2016. Quercetin protects human peripheral blood mononuclear cells from OTA-induced oxidative stress, genotoxicity, and inflammation. *Environ Toxicol* 31, 855-865. doi: 10.1002/tox.22096

Ramyaa, P., Krishnaswamy, R., Padma, V.V., 2014. Quercetin modulates OTA-induced oxidative stress and redox signalling in HepG2 cells - up regulation of Nrf2 expression and down regulation of NF-kappaB and COX-2. *Biochim Biophys Acta* 1840, 681-692. doi: 10.1016/j.bbagen.2013.10.024

Ramyaa, P., Padma, V.V., 2013. Ochratoxin-induced toxicity, oxidative stress and apoptosis ameliorated by quercetin--modulation by Nrf2. *Food Chem Toxicol* 62, 205-216. doi: 10.1016/j.fct.2013.08.048

Ruiz, M.J., Festila, L.E., Fernández, M., 2006. Comparison of basal cytotoxicity of seven carbamates in CHO-K1 cells. *Environ. Toxicol. Chem.* 88, 345-354. doi: 10.1080/02772240600630622

Russo, M., Spagnuolo, C., Tedesco, I., Bilotto, S., Russo, G.L., 2012. The flavonoid quercetin in disease prevention and therapy: facts and fancies. *Biochem Pharmacol* 83, 6-15. doi: 10.1016/j.bcp.2011.08.010

Salim, S., 2014. Oxidative stress and psychological disorders. *Curr Neuropharmacol* 12, 140-147. doi: 10.2174/1570159X11666131120230309

Sanchez-Carranza, J.N., Diaz, J.F., Redondo-Horcajo, M., Barasoain, I., Alvarez, L., Lastres, P., et al., 2018. Gallic acid sensitizes paclitaxel-resistant

human ovarian carcinoma cells through an increase in reactive oxygen species and subsequent downregulation of ERK activation. *Oncol Rep* 39, 3007-3014. doi: 10.3892/or.2018.6382

Sharma, D.R., Wani, W.Y., Sunkaria, A., Kandimalla, R.J., Sharma, R.K., Verma, D., et al., 2016. Quercetin attenuates neuronal death against aluminum-induced neurodegeneration in the rat hippocampus. *Neuroscience* 324, 163-176. doi: 10.1016/j.neuroscience.2016.02.055

Silvester, A.J., Aseer, K.R., Yun, J.W., 2019. Dietary polyphenols and their roles in fat browning. *J Nutr Biochem* 64, 1-12. doi: 10.1016/j.jnutbio.2018.09.028

Sivakumar, V., Thanisslass, J., Niranjali, S., Devaraj, H., 2001. Lipid peroxidation as a possible secondary mechanism of sterigmatocystin toxicity. *Hum Exp Toxicol* 20, 398-403. doi: 10.1191/096032701682692955

Thannickal, V.J., Fanburg, B.L., 2000. Reactive oxygen species in cell signaling. *Am J Physiol Lung Cell Mol Physiol* 279, L1005-1028. doi: 10.1152/ajplung.2000.279.6.L1005

Tian, H., Lou, J., Du, C., 1995. Determination of sterigmatocystin in cancerous tissues, blood and urine in patients with liver and stomach cancer. *Zhonghua Yu Fang Yi Xue Za Zhi* 29, 276-278.

Vanella, L., Li Volti, G., Distefano, A., Raffaele, M., Zingales, V., Avola, R., et al., 2017. A new antioxidant formulation reduces the apoptotic and damaging effect of cigarette smoke extract on human bronchial epithelial cells. *Eur Rev Med Pharmacol Sci* 21, 5478-5484. doi: 10.26355/eurrev\_201712\_13938

Vina, J., Borrás, C., Gomez-Cabrera, M.C., Orr, W.C., 2006. Part of the series: from dietary antioxidants to regulators in cellular signalling and gene

---

expression. Role of reactive oxygen species and (phyto)oestrogens in the modulation of adaptive response to stress. *Free Radic Res* 40, 111-119. doi: 10.1080/10715760500405778

Xiao, L., Luo, G., Tang, Y., Yao, P., 2018. Quercetin and iron metabolism: What we know and what we need to know. *Food Chem Toxicol* 114, 190-203. doi: 10.1016/j.fct.2018.02.022

Ye, J., Coulouris, G., Zaretskaya, I., Cutcutache, I., Rozen, S., Madden, T.L., 2012. Primer-BLAST: a tool to design target-specific primers for polymerase chain reaction. *BMC Bioinf.* 13, 134. doi: 10.1186/1471-2105-13-134

Zaplatic, E., Bule, M., Shah, S.Z.A., Uddin, M.S., Niaz, K., 2019. Molecular mechanisms underlying protective role of quercetin in attenuating Alzheimer's disease. *Life Sci* 224, 109-119. doi: 10.1016/j.lfs.2019.03.055

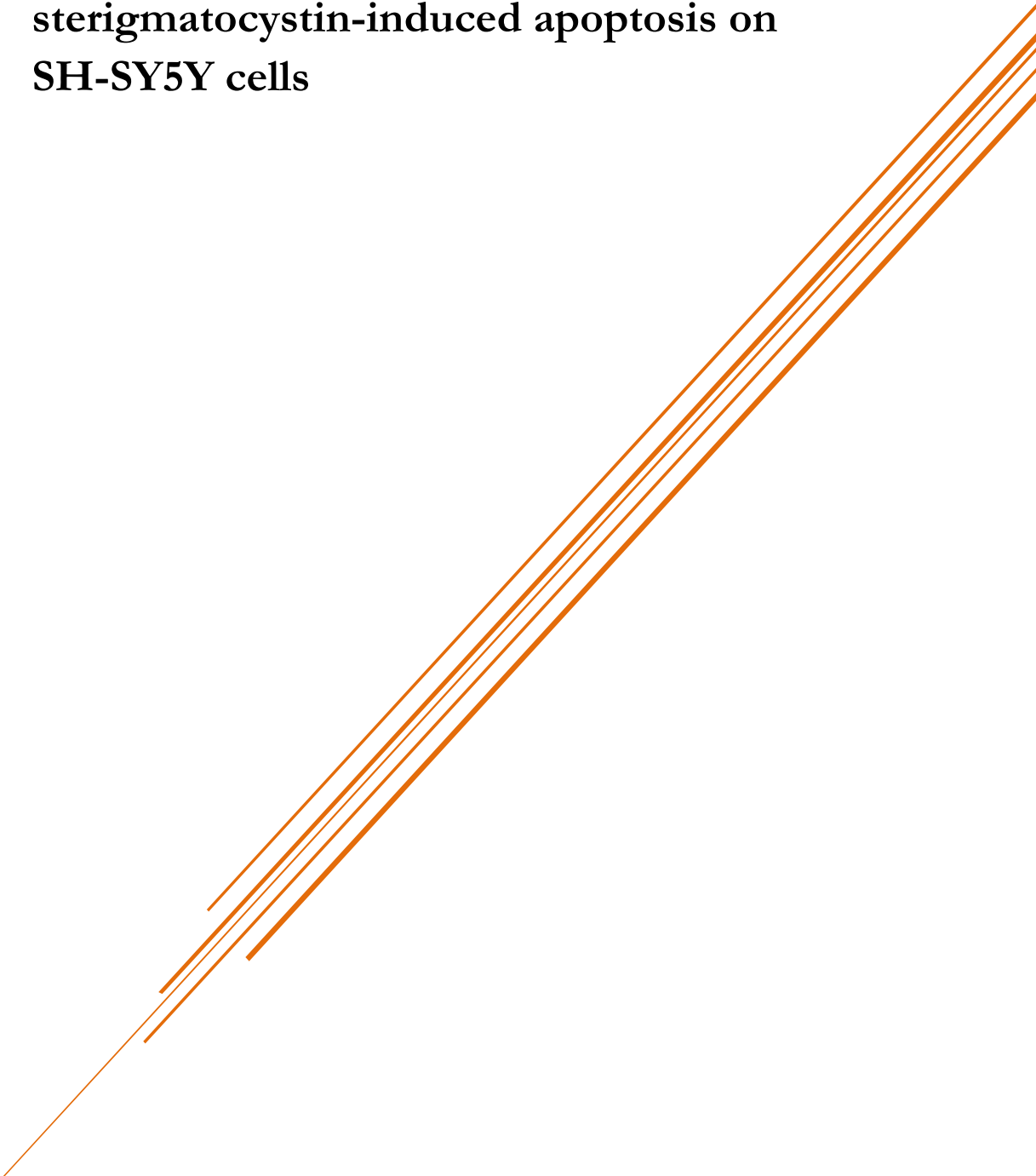
Zhang, Y., Yao, Z.G., Wang, J., Xing, L.X., Xia, Y., Zhang, X.H., 2012. Effects of sterigmatocystin on TNF- $\alpha$ , IL-6 and IL-12 expression in murine peripheral blood mononuclear cells and peritoneal macrophages in vivo. *Mol Med Rep* 5, 1318-1322. doi: 10.3892/mmr.2012.788

Zingales, V., Fernandez-Franzon, M., Ruiz, M.J., 2020a. Sterigmatocystin-induced cytotoxicity via oxidative stress induction in human neuroblastoma cells. *Food Chem Toxicol* 136, 110956. doi: 10.1016/j.fct.2019.110956

Zingales, V., Fernandez-Franzon, M., Ruiz, M.J., 2020b. Sterigmatocystin: Occurrence, toxicity and molecular mechanisms of action - A review. *Food Chem Toxicol* 146, 111802. doi: 10.1016/j.fct.2020.111802

Zingales, V., Fernandez-Franzon, M., Ruiz, M.J., 2020c. The role of mitochondria in sterigmatocystin-induced apoptosis on SH-SY5Y cells. *Food Chem Toxicol* 142, 111493. doi: 10.1016/j.fct.2020.111493

### **3.4. The role of mitochondria in sterigmatocystin-induced apoptosis on SH-SY5Y cells**







Food and Chemical Toxicology

**The role of mitochondria in sterigmatocystin-induced  
apoptosis on SH-SY5Y cells**

Veronica Zingales\*, Mónica Fernández-Franzón, Maria-José Ruiz

Laboratory of Food Chemistry and Toxicology, Faculty of Pharmacy, University of

Valencia, Av. Vicent Andrés Estellés s/n, 46100, Valencia, Spain

\*Corresponding author. Laboratory of Toxicology, Faculty of Pharmacy, University of Valencia, Av. Vicent Andrés Estellés, s/n, 46100, Burjassot, Valencia, Spain. *E-mail address:* [vezin@uv.es](mailto:vezin@uv.es) (V. Zingales).

### Abstract

Mitochondria are cellular organelles involved in many crucial functions, such as generation of energy (ATP) and initiation of apoptosis. The aim of the present study was to evaluate the role of mitochondria in the toxicity induced by sterigmatocystin (STE), a mycotoxin produced by fungi of the genus *Aspergillus*, on SH-SY5Y cells. Our results showed that STE exposure decreased cell viability in a time- and concentration-dependent manner by MTT assay and caused mitochondrial dysfunction, as highlighted by the increase of STE cytotoxicity in cells forced to rely on mitochondrial oxidative phosphorylation. Furthermore, intracellular ATP depletion and increased mitochondrial reactive oxygen species were also observed. Since mitochondria play a pivotal role in apoptosis, the induction of this process in response to STE exposure was decided to study. Our results showed an increase in apoptotic cell population by flow cytometry, further confirmed by the up-regulation of the expression levels of the pro-apoptotic genes *Bax* and *Casp-3* and the down-regulation of the anti-apoptotic gene *Bcl-2* by qPCR technique. Taken together, our results provide novel insights in the signalling pathways of the cell death process induced by STE in SH-SY5Y cells, highlighting the key role played by mitochondria in STE toxicity.

**Keywords:** Sterigmatocystin, SH-SY5Y cells, Cytotoxicity, Mitochondria, Apoptosis.

## 1. Introduction

Mitochondria are key cellular organelles known to guarantee many physiological processes, such as cell proliferation and differentiation, production of cellular energy, signal transduction and cell death. Alterations of one or more of these functions can lead to cellular stress and impairment of cell viability. In particular, the synthesis of high-energy molecules, mainly adenosine-5'-triphosphate (ATP), is a crucial process for cell survival. Considering that ATP synthesis from ADP and inorganic phosphate (Pi) involves a complex reaction network, any process that disturbs or blocks it results in a reduction of the ATP generation. In eukaryotic cells, mitochondria produce ATP through oxidative phosphorylation (OXPHOS), a process that involves the electron transport chain (ECT), a series of protein complexes and electron carrier molecules embedded in the inner mitochondrial membrane. The ECT pumps protons out of the mitochondrial matrix into the intermembrane space, generating an electrochemical gradient and, consequently, a membrane potential ( $\Delta\Psi_m$ ), used to synthesize ATP. However, in *in vitro* conditions, cell lines are metabolically adapted to growth rapidly and, for this reason, they derive most of their energy from glycolysis rather than OXPHOS, a phenomenon known as the Crabtree effect (Marroquin et al., 2007; Rodriguez-Enriquez et al., 2001). Evidence suggests that the Crabtree effect can be reversed by culturing cells in galactose as the main fuel source; these conditions abolish net yield of ATP from glycolysis and, correspondingly, cells are forced to rely on mitochondrial OXPHOS (Rossignol et al., 2004). The substitution of galactose for glucose in the culture medium is used as a method not only to shift the energy metabolism toward OXPHOS, but also as an expeditious way to determine mitochondrial toxicity and reveal mitochondrial dysfunction (Marroquin et al., 2007). Several chronic

diseases, including neurodegenerative diseases such as Parkinson's and Alzheimer's, are associated to mitochondrial dysfunction. The latter is characterized by losing efficiency in the ETC and reduction in ATP synthesis (Karbowski and Neutzner, 2012). To date, a lot of mitochondrial toxins are known (Wallace and Starkov, 2000). Among these, natural products, such as the *Streptomyces*-derived ETC inhibitor antimycin A or mycotoxins, have been recognized to contribute to the occurrence of mitochondrial dysfunction (Islam et al., 2018). Mycotoxins are toxic secondary metabolites that can occur in a variety of food and feed. They are produced by a number of fungal genera, primarily *Aspergillus*, *Penicillium*, *Alternaria* and *Fusarium* genus (Marin et al., 2013). Sterigmatocystin (STE) is a mycotoxin mainly produced by several species of the genus *Aspergillus*. Because this genus of fungi grows under a wide range of environmental conditions, including at low and high temperature (4-40 °C), fungal contamination may occur at various points in the food chain, such as the pre- and post-harvest stage or in food kept under refrigeration. Particularly, STE has been detected in animal feed and in human food, such as grains, cheese, spices, green coffee beans, in varying amounts depending on food (Versilovskis and De Saeger, 2010). Being the precursor of aflatoxin B1 (AFB1), one of the most potent carcinogen mycotoxin known, the dietary, dermal or respiratory exposure to STE might be an important health risk factor. In the past decades *in vivo* studies have demonstrated that STE is able to induce from acute symptoms to tumours, varying with species of animals tested, route and frequency of administrations (Fujii et al., 1976; Purchase and Van der Watt, 1973; Vesonder and Horn, 1985). In light of all this, STE has been classified in the Group 2B (possible human carcinogen) by the International Agency for Research on Cancer (IARC, 1987). Recently, several researchers have carried out

*in vitro* studies on different human cell cultures in order to clarify the role of STE as a human health hazard, highlighting the ability of STE to induce malignant transformation by influencing cell proliferation, inducing genotoxic effects, oxidative stress and apoptosis (Gao et al., 2015; Liu et al., 2014; Sun et al., 2002; Zouaoui et al., 2016).

We previously showed that oxidative stress plays a central role in STE-induced cytotoxicity in human neuroblastoma SH-SY5Y cells (Zingales et al., 2019). However, little is known about the effects of STE on cellular energy metabolism. So, the aim of the present study was to elucidate the underlying molecular mechanisms through which STE exerts its toxicity on SH-SY5Y cells. In particular, we hypothesised that STE affects mitochondrial functionality and thus investigated its effects on the ECT, ATP production, mitochondrial superoxide generation,  $\Delta\Psi_m$ , apoptosis and apoptosis related factors using MTT and fluorescence assay, flow cytometric analysis and qPCR technique.

## **2. Material and methods**

### *2.1. Reagents*

The reagent grade chemicals and cell culture compounds used, namely culture medium DMEM Ham's-F12, penicillin, streptomycin, trypsin/EDTA solutions, phosphate buffer saline (PBS), fetal bovin serum (FBS), tetrazolium bromide (MTT), propidium iodide (PI), HEPES, Rhodamine 123 (Rh123), 4',6-diamidine-2'-phenylindole dihydrochloride (DAPI), Antimycin A, Rotenone, D-(+)-Glucose and D-(+)-Galactose were from Sigma Chemical Co (St. Louis, MO, USA). The NaCl and ethanol were from Merck KGaA (Germany). The  $\text{CaCl}_2$  was from Scharlau Chemie S.A. (Barcelona, Spain). Methanol (MeOH) was from VWR International (LLC, Pennsylvania, USA). Human recombinant

annexin V-FITC conjugate was from Invitrogen (USA). Standard of the selected mycotoxin STE (MW: 324.28 g/mol) was purchased from Sigma-Aldrich (St. Louis Mo. USA). Stock solutions of the mycotoxin were prepared in methanol and maintained at  $-20\text{ }^{\circ}\text{C}$ .

### 2.2. *Cell culture and treatment*

Human neuroblastoma SH-SY5Y cells were cultured in DMEM Ham's-F12 medium supplemented with 10% FBS, 100 U/ml penicillin and 100 mg/ml streptomycin. The incubation conditions were pH 7.4, 5% CO<sub>2</sub> at 37 °C and 95% air atmosphere at constant humidity. The medium was changed every 2–3 days.

Moreover, SH-SY5Y cells were grown in glucose- or galactose-supplemented media and kept in 5% CO<sub>2</sub> at 37 °C and 95% air atmosphere at constant humidity. Glucose medium was prepared from DMEM Ham's-F12 medium supplemented with 25 mM glucose, 10% FBS, 100 U/ml penicillin and 100 mg/ml streptomycin. Galactose medium was prepared from DMEM Ham's-F12 medium supplemented with 10 mM galactose, 10% FBS, 100 U/ml penicillin and 100 mg/ml streptomycin. The final STE concentrations tested were achieved by adding STE solutions to the culture medium with a final methanol concentration of 1% (v/v). Appropriate controls containing the same amount of solvent were included in each experiment.

### 2.3. *In vitro cytotoxicity*

The tetrazolium bromide (MTT) assay was performed to determine cell proliferation. The MTT assay is a method based on the ability of viable cells to

metabolize the yellow soluble tetrazolium salt to a blue insoluble formazan product by the mitochondrial succinic dehydrogenase. The MTT assay was performed as described by Ruiz et al. (2006). For this endpoint bioassay, the SH-SY5Y cells were plated in 96-well microplates at a density of  $3 \times 10^4$  cells/well. After 48 h, when the cells reached 80% of confluence, the culture medium was replaced with fresh medium containing eight serial dilutions (serial dilution factor = 2) of the mycotoxin ranging from 25 to 0.19  $\mu\text{M}$ . The STE was exposed during 24, 48 and 72 h. During the exposure time, neither the medium nor the mycotoxin were replenished. For the MTT assay, after the time exposure, the medium containing STE was replaced with fresh medium containing 50  $\mu\text{l}$  (5 mg/ml PBS) of MTT salt. After 4 h of incubation at 37 °C under darkness, the resulting formazan crystals were solubilized in DMSO. The absorbance was measured at 540 nm using an automatic ELISA plate reader (MultiSkanEX, Labsystem, Helsinki, Finland). Cell viability was expressed as a percentage relative to the solvent control (1% MeOH). Two independent experiments for each time of exposure were conducted with 8 replicates each. The mean 50% inhibitory concentration ( $\text{IC}_{50}$ ) values were calculated using SigmaPlot version 11 (Systat Software Inc., GmbH, Germany).

#### 2.4. *Assessment of mitochondrial toxicity*

In order to evaluate the mitochondrial toxicity of STE, cell viability was determined by MTT assay refining the cell culture conditions. In particular, cells were cultured in the presence of glucose or galactose as the only available sugar. Briefly, SH-SY5Y cells were seeded in 96-well microplates at a density of  $3 \times 10^4$  cells/well. After 48 h, when the cells reached 80% of confluence, the culture medium was replaced with fresh glucose- or galactose-supplemented medium

containing six serial dilutions (serial dilution factor = 2) of the mycotoxin ranging from 25 to 0.78  $\mu\text{M}$ . After 24 h of exposure, the medium containing STE was removed and the MTT assay was performed as described above.

Additionally, cell viability was evaluated by MTT assay in SH-SY5Y grown in galactose-supplemented medium and exposed to STE 6.24  $\mu\text{M}$  and ETC inhibitors (antimycin A 10  $\mu\text{M}$  or rotenone 10  $\mu\text{M}$ ) for 24 h. The concentration of STE assayed was selected according to the results obtained in the previous cytotoxic assays carried out.

Cell viability was expressed as a percentage relative to the solvent control (1% MeOH). For each experiment, determinations were performed in three independent experiments with 4 replicates each.

### 2.5. *Measurement of intracellular adenosine triphosphate (ATP)*

Intracellular ATP levels were measured using the CellTiter-Glo<sup>®</sup> Luminescent Cell Viability Assay (Promega, USA), a method based on the properties of a thermostable luciferase, which generates a luminescent signal proportional to the amount of ATP present. The assay was performed according to manufacturer's instructions. Briefly, SHSY5Y cells were plated in opaque-walled 96-well microplates at a density of  $3 \times 10^4$  cells/well. The assay was conducted in the presence of glucose or galactose as the only available sugar. After 48 h, when the cells reached 80% of confluence, the culture medium was replaced with fresh glucose- or galactose-supplemented medium containing six serial dilutions (serial dilution factor = 2) of the mycotoxin ranging from 25 to 0.78  $\mu\text{M}$ . After 24 h of STE exposure, the medium was replaced with fresh medium and an equal volume of CellTiter-Glo reagent was added to each well.



Therefore, the plate was incubated at room temperature in the dark for 10 min. Luminescence was measured on a Fluoreskan Ascent FL (Thermo Fisher Scientific, Finland). The ATP content was expressed as a percentage relative to the solvent control (1% MeOH). Three independent experiments with 4 replicates each were performed.

### 2.6. *Mitochondrial superoxide measurement*

Mitochondrial superoxide was detected using MitoSOX™ Red Mitochondrial Superoxide Indicator (M36008, Thermo Fisher Scientific), a fluorogenic dye for highly selective detection of superoxide in the mitochondria of live cells. In fact, once in the mitochondria, MitoSOX™ Red reagent is oxidized by superoxide but not by other reactive oxygen species (ROS). In an oxidized state, the probe exhibits excitation/emission maxima at 510/580 nm. The assay was performed as described by Quintana-Cabrera et al. (2012), with some modifications. Briefly, a number of  $7 \times 10^5$  cells/well were seeded in six-well plates. After 24 h of exposure at STE (0.78, 1.56 and 3.12  $\mu\text{M}$ ), SH-SY5Y cells were trypsinized and MitoSOX Red reagent was added at a final concentration of 5  $\mu\text{M}$  in Hank's buffer to the cells. After incubation for 15 min at 37 °C in the dark, the medium was removed and the cells were washed three times with pre-warmed Hank's buffer. The three different concentrations assayed were set according to the results obtained by cell viability assay and our previously studies (Zingales et al., 2019). Three independent experiments were carried out and 10,000 live cells were acquired and analysed by a BD LSRFortessa (BD Biosciences) flow cytometry. Dead cells were not considered by staining with DAPI (20  $\mu\text{g}/\mu\text{l}$ ).

### 2.7. *Measurement of mitochondrial membrane potential ( $\Delta\Psi_m$ )*

The  $\Delta\Psi_m$  was evaluated in living cells using Rh123 as described by Liu et al. (2018). The Rh123 is a green-fluorescent dye that is rapidly sequestered by the cells with active mitochondria without cytotoxic effects. Briefly, SH-Y5Y cells were seeded in 96-well black culture microplates at a density of  $4 \times 10^4$  cells/well. After 24 h of STE exposure (0.78, 1.56 and 3.12  $\mu\text{M}$ ), the medium was removed and the cells were incubated with 5  $\mu\text{M}$  Rh123 in fresh medium for 15 min at 37 °C in the dark. The fluorescence was measured on a Wallace Victor2, model 1420 multilabel counter (PerkinElmer, Turku, Finland) at excitation/emission wavelengths of 485/535 nm. Results are expressed as decrease in fluorescence respect to the control (1% MeOH). Three independent experiments were performed.

### 2.8. *Measurement of necrosis-apoptosis by annexin V-FITC/PI*

Cell death generally proceeds through two molecular mechanisms: necrosis and apoptosis. The first one is an accidentally unregulated cell death, whereas apoptosis is a strictly genetically regulated cell death process. During apoptosis, the externalization of phosphatidylserine (PS) to the outer leaflet of the plasma membrane occurs. The different populations of apoptotic cells (early or late), necrotic and dead cells were identified by Annexin V-FITC/PI double staining (Vermes et al., 1995). Annexin V is a  $\text{Ca}^{2+}$ -dependent phospholipid-binding protein with high affinity for PS and binds to cells exposing PS to the extracellular side of the plasma membrane, whereas PI binds to the DNA of necrotic/dead cells. Viable cells with intact membranes exclude PI, whereas the membranes of dead and damaged cells are permeable to PI. Cells considered as viable are both Annexin V-FITC<sup>-</sup>/PI<sup>-</sup>; cells in early apoptosis (pro-

apoptotic/apoptotic) are Annexin V-FITC<sup>+</sup>/PI<sup>-</sup>; cells in late apoptosis, that have completed the apoptotic and start the necrotic process (apoptotic/necrotic), are both Annexin V-FITC<sup>+</sup>/PI<sup>+</sup>.

For the Annexin V-FITC assay,  $7 \times 10^5$  cells/well were seeded in six-well plates. After 2 and 24 h of exposure at 0.78, 1.56 and 3.12  $\mu$ M of STE, cells were trypsinized and resuspended in 360  $\mu$ l of HEPES-Ca<sup>2+</sup> buffer prepared as follows: 10 mM HEPES-NaOH (pH 7.4), 135 mM NaCl and 2.5 mM CaCl<sub>2</sub>. After incubation at 4 °C for 30 min in the dark, 10,000 cells were acquired and analysed by a BD LSRFortessa (BD Biosciences) flow cytometry. Quadrant statistics were performed to determine viable cells, early apoptotic, apoptotic/necrotic and necrotic cells from the total population of cells. Three independent experiments were performed for each time of STE exposure.

### 2.9. RNA extraction and quantification

Total RNA of SH-SY5Y cells exposed to methanol (solvent control) or different concentrations of STE (0.78, 1.56 and 3.12  $\mu$ M) was isolated using ReliaPrep<sup>™</sup> RNA Cell Miniprep System kit and treated with RNase free DNase (Promega) to remove genomic DNA contamination, according to the manufacturer's instructions. The extracted RNA of each sample was firstly checked for quantity and quality using Nanodrop2000 (Thermo Scientific), showing concentrations between 1244 and 277 ng/ $\mu$ l and appropriate 260/280 and 260/230 ratios both  $\geq 2$ . The RNA samples were stored at -20 °C until their dilution to 100 ng/ $\mu$ l with pure Milli-Q H<sub>2</sub>O until their reverse transcription to complementary DNA (cDNA). The protein content was determined by the Bio-Rad DC Protein Assay, catalogue number 5000116. Protein concentration ( $\mu$ g/ml) was measured at 690 nm.

### 2.10. Reverse transcription and qPCR reaction

First, synthesis of cDNA was carried out using 5  $\mu$ l of total RNA (500 ng) according to the instructions of TaqMan™ MicroRNA Reverse Transcription Kit protocol (Thermo Fisher Scientific, Spain). The cDNA was subsequently stored at  $-20$  °C until use for qPCR reactions. The qPCR was performed for all primer pairs and a single amplification product was obtained for each gene by the melting curve assay. Primer pairs for each gene were designed based on the entire coding region of the candidate genes using Primer-BLAST (Ye et al., 2012), according to the following parameters: primer length of about 20 bases, GC content of 45–60%, melting temperature ( $T_m$  value) between 58 and 59 °C, and amplicon product size ranging from 50 to 150 base pair. Primer amplification efficiency was determined from standard curve generated by cDNA serial dilution (serial dilution factor = 2) for each gene in triplicate. The gene-specific primers used in the present study are listed in Table 1. Correlation coefficients ( $R^2$ ) and amplification efficiencies (E) for each primer pairs were calculated from slope of regression line by plotting mean  $C_q$  values against the log cDNA dilution factor in StepOne software (Table 1). Real-time amplification reactions were performed in 96 well plates using SYBR Green detection reactive and run with the StepOne Plus Real-time PCR instrument (Applied Biosystems). Reactions were prepared in a total volume of 10  $\mu$ l containing: 3  $\mu$ l of 1:2 diluted template, 2  $\mu$ l of amplification primer mix (forward/reverse of each gene; 2.5  $\mu$ M) and 5  $\mu$ l of SYBR Green (Applied Biosystems). Non-template controls (NTC) were also included for each primer pair, replacing the template by DNase and RNase free water from the RNA extraction kit. Determinations were performed in two independent experiments with 3 replicates each. The cycling

conditions were set as default: initial denaturation step of 95 °C for 5 min to activate the Taq DNA polymerase, followed by 40 cycles of denaturation at 95°C for 15 s, annealing temperatures ranging from 58 to 59 °C (depending on the primers) for 15 s and elongation at 72 °C for 45 s. The melting curve was generated by heating the amplicon from 60 to 90 °C. Baseline, threshold cycles (Ct) and primer parameters analysis were automatically determined using the StepOne Plus Software version 2.3 (Applied Biosystems).

### *2.11. Statistical analysis*

Statistical analysis of data was carried out using GraphPad Prism version 7 (GraphPad Software, California, USA), statistical software package. Data were expressed as mean  $\pm$  SEM of different independent experiments. The statistical analysis of the results was performed by Student's t-test for paired samples. Differences between groups were analysed statistically with one-way ANOVA followed by the Tukey HDS post-hoc test for multiple comparisons. The difference level of  $p \leq 0.05$  was considered statistically significant.

Table 1.

Gene Symbol	Gene Name	Optimum Temp. (C°)	Forward primer/Reverse primer	Efficiency (%)	Linearity (R <sup>2</sup> )
<i>Bax</i>	Bcl-2-associated X protein	58.2	ATGCGTTTTTCCTTACGTGTCT/ GAGGTCAGCAGGGTAGATGA	105.3	0.982
<i>Bcl-2</i>	B-cell lymphoma 2	58.4	CTTCTTTGAGTTCGGTGGGG/ AAATCAAACAGAGGCCGCAT	111.0	0.984
<i>Casp-3</i>	Caspase-3	58	GGAGGCCGACTTCTTGTATG/ GCCATCCTTTGAATTTGCGC	106.9	0.989
<i>18S rRNA</i>	18S ribosomal RNA	58	CGGCTACCACATCCAAGGAA/ GCTGGAATTACCGCGGCT	105.0	0.994

### 3. Results

#### 3.1. *In vitro* cytotoxicity

The cytotoxic effect of STE on SH-SY5Y cells was evaluated by MTT assay over 24, 48 and 72 h in order to determine the molar concentration of mycotoxin able to reach the IC<sub>50</sub>. Cells exposed to STE revealed a decrease in cell viability in a time- and concentration-dependent manner (data not shown). After 24 h of exposure, STE did not show an IC<sub>50</sub> value at the range of concentration tested, while after 48 and 72 h of exposure, STE showed IC<sub>50</sub> values equal to 2.12  $\mu\text{M} \pm 1.18$  and 0.52  $\mu\text{M} \pm 0.05$ , respectively. After 24 h of exposure, STE only reduced significantly ( $p \leq 0.05$ ) cell proliferation at the concentrations ranging from 3.12 to 25  $\mu\text{M}$  by MTT assay, showing a decrease ranging from 80% to 28% respect to the control. However, after 48 and 72 h STE induced a significant reduction already starting from the lowest concentration (0.19  $\mu\text{M}$ ). The cell proliferation decrease obtained at these two times of exposure was ranging from 86% to 16% and from 78% to 9% respect to the control, respectively.

#### 3.2. *Assessment of mitochondrial toxicity and ATP content*

In order to assess loss of mitochondrial function in response to STE exposure, SH-SY5Y cells were cultured in presence of glucose (25 mM) or galactose (10 mM) as the only sugar available, switching cellular energy metabolism from glycolysis to OXPHOS. In these conditions, the cells are more susceptible to mitochondrial toxins. As shown in Fig. 1, the change in the fuel source caused a decrease in cell viability of galactose-grown cells compared to glucose-grown cells, suggesting that STE exhibited an increased level of toxicity in SH-SY5Y cells following the switch to OXPHOS. In particular, after 24 h of

exposure, in glucose-grown cells STE reduced significantly ( $p \leq 0.05$ ) cell proliferation at the concentrations ranging from 6.24 to 25  $\mu\text{M}$ , not showing an  $\text{IC}_{50}$  value at the range of concentration tested. On the other hand, in galactose-grown cells STE reduced cell viability already starting from 3.12  $\mu\text{M}$ , showing an  $\text{IC}_{50}$  value equal to  $2.57 \mu\text{M} \pm 0.46$ . Significant differences between the two culture conditions were observed at the concentrations ranging from 6.24 to 25  $\mu\text{M}$ . In contrast, no differences were obtained in the ATP content, except at the lowest STE concentration (Fig. 2). In fact, while in cells grown in glucose a significant decrease in ATP levels was observed when exposed to STE 0.78  $\mu\text{M}$ , in cells grown in galactose the ATP content slightly increased, suggesting that at this concentration the effect of STE differs depending on the route of ATP production. However, at the concentrations of STE ranging from 1.56 to 25  $\mu\text{M}$ , this difference disappeared, obtaining in both growth conditions a significant reduction in the ATP content starting from a STE concentration of 3.12  $\mu\text{M}$ . Finally, considering the crucial importance of a functional ETC in OXPHOS conditions, we also compared the effect of 24 h of exposure to STE 6.24  $\mu\text{M}$  in the presence or not of known ETC inhibitors (antimycin A and rotenone) in cells grown in galactose-supplemented medium. To carry out the assay, the lowest concentration of STE that had caused a significant difference in cell viability decrease between the two growth conditions was chosen (Fig. 1). Treatment with STE 6.24  $\mu\text{M}$  and 10  $\mu\text{M}$  rotenone resulted in a further significant decrease in SH-SY5Y cell viability respect to cells only exposed to the mycotoxin, while no effect was observed in the presence of 10  $\mu\text{M}$  antimycin A (Fig. 3). These data suggest that STE might affect the complex I but not the complex III of the ETC.



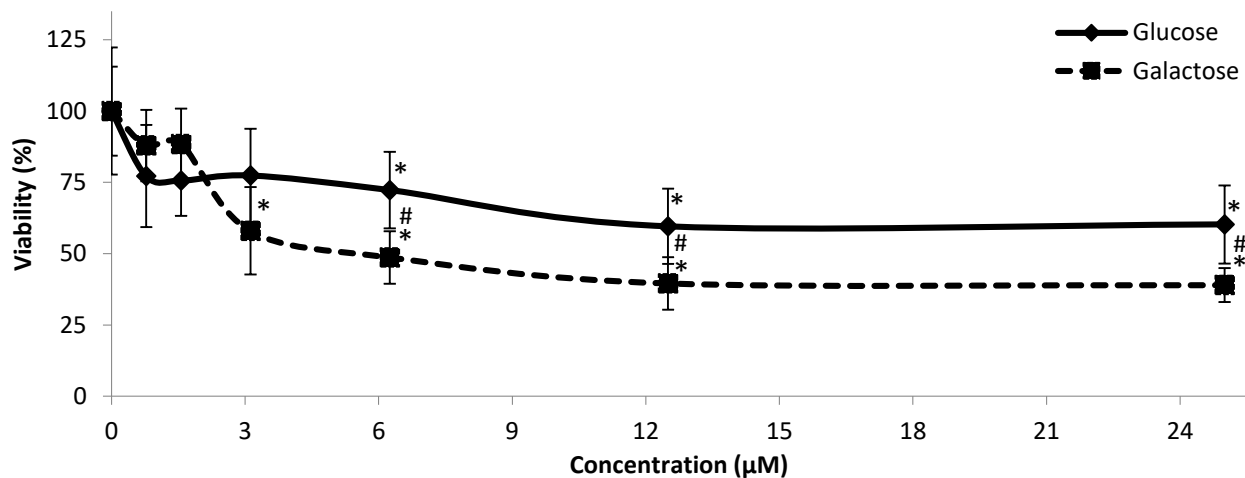


**Fig. 1.** Effect of STE (from 0.78 to 25 μM) on the viability of SH-SY5Y cells. Cells were grown in the presence of glucose (25 mM) or galactose (10 mM), following 24 h of exposure to STE. Measurements were performed in a microplate reader using the MTT viability assay. Data are expressed as mean ± SEM of three independent experiments with 4 replicates each. (\*)  $p \leq 0.05$  indicates a significant difference compared to the control. (#)  $p \leq 0.05$  indicates a significant difference respect to the corresponding cells grown in glucose-supplemented medium.

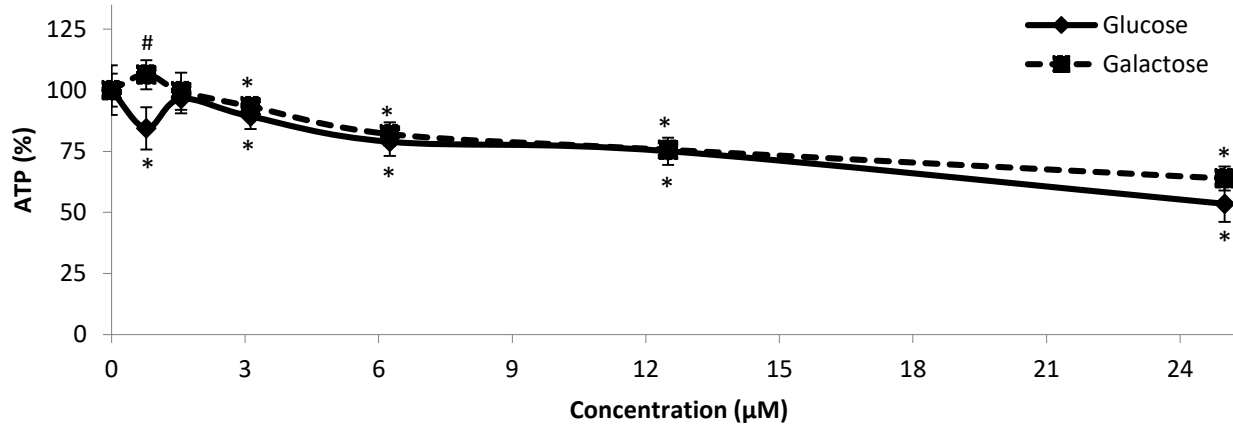


**Fig. 2.** Effect of STE (from 0.78 to 25 µM) on ATP levels in SH-SY5Y cells. Cells were grown in the presence of glucose (25 mM) or galactose (10 mM), following 24 h of exposure to STE. Measurements were performed in a microplate reader using the CellTiter-Glo® Luminescent Cell Viability Assay (Promega). Data are expressed as mean ± SEM of three independent experiments with 4 replicates each. (\*)  $p \leq 0.05$  indicates a significant difference compared to the control. (#)  $p \leq 0.05$  indicates a significant difference respect to the corresponding cells grown in glucose-supplemented medium.

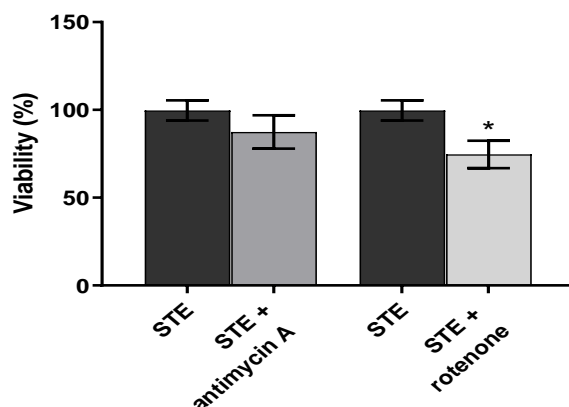


**Fig. 3.** Effect of 24 h of exposure to STE 6.24  $\mu\text{M}$  with or without antimycin A (10  $\mu\text{M}$ ) or rotenone (10  $\mu\text{M}$ ) on the viability of SH-SY5Y cells cultured in galactose-supplemented medium. Measurements were performed in a microplate reader using the MTT viability assay. Data are expressed as mean  $\pm$  SEM of three independent experiments with 4 replicates each. (\*)  $p \leq 0.05$  indicates a significant difference compared to STE 6.24  $\mu\text{M}$ .

### 3.3. Mitochondrial superoxide measurement

As shown in Fig. 4a, the levels of mitochondrial superoxide were detected after 24 h of exposure to STE (0.78, 1.56 and 3.12  $\mu\text{M}$ ) using the mitochondria-targeted superoxide-sensitive fluorogenic probe MitoSOX<sup>TM</sup> Red. The results indicated that stimulation of SH-SY5Y cells with STE significantly induced a concentration-dependent production of mitochondrial superoxide. An example of the dot plots representative of the control and the cells exposed to the highest concentration tested (3.12  $\mu\text{M}$ ) of STE can be observed in Fig. 4b and c, respectively.

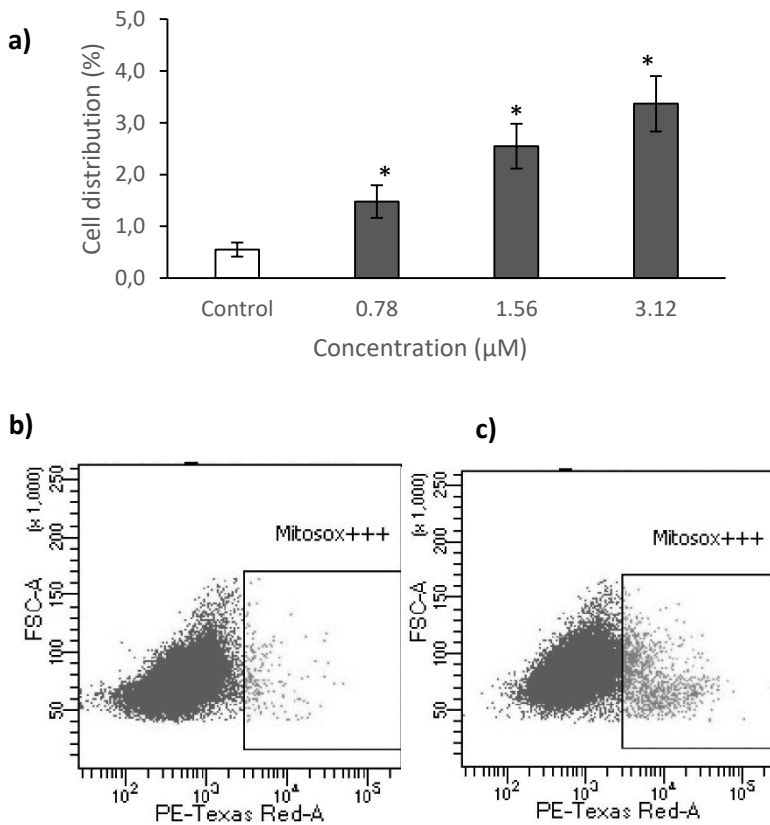


**Fig. 4.** Analysis of mitochondrial superoxide induction in SH-SY5Y cells after exposure to different concentrations (0.78, 1.56 and 3.12  $\mu\text{M}$ ) of STE for 24 h. Mitochondrial superoxide was measured by MitoSOX™ Red Mitochondrial Superoxide Indicator by flow cytometry. a) Data are expressed as mean  $\pm$  SEM of three independent experiments. (\*)  $p \leq 0.05$  indicates a significant difference compared to the control. b) Dot plot representative of control SH-SY5Y cells and c) Dot plot representative of SH-SY5Y cells exposed to 3.12  $\mu\text{M}$  of STE.

### 3.4. Measurement of mitochondrial membrane potential ( $\Delta\Psi_m$ )

Considering that the  $\Delta\Psi_m$  is used to drive the mitochondrial ATP synthesis, mitochondrial function was also evaluated by analysing the changes in  $\Delta\Psi_m$  induced in SH-SY5Y cells exposed to 0.78, 1.56 and 3.12  $\mu\text{M}$  STE for 24 h. The alteration of  $\Delta\Psi_m$  was determined by using the fluorescent probe Rh123. As shown in Fig. 5, incubation of SH-SY5Y cells in the presence of increasing concentrations of STE resulted in no alteration of the  $\Delta\Psi_m$ , as demonstrated by no significant variation in the Rh123 fluorescence intensity observed with respect to the control cells. These results indicate that the cytotoxic effects induced by STE are not necessarily linked to an alteration of the  $\Delta\Psi_m$ .

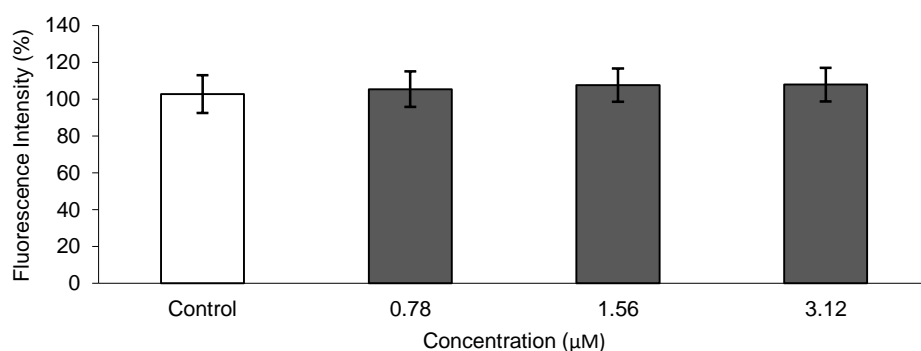


**Fig. 5.** Effect of STE (0.78, 1.56 and 3.12  $\mu\text{M}$ ) on mitochondrial membrane potential ( $\Delta\Psi_m$ ) determined by Rh123 assay. The SH-SY5Y cells were exposed to STE or control (1% methanol) for 24 h in 96-well black plate and then loaded with Rh123 for 15 min. Data are expressed as mean  $\pm$  SEM of three independent experiments with 24 replicates each. There were no significant differences between the concentrations tested and the control.

### 3.5. Necrosis-apoptosis analysis

To determine the death pathway underlying the observed decline on cell proliferation, the mechanism of induction of cell death was decided to study. The early apoptotic, apoptotic/necrotic and/or necrotic cells induced by the studied concentrations (0.78, 1.56 and 3.12  $\mu\text{M}$ ) of STE after 2 and 24 h of exposure in SH-SY5Y cells are shown in Fig. 6 and Fig. 7, respectively. Firstly, after 2 h of exposure, a concentration-dependent increase of early apoptotic cells was observed. In particular, early apoptotic cell population increased from  $3.67 \pm 0.16\%$  and  $4.23 \pm 0.37\%$  as compared with  $1.27 \pm 0.24\%$  of control cells (Fig. 6a). However, after 24 h of STE exposure the experimental results showed that for the samples exposed to STE (Fig. 7b–d), the apoptotic/necrotic cell population in the upper right quadrant increased in a concentration-dependent manner respect to the control cells (Fig. 7a). Fig. 7e shows that this increase was detected to be equal to  $18.43 \pm 2.07\%$ ,  $30.83 \pm 2.00\%$  and  $39.08 \pm 0.96\%$  respect to the control ( $3.6 \pm 0.92$ ) for 0.78, 1.56 and 3.12  $\mu\text{M}$ , respectively. No significant increase was observed in early apoptotic cells exposed to STE for 24 h respect to the control. Finally, necrotic cells proportion was not produced at 2 h (Fig. 6b) and 24 h (Fig. 7) indicating that under the studied conditions, necrotic pathway is not activated in SH-SY5Y cells.

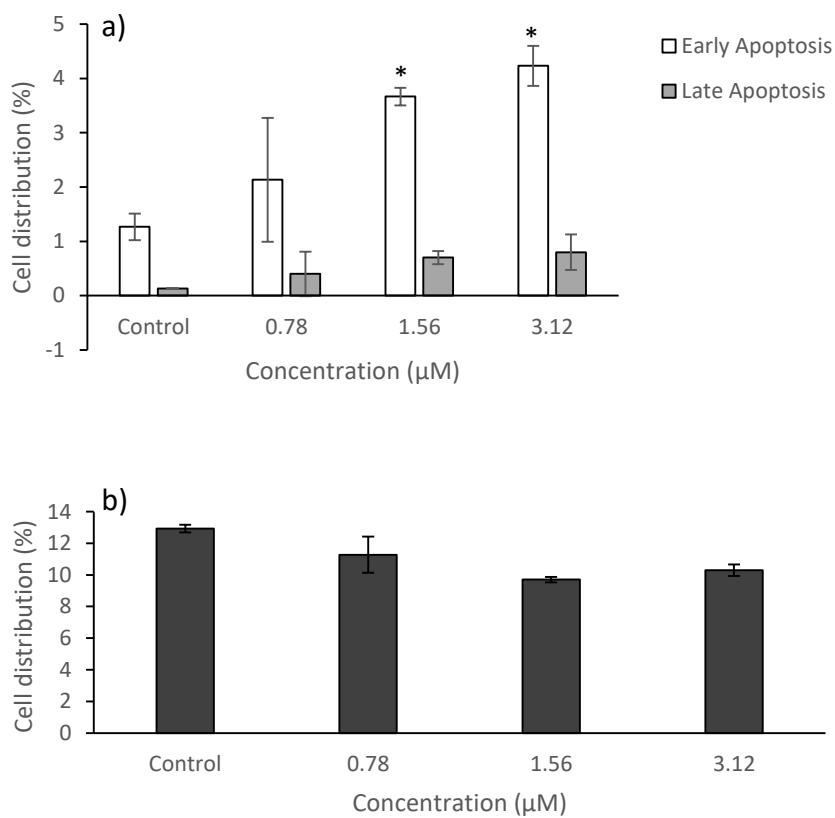


**Fig. 6.** Analysis of apoptosis/necrosis induction in SH-SY5Y cells after exposure to different concentrations (0.78, 1.56 and 3.12  $\mu\text{M}$ ) of STE for 2 h. Cells were stained with Annexin V-FITC and PI to distinguish a) early apoptotic and apoptotic/necrotic cells and b) necrotic cells. Data are expressed as mean  $\pm$  SEM of three independent experiments. (\*)  $p \leq 0.05$  indicates a significant difference compared to the control.

## Results

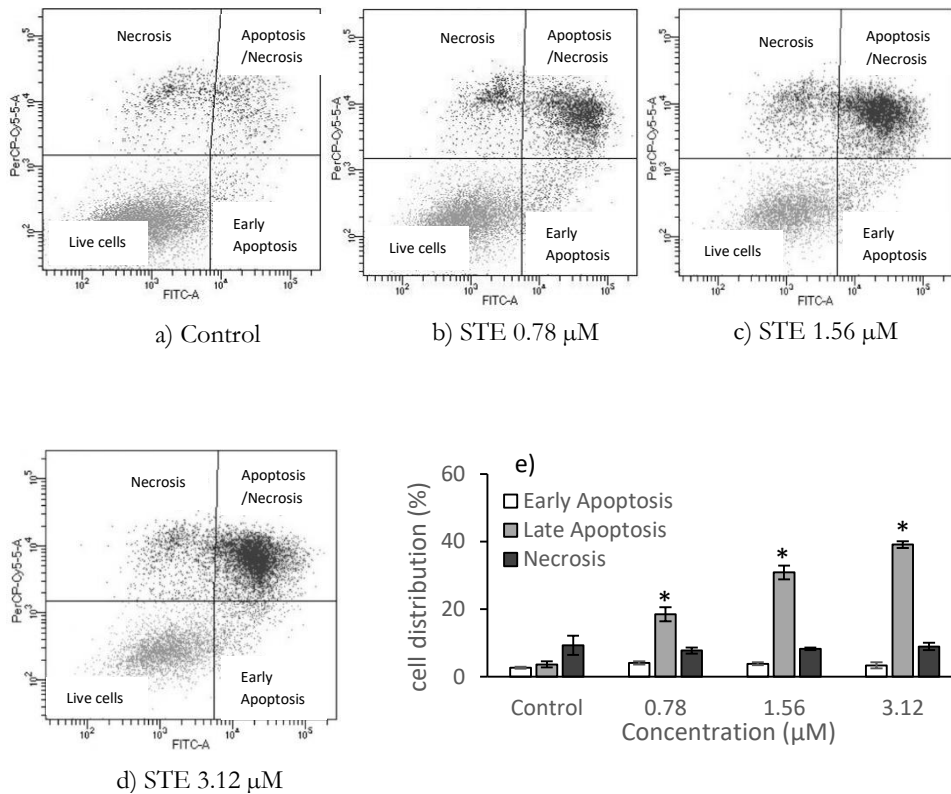


**Fig. 7.** Analysis of apoptosis/necrosis induction in SH-SY5Y cells after exposure to different concentrations (0.78, 1.56 and 3.12  $\mu\text{M}$ ) of STE for 24 h. Cells were stained with Annexin V-FITC and PI to distinguish early apoptotic, apoptotic/necrotic and necrotic cells. (a-d) Two-dimensional dot plots of FITC Annexin V vs. PI through flow cytometry. Cells stained negative for Annexin V-FITC and PI in the lower left quadrant shows alive cells. Cells stained positive for Annexin V-FITC and negative for PI in the lower right quadrant are representing early apoptosis. Cells stained negative for Annexin V-FITC and positive for PI in the upper left quadrant representing necrotic cells. Cells stained positive for both Annexin V-FITC and PI in the upper right quadrant are the late apoptotic/necrotic cells. (e) Percentage of early apoptotic, late apoptotic/necrotic and necrotic cells. Data are expressed as mean  $\pm$  SEM of three independent experiments. (\*)  $p \leq 0.05$  indicates a significant difference compared to the control.



### 3.6. Gene expression analysis

In order to confirm that STE induces apoptosis in SH-SY5Y cells, the mRNA expression levels of *Bax*, *Bcl-2* and *Casp-3* genes were determined by real-time PCR after 24 h of cell exposure to increasing concentrations of the mycotoxin (0.78, 1.56 and 3.12  $\mu\text{M}$ ). As it can be observed in Fig. 8, *Bax* and *Casp-3* mRNA were up-regulated in a concentration-dependent manner, while *Bcl-2* mRNA was down-regulated at the three studied concentrations but its expression was not correlated with the concentration. These results are perfectly in accordance with the increase in the apoptotic cell population observed at the same STE concentrations and suggest that the STE-induced apoptosis process results from an alteration of the cellular levels of *Bax*, *Casp-3* and *Bcl-2* mRNA.

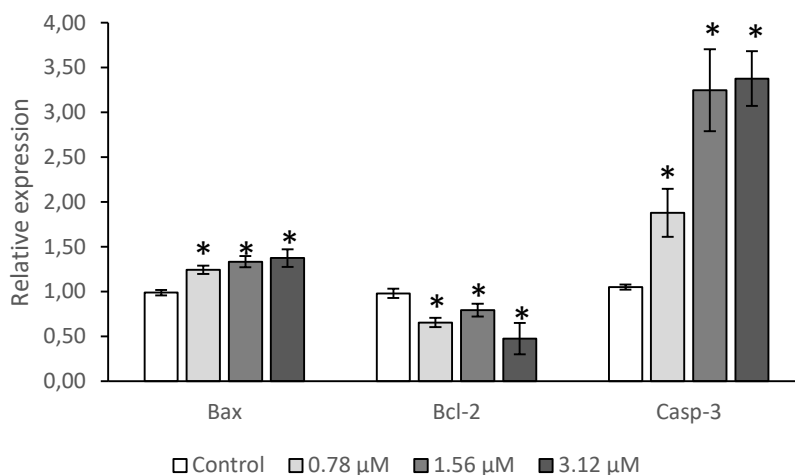


**Fig. 8.** Analysis of the relative mRNA expression levels of *Bax*, *Bcl-2* and *Casp-3* quantified in SH-SY5Y cells after 24 h of STE exposure using real-time PCR. The average of the target gene values was normalized to the corresponding 18S rRNA value and expressed as fold change compared with the solvent control. (\*)  $p \leq 0.05$  indicates a significant difference compared to the control.

#### 4. Discussion

The STE is known to induce reduction of cell viability and cell proliferation (Anninou et al., 2014; Cui et al., 2017; Liu et al., 2014; Zouaoui et al., 2016), DNA-double strand breaks (Huang et al., 2014) and cell cycle arrest (Wang et al., 2013; Xing et al., 2011; Zhang et al., 2013). Moreover, mutagenic and carcinogenic properties have been attributed to STE (Versilovskis and De Saeger, 2010). Additionally, we have recently demonstrated that STE causes oxidative stress, lipid peroxidation and produces changes in the antioxidant defence system on human neuroblastoma cells (Zingales et al., 2019). On the basis of our previous studies, in the present study we further explored the effects of STE on viability, mitochondrial function and mitochondria-mediated apoptosis in SH-SY5Y cells. Our results demonstrate that STE reduced in a time- and concentration-dependent manner the cell viability of SH-SY5Y cells by MTT assay, confirming our previous results obtained by NR assay (Zingales et al., 2019). However, the two methods are based on different physiological endpoints. In fact, if the latter is based on the incorporation of the dye neutral red into the lysosomes of viable cells, allowing to evaluate the lysosome functionality, on the other hand the ability of cells to reduce MTT provides an indication of mitochondrial integrity and activity. Thus, the data obtained by MTT assay is interpreted not only as a measure of cell viability but indirectly serves also to assess the cellular energy capacity of the cells. Finally, *in vitro* cytotoxicity assays, besides being useful to define the basal cytotoxicity, allow to define the concentration range for further assays. In order to gain further insights into the mechanisms of STE-mediated cytotoxicity, aspects of metabolic and mitochondrial function were investigated. It has been demonstrated that in cultured cells, despite aerobic conditions, the majority of ATP is obtained via

glycolysis in the cytoplasm, with a concomitant significant decrease in levels of OXPHOS (Crabtree effect). However, since galactose produces no net ATP from glycolysis, culturing cells in galactose-supplemented medium rather than glucose leads to circumvention of the Crabtree effect and stimulates OXPHOS (Marroquin et al., 2007). Thus, we forced SH-SY5Y cells to use OXPHOS by replacing the glucose in the medium with galactose. Using this approach, we developed a cell model that more faithfully reports mitochondrial physiology and probes the functional status of the mitochondria of SH-SY5Y cells exposed to STE. Our results suggest that the switch in substrate caused a striking change in the growth behaviour of the galactose-grown cells when compared to glucose-grown SH-SY5Y cells exposed to increasing concentrations of STE (Fig. 1). In particular, cells grown in glucose tolerated up to 6.24  $\mu\text{M}$  STE without a significant loss in cell viability. In contrast, cells grown in galactose were highly susceptible with a significant loss of viability starting from 3.12  $\mu\text{M}$  STE. The differences in the response between SHSY5Y cells grown in glucose and those grown in galactose suggest that the etiology of STE cytotoxicity depends on mitochondrial impairment. The ability of cells to produce high-energy molecules, such as ATP, is directly related to mitochondrial metabolism. For this reason, we measured the ATP content in SH-SY5Y cells exposed to STE in glucose and galactose culture conditions. A significant decrease in ATP levels was observed in SH-SY5Y cells starting from a STE concentration of 3.12  $\mu\text{M}$  and was equivalent in both growth conditions (Fig. 2). These data suggest that STE affects ATP production in SH-SY5Y cells, although the mechanism underlying this impairment is not dependent by the route through which cells derive their energy. However, in galactose-grown cells a slight increase in ATP content was obtained at the lowest STE concentration (0.78  $\mu\text{M}$ ). It could be

assumed that under these conditions the response of SH-SY5Y cells to STE is a hormetic response characterized by low concentration stimulation and high concentration inhibition (Calabrese and Baldwin, 2003). The exact mechanisms underlying this phenomenon are unknown. Further studies are needed to elucidate the extent of such hormesis induced by STE. A decrease of ATP levels along the treatment concentrations of STE (0.5–7  $\mu\text{M}$ ) was reported also by Liu et al. (2014) in HepG2 cells. However, only limited reports about the ability of STE to alter mitochondrial functions are available. In contrast, several other mycotoxins were reported to cause mitochondrial dysfunctions. In particular, patulin was found to cause ATP depletion and mitochondrial dysfunction in murine neuroblastoma neuro-2a cells and in human fetal kidney HEK293 cells (Malekinejad et al., 2015; Zhong et al., 2017). In rat cardiomyocytes deoxynivalenol and T-2 toxin have been shown to cause mitochondrial dysfunction by inhibition of the mitochondrial ETC function (Ngampongsa et al., 2013). Similarly, Moosavi et al. (2016) revealed a decrease of the activity of mitochondrial complexes III, IV and V,  $\Delta\Psi\text{m}$  and ATP content in rat hepatocytes following T-2 toxin administration. In ATP synthesis two components play a crucial role: the transmembrane proton concentration gradient (pH) and the  $\Delta\Psi\text{m}$  (Dimroth et al., 2000; Mazat et al., 2013). Although in mitochondria the  $\Delta\Psi\text{m}$  component is the main driving force for ATP production, under our experimental conditions no alterations of  $\Delta\Psi\text{m}$  were reported to be related to the decreased ATP content observed (Fig. 5). However, according to our results, Bohler et al. (2018) showed that in Jurkat cells not even the ETC inhibitors, known to block the electron transport and thus inhibit the ATP synthetase, affected  $\Delta\Psi\text{m}$ . It has to be taken into account that, in OXPHOS condition another crucial requirement for ATP synthesis consists in

a functional ETC. For this reason, in subsequent experiments we evaluated the effect of STE on cell viability of SH-SY5Y cells grown in galactose-supplemented medium in presence of ETC inhibitors (Fig. 3). The further decrease in cell viability obtained when cells were exposed to STE in presence of rotenone, a selective inhibitor of the complex I, highlights that the mechanism of STE-cytotoxicity is directly dependent on changes in ETC activity. However, no effects were observed in presence of antimycin A, an inhibitor of the complex III, suggesting that this latter complex is not involved in STE toxicity. Overall, these observations establish clearly that mitochondria play a central role in the cytotoxic activity of STE, although its cytotoxicity appears not necessarily a result of its effects on the  $\Delta\Psi_m$  and on the complex III of the ETC. Mitochondria are the main source of intracellular ROS production (Zhan et al., 2019). However, endogenous antioxidant systems scavenge ROS, maintaining them at no toxic levels. A decrease in mitochondrial function has been linked to an increase in mitochondrial ROS generation (Leon et al., 2016). Our study showed that in SH-SY5Y cells, STE triggered a concentration-dependent enhancement of mitochondrial superoxide levels after 24 h of exposure (Fig. 4), demonstrating its implication in cell toxicity. In fact, mycotoxins-induced oxidative stress might be one of the major causes of mitochondrial dysfunction (Islam et al., 2018). Particularly, increased levels of mitochondrial ROS are known to cause damages to mitochondrial DNA (mtDNA), with consequent production of dysfunctional proteins essential for proper mitochondrial functioning (Yang et al., 2016). Several mycotoxins were reported to induce mitochondrial dysfunction by increasing oxidative stress. Sahu et al. (2010) showed that deoxynivalenol causes oxidative stress and thus mitochondrial dysfunction in liver cells of rats (Clone9 and MH1C1), mice (NBL CL2) and

humans (WRL68 and HepG2). Ochratoxin A has been demonstrated to trigger accelerated respiration and increase the production of mitochondrial ROS, causing an opening of ROS-dependent mitochondrial permeability transition (mPT) pores. This led to a decrease in  $\Delta\Psi_m$  and the release of cytochrome c into the cytosol, resulting in the induction of mitochondrial intrinsic apoptosis (Wang et al., 2017). Apoptosis is a specialized process of cell death included in the normal development of organs and tissue maintenance, but may also occur as a response to various toxic environmental stimuli. It is an extremely complex process in which mitochondria play a pivotal role. It is tightly regulated through a number of checkpoints in order to preserve a healthy balance between cell death and cell survival and maintain genome integrity (Blatt and Glick, 2001). One of the main and crucial disruptors of this balance is represented by the excessive oxidative stress. In fact, the mPT pores, whose opening causes the release of death factors, are redox-sensitive. Moreover, a series of well-known molecular pathways results to be involved in the regulation of apoptosis. In particular, this process is strictly controlled by a balance between the pro-apoptotic proteins, such as *Bax*, and the anti-apoptotic proteins, such as *Bcl-2*, resulting ultimately in the activation of the apoptotic effector molecule *Casp-3* and the execution of the cell death program (Blatt and Glick, 2001). Definitely, *Bcl-2* keeps the mPT pores in a closed state and thus prevents cytochrome c from crossing mitochondrial outer membrane and leaking out to activate caspases. In contrast, *Bax* leads to an opening of mPT pores, promoting apoptosis. Accumulating evidences highlight that the induction of apoptosis is one of the main effects of many carcinogenic mycotoxins, such as fumonisin B1, patulin and zearalenone (Alizadeh et al., 2015; Ayed-Boussema et al., 2008; Boussabbeh et al., 2015; Ribeiro et al., 2010). In the present study, we found that STE induced

early- and late-stage apoptotic events in SH-SY5Y cells after 2 and 24 h of exposure, respectively (Figs. 6 and 7). These results suggest that the observed loss of cell viability resulting from the exposition of SH-SY5Y cells to STE is due to the induction of an apoptotic process. Our findings are consistent with other previous studies, demonstrating that apoptosis is a common effect of STE in different cell lines. Cui et al. (2017) showed that in adenocarcinomic human alveolar basal epithelial A549 cells and in human bronchial epithelial BEAS-2B cells STE induced apoptosis in a concentration-dependent manner. The STE has been demonstrated to cause apoptosis also in human gastric epithelial GES-1 cells (Zhang et al., 2013). In order to obtain a further confirmation of our results, the evaluation of the expression levels of apoptosis-related proteins was carried out. In particular, the changes in the mRNA expression levels of the key proteins *Bax*, *Bcl-2* and *Casp-3* were evaluated (Fig. 8). Compared to control, the mRNA expression levels of *Bax* were increased by STE exposure, while *Bcl-2* mRNA resulted to be down-regulated in SHSY5Y cells exposed to the mycotoxin. In addition, the up-regulation of *Casp-3* mRNA confirmed that STE inhibits the proliferation of SH-SY5Y cells by inducing apoptosis. Our results are in accordance with those reported by Cui et al. (2017) and Zhang et al. (2013), who demonstrated that STE induced apoptosis by increasing the *Bax/Bcl-2* ratio and activating *Casp-3* in HepG2, A549 and BEAS-2B cells. Other studies have demonstrated that the mycotoxin zearalenone and T-2 toxin induce apoptosis through the caspase-dependent apoptotic pathway by increasing *Bax/Bcl-2* ratio and activating *Casp-3* in in vitro studies (Ayed-Boussema et al., 2008; Chaudhari et al., 2009). In Het-1A and A549 cells, apoptosis was induced by ochratoxin A and aflatoxin G1 via activation and cleavage of *Casp-3* and up- and down-regulation of *Bax* and *Bcl-2* genes, respectively (Liu et al., 2015; Shen et al., 2013).

In summary, our results provide further novel insights in the signaling pathways of the cell death process induced by STE in SH-SY5Y cells. We identify for the first time STE as a mitochondrial mycotoxin, with a mode of action that involves a modulation of mitochondrial function, ATP depletion, oxidative stress and the activation of mitochondrial-related pathway of apoptosis. With metabolic disorders rising at an alarming rate in Western and developed countries, it is becoming increasingly important to understand how foodborne mycotoxins, such as STE, can affect the energy metabolism. Furthermore, the identification of mitochondria as one of the targets of STE might provide a useful tool for the study of the use of neuroprotective mitochondria-target functional peptides, known for protect mitochondria against oxidative stress and prevent neuronal cell death (Szeto, 2006).

### **CRedit authorship contribution statement**

**Veronica Zingales:** Investigation, Validation, Formal analysis, Writing - original draft, Writing - review & editing. **Mónica Fernández-Franzón:** Supervision. **Maria-José Ruiz:** Conceptualization, Supervision, Project administration, Funding acquisition.

### **Declaration of competing interest**

The authors declare that they have no known competing financial interests or personal relationships that could have appeared to influence the work reported in this paper.



## Acknowledgments

We are grateful for the technical assistance from the SCSIE of the University of Valencia. This research has been supported by the Spanish Ministry of Economy and Competitiveness (AGL2016-77610-R), the Generalitat Valenciana grant (Prometeo 2018/216) and the pre-doctoral research training program "Santiago Grisolia (GRISOLIAP/2018/092) CPI-18-117".

## References

Alizadeh, A.M., Mohammadghasemi, F., Zندهدل, K., Kamyabi-Moghaddam, Z., Tavassoli, A., Amini-Najafi, F., Khosravi, A., 2015. Apoptotic and proliferative activity of mouse gastric mucosa following oral administration of fumonisin B1. *Iran J Basic Med Sci* 18, 8–13.

Anninou, N., Chatzaki, E., Papachristou, F., Pitiakoudis, M., Simopoulos, C., 2014. Mycotoxins' activity at toxic and sub-toxic concentrations: differential cytotoxic and genotoxic effects of single and combined administration of sterigmatocystin, ochratoxin A and citrinin on the hepatocellular cancer cell line Hep3B. *Int. J. Environ. Res. Publ. Health* 11, 1855–1872.

Ayed-Boussema, I., Bouaziz, C., Rjiba, K., Valenti, K., Laporte, F., Bacha, H., Hassen, W., 2008. The mycotoxin Zearalenone induces apoptosis in human hepatocytes (HepG2) via p53-dependent mitochondrial signaling pathway. *Toxicol. Vitro* 22, 1671–1680.

Blatt, N.B., Glick, G.D., 2001. Signaling pathways and effector mechanisms pre-programmed cell death. *Bioorg. Med. Chem.* 9, 1371–1384.

Bohler, P., Stuhldreier, F., Anand, R., Kondadi, A.K., Schlutermann, D., Berleth, N., Deitersen, J., Wallot-Hieke, N., Wu, W., Frank, M., Niemann,

H., Wesbuer, E., Barbian, A., Luyten, T., Parys, J.B., Weidtkamp-Peters, S., Borchardt, A., Reichert, A.S., Pena-Blanco, A., Garcia-Saez, A.J., Itskanov, S., van der Blik, A.M., Proksch, P., Wesselborg, S., Stork, B., 2018. The mycotoxin phomoxanthone A disturbs the form and function of the inner mitochondrial membrane. *Cell Death Dis.* 9, 286. <https://doi.org/10.1038/s41419-018-0312-8>.

Boussabbeh, M., Ben Salem, I., Prola, A., Guilbert, A., Bacha, H., Abid-Essefi, S., Lemaire, C., 2015. Patulin induces apoptosis through ROS-mediated endoplasmic reticulum stress pathway. *Toxicol. Sci.* 144, 328–337.

Calabrese, E.J., Baldwin, L.A., 2003. The hormetic dose-response model is more common than the threshold model in toxicology. *Toxicol. Sci.* 71, 246–250.

Chaudhari, M., Jayaraj, R., Bhaskar, A.S., Lakshmana Rao, P.V., 2009. Oxidative stress induction by T-2 toxin causes DNA damage and triggers apoptosis via caspase pathway in human cervical cancer cells. *Toxicology* 262, 153–161.

Cui, J., Wang, J., Huang, S., Jiang, X., Li, Y., Wu, W., Zhang, X., 2017. Sterigmatocystin induced apoptosis in human pulmonary cells in vitro. *Exp. Toxicol. Pathol.* 69, 695–699.

Dimroth, P., Kaim, G., Matthey, U., 2000. Crucial role of the membrane potential for ATP synthesis by F(1)F(o) ATP synthases. *J. Exp. Biol.* 203, 51–59.

Fujii, K., Kurata, H., Odashima, S., Hatsuda, Y., 1976. Tumor induction by a single subcutaneous injection of sterigmatocystin in newborn mice. *Canc. Res.* 36, 1615–1618.

Gao, W., Jiang, L., Ge, L., Chen, M., Geng, C., Yang, G., Li, Q., Ji, F., Yan, Q., Zou, Y., Zhong, L., Liu, X., 2015. Sterigmatocystin-induced oxidative DNA damage in human liver-derived cell line through lysosomal damage. *Toxicol. Vitro* 29, 1–7.

Huang, S., Wang, J., Xing, L., Shen, H., Yan, X., Wang, J., Zhang, X., 2014. Impairment of cell cycle progression by sterigmatocystin in human pulmonary cells in vitro. *Food Chem. Toxicol.* 66, 89–95.

IARC, 1987. Overall Evaluations of Carcinogenicity: an Updating of IARC Monographs Volumes 1 to 42, Supplement 7. (Lyon, France).

Islam, M.T., Mishra, S.K., Tripathi, S., de Alencar, M., JMC, E.S., Rolim, H.M.L., de Medeiros, M., Ferreira, P.M.P., Rouf, R., Uddin, S.J., Mubarak, M.S., Melo-Cavalcante, A.A.C., 2018. Mycotoxin-assisted mitochondrial dysfunction and cytotoxicity: unexploited tools against proliferative disorders. *IUBMB Life* 70, 1084–1092.

Karbowski, M., Neutzner, A., 2012. Neurodegeneration as a consequence of failed mitochondrial maintenance. *Acta Neuropathol.* 123, 157–171.

Leon, J., Sakumi, K., Castillo, E., Sheng, Z., Oka, S., Nakabeppu, Y., 2016. 8-Oxoguanine accumulation in mitochondrial DNA causes mitochondrial dysfunction and impairs neuritogenesis in cultured adult mouse cortical neurons under oxidative conditions. *Sci. Rep.* 6, 22086. <https://doi.org/10.1038/srep22086>.

Liu, C.X., Tan, Y.R., Xiang, Y., Liu, C., Liu, X.A., Qin, X.Q., 2018. Hydrogen sulfide protects against chemical hypoxia-induced injury via attenuation of ROS-mediated Ca (2+) overload and mitochondrial dysfunction

in human bronchial epithelial cells. *BioMed Res. Int.* 2018, 2070971.

<https://doi.org/10.1155/2018/2070971>.

Liu, J., Wu, S., Shen, H., Cui, J., Wang, Y., Xing, L., Wang, J., Yan, X., Zhang, X., 2015. Ochratoxin A induces DNA damage and G2 phase arrest in human esophageal epithelium Het-1A cells in vitro. *J. Toxicol. Sci.* 40, 657–665.

Liu, Y., Du, M., Zhang, G., 2014. Proapoptotic activity of aflatoxin B1 and sterigmatocystin in HepG2 cells. *Toxicol. Rep.* 1, 1076–1086.

Malekinejad, H., Aghazadeh-Attari, J., Rezaabakhsh, A., Sattari, M., Ghasemsoltani-Momtaz, B., 2015. Neurotoxicity of mycotoxins produced in vitro by *Penicillium roqueforti* isolated from maize and grass silage. *Hum. Exp. Toxicol.* 34, 997–1005.

Marin, S., Ramos, A.J., Cano-Sancho, G., Sanchis, V., 2013. Mycotoxins: occurrence, toxicology, and exposure assessment. *Food Chem. Toxicol.* 60, 218–237.

Marroquin, L.D., Hynes, J., Dykens, J.A., Jamieson, J.D., Will, Y., 2007. Circumventing the Crabtree effect: replacing media glucose with galactose increases susceptibility of HepG2 cells to mitochondrial toxicants. *Toxicol. Sci.* 97, 539–547.

Mazat, J.P., Ransac, S., Heiske, M., Devin, A., Rigoulet, M., 2013. Mitochondrial energetic metabolism-some general principles. *IUBMB Life* 65, 171–179.

Moosavi, M., Rezaei, M., Kalantari, H., Behfar, A., Varnaseri, G., 2016. l-carnitine protects rat hepatocytes from oxidative stress induced by T-2 toxin. *Drug Chem. Toxicol.* 39, 445–450.

Ngampongsa, S., Hanafusa, M., Ando, K., Ito, K., Kuwahara, M., Yamamoto, Y., Yamashita, M., Tsuru, Y., Tsubone, H., 2013. Toxic effects of

T-2 toxin and deoxynivalenol on the mitochondrial electron transport system of cardiomyocytes in rats. *J. Toxicol. Sci.* 38, 495–502.

Purchase, I.F., Van der Watt, J.J., 1973. Carcinogenicity of sterigmatocystin to rat skin. *Toxicol. Appl. Pharmacol.* 26, 274–281.

Quintana-Cabrera, R., Fernandez-Fernandez, S., Bobo-Jimenez, V., Escobar, J., Sastre, J., Almeida, A., Bolanos, J.P., 2012.  $\gamma$ -Glutamylcysteine detoxifies reactive oxygen species by acting as glutathione peroxidase-1 cofactor. *Nat. Commun.* 3, 718. <https://doi.org/10.1038/ncomms1722>.

Ribeiro, D.H., Ferreira, F.L., da Silva, V.N., Aquino, S., Correa, B., 2010. Effects of aflatoxin B(1) and fumonisin B(1) on the viability and induction of apoptosis in rat primary hepatocytes. *Int. J. Mol. Sci.* 11, 1944–1955.

Rodriguez-Enriquez, S., Juarez, O., Rodriguez-Zavala, J.S., Moreno-Sanchez, R., 2001. Multisite control of the Crabtree effect in ascites hepatoma cells. *Eur. J. Biochem.* 268, 2512–2519.

Rosignol, R., Gilkerson, R., Aggeler, R., Yamagata, K., Remington, S.J., Capaldi, R.A., 2004. Energy substrate modulates mitochondrial structure and oxidative capacity in cancer cells. *Canc. Res.* 64, 985–993.

Ruiz, M.J., Festila, L.E., Fernández, M., 2006. Comparison of basal cytotoxicity of seven carbamates in CHO-K1 cells. *Environ. Toxicol. Chem.* 88, 345–354.

Sahu, S.C., O'Donnell Jr., M.W., Wiesenfeld, P.L., 2010. Comparative hepatotoxicity of deoxynivalenol in rat, mouse and human liver cells in culture. *J. Appl. Toxicol.* 30, 566–573.

Shen, H., Liu, J., Wang, Y., Lian, H., Wang, J., Xing, L., Yan, X., Wang, J., Zhang, X., 2013. Aflatoxin G1-induced oxidative stress causes DNA

damage and triggers apoptosis through MAPK signaling pathway in A549 cells. *Food Chem. Toxicol.* 62, 661–669.

Sun, X.M., Zhang, X.H., Wang, H.Y., Cao, W.J., Yan, X., Zuo, L.F., Wang, J.L., Wang, F.R., 2002. Effects of sterigmatocystin, deoxynivalenol and aflatoxin G1 on apoptosis of human peripheral blood lymphocytes in vitro. *Biomed. Environ. Sci.* 15, 145–152.

Szeto, H.H., 2006. Mitochondria-targeted peptide antioxidants: novel neuroprotective agents. *AAPS J.* 8 (3), E521–E531.  
<https://doi.org/10.1208/aapsj080362>.

Vermes, I., Haanen, C., Steffens-Nakken, H., Reutelingsperger, C., 1995. A novel assay for apoptosis. Flow cytometric detection of phosphatidylserine expression on early apoptotic cells using fluorescein labelled Annexin V. *J. Immunol. Methods* 184, 39–51.

Versilovskis, A., De Saeger, S., 2010. Sterigmatocystin: occurrence in foodstuffs and analytical methods-an overview. *Mol. Nutr. Food Res.* 54, 136–147.

Vesonder, R.F., Horn, B.W., 1985. Sterigmatocystin in dairy cattle feed contaminated with *Aspergillus versicolor*. *Appl. Environ. Microbiol.* 49, 234–235.

Wallace, K.B., Starkov, A.A., 2000. Mitochondrial targets of drug toxicity. *Annu. Rev. Pharmacol. Toxicol.* 40, 353–388.

Wang, J., Huang, S., Xing, L., Shen, H., Yan, X., Wang, J., Zhang, X., 2013. Role of hMLH1 in sterigmatocystin-induced G(2) phase arrest in human esophageal epithelial Het-1A cells in vitro. *Toxicol. Lett.* 217, 226–234.

Wang, Y., Peng, X., Yang, Z., Zhao, W., Xu, W., Hao, J., Wu, W., Shen, X.L., Luo, Y., Huang, K., 2017. iTRAQ mitoproteome analysis reveals

mechanisms of programmed cell death in *Arabidopsis thaliana* induced by ochratoxin A. *Toxins* 9 (5), 167. <https://doi.org/10.3390/toxins9050167>.

Xing, X., Wang, J., Xing, L.X., Li, Y.H., Yan, X., Zhang, X.H., 2011. Involvement of MAPK and PI3K signaling pathway in sterigmatocystin-induced G2 phase arrest in human gastric epithelium cells. *Mol. Nutr. Food Res.* 55, 749–760.

Yang, Y., Karakhanova, S., Hartwig, W., D'Haese, J.G., Philippov, P.P., Werner, J., Bazhin, A.V., 2016. Mitochondria and mitochondrial ROS in cancer: novel targets for anticancer therapy. *J. Cell. Physiol.* 231, 2570–2581.

Ye, J., Coulouris, G., Zaretskaya, I., Cutcutache, I., Rozen, S., Madden, T.L., 2012. Primer-BLAST: a tool to design target-specific primers for polymerase chain reaction. *BMC Bioinf.* 13, 134. <https://doi.org/10.1186/1471-2105-13-134>.

Zhan, W., Liao, X., Li, L., Chen, Z., Tian, T., Yu, L., Chen, Z., 2019. In vitro mitochondrial-targeted antioxidant peptide induces apoptosis in cancer cells. *OncoTargets Ther.* 12, 7297–7306.

Zhang, D., Cui, Y., Shen, H., Xing, L., Cui, J., Wang, J., Zhang, X., 2013. Sterigmatocystin-induced DNA damage triggers G2 arrest via an ATM/p53-related pathway in human gastric epithelium GES-1 cells in vitro. *PLoS One* 8 (5), e65044. <https://doi.org/10.1371/journal.pone.0065044>.

Zhong, Y., Jin, C., Gan, J., Wang, X., Shi, Z., Xia, X., Peng, X., 2017. Apigenin attenuates patulin- induced apoptosis in HEK293 cells by modulating ROS-mediated mitochondrial dysfunction and caspase signal pathway. *Toxicon* 137, 106–113.

Zingales, V., Fernandez-Franzon, M., Ruiz, M.J., 2019. Sterigmatocystin-induced cytotoxicity via oxidative stress induction in human

## Results

---

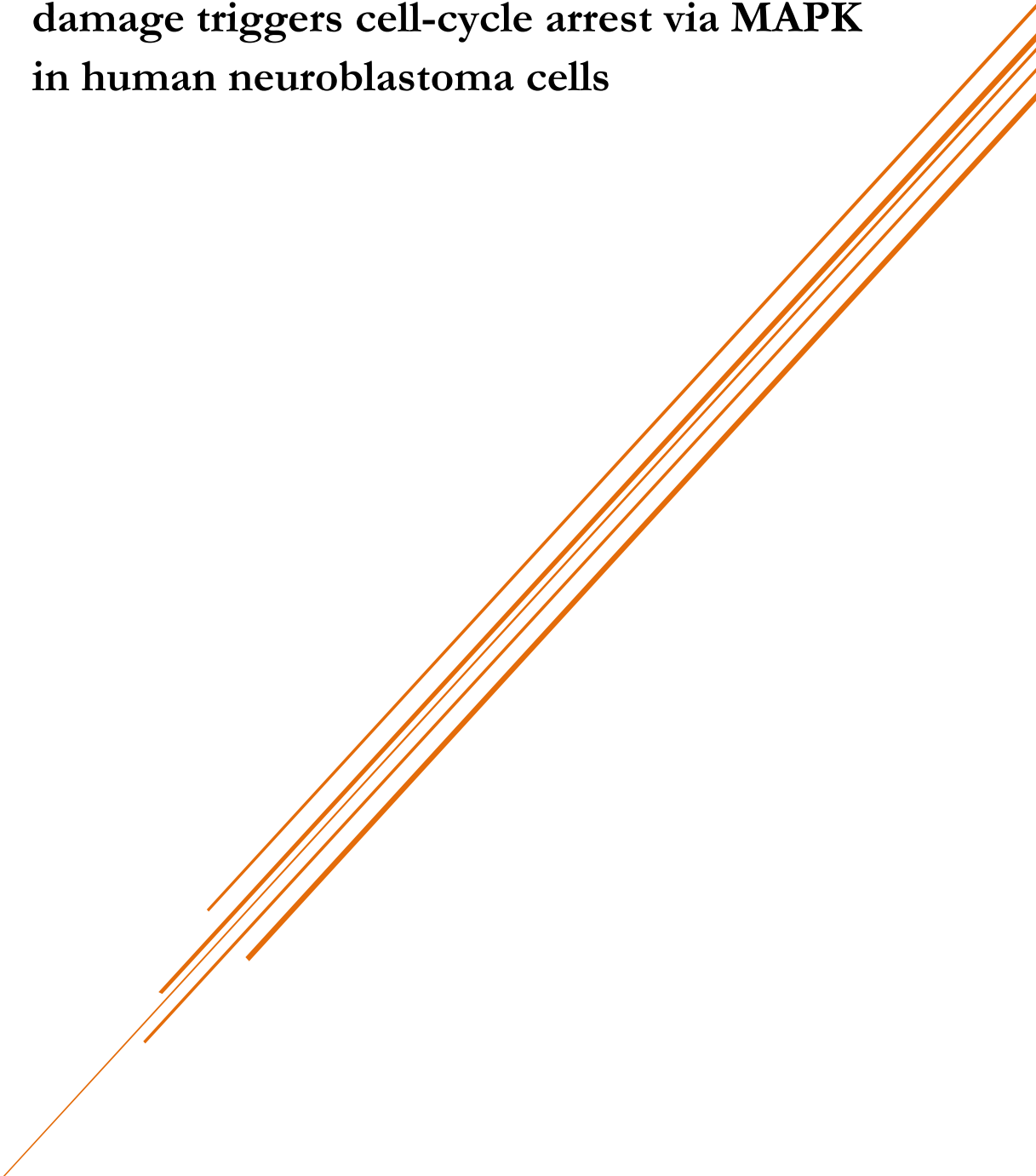
neuroblastoma cells. *Food Chem. Toxicol.*

136 <https://doi.org/10.1016/j.fct.2019.110956>. 110956.

Zouaoui, N., Mallebrera, B., Berrada, H., Abid-Essefi, S., Bacha, H., Ruiz, M.J., 2016. Cytotoxic effects induced by patulin, sterigmatocystin and beauvericin on CHO-K1 cells. *Food Chem. Toxicol.* 89, 92–103.



### **3.5. Sterigmatocystin-induced DNA damage triggers cell-cycle arrest via MAPK in human neuroblastoma cells**





Toxicology Mechanisms and Methods

**Sterigmatocystin-induced DNA damage triggers cell-cycle arrest via MAPK in human neuroblastoma cells**

Veronica Zingales\*, Mónica Fernández-Franzón, Maria-José Ruiz

Laboratory of Food Chemistry and Toxicology, Faculty of Pharmacy, University of

Valencia, Av. Vicent Andrés Estellés s/n, 46100, Valencia, Spain

\*Corresponding author. Laboratory of Toxicology, Faculty of Pharmacy, University of Valencia, Av. Vicent Andrés Estellés, s/n, 46100, Burjassot, Valencia, Spain. *E-mail address:* [vezin@uv.es](mailto:vezin@uv.es) (V. Zingales).

### Abstract

Sterigmatocystin (STE) is a common mycotoxin found in food and feed. Many studies showed that STE is genotoxic. However, up to now, the potential genotoxicity of STE on human neuronal system remains unknown. In this study, we explored the effect of STE on DNA damage and cell-cycle progression on human neuroblastoma SH-SY5Y cells exposed to various concentrations of STE (0.78, 1.56 and 3.12  $\mu\text{M}$ ) for 24 h. The results indicated that STE exposure induced DNA damage, as evidenced by DNA comet tails formation and increased  $\gamma\text{H2AX}$  foci. Additionally, genotoxicity was confirmed by micronuclei (MN) analysis. Furthermore, we found that STE exposure led to cell-cycle arrest at the S and the  $\text{G}_2/\text{M}$  phase. Considering the important role played by MAPK and p53 signaling pathways in cell-cycle arrest, we explored their potential involvement in STE-induced cell-cycle arrest by using specific inhibitors. The inhibition of JNK and ERK resulted to attenuate S and  $\text{G}_2/\text{M}$  arrest, whereas the inhibition of p38 and p53 attenuated only STE-induced S phase arrest. In conclusion, the present study demonstrates that STE induced DNA damage and triggered MAPK and p53 pathways activation, resulting in cell-cycle arrest at the S and the  $\text{G}_2/\text{M}$  phase.

**Keywords:** Sterigmatocystin, SH-SY5Y cells, Genotoxicity, DNA damage, Cell cycle.

## 1. Introduction

Sterigmatocystin (STE) is a toxic secondary fungal metabolite mainly produced by *Aspergillus versicolor* and *A. nidulans* fungi. The STE producing fungi have been frequently isolated from several foodstuffs, with a consequent strong economic impact for the biotechnological, agricultural and food industries. However, in literature only limited information is available on the presence of STE in food and feed (Zingales et al. 2020c). Due to the limited STE occurrence data, STE is not included in the European Commission Regulation (EC) no. 1881/2006, which established maximum levels for certain contaminants in foodstuffs to ensure animal and public health, as well as agricultural productivity (Commission Regulation 2006). However, efforts are focused on this mycotoxin to establish a better risk assessment. In fact, epidemiological evidence highlighted the existence of associations between STE exposure and the risk of cancer development. A large number of studies performed in China revealed that STE may be a putative etiological factor for gastric carcinoma, as suggested by the strong positive correlations existing between high levels of STE contamination in foodstuffs and a higher incidence of gastric cancer (Lou et al. 1995; Zhang X et al. 2003; Tian and Liu 2004; Hutanasu et al. 2011). Furthermore, STE has been shown to be hepatotoxic and nephrotoxic in animal models. Accordingly, in light of the animal studies performed and of the cases of human cancer analyzed as far, STE has been classified in the group 2B (possibly carcinogenic to humans) by the International Agency for Research on Cancer (IARC 1987; Pitt et al. 2012).

It has been generally accepted that one of the most common mechanism of action through which many carcinogenic mycotoxins induce abnormal cell

proliferation and carcinogenesis consists in the alteration of cell-cycle progression. For example, the ochratoxin A (OTA), a nephrotoxic mycotoxin associated to urinary tract tumors, was shown to inhibit cell-cycle progression at the G<sub>2</sub> phase in human gastric epithelium GES-1 cells and at the G<sub>2</sub>/M phase in V79 Chinese hamster lung fibroblast, whereas cell-cycle arrest in G<sub>0</sub>/G<sub>1</sub> phase was detected in human liver cancer cells (HepG2) exposed to OTA and OTA+beauvericin (BEA), indicating that different effects on cell-cycle distribution can be induced in different cell lines (Palma et al. 2007; Cui et al. 2010; Juan-Garcia et al. 2019). Cell-cycle arrest in G<sub>2</sub>/M phase has been observed to be caused also by T-2 toxin in HepG2 cells and by zearalenone (ZEA) in human colon cancer cells (Abid-Essefi et al. 2004; Taroncher et al. 2020). Additionally, ZEA has been shown to induce G<sub>1</sub> phase arrest in human peripheral blood mononuclear cells (hPBMCs) (Banjerdpongchai et al. 2010). Similar results were obtained in hPBMCs exposed to OTA (Liu J et al. 2012).

The cell-cycle arrest is frequently a consequence of DNA damage that can be caused by environmental or metabolic factors. Indeed, in the presence of DNA damage, cells respond by undergoing cell-cycle arrest, to minimize the replication of damaged DNA and prevent the transmission of damaged chromosome to the daughter cells, or apoptosis, if the cellular damage cannot be properly repaired (Ishikawa et al. 2006). In fact, continued proliferation in the presence of unrepaired or inappropriately repaired DNA damage may facilitate the propagation of unstable genomes and acquisition of genetic alteration, which may significantly contribute to cancer development (Sancar et al. 2004; Aziz et al. 2012).

The cell cycle is a highly complex process tightly regulated at several levels. A number of checkpoints are involved to allow the arrest of cell cycle in the presence of various types of DNA damage (Flatt and Pietsenpol 2000; Stewart and Pietsenpol 2001). Among the intracellular signaling pathway implicated in the regulation of cell cycle, mitogen-activated protein kinase (MAPK) signaling pathway is involved and activated in response to cellular stress. The c-Jun-N-terminal kinase (JNK), the extracellular signal-regulated kinase (ERK) and p38 represent three of the major and well-characterized members of the MAPKs family (Schafer 1998). The activation of ERK, JNK and p38 MAPK signaling pathway in response to cell-cycle arrest induced by some carcinogenic mycotoxins (deoxynivalenol, fumonisin B1, OTA) was reported by several studies (Johnson et al. 2003; Yang et al. 2008; Wang Y et al. 2012; Dai et al. 2017; Lee et al. 2019a, 2019b).

In eukaryotic cells, the progression of cell cycle concerns also other molecular regulators, such as the p53 transcriptional factor, whose role at the G<sub>1</sub>/S and G<sub>2</sub> checkpoints is well documented (Stewart and Pietsenpol 2001).

Based on our knowledge, to date, no studies have been reported looking at the putative effects of STE on DNA damage and cell-cycle progression specifically in human neuronal system. Our study aimed at filling this gap. We used human neuroblastoma (SH-SY5Y) cells to investigate the effect of STE exposure on DNA damage and cell-cycle distribution. Furthermore, the role of ERK, JNK, p38, and p53 in STE-induced cell-cycle arrest was evaluated by using specific inhibitors.

### 2. Material and methods

#### 2.1. Reagents

The reagent grade chemicals and cell culture compounds used, namely culture medium DMEM Ham's-F12, penicillin, streptomycin, trypsin/EDTA solutions, phosphate buffer saline (PBS), fetal bovin serum (FBS), trizma base (Tris), propidium iodide (PI), Ribonuclease A (RNase), *t*-octylphenoxypolyethoxyethanol (Triton-X 100), 40,6-diamidine-20-phenylindole dihydrochloride (DAPI), SB203580 (p38 inhibitor), PD98059 (ERK inhibitor), SP600125 (JNK inhibitor), PFT (p53 inhibitor), agarose, low gelling temperature agarose (LMA), disodium ethylenediaminetetraacetate dihydrate (Na<sub>2</sub>-EDTA), sodium dihydrogen phosphate (NaH<sub>2</sub>PO<sub>4</sub>), disodium hydrogen phosphate (Na<sub>2</sub>HPO<sub>4</sub>) and paraformaldehyde were from Sigma Chemical Co (St. Louis, MO). Ethanol (EtOH) and sodium hydroxide (NaOH) were from Merck KGaA (Gernsheim, Germany). Dimethyl sulfoxide (DMSO) was obtained from Fisher Scientific (Geel, Belgium). Methanol (MeOH), sodium chloride (NaCl) and hydrochloric acid (HCl) were from VWR International (LLC, Monroeville, PA). The Litron In Vitro Microflow Kit for the micronucleus assay by flow cytometry was purchased from the Litron Laboratories (Litron Laboratories, Rochester, NY). The primary monoclonal antibody rabbit anti-human phospho-histone H2AX (Ser-139) was purchased from Cell Signaling Technology (Beverly, MA). Standard of the selected mycotoxin STE (MW: 324.28 g/mol) was purchased from Sigma-Aldrich (St. Louis, MO). Stock solutions of the mycotoxin were prepared in methanol and maintained at -20 °C.



## 2.2. *Cell culture and treatment*

Human neuroblastoma SH-SY5Y cells were cultured in DMEM Ham's-F12 medium supplemented with 10% FBS, 100 U/mL penicillin, and 100 mg/mL streptomycin. The incubation conditions were pH 7.4, 5% CO<sub>2</sub> at 37°C and 95% air atmosphere at constant humidity. The medium was changed every 2–3 days. The final STE concentrations tested were achieved by adding STE solutions to the culture medium with a final methanol concentration ≤1% (v/v). Appropriate controls containing the same amount of solvent were included in each experiment.

The concentrations of STE for the following assays performed were set based on the results obtained from the cell viability assays in our previous studies. Particularly, the median inhibitory concentrations (IC<sub>50</sub>) obtained after 24 h of exposure to STE by the tetrazolium salt (MTI) and the neutral red (NR) assays were >25 μM and 19.26 ± 39.53 μM, respectively (Zingales et al. 2020a, 2020b). The STE concentrations selected in the present study (0.78, 1.56, and 3.12 μM) were below the IC<sub>50</sub> obtained.

## 2.3. *Alkaline comet assay (pH > 13)*

The induction of DNA strand breaks was determined by alkaline comet assay (pH > 13), as described by Mallebrera et al. (2016), with some modifications. Briefly, SH-SY5Y cells (7×10<sup>5</sup> cells/well) were seeded in six-well plates. Once the cells reached 90% confluence, cells were exposed to 0.78, 1.56, and 3.12 μM STE for 24 h. Then, 3×10<sup>4</sup> cells were suspended in pre-warmed LMA (1% PBS; 37 °C) and 70 ml of the suspension were rapidly transferred to agarose pre-coated slides (1% H<sub>2</sub>O) and covered with a coverslip (24×24 cm).

After gelling for 10 min at 4 °C, the coverslip was gently removed and the slides were immersed in lysis solution (2.5 M NaCl, 100 mM Na<sub>2</sub>-EDTA, 10 mM Tris and 250 mM NaOH, 10% DMSO and 1% Triton X-100, freshly added; pH 10) for at least 1 h at 4 °C in the dark. After lysis, the slides were covered by electrophoresis buffer (300 mM NaOH, 1 mM Na<sub>2</sub>-EDTA; pH 13) for 40 min at room temperature to allow the DNA to unwind. Electrophoresis was run in the same solution for 20 min at 1 V/cm and 300 mA. When an electric field is applied, intact DNA strands remain in the head, while the broken pieces of DNA migrate toward the anode forming a typical comet tail. After electrophoresis, the slides were dried in 96% ethanol (-20 °C, 5 min) and left to dry completely at room temperature overnight. Cells were stained with 500 µl of PI (20 µg/ml) and analyzed using a Leica DM-4500B microscope (Leica Microsystems, Wetzlar, Germany) at 20× magnification. Two slides were prepared for each treatment condition and three independent replicate experiments were performed. A minimum of 50 randomly selected individual cells per slide were analyzed by using Comet Assay Software Project Lab (CaspLab) 1.2.3b1 version. The results were expressed in terms of three comet assay parameters, namely the percentage of DNA in the tail (% tail DNA), tail length, and olive tail moment.

### 2.4. *Immunofluorescence staining*

To determine the levels of the phosphorylated histone H2AX ( $\gamma$ H2AX), SH-SY5Y cells ( $9 \times 10^4$  cells/well) were seeded in 48-well plates and exposed to 0.78, 1.56, and 3.12 µM of STE for 24 h. The cells were then fixed with 4% paraformaldehyde for 20 min, washed three times with 0.1M phosphate buffer PB (prepared by mixing 0.2 M Na<sub>2</sub>HPO<sub>4</sub> and 0.2 M NaH<sub>2</sub>PO<sub>4</sub>) and incubated in blocking solution (0.1 M PB, 0.1% Triton X-100, and 10% FBS) for 1 h at room

---

temperature. Subsequently, cells were incubated with primary rabbit monoclonal antibody anti- $\gamma$ H2AX (1:400 dilution in blocking solution) at 4 °C overnight. The cells were then washed three times with 0.1 M PB and incubated with Alexa FluorVR 488 affinity purified anti-rabbit IgG secondary antibody (1:800 dilution in blocking solution) for 1 h at room temperature. Nuclei were stained with DAPI for 10 min. The images were captured and analyzed using IN Cell Analyzer 2000 (GE Healthcare, Chicago, IL). For quantification, 30 fields for well were observed at a magnification of 40 $\times$ . Three independent experiments were performed and at least 300 cells per field were counted; a cell was verified by the presence of a DAPI-stained nucleus. The results were expressed as fluorescence intensity of cells positive for the antibody under study.

### 2.5. *Micronucleus detection through flow cytometry*

Micronucleus (MN) assay was carried out using the Litron In Vitro Microflow Kit (Litron Laboratories, Rochester, NY), according to the OECD TG 487. Conditions set for this assay point that it must be carried out exposing logarithmically dividing cells to the toxic for a duration of time that approximates 1.5–2 normal cell cycles. At this time, cells must be harvested and processed for MN scoring. The assay was performed according to manufacturer's instructions based on previous reports (Bryce et al. 2007, 2008). Briefly,  $7 \times 10^5$  cells/well were seeded in six-well plates and exposed to 0.78, 1.56, and 3.12  $\mu$ M of STE for 48 h, which is equal to 1.5–2 doubling times for this cell line. The day of the experiment, cells were stained with Nucleic Acid Dye A Solution and placed on ice near a light source for 30 min, to induce the photoactivation of the EMA fluorochrome dye, a reagent that crosses the compromised outer membrane of apoptotic and necrotic cells. Afterwards, cells were washed, lysed with the Litron

Lysis kit-solution and preserved from light for 60 min. During the lysis step, cytoplasmic membranes were digested to liberate nuclei and MN. Finally, a lysis solution 2 containing Nucleic Acid Dye B (SYTOX fluorochrome), which labels all chromatin, was added and cells were incubated for 30 min at room temperature in the dark. The differential staining allows to distinguish between healthy chromatin and dead/dying cells. Gating and analysis strategies were performed by using a BD FACSVersé (BD Biosciences, Franklin Lakes, NJ) flow cytometry, following the instructions and templates provided by the Litron In Vitro Microflow Kit manual and as described by Bryce et al. (2010, 2008). Three independent experiments were performed.

### 2.6. *Cell-cycle analysis by flow cytometry*

Cell-cycle analysis was performed using Vindelov's PI staining solution as described previously by Juan-Garcia et al. (2013). The PI is a fluorescent DNA intercalating agent capable of binding and labeling double-stranded nucleic acids, making possible to achieve a rapid and precise evaluation of cellular DNA content by flow cytometric analysis. Briefly, a number of  $7 \times 10^5$  cells/well were seeded in six-well plates and exposed to 0.78, 1.56, and 3.12  $\mu\text{M}$  of STE for 24 h. Then, cells were trypsinized and placed on ice for 30 min with 860  $\mu\text{l}$  of fresh medium containing Vindelov's PI staining solution prepared as follow: 40  $\mu\text{g/ml}$  RNase, 0.1% Triton X-100, 10 mM Tris, 10 mM NaCl, and 50  $\mu\text{g/ml}$  of PI in PBS. Three independent experiments were performed and 100 000 cells for each sample were analyzed by using a BD LSRFortessa (BD Biosciences, Franklin Lakes, NJ) flow cytometry.

### 2.7. Pretreatment with inhibitors

To evaluate the putative role of MAPK signaling pathways and tumor suppressor p53 on STE-mediated cell-cycle effect, the cells were pre-treated with medium containing 10  $\mu\text{M}$  SB203580, 20  $\mu\text{M}$  PD98059, 20  $\mu\text{M}$  SP600125 or 50  $\mu\text{M}$  PFT for 2 h and then incubated with 3.12  $\mu\text{M}$  STE for 24 h. The effect of the inhibitors on STE-induced cell-cycle arrest was determined by flow cytometry, as previously described.

### 2.8. Statistical analysis

Statistical analysis of data was carried out using GraphPad Prism version 7 (GraphPad Software, San Diego, CA), statistical software package. Data were expressed as mean  $\pm$  SEM of different independent experiments. The statistical analysis of the results was performed by Student's *t*-test for paired samples. Differences between groups were analyzed statistically with one-way ANOVA followed by the Tukey HDS *post-hoc* test for multiple comparisons. The difference level of  $p \leq 0.05$  was considered statistically significant.

## 3. Results

### 3.1. Effect of STE on DNA damage

To investigate whether STE exposure caused DNA damage, the comet assay was performed under alkaline condition. Cells exposed to different concentrations of STE (0.78, 1.56, and 3.12  $\mu\text{M}$ ) for 24 h showed clearly visible comet tails, which is an evident indicator of DNA strand breakage (Figure 1(b–d)). Conversely, in the solvent control group, almost all comet heads were

concentrated with high-density DNA, accompanied by a smooth margin and intact nuclei (Figure 1(a)). The analysis indicated that treatment with STE caused a significant concentration-dependent increase in % tail DNA, tail length, and olive tail moment (Table 1;  $p \leq 0.05$ ). These results suggested that SH-SY5Y cells exposed to different concentrations of STE exhibited markedly higher DNA damage than control cells.

To validate if STE induced DNA double-strand breaks (DSBs), the phosphorylation of the histone H2AX at Ser-139 ( $\gamma$ H2AX), a well-known marker of DBSs, was detected by immunofluorescence staining. In the solvent control cells, no  $\gamma$ H2AX foci were detected (Figure 2(a)). However, significantly more cells displayed  $\gamma$ H2AX foci after 24 h of exposure to STE at all concentrations tested (Figure 2(a)). The bar graph of nuclear staining intensity of cells positive for the antibody under study is shown in Figure 2(b). These results confirm that STE induced significant DNA damage in SH-SY5Y cells.

### 3.2. *Effect of STE on micronuclei induction*

Figure 3 collects MN frequencies in SH-SY5Y cells exposed to STE (0.78, 1.56, and 3.12  $\mu$ M). All concentrations tested induced a significant increase in MN frequencies, exhibiting a similar genotoxic potential. The increase effect resulted in MN frequencies ranging from  $4.1 \pm 0.98\%$  to  $4.3 \pm 0.96\%$  with respect to the control ( $1.0 \pm 0.09\%$ ). These results confirmed that STE was genotoxic to SH-SY5Y cells.

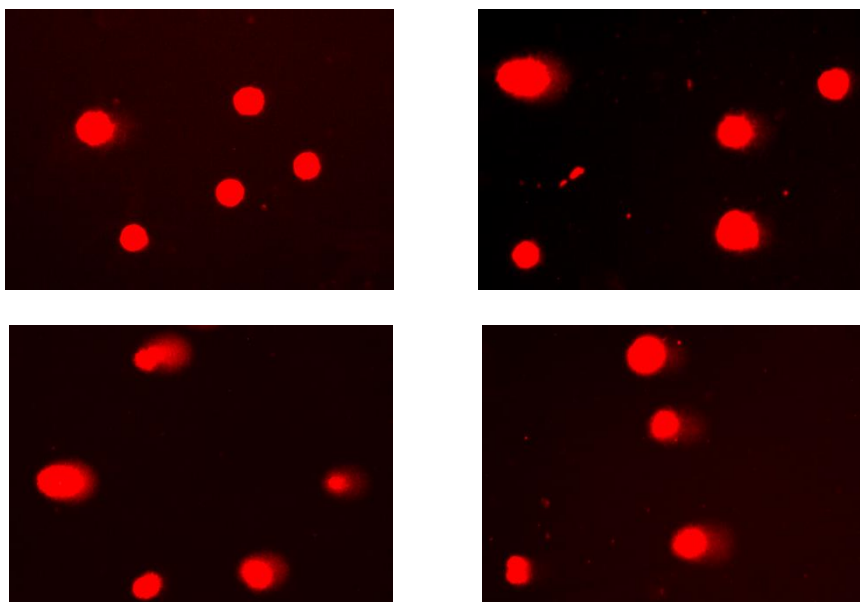
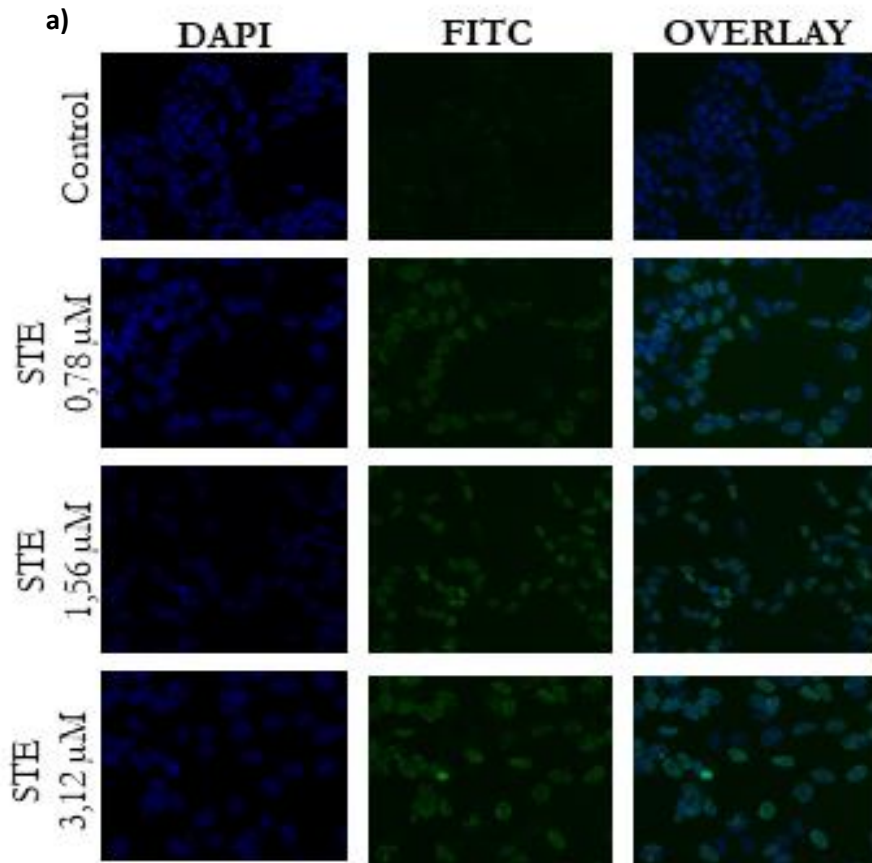


**Figure 1.** The DNA strand breaks in SH-SY5Y cells measured by alkaline comet assay. The cells were treated with the vehicle (a), 0.78  $\mu\text{M}$  (b), 1.56  $\mu\text{M}$  (c) and 3.12  $\mu\text{M}$  (d) for 24 h. Cells were observed under a fluorescent microscope and quantified (20x magnification). The data shown are representative of three independent experiments.

**Table 1.** The tail DNA %, tail length and olive tail moment in SH-SY5Y cells exposed to STE at 0.78, 1.56 and 3.12  $\mu\text{M}$  for 24 h. Data represent the means  $\pm$  SEM. (\*)  $p \leq 0.05$  indicates a significant difference compared to the control.

Group	Tail DNA %	Tail length	Olive tail moment
Control	1,27 $\pm$ 0.88	8,79 $\pm$ 5.77	0,70 $\pm$ 0.84
STE 0.78 $\mu\text{M}$	4,78 $\pm$ 2.99*	20,86 $\pm$ 7.87*	2,10 $\pm$ 2.45*
STE 1.56 $\mu\text{M}$	7,92 $\pm$ 4.59*	30,03 $\pm$ 11.30*	3,82 $\pm$ 3.02*
STE 3.12 $\mu\text{M}$	10,09 $\pm$ 5.28*	32,94 $\pm$ 11.54*	4,69 $\pm$ 3.12*



(Caption of the figure on the next page)



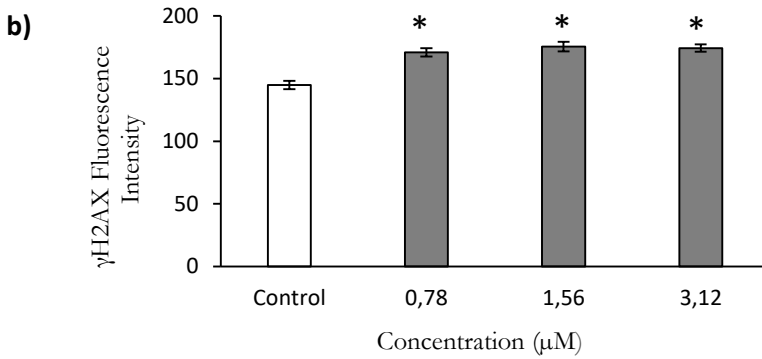


**Figure 2.** Effect of STE exposure on histone H2AX phosphorylation. a) The SH-SY5Y cells were exposed to STE (0.78, 1.56 and 3.12  $\mu\text{M}$ ) for 24 h, fixed and stained with DAPI to visualize nuclei (blue) and with anti- $\gamma\text{H2AX}$  antibody as DSBs marker (green). Figures show DAPI staining, FITC staining and overlay. Images were obtained by using the automated microscope IN Cell Analyzer 2000 (40x magnification). The data shown are representative of three independent experiments. b) Quantification of the  $\gamma\text{H2AX}$  nuclear staining intensity. Data are expressed as mean  $\pm$  SEM ( $n = 3$ ). (\*)  $p \leq 0.05$  indicates a significant difference compared to the control.

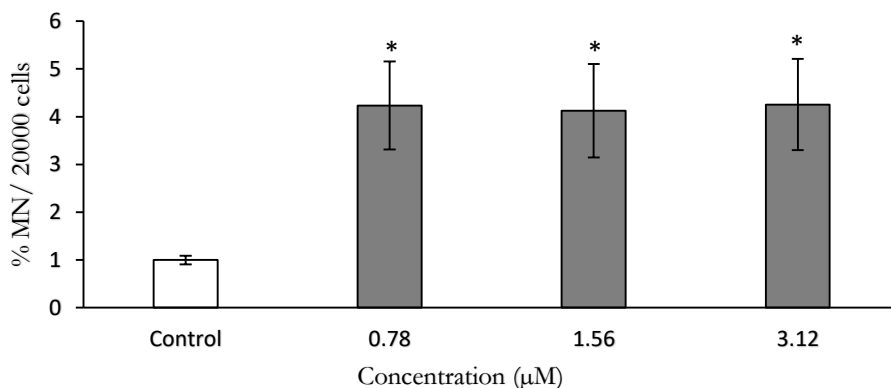


**Figure 3.** Genotoxicity assessment by micronucleus assay in SH-SY5Y cells exposed to STE (0.78, 1.56, and 3.12  $\mu\text{M}$ ) for 48 h. Data are expressed as percentage of MN per 20 000 cells  $\pm$  SEM ( $n = 3$ ). (\*)  $p \leq 0.05$  indicates a significant difference compared to the control.

### 3.3. *Effect of STE on cell-cycle progression*

Because DNA damage is often accompanied by alteration of cell-cycle progression, flow cytometry analysis by PI-staining was performed on SH-SY5Y cells after 24 h of exposure to STE. Exposure to STE at all concentrations assayed resulted in statistically significant differences with respect to the control for all phases. In particular, as shown in Figure 4, a significant reduction in the proportion of cells in the  $G_0/G_1$  phase accompanied by an increase in the percentage of number of cells in S and  $G_2/M$  phases was observed. The percentage of SH-SY5Y cells in the  $G_0/G_1$  phase decreased until  $34.0 \pm 2.26\%$ ,  $30.4 \pm 1.75\%$ , and  $29.3 \pm 1.18\%$  after 0.78, 1.56, and 3.12  $\mu\text{M}$  STE, respectively, as compared to the control ( $62.5 \pm 2.17\%$ ). For the S phase, the percentage of cells increased until  $41.2 \pm 2.08\%$ ,  $46.1 \pm 2.47\%$ , and  $48.0 \pm 2.28\%$  at the three

concentrations tested, respectively, as compared to the control ( $19.2 \pm 2.28\%$ ). Similarly, for the G<sub>2</sub>/M phase, the number of cells increased until  $24.4 \pm 0.28\%$ ,  $23.0 \pm 1.05\%$ , and  $22.1 \pm 1.23\%$ , respectively, as compared to the control ( $18.0 \pm 0.78\%$ ). Nevertheless, the highest increase was observed in the S phase at all concentrations tested. An example of the histograms representative of the control and the highest concentration tested ( $3.12 \mu\text{M}$ ) of STE after 24 h of exposure can be observed in Figure 5.

### 3.4. Role of MAPK and p53 inhibitors on STE-induced cell-cycle arrest

To clarify the role of ERK, JNK, p38, and p53 on the cell-cycle arrest induced by STE, specific inhibitors were applied and the effects on the cell cycle were evaluated using PI-staining method by flow cytometry. As shown in Figure 6(a), in cells exposed to  $3.12 \mu\text{M}$  STE and pre-treated with PD98059 the percentage of cells in the G<sub>0</sub>/G<sub>1</sub> phase significantly increased until  $61.6 \pm 0.71\%$  compared to cells exposed to STE ( $49.07 \pm 4.6\%$ ), up to not being significantly different from control cells ( $65.9 \pm 0.98\%$ ). For the S phase, the percentage of cells significantly decreased until  $24.45 \pm 1.77\%$  compared to cells exposed to STE ( $37.07 \pm 4.44\%$ ) and resulted not significantly different compared to control cells ( $16.67 \pm 2.4\%$ ). Finally, for the G<sub>2</sub>/M phase, a significant decrease until  $13.2 \pm 0.99\%$  was observed in cells exposed to STE and pretreated with PD98059 compared to cells exposed to the mycotoxin ( $22.1 \pm 2.13\%$ ), while no significant changes were observed respect to control cells ( $17.43 \pm 1.53\%$ ). The SP600125 induced similar results (Figure 6(b)), suggesting that STE-mediated S and G<sub>2</sub>/M cell-cycle arrest is markedly attenuated by ERK and JNK inhibitors. No effects on STE-induced cell-cycle arrest were obtained in cells pre-treated with SB203580 and PFT, except for the G<sub>2</sub>/M phase, where both of these

## Resultados

inhibitors induced a decrease of the number of cells (until  $14.35 \pm 0.35\%$  and  $11.33 \pm 0.9\%$ , respectively) respect to cells exposed to STE and, for the second one, also respect to control cells (Figure 6(c,d)).

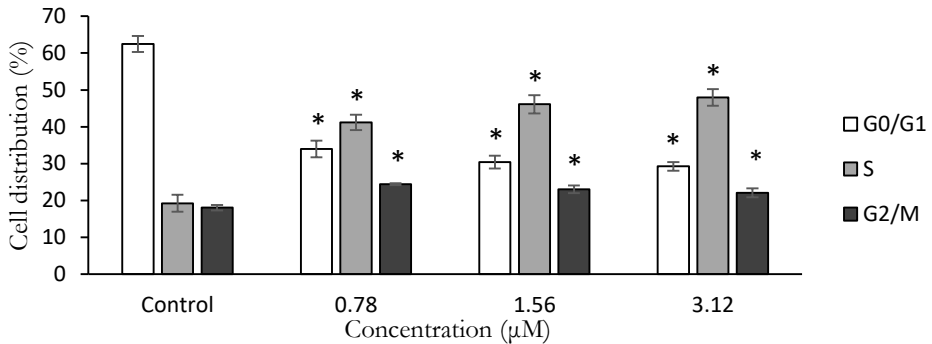


**Figure 4.** Analysis of cell-cycle distribution of SH-SY5Y cells treated with STE at 0.78, 1.56, and  $3.12 \mu\text{M}$  for 24 h. Data are expressed as mean  $\pm$  SEM ( $n = 3$ ). (\*)  $p \leq 0.05$  indicates a significant difference compared to the control.

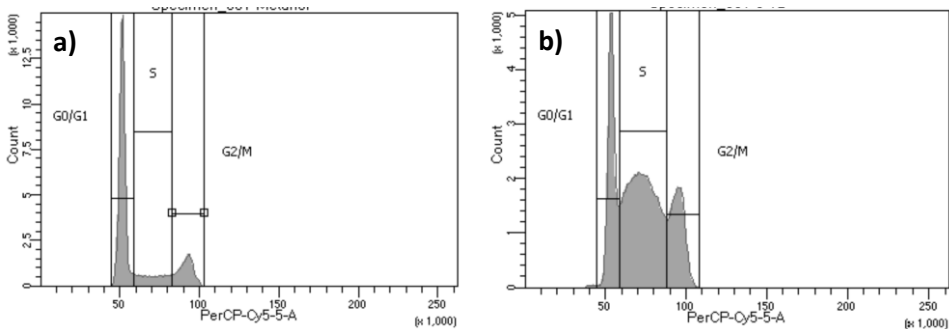


**Figure 5.** Cells were exposed to STE, stained with PI and subjected to cell-cycle analysis by flow cytometry. The cell-cycle histograms are representative of SH-SY5Y cells: (a) control and (b) exposed to  $3.12 \mu\text{M}$  of STE for 24 h.

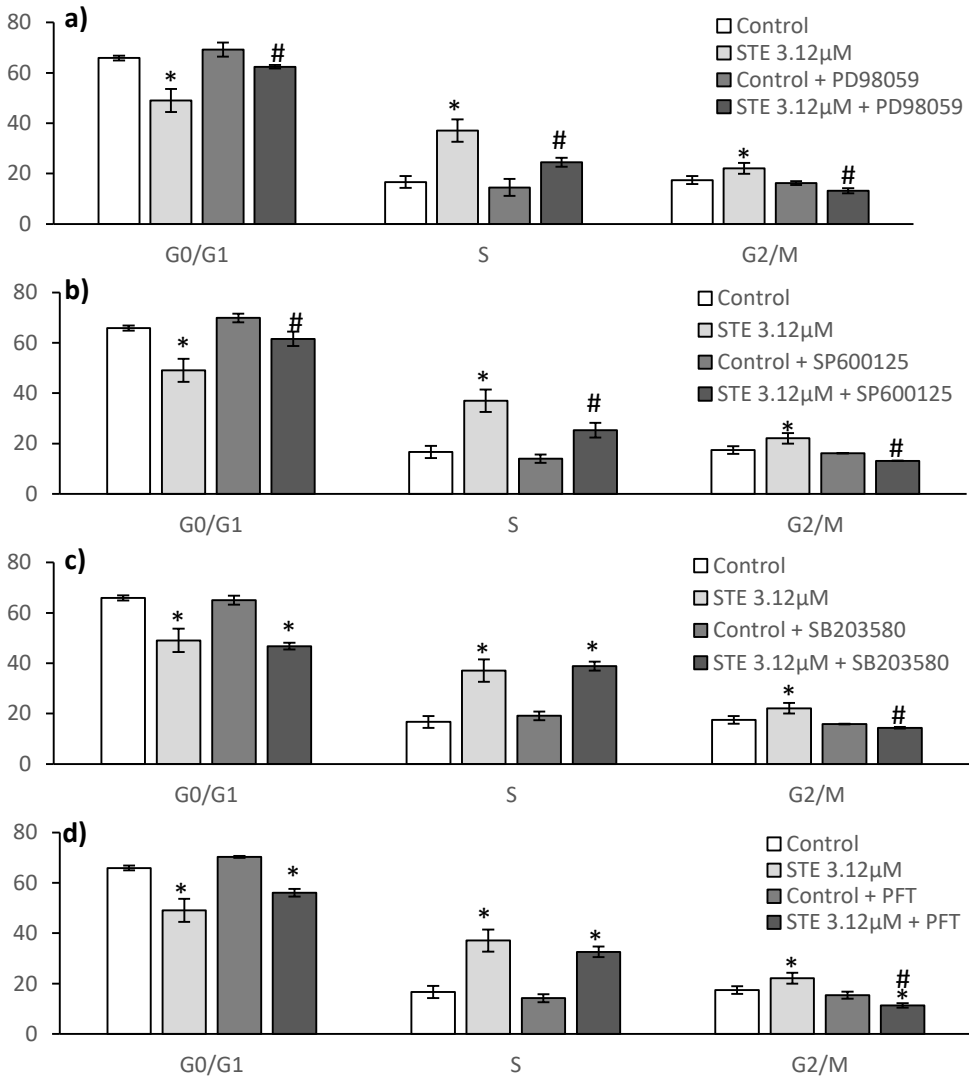


**Figure 6.** Analysis of cell-cycle distribution of SH-SY5Y cells pre-treated with 20 µM PD98059 (a), 20 µM SP600125 (b), 10 µM SB203580 (c), or 50 µM PFT (d) and exposed to 3.12 µM STE for 24 h. Data are expressed as mean ± SEM ( $n = 3$ ). (\*)  $p \leq 0.05$  indicates a significant difference compared to the control; (#)  $p \leq 0.05$  indicates a significant difference compared to cells exposed to 3.12 µM STE.

### 4. Discussion

The STE is known to induce reduction of cell viability and cell proliferation (Anninou et al., 2014; Cui et al., 2017; Liu et al., 2014; Zouaoui et al., 2016), DNA-double strand breaks (Huang et al., 2014) and cell cycle arrest (Wang et al., 2013; Xing et al., 2011; Zhang et al., 2013). Moreover, mutagenic and carcinogenic properties have been attributed to STE (Versilovskis and De Saeger, 2010). Additionally, we have recently demonstrated that STE causes oxidative stress, lipid peroxidation and produces changes in the antioxidant defence system on human neuroblastoma cells (Zingales et al., 2019). On the basis of our previous studies, in the present study we further explored the effects of STE on viability, mitochondrial function and mitochondria-mediated apoptosis in SH-SY5Y cells. Our results demonstrate that STE reduced in a time- and concentration-dependent manner the cell viability of SH-SY5Y cells by MTT assay, confirming our previous results obtained by NR assay (Zingales et al., 2019). However, the two methods are based on different physiological endpoints. In fact, if the latter is based on the incorporation of the dye neutral red into the lysosomes of viable cells, allowing to evaluate the lysosome functionality, on the other hand the ability of cells to reduce MTT provides an indication of mitochondrial integrity and activity. Thus, the data obtained by MTT assay is interpreted not only as a measure of cell viability but indirectly serves also to assess the cellular energy capacity of the cells. Finally, *in vitro* cytotoxicity assays, besides being useful to define the basal cytotoxicity, allow to define the concentration range for further assays. In order to gain further insights into the mechanisms of STE-mediated cytotoxicity, aspects of metabolic and mitochondrial function were investigated. It has been demonstrated that in cultured cells, despite aerobic conditions, the majority of ATP is obtained via

---

glycolysis in the cytoplasm, with a concomitant significant decrease in levels of OXPHOS (Crabtree effect). However, since galactose produces no net ATP from glycolysis, culturing cells in galactose-supplemented medium rather than glucose leads to circumvention of the Crabtree effect and stimulates OXPHOS (Marroquin et al., 2007). Thus, we forced SH-SY5Y cells to use OXPHOS by replacing the glucose in the medium with galactose. Using this approach, we developed a cell model that more faithfully reports mitochondrial physiology and probes the functional status of the mitochondria of SH-SY5Y cells exposed to STE. Our results suggest that the switch in substrate caused a striking change in the growth behaviour of the galactose-grown cells when compared to glucose-grown SH-SY5Y cells exposed to increasing concentrations of STE (Fig. 1). In particular, cells grown in glucose tolerated up to 6.24  $\mu\text{M}$  STE without a significant loss in cell viability. In contrast, cells grown in galactose were highly susceptible with a significant loss of viability starting from 3.12  $\mu\text{M}$  STE. The differences in the response between SHSY5Y cells grown in glucose and those grown in galactose suggest that the etiology of STE cytotoxicity depends on mitochondrial impairment. The ability of cells to produce high-energy molecules, such as ATP, is directly related to mitochondrial metabolism. For this reason, we measured the ATP content in SH-SY5Y cells exposed to STE in glucose and galactose culture conditions. A significant decrease in ATP levels was observed in SH-SY5Y cells starting from a STE concentration of 3.12  $\mu\text{M}$  and was equivalent in both growth conditions (Fig. 2). These data suggest that STE affects ATP production in SH-SY5Y cells, although the mechanism underlying this impairment is not dependent by the route through which cells derive their energy. However, in galactose-grown cells a slight increase in ATP content was obtained at the lowest STE concentration (0.78  $\mu\text{M}$ ). It could be

assumed that under these conditions the response of SH-SY5Y cells to STE is a hormetic response characterized by low concentration stimulation and high concentration inhibition (Calabrese and Baldwin, 2003). The exact mechanisms underlying this phenomenon are unknown. Further studies are needed to elucidate the extent of such hormesis induced by STE. A decrease of ATP levels along the treatment concentrations of STE (0.5–7  $\mu\text{M}$ ) was reported also by Liu et al. (2014) in HepG2 cells. However, only limited reports about the ability of STE to alter mitochondrial functions are available. In contrast, several other mycotoxins were reported to cause mitochondrial dysfunctions. In particular, patulin was found to cause ATP depletion and mitochondrial dysfunction in murine neuroblastoma neuro-2a cells and in human fetal kidney HEK293 cells (Malekinejad et al., 2015; Zhong et al., 2017). In rat cardiomyocytes deoxynivalenol and T-2 toxin have been shown to cause mitochondrial dysfunction by inhibition of the mitochondrial ETC function (Ngampongsa et al., 2013). Similarly, Moosavi et al. (2016) revealed a decrease of the activity of mitochondrial complexes III, IV and V,  $\Delta\Psi\text{m}$  and ATP content in rat hepatocytes following T-2 toxin administration. In ATP synthesis two components play a crucial role: the transmembrane proton concentration gradient (pH) and the  $\Delta\Psi\text{m}$  (Dimroth et al., 2000; Mazat et al., 2013). Although in mitochondria the  $\Delta\Psi\text{m}$  component is the main driving force for ATP production, under our experimental conditions no alterations of  $\Delta\Psi\text{m}$  were reported to be related to the decreased ATP content observed (Fig. 5). However, according to our results, Bohler et al. (2018) showed that in Jurkat cells not even the ETC inhibitors, known to block the electron transport and thus inhibit the ATP synthetase, affected  $\Delta\Psi\text{m}$ . It has to be taken into account that, in OXPHOS condition another crucial requirement for ATP synthesis consists in



---

a functional ETC. For this reason, in subsequent experiments we evaluated the effect of STE on cell viability of SH-SY5Y cells grown in galactose-supplemented medium in presence of ETC inhibitors (Fig. 3). The further decrease in cell viability obtained when cells were exposed to STE in presence of rotenone, a selective inhibitor of the complex I, highlights that the mechanism of STE-cytotoxicity is directly dependent on changes in ETC activity. However, no effects were observed in presence of antimycin A, an inhibitor of the complex III, suggesting that this latter complex is not involved in STE toxicity. Overall, these observations establish clearly that mitochondria play a central role in the cytotoxic activity of STE, although its cytotoxicity appears not necessarily a result of its effects on the  $\Delta\Psi_m$  and on the complex III of the ETC. Mitochondria are the main source of intracellular ROS production (Zhan et al., 2019). However, endogenous antioxidant systems scavenge ROS, maintaining them at no toxic levels. A decrease in mitochondrial function has been linked to an increase in mitochondrial ROS generation (Leon et al., 2016). Our study showed that in SH-SY5Y cells, STE triggered a concentration-dependent enhancement of mitochondrial superoxide levels after 24 h of exposure (Fig. 4), demonstrating its implication in cell toxicity. In fact, mycotoxins-induced oxidative stress might be one of the major causes of mitochondrial dysfunction (Islam et al., 2018). Particularly, increased levels of mitochondrial ROS are known to cause damages to mitochondrial DNA (mtDNA), with consequent production of dysfunctional proteins essential for proper mitochondrial functioning (Yang et al., 2016). Several mycotoxins were reported to induce mitochondrial dysfunction by increasing oxidative stress. Sahu et al. (2010) showed that deoxynivalenol causes oxidative stress and thus mitochondrial dysfunction in liver cells of rats (Clone9 and MH1C1), mice (NBL CL2) and

humans (WRL68 and HepG2). Ochratoxin A has been demonstrated to trigger accelerated respiration and increase the production of mitochondrial ROS, causing an opening of ROS-dependent mitochondrial permeability transition (mPT) pores. This led to a decrease in  $\Delta\Psi_m$  and the release of cytochrome c into the cytosol, resulting in the induction of mitochondrial intrinsic apoptosis (Wang et al., 2017). Apoptosis is a specialized process of cell death included in the normal development of organs and tissue maintenance, but may also occur as a response to various toxic environmental stimuli. It is an extremely complex process in which mitochondria play a pivotal role. It is tightly regulated through a number of checkpoints in order to preserve a healthy balance between cell death and cell survival and maintain genome integrity (Blatt and Glick, 2001). One of the main and crucial disruptors of this balance is represented by the excessive oxidative stress. In fact, the mPT pores, whose opening causes the release of death factors, are redox-sensitive. Moreover, a series of well-known molecular pathways results to be involved in the regulation of apoptosis. In particular, this process is strictly controlled by a balance between the pro-apoptotic proteins, such as *Bax*, and the anti-apoptotic proteins, such as *Bcl-2*, resulting ultimately in the activation of the apoptotic effector molecule *Casp-3* and the execution of the cell death program (Blatt and Glick, 2001). Definitely, *Bcl-2* keeps the mPT pores in a closed state and thus prevents cytochrome c from crossing mitochondrial outer membrane and leaking out to activate caspases. In contrast, *Bax* leads to an opening of mPT pores, promoting apoptosis. Accumulating evidences highlight that the induction of apoptosis is one of the main effects of many carcinogenic mycotoxins, such as fumonisin B1, patulin and zearalenone (Alizadeh et al., 2015; Ayed-Boussema et al., 2008; Boussabbeh et al., 2015; Ribeiro et al., 2010). In the present study, we found that STE induced

early- and late-stage apoptotic events in SH-SY5Y cells after 2 and 24 h of exposure, respectively (Figs. 6 and 7). These results suggest that the observed loss of cell viability resulting from the exposition of SH-SY5Y cells to STE is due to the induction of an apoptotic process. Our findings are consistent with other previous studies, demonstrating that apoptosis is a common effect of STE in different cell lines. Cui et al. (2017) showed that in adenocarcinomic human alveolar basal epithelial A549 cells and in human bronchial epithelial BEAS-2B cells STE induced apoptosis in a concentration-dependent manner. The STE has been demonstrated to cause apoptosis also in human gastric epithelial GES-1 cells (Zhang et al., 2013). In order to obtain a further confirmation of our results, the evaluation of the expression levels of apoptosis-related proteins was carried out. In particular, the changes in the mRNA expression levels of the key proteins *Bax*, *Bcl-2* and *Casp-3* were evaluated (Fig. 8). Compared to control, the mRNA expression levels of *Bax* were increased by STE exposure, while *Bcl-2* mRNA resulted to be down-regulated in SHSY5Y cells exposed to the mycotoxin. In addition, the up-regulation of *Casp-3* mRNA confirmed that STE inhibits the proliferation of SH-SY5Y cells by inducing apoptosis. Our results are in accordance with those reported by Cui et al. (2017) and Zhang et al. (2013), who demonstrated that STE induced apoptosis by increasing the *Bax/Bcl-2* ratio and activating *Casp-3* in HepG2, A549 and BEAS-2B cells. Other studies have demonstrated that the mycotoxin zearalenone and T-2 toxin induce apoptosis through the caspase-dependent apoptotic pathway by increasing *Bax/Bcl-2* ratio and activating *Casp-3* in in vitro studies (Ayed-Boussema et al., 2008; Chaudhari et al., 2009). In Het-1A and A549 cells, apoptosis was induced by ochratoxin A and aflatoxin G1 via activation and cleavage of *Casp-3* and up- and down-regulation of *Bax* and *Bcl-2* genes, respectively (Liu et al., 2015; Shen et al., 2013).

In summary, our results provide further novel insights in the signaling pathways of the cell death process induced by STE in SH-SY5Y cells. We identify for the first time STE as a mitochondrial mycotoxin, with a mode of action that involves a modulation of mitochondrial function, ATP depletion, oxidative stress and the activation of mitochondrial-related pathway of apoptosis. With metabolic disorders rising at an alarming rate in Western and developed countries, it is becoming increasingly important to understand how foodborne mycotoxins, such as STE, can affect the energy metabolism. Furthermore, the identification of mitochondria as one of the targets of STE might provide a useful tool for the study of the use of neuroprotective mitochondria-target functional peptides, known for protect mitochondria against oxidative stress and prevent neuronal cell death (Szeto, 2006).

### **Acknowledgments**

The authors thank the cell culture and flow cytometry service from the SCSIE of the University of Valencia for their technical support.

### **Disclosure statement**

No potential conflict of interest was reported by the author(s).

### **Funding**

This work has been supported by the Generalitat Valenciana under Grant Prometeo 2018/216 and under the pre-doctoral research training program ‘Santiago Grisolia [GRISOLIAP/2018/092] CPI-18-117’.

---

## References

- Abid-Essefi S, Ouanes Z, Hassen W, Baudrimont I, Creppy E, Bacha H. 2004. Cytotoxicity, inhibition of DNA and protein syntheses and oxidative damage in cultured cells exposed to zearalenone. *Toxicol in Vitro*. 18(4):467–474.
- Agrawal M, Bhaskar AS, Lakshmana Rao PV. 2015. Involvement of mitogen-activated protein kinase pathway in T-2 toxin-induced cell cycle alteration and apoptosis in human neuroblastoma cells. *Mol Neurobiol*. 51(3):1379–1394.
- Anninou N, Chatzaki E, Papachristou F, Pitiakoudis M, Simopoulos C. 2014. Mycotoxins' activity at toxic and sub-toxic concentrations: differential cytotoxic and genotoxic effects of single and combined administration of sterigmatocystin, ochratoxin A and citrinin on the hepatocellular cancer cell line Hep3B. *Int J Environ Res Public Health*. 11(2):1855–1872.
- Axelsson V, Holback S, Sjogren M, Gustafsson H, Forsby A. 2006. Gliotoxin induces caspase-dependent neurite degeneration and calpain-mediated general cytotoxicity in differentiated human neuroblastoma SH-SY5Y cells. *Biochem Biophys Res Commun*. 345(3): 1068–1074.
- Aziz K, Nowsheen S, Pantelias G, Iliakis G, Gorgoulis VG, Georgakilas AG. 2012. Targeting DNA damage and repair: embracing the pharmacological era for successful cancer therapy. *Pharmacol Ther*. 133(3): 334–350.
- Banjerdpongchai R, Kongtawelert P, Khantamat O, Srisomsap C, Chokchaichamnankit D, Subhasitanont P, Svasti J. 2010. Mitochondrial and endoplasmic reticulum stress pathways cooperate in zearalenone-induced apoptosis of human leukemic cells. *J Hematol Oncol*. 3: 50.

Bryce SM, Avlasevich SL, Bemis JC, Lukamowicz M, Elhajouji A, Van Goethem F, De Boeck M, Beerens D, Aerts H, Van Gompel J, et al. 2008. Interlaboratory evaluation of a flow cytometric, high content in vitro micronucleus assay. *Mutat Res.* 650(2):181–195.

Bryce SM, Bemis JC, Avlasevich SL, Dertinger SD. 2007. In vitro micronucleus assay scored by flow cytometry provides a comprehensive evaluation of cytogenetic damage and cytotoxicity. *Mutat Res.* 630(1–2):78–91.

Bryce SM, Shi J, Nicolette J, Diehl M, Sonders P, Avlasevich S, Raja S, Bemis JC, Dertinger SD. 2010. High content flow cytometric micronucleus scoring method is applicable to attachment cell lines. *Environ Mol Mutagen.* 51(3):260–266.

Chatzimichail E, Matthaïos D, Bouros D, Karakitsos P, Romanidis K, Kakolyris S, Papashinopoulos G, Rigas A. 2014. gamma-H2AX: a novel prognostic marker in a prognosis prediction model of patients with early operable non-small cell lung cancer. *Int J Genomics.* 2014:1–6.

Commission Regulation. 2006. (EC) No. 1881/2006 of 19 December Setting Maximum Levels for Certain Contaminants in Foodstuffs. Available online: <https://eur-lex.europa.eu/LexUriServ/LexUriServ.do?uri=OJ:L:2006:364:0005:0024:EN:PDF>.

Cui J, Wang J, Huang S, Jiang X, Li Y, Wu W, Zhang X. 2017. Sterigmatocystin induced apoptosis in human pulmonary cells in vitro. *Exp Toxicol Pathol.* 69(8):695–699.

Cui J, Wang J, Huang S, Jiang X, Li Y, Wu W, Zhang X. 2018. The G2 phase arrest induced by sterigmatocystin is dependent on hMLH1-ERK/p38-p53 pathway in human esophageal epithelium cells in vitro. *Food Chem Toxicol.* 115:205–211.

---

Cui J, Xing L, Li Z, Wu S, Wang J, Liu J, Wang J, Yan X, Zhang X. 2010. Ochratoxin A induces G(2) phase arrest in human gastric epithelium GES-1 cells in vitro. *Toxicol Lett.* 193(2):152–158.

Dai Y, Xie H, Xu Y. 2017. Evaluation of deoxynivalenol-induced toxic effects on mouse endometrial stromal cells: cell apoptosis and cell cycle. *Biochem Biophys Res Commun.* 483(1):572–577.

Flatt PM, Pietsenpol JA. 2000. Mechanisms of cell-cycle checkpoints: at the crossroads of carcinogenesis and drug discovery. *Drug Metab Rev.* 32(3–4):283–305.

Gao W, Jiang L, Ge L, Chen M, Geng C, Yang G, Li Q, Ji F, Yan Q, Zou Y, et al. 2015. Sterigmatocystin-induced oxidative DNA damage in human liver-derived cell line through lysosomal damage. *Toxicol in Vitro.* 29(1):1–7.

Harper JW, Elledge SJ. 2007. The DNA damage response: ten years after. *Mol Cell.* 28(5):739–745.

Hayashi A, Jose Dorantes-Aranda J, Bowman JP, Hallegraef G. 2018. Combined cytotoxicity of the phycotoxin okadaic acid and mycotoxins on intestinal and neuroblastoma human cell models. *Toxins.* 10(12):526.

Huang S, Wang J, Xing L, Shen H, Yan X, Wang J, Zhang X. 2014. Impairment of cell cycle progression by sterigmatocystin in human pulmonary cells in vitro. *Food Chem Toxicol.* 66:89–95.

Hutanasu C, Sfarti C, Trifan A, Cojocariu C, Singeap AM, Spac A, Stanciu C. 2011. High levels of sterigmatocystin in patients with chronic liver diseases. *Rev Med Chir Soc Med Nat Iasi.* 115(1):33–37.

IARC. 1987. Overall evaluations of carcinogenicity: an updating of IARC monographs, Volumes 1–42. Supplement 7. Lyon, France.

Ishikawa K, Ishii H, Saito T. 2006. DNA damage-dependent cell cycle checkpoints and genomic stability. *DNA Cell Biol.* 25(7):406–411.

Jeggo PA, Lobrich M. 2007. DNA double-strand breaks: their cellular and clinical impact? *Oncogene.* 26(56):7717–7719.

Jiang X, Wang J, Xing L, Shen H, Lian W, Yi L, Zhang D, Yang H, Liu J, Zhang X. 2017. Sterigmatocystin-induced checkpoint adaptation depends on Chk1 in immortalized human gastric epithelial cells in vitro. *Arch Toxicol.* 91(1):259–270.

Johnson VJ, He Q, Kim SH, Kanti A, Sharma RP. 2003. Increased susceptibility of renal epithelial cells to TNFalpha-induced apoptosis following treatment with fumonisin B1. *Chem Biol Interact.* 145(3):297–309.

Juan-Garcia A, Manyes L, Ruiz MJ, Font G. 2013. Involvement of enniatins-induced cytotoxicity in human HepG2 cells. *Toxicol Lett.* 218(2): 166–173.

Juan-Garcia A, Tolosa J, Juan C, Ruiz MJ. 2019. Cytotoxicity, genotoxicity and disturbance of cell cycle in HepG2 cells exposed to OTA and BEA: single and combined actions. *Toxins.* 11(6):341.

Lee JY, Lim W, Park S, Kim J, You S, Song G. 2019a. Deoxynivalenol induces apoptosis and disrupts cellular homeostasis through MAPK signaling pathways in bovine mammary epithelial cells. *Environ Pollut.* 252(Pt A):879–887.

Lee JY, Lim W, Ryu S, Kim J, Song G. 2019b. Ochratoxin A mediates cytotoxicity through the MAPK signaling pathway and alters intracellular homeostasis in bovine mammary epithelial cells. *Environ Pollut.* 246: 366–373.

Liu J, Wang Y, Cui J, Xing L, Shen H, Wu S, Lian H, Wang J, Yan X, Zhang X. 2012. Ochratoxin A induces oxidative DNA damage and G1 phase



---

arrest in human peripheral blood mononuclear cells in vitro. *Toxicol Lett.* 211(2):164–171.

Liu Y, Du M, Zhang G. 2014. Proapoptotic activity of aflatoxin B1 and sterigmatocystin in HepG2 cells. *Toxicol Rep.* 1:1076–1086.

Lou JL, Tian HJ, Meng ZH, Gou ZQ. 1995. Detection of sterigmatocystin in food/feed samples from areas with various liver/stomach cancer incidences by enzyme-linked immunosorbent assay. *Wei Sheng Yan Jiu.* 24:28–31.

Mallebrera B, Juan-Garcia A, Font G, Ruiz MJ. 2016. Mechanisms of beauvericin toxicity and antioxidant cellular defense. *Toxicol Lett.* 246: 28–34.

Matthaios D, Hountis P, Karakitsos P, Bouros D, Kakolyris S. 2013. H2AX a promising biomarker for lung cancer: a review. *Cancer Invest.* 31(9): 582–599.

Nicolai S, Rossi A, Di Daniele N, Melino G, Annicchiarico-Petruzzelli M, Raschella G. 2015. DNA repair and aging: the impact of the p53 family. *Aging (Albany NY).* 7(12):1050–1065.

Niida H, Nakanishi M. 2006. DNA damage checkpoints in mammals. *Mutagenesis.* 21(1):3–9.

Palma N, Cinelli S, Saporita O, Wilson SH, Dogliotti E. 2007. Ochratoxin A induced mutagenesis in mammalian cells is consistent with the production of oxidative stress. *Chem Res Toxicol.* 20(7):1031–1037.

Pastor S, Gutierrez S, Creus A, Xamena N, Piperakis S, Marcos R. 2001. Cytogenetic analysis of Greek farmers using the micronucleus assay in peripheral lymphocytes and buccal cells. *Mutagenesis.* 16(6):539–545.

Pitt JI, Wild CP, Baan RA, Gelderblom WCA, Miller JD, Riley RT, Wu F. 2012. Improving Public Health through Mycotoxin Control. *International*

Agency for Research on Cancer (IARC Scientific Publications Series, No. 158), Lyon, France.

Reinhardt HC, Schumacher B. 2012. The p53 network: cellular and systemic DNA damage responses in aging and cancer. *Trends Genet.* 28(3):128–136.

Sancar A, Lindsey-Boltz LA, Unsal-Kacmaz K, Linn S. 2004. Molecular mechanisms of mammalian DNA repair and the DNA damage checkpoints. *Annu Rev Biochem.* 73:39–85.

Schafer KA. 1998. The cell cycle: a review. *Vet Pathol.* 35(6):461–478.  
Stewart ZA, Pietsenpol JA. 2001. p53 signaling and cell cycle checkpoints. *Chem Res Toxicol.* 14(3):243–263.

Stockmann-Juvala H, Naarala J, Loikkanen J, Vahakangas K, Savolainen K. 2006. Fumonisin B1-induced apoptosis in neuroblastoma, glioblastoma and hypothalamic cell lines. *Toxicology.* 225(2–3):234–241.

Taroncher M, Rodriguez-Carrasco Y, Ruiz MJ. 2020. T-2 toxin and its metabolites: Characterization, cytotoxic mechanisms and adaptive cellular response in human hepatocarcinoma (HepG2) cells. *Food Chem Toxicol.* 145(111654):111654.

Tian H, Liu X. 2004. Survey and analysis on sterigmatocystin contaminated in grains in China. *Wei Sheng Yan Jiu.* 33(5):606–608.

van Gent DC, Hoeijmakers JH, Kanaar R. 2001. Chromosomal stability and the DNA double-stranded break connection. *Nat Rev Genet.* 2(3): 196–206.

Vousden KH, Lane DP. 2007. p53 in health and disease. *Nat Rev Mol Cell Biol.* 8(4):275–283.

Wang J, Huang S, Xing L, Cui J, Tian Z, Shen H, Jiang X, Yan X, Wang J, Zhang X. 2015. Sterigmatocystin induces G1 arrest in primary human

---

esophageal epithelial cells but induces G2 arrest in immortalized cells: key mechanistic differences in these two models. *Arch Toxicol.* 89(11): 2015–2025.

Wang J, Huang S, Xing L, Shen H, Yan X, Wang J, Zhang X. 2013. Role of hMLH1 in sterigmatocystin-induced G(2) phase arrest in human esophageal epithelial Het-1A cells in vitro. *Toxicol Lett.* 217(3): 226–234.

Wang Y, Liu J, Cui J, Xing L, Wang J, Yan X, Zhang X. 2012. ERK and p38 MAPK signaling pathways are involved in ochratoxin A-induced G2 phase arrest in human gastric epithelium cells. *Toxicol Lett.* 209(2):186–192.

Wu GS. 2004. The functional interactions between the p53 and MAPK signaling pathways. *Cancer Biol Ther.* 3(2):156–161.

Xie TX, Misumi J, Aoki K, Zhao WY, Liu SY. 2000. Absence of p53-mediated G1 arrest with induction of MDM2 in sterigmatocystin-treated cells. *Int J Oncol.* 17(4):737–742.

Xing X, Wang J, Xing LX, Li YH, Yan X, Zhang XH. 2011. Involvement of MAPK and PI3K signaling pathway in sterigmatocystin-induced G2 phase arrest in human gastric epithelium cells. *Mol Nutr Food Res.* 55(5):749–760.

Yang H, Chung DH, Kim YB, Choi YH, Moon Y. 2008. Ribotoxic mycotoxin deoxynivalenol induces G2/M cell cycle arrest via p21Cip/WAF1 mRNA stabilization in human epithelial cells. *Toxicology.* 243(1–2):145–154.

Yuan J, Adamski R, Chen J. 2010. Focus on histone variant H2AX: to be or not to be. *FEBS Lett.* 584(17):3717–3724.

Zhang D, Cui Y, Shen H, Xing L, Cui J, Wang J, Zhang X. 2013.

Sterigmatocystin-induced DNA damage triggers G2 arrest via an ATM/p53-related pathway in human gastric epithelium GES-1 cells in vitro. *PLoS One.* 8(5): e65044.

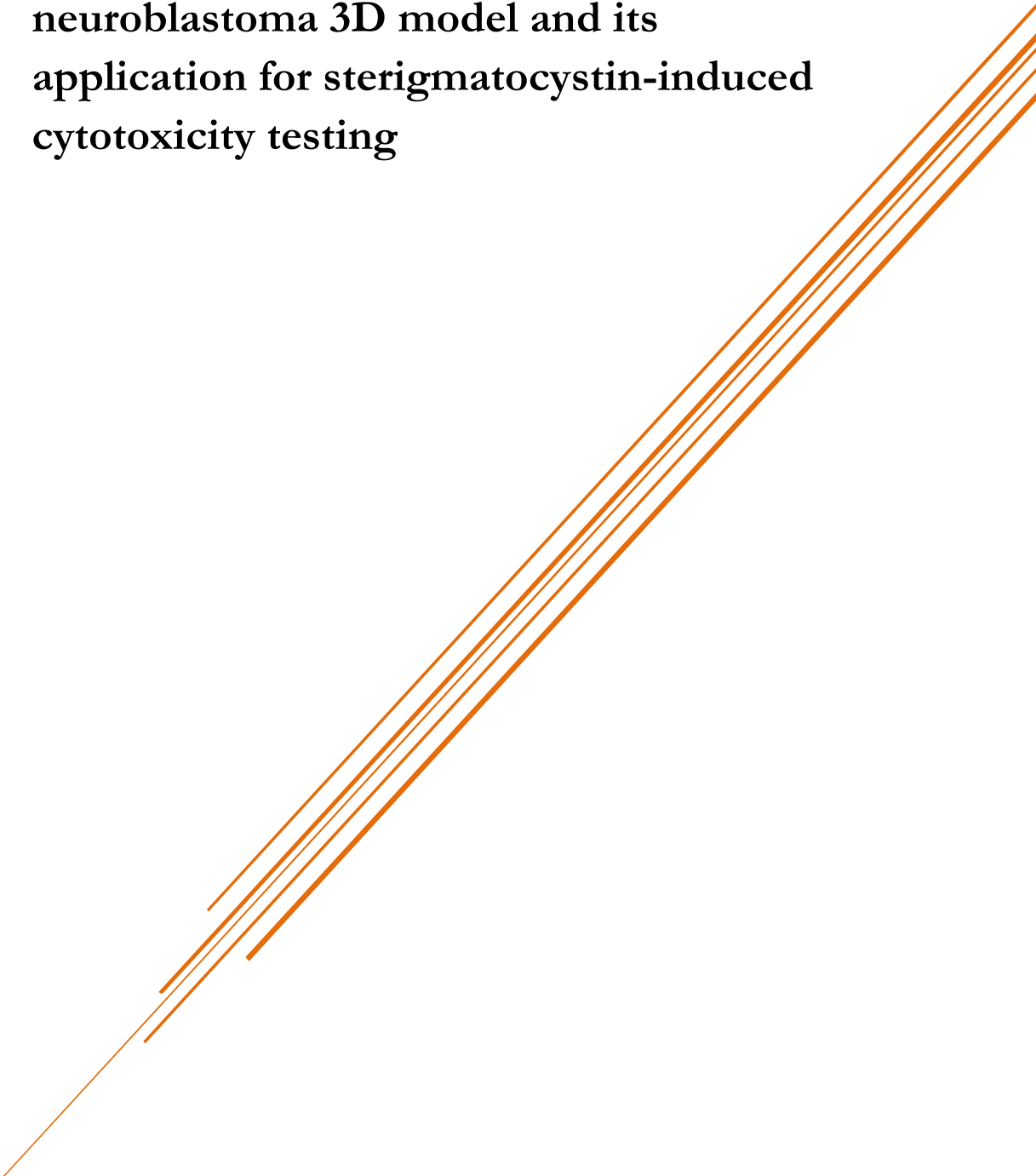
Zhang X, Wang F, Wang J, Yan X, Huang X, Xie T, Zhang Z. 2003. Experimental lung carcinoma induced by fungi and mycotoxins – a review. *Beijing Da Xue Xue Bao Yi Xue Ban*. 35(1):4–6.

Zingales V, Fernandez-Franzon M, Ruiz MJ. 2020a. The role of mitochondria in sterigmatocystin-induced apoptosis on SH-SY5Y cells. *Food Chem Toxicol*. 142:111493.

Zingales V, Fernandez-Franzon M, Ruiz MJ. 2020b. Sterigmatocystin-induced cytotoxicity via oxidative stress induction in human neuroblastoma cells. *Food Chem Toxicol*. 136:110956.

Zingales V, Fernandez-Franzon M, Ruiz MJ. 2020c. Sterigmatocystin: occurrence, toxicity and molecular mechanisms of action – a review. *Food Chem Toxicol*. 146:111802.

### **3.6. Development of an in vitro neuroblastoma 3D model and its application for sterigmatocystin-induced cytotoxicity testing**





Food and Chemical Toxicology

(Under Review)

**Development of an in vitro neuroblastoma 3D model  
and its application for sterigmatocystin-induced cytotoxicity  
testing**

Veronica Zingales<sup>1</sup>, Noemi Torriero<sup>2,3</sup>, Luca Zanella<sup>2</sup>, Mónica Fernández-  
Franzón<sup>1</sup>, Maria-José Ruiz<sup>1</sup>, Maria Rosaria Esposito<sup>2,3</sup>, Elisa Cimetta<sup>2,3,4</sup>

<sup>1</sup>Laboratory of Food Chemistry and Toxicology, Faculty of Pharmacy, University of  
Valencia, Av. Vicent Andrés Estellés s/n, 46100, Valencia, Spain

<sup>2</sup>Department of Industrial Engineering (DII), University of Padua, Via Marzolo 9,  
35131, Padova, Italy

<sup>3</sup>Fondazione Istituto di Ricerca Pediatrica Città Della Speranza (IRP) – Lab  
NBTECH, Corso Stati Uniti 4, 35127, Padova, Italy

<sup>4</sup>Centro di Ricerca Interdipartimentale per le Biotecnologie Innovative (CRIBI) - Viale  
G. Colombo 3, 35131 Padova, Italy

\*Corresponding author. Laboratory of Toxicology, Faculty of Pharmacy,  
University of Valencia, Av. Vicent Andrés Estellés, s/n, 46100, Burjassot,  
Valencia, Spain. *E-mail address:* [vezin@uv.es](mailto:vezin@uv.es) (V. Zingales).

### **Abstract**

Given the increasing importance of establishing better risk assessments for mycotoxins, novel *in vitro* tools for the evaluation of their toxicity are mandatory. In this study, an *in vitro* 3D spheroid model from SH-SY5Y and SK-N-DZ cells, human neuroblastoma cell lines, was developed and optimized to test the cytotoxic effects caused by the mycotoxin sterigmatocystin (STE). The STE induced a concentration- and time-dependent cell viability decrease in spheroids, with higher susceptibility of SH-SY5Y than SK-N-DZ cells. Spheroids displayed cell disaggregation after STE exposure, increasing in a dose-dependent manner and over time; these effects were stronger for the SH-SY5Y cells. The STE induced apoptosis as confirmed by immunofluorescence staining and western blot. Following the decreased proliferation and increased apoptosis, STE cytostasis effects were observed by migration assays both in 2D and 3D cell culture. Increased ROS generation, as well as DNA damage were also observed. Taken together, these data highlight the cytotoxic properties of STE and suggest that cell culture models play a pivotal role in the toxicological risk assessment of mycotoxins. The evaluation of cytotoxicity in spheroids (3D) rather than monolayer cultures (2D) is expected to more accurately reflect *in vivo*-like cell behaviour.

**Keywords:** Sterigmatocystin, 3D spheroid, neuroblastoma, cytotoxicity, mechanisms of action.



## 1. Introduction

Sterigmatocystin (STE) is a mycotoxin, a low-molecular weight secondary metabolite produced by fungi mainly belonging to the genus *Aspergillus*. Fungi capable of producing STE are common food and feed contaminants. Nevertheless, only limited information is available on the occurrence of STE (EFSA, 2013) in the literature. On the other hand, there is a growing awareness of the importance of establishing a better risk assessment for this mycotoxin. In fact, *in vivo* studies demonstrated that STE may induce toxic effects in different species of animals, from acute symptoms to tumours, varying according to the species, route and frequency of administration (Fujii et al., 1976; Purchase and Van der Watt, 1973; Vesonder and Horn, 1985). Furthermore, epidemiological evidence has highlighted the existence of associations between exposure to STE and an increased risk of developing cancer (Cao et al., 2018; Hutanasu et al., 2011). In the last years, the role of STE as human health hazard as well as the potential mechanisms of action underlying its toxicity have been importantly investigated also by means of *in vitro* studies (Gao et al., 2015; Liu et al., 2014; Zouaoui et al., 2016). However, most current *in vitro* investigations on STE toxicity have been performed in two-dimensional (2D) cell cultures. If on the one hand this approach is well-accepted as well as convenient and essential for testing the effects of toxic substances, on the other, cytotoxic effects observed in conventional monolayer cultures often do not adequately resemble the complexity of the microenvironment *in vivo* (Kapalczynska et al., 2018; Langhans, 2018). To overcome this limitation and fill the gap between the oversimplified structure of monolayer cultures and the highly complex whole-animal systems, important efforts have been made in the development of a variety of three-dimensional (3D) models. According to Mikhail et al. (2013), 3D

cell cultures may serve as an intermediate step, offering a model closer to the *in vivo* architecture of natural tissues and organs, due to the enhanced cell-to-cell and cell-to-matrix interactions that contribute to the generation of a complex microenvironment. Moreover, 3D cultures can be grown undisturbed over a long period of time, making them an appropriate model for long-term exposure studies, a condition that appears frequently *in vivo* (Stampar et al., 2019).

Several 3D culture systems have been established, varying from the long-known spheroids (small 3D cellular aggregates with a spontaneous self-organization in a spherical-like shape) to the more sophisticated recent developments, such as organotypic cultures and organoids, organ-on-a-chip and 3D-printed tissues (Pati et al., 2016; Skardal et al., 2016; Stampar et al., 2019; Weiswald et al., 2015).

To date, the spheroid-based model is the best characterized and most widely used 3D system thanks to its easy standardization and sufficient recapitulation of key characteristics of natural tissues, such as the production of extracellular matrix and the formation of networks of cell-cell contacts (Hirschhaeuser et al., 2010; Nath and Devi, 2016). In addition, spheroids larger than 500  $\mu\text{m}$  in diameter lead to the generation of different proliferation areas (a necrotic core, quiescent intermediate and proliferating periphery regions), ultimately inducing corresponding cellular behaviours that cannot be replicated in 2D systems (Maltman and Przyborski, 2010).

To the best of our knowledge, no studies have yet been reported examining the putative effects of STE on a 3D cell culture system. Thus, the proposed use of spheroids as a model for screening of toxins and for detecting effects caused by long exposure is fairly novel. The aim of the present study was

to develop and optimize the culturing technique to obtain a viable 3D spheroid model of human neuroblastoma (NB) SH-SY5Y and SK-N-DZ cells useful to test STE toxic effects. Our results on the STE effects on 3D models have been compared with previous findings on SH-SY5Y monolayer cell cultures. The use of different NB cell lines also enabled assessing putative differences of the STE effects based on the differential amplification of the MYCN oncogene (v-myc myelocytomatosis viral-related oncogene, neuroblastoma-derived). Overall, our findings provided a more realistic portrait of STE cytotoxicity using a system resembling *in vivo*-like cell behaviour.

## 2. Material and methods

### 2.1. Reagents

The reagent grade chemicals and cell culture compounds used, namely culture medium DMEM high glucose with L-glutamine and fetal bovine serum (FBS) were from ATCC. Minimum essential medium non-essential amino acids (MEM NEAA) and trypsin/EDTA solutions were obtained from Gibco (USA). Penicillin, streptomycin, phosphate buffer saline (PBS), tetrazolium bromide (MTT), 2',7'-dichlorodihydrofluorescein diacetate (H<sub>2</sub>-DCFDA), bovine serum albumin (BSA), disodium ethylenediaminetetraacetate dihydrate (Na<sub>2</sub>-EDTA), sodium hydroxide (NaOH), sodium chloride (NaCl), trizma base (Tris), t-octylphenoxypolyethoxyethanol (Triton-X 100), crystal violet solution, methanol (MeOH), dimethyl sulfoxide (DMSO), 4',6-diamidine-2'-phenylindole dihydrochloride (DAPI), propidium iodide (PI) and paraformaldehyde were from Sigma Chemical Co (St. Louis, MO, USA). Agarose and low gelling temperature agarose (LMA) were from Invitrogen (Carlsbad, CA, USA).

Dimethyl sulfoxide (DMSO) was obtained from Fisher Scientific (Geel, Belgium). I-Block was purchased from Applied Biosystems (Foster City, CA, USA). Primary monoclonal antibodies for GAPDH, Ki-67 and MMP9 were purchased from GeneTex (Irvine, CA, USA). Primary antibodies for cleaved PARP (cPARP) and Casp-3 were purchased from Cell Signaling Technology (Beverly, MA, USA). Standard of the selected mycotoxin STE (MW: 324.28 g/mol) was purchased from Sigma-Aldrich (St. Louis, MO, USA). Stock solutions of the mycotoxin were prepared in methanol and maintained at -20°C.)

### 2.2. *Cell culture and spheroid formation*

Human neuroblastoma SH-SY5Y (ATCC-CRL-2266, MYCN not amplified) and SK-N-DZ (ATCC-CRL-2149, MYCN amplified) cells were cultured in monolayer in DMEM high glucose with L-glutamine medium supplemented with 10% FBS, 1% MEM NEAA (100X) and 1% penicillin-streptomycin. The incubation conditions were pH 7.4, 5% CO<sub>2</sub> at 37°C and 95% air atmosphere at constant humidity. The medium was changed every 2-3 days.

To obtain a single, centred and highly reproducible spheroid per well, ultra-low attachment (ULA) 96-well round bottom plates were used. In contrast to other approaches, they do not require coating to prevent cell adhesion and promote the self-aggregation of cells into spheroids (Vinci et al., 2012).

The 3D spheroid cultures were generated from single-cell suspensions obtained from trypsinized monolayers of both cell lines (SH-SY5Y and SK-N-DZ) and diluted to the optimum cell plating density of  $1 \times 10^4$  cells/ml. Then, 200  $\mu$ l of cell suspension ( $2 \times 10^3$  cells) were dispensed into each well of Corning® ULA 96-well round bottom plates. Plates were centrifuged at 1200

revolution per minute (RPM) for 5 minutes for SH-SY5Y cells and for 10 minutes for SK-N-DZ, to help the cells settle rapidly to the bottom of the wells. The initial optimal seeding densities were established such that each spheroid for both cell lines sized approximately 500  $\mu\text{m}$  in diameter. This size is considered appropriate for the spontaneous formation of gradients of oxygen and other nutrients, and of differential proliferation rates, all essential for bio-relevant 3D experimental studies (Vinci et al., 2012).

The SK-N-DZ and SH-SY5Y spheroids were cultured for 3 and 7 days, respectively, with a gentle 50% medium replenishment for SH-SY5Y spheroids on day 4.

Culture media and conditions used to grow the cells as 3D spheroids were the same as monolayer cell culture.

### 2.3. 3D cell viability assay

The effect of STE on 3D spheroids was determined after 1, 2, 3 and 4 days of exposure evaluating spheroid morphology by microscope observation and 3D cell viability by MTT and ATP assays. The MTT assay is a method based on the ability of viable cells to metabolize the yellow soluble tetrazolium salt to a blue insoluble formazan product by the mitochondrial succinic dehydrogenase. The ATP test, as an alternative, is based on the properties of a thermostable luciferase, which generates a luminescent signal proportional to the amount of ATP present.

SH-SY5Y and SK-N- DZ cultures were exposed to STE at day 7 and 3 after spheroids formation, respectively, by replacing 100  $\mu\text{l}$  of culture medium with medium containing STE to obtain final concentrations ranging from 2.5 to

20  $\mu$ M. Appropriate controls containing the same amount of solvent ( $\leq 1\%$  v/v) were included in each experiment. Intracellular ATP levels were measured using the CellTiter-Glo<sup>®</sup> Luminescent Cell Viability Assay (Promega, USA), according to manufacturer's instructions. Briefly, at the end of the exposure time (1, 2, 3 and 4 days), spheroids were transferred to an opaque white flat bottom 96-well plate with 50  $\mu$ l of supernatant. Afterwards, an equal volume of CellTiter-Glo reagent was added to each well and the plate was incubated at room temperature for 30 min protected from light. Luminescence was measured on a Wallace Victor2, model 1420 multilabel counter (PerkinElmer, Turku, Finland).

The MTT assay was performed as described by Salehi et al. (2017), with slight modifications. Briefly, at the end of each exposure time (2, 3 and 4 days), spheroids were individually transferred to a flat bottom 96-well plate with 100  $\mu$ l of supernatant and 50  $\mu$ l/well of MTT solution (5 mg/ml PBS). After 4 h of incubation at 37 °C protected from light, the resulting formazan crystals were solubilized in DMSO (50  $\mu$ l/well). The absorbance was measured at 560 nm using Wallace Victor2, model 1420 multilabel counter (PerkinElmer, Turku, Finland).

For both viability assays, cell viability was expressed as a percentage relative to the solvent control (1% MeOH). The mean 50% inhibitory concentration (IC<sub>50</sub>) values were calculated using SigmaPlot version 11 (Systat Software Inc., GmbH, Germany).

### 2.4. *Immunofluorescence staining*

To assess cellular viability rates (live/dead), apoptosis and proliferation were determined by immunofluorescence in SH-SY5Y spheroids after 2 and 3

days of STE exposure. At day 7, 3D spheroids were exposed to STE by replacing 100  $\mu$ l of culture medium with medium containing the mycotoxin to obtain final concentrations of 2.5 and 5  $\mu$ M. The two concentrations were selected according to the concentrations of STE found in food, as well as taking into account the previous cytotoxic assays carried out (all of these concentrations resulted to be below the IC<sub>50</sub> values obtained). At the end of each exposure time, spheroids from each well were transferred to a 48-well plate and the supernatant was removed. Spheroids were then fixed with 4% paraformaldehyde for 1 h at room temperature, washed with PBS and incubated in blocking solution (1% BSA and 0.5% Triton X-100 in PBS) for 1 h at room temperature. Subsequently, spheroids were incubated with the primary mouse monoclonal antibody anti-Ki-67 (1:100 dilution in PBS, 1% BSA and 0.1% Triton X-100) as marker of proliferation and with the primary rabbit monoclonal antibody anti-Casp3 (1:200 dilution in PBS, 1% BSA and 0.1% Triton X-100) as marker of apoptosis, both incubated at 4 °C overnight. Finally, spheroids were washed two times with PBS and incubated with Alexa Fluor® 488 affinity purified anti-mouse IgG secondary antibody (1:800 dilution in PBS, 1% BSA and 0.1% Triton X-100), Alexa Fluor® 594 affinity purified anti-rabbit IgG secondary antibody (1:800 dilution in PBS, 1% BSA and 0.1% Triton X-100) and DAPI for 2 h at room temperature. The stained spheroids were immediately imaged under a confocal fluorescence microscope (Zeiss LSM 800, Zeiss Microscopy, Germany).

### 2.5. *Western blotting*

The expression of the selected proteins in SH-SY5Y spheroids was determined by western blot, as described by Stampar et al. (2019), with some modification. The proteins were isolated from a pool of 60 spheroids for each

condition and quantified using the BCA™ Protein Assay Kit (Thermo Scientific, USA). Ten µg of total proteins were applied to SDS-PAGE electrophoresis with 4-12% polyacrylamide gel. After the electrophoresis, the gel with the resolved proteins was transferred to a nitrocellulose membrane. The membrane was incubated in blocking solution (0.2 g I-Block and 0.1% Tween in PBS), and then probed with the rabbit monoclonal primary antibody against cPARP (1:1000 dilution in blocking solution) and mouse monoclonal primary antibody against MMP9 (1:1000 dilution in blocking solution). The GAPDH mouse monoclonal primary antibody (1:5000 dilution in blocking solution) represented the control for equal loading. After washing for the removal of unconjugated antibodies, membranes were incubated with appropriated anti-rabbit (1:25000 dilution in blocking solution) and anti-mouse (1:20000 dilution in blocking solution) secondary antibodies. Chemiluminescence was developed by using Western Hypernova Chemiluminescence Reagent (Cyanagen, Bologna, Italy), according to the manufacturer's protocol and detected with the iBright™ CL1500 Imaging System (Invitrogen, USA). Band intensities were quantified using ImageJ software version 1.53e (Java 1.8.0\_172, USA) and normalized to the internal control.

### 2.6. *Reactive oxygen species (ROS) assay*

Intracellular ROS production was detected in SH-SY5Y spheroids by H<sub>2</sub>-DCFDA assay. The H<sub>2</sub>-DCFDA is taken up by cells and then deacetylated by intracellular esterases; the resulting non-fluorescent 2',7'-dichlorodihydrofluorescein (H<sub>2</sub>-DCF) is switched to highly fluorescent dichlorofluorescein (DCF) when oxidized by ROS. SH-SY5Y spheroids were exposed to STE at day 7 by replacing 100 µl of culture medium with medium



---

containing STE for the final concentrations of 2.5 and 5  $\mu\text{M}$ . The effect of STE on ROS generation was measured after 1, 2 and 3 days of exposure. At the end of each exposure time, supernatant was removed and 100  $\mu\text{l}$  of 50  $\mu\text{M}$   $\text{H}_2\text{-DCFDA}$  were added. The plate was incubated at 37  $^\circ\text{C}$  for 30 min protected from light. Increases in fluorescence were measured on a Spark<sup>®</sup> Multimode Microplate Reader by Tecan (Männedorf, Switzerland), at excitation/emission wavelengths of 485/535 nm. Results were expressed as increase in fluorescence with respect to solvent control.

### 2.7. Comet assay

The induction of DNA strand breaks in SH-SY5Y spheroids after 3 days of exposure to STE 2.5  $\mu\text{M}$  was evaluated by comet assay, according to Stampar et al. (2019), with some modifications. Briefly, 3D spheroids were exposed to STE at day 7 by replacing 100  $\mu\text{l}$  of culture medium with medium containing the mycotoxin for the final desired concentration. After the exposure time, single cell suspension was obtained by mechanical degradation and enzymatic digestion. Specifically, 24 spheroids per condition were left in trypsin–EDTA for 5 min and reduced to a single cell suspension. The viability of cells in the suspension was checked with Trypan Blue staining. Subsequently, 30  $\mu\text{l}$  of cell suspension were mixed with 140  $\mu\text{l}$  of pre-warmed LMA (1% in PBS) and 70  $\mu\text{l}$  of the suspension were rapidly transferred to agarose pre-coated slides (1% in  $\text{dH}_2\text{O}$ ) and covered with a coverslip (24  $\times$  24 cm). After gelling for 10 min at 4  $^\circ\text{C}$ , the coverslip was gently removed and the slides were immersed in lysis solution (2.5 M NaCl, 100 mM  $\text{Na}_2\text{-EDTA}$ , 10 mM Tris and 250 mM NaOH, 10% DMSO and 1% Triton X-100, freshly added; pH 10) for at least 1 h at 4  $^\circ\text{C}$  in the dark. After lysis, the slides were covered in electrophoresis buffer (300

mM NaOH, 1 mM Na<sub>2</sub>-EDTA; pH 13) for 40 min at room temperature to allow the DNA to unwind. Electrophoresis was run in the same solution for 30 min at 1 V/cm and 300 mA. When an electric field is applied, intact DNA strands remain in the head, while broken DNA pieces migrate toward the anode forming a typical comet tail. After electrophoresis, the slides were dried in 96% ethanol (-20 °C, 5 min) and the process completed at room temperature overnight. Cells were stained with 500 µl of Propidium Iodie (PI, 20 µg/ml) and analysed using a fluorescence microscope (Zeiss Axio Imager M1, Zeiss Microscopy, Germany) at 40× magnification. Two independent experiments were performed and a minimum of 50 randomly selected individual cells per slide were analysed by using Comet Assay Software Project Lab (CaspLab) 1.2.3b1 version. The results were expressed in terms of three comet assay parameters: the percentage of DNA in the tail (% tail DNA), tail length, and olive tail moment.

### 2.8. 2D cell migration assays

Culture inserts and transwell chambers were used to evaluate the ability of STE to stimulate cell migration in 2D SH-SY5Y cell cultures. For the assays, three concentrations (0.78, 1.56 and 3.12 µM) were selected, according to our previous cytotoxic assays carried out (Zingales et al., 2020a, b).

For the first approach,  $3.5 \times 10^4$  cells/well were seeded in a two well silicone Ibidi's Culture-Insert with a defined cell-free gap. Filling each compartment of the insert with the cell suspension allows cells to grow in each designated area until confluence. After 24 h, when cells reached 100% confluence, the culture insert was removed, engendering in two precisely defined cell patches separated by a zone with the width of the separation wall. Medium containing the three concentrations of STE tested was thus added, and cell

migration was monitored taking photos under the inverted light microscope Zeiss Primo Vert equipped with a Zeiss camera (Axiocam 208 color, Zeiss Microscopy, Germany) at 10× magnification with 24 h of intervals for 2 days. Three independent experiments were performed, and three different areas were captured for each sample. The area that remained clear of cells was quantified using ImageJ software version 1.53e (Java 1.8.0\_172, USA).

Additionally, the effect of STE on cell migration was evaluated by transwell migration assay, as described by Wang et al. (2019) with some modifications. Briefly,  $7 \times 10^5$  cells/well were seeded in six-well plates for 48 h. Then,  $2 \times 10^5$  cells suspended in a DMEM-only medium were loaded in triplicate upper chambers of the transwell chambers (Costar) with an 8- $\mu\text{m}$  pore size and 600- $\mu\text{L}$  DMEM medium with 10% FBS was added into the lower chamber. After incubating for 24 h in a 37 °C humidified incubator with 5% CO<sub>2</sub>, transwell chambers were washed twice with PBS. The cells on the inside of the transwell were gently removed using moistened cotton swabs, whereas the migrated cells on the lower surface were fixed with MeOH for 15 min, washed, and stained with crystal violet for 10 min. The transwell inserts were washed twice with PBS to remove the unbound crystal violet and then air-dried. The migrated cells were observed and imaged under an inverted light microscope Zeiss Primo Vert equipped with a Zeiss camera (Axiocam 208 color, Zeiss Microscopy, Germany) at 10× magnification. The number of cells that migrated through the transwell was calculated using the ImageJ software version 1.53e (Java 1.8.0\_172, USA).

### 2.9. 3D spheroid-based migration assay on matrix protein

The STE effects on cell migration in the 3D SH-SY5Y spheroids was evaluated according to Vinci et al. (2012), with some modifications. On day 7, 3D spheroids were exposed to STE (2.5  $\mu\text{M}$ ) by replacing 100  $\mu\text{l}$  of culture medium with medium containing the mycotoxin for the final desired concentration. Subsequently, 100  $\mu\text{l}$  of STE-contaminated medium including the spheroid were transferred (one single spheroid/well) into a gelatin-coated “migration” plate (U-bottom 96-well plate coated with 0.2% v/v gelatin in sterile water for 1 h at 37 °C). Spheroids were allowed to adhere, and images were captured at time 0, 1, 2 and 3 days, using the inverted light microscope Zeiss Primo Vert equipped with a Zeiss camera (Axiocam 208 color, Zeiss Microscopy, Germany) at 4 $\times$  and 10 $\times$  magnification. Image analysis was based on the sequential application of several image processing techniques (Fig. 1a). At first, RGB images containing spheroids were converted to grayscale. When dealing with low contrast images, we increased the contrast by performing a linear remapping of the original intensity values to the full display range. These (optionally) pre-processed images were then fed to our routine, which uses the Sobel method for edge detection (Kanopoulos et al., 1988). Edges are returned at those pixels where the gradient of the image is above a threshold, producing a binary image. To close the contours of the spheroids, a dilation followed by a flood-fill operation was applied. Since dilation leads to segmentations which are larger than the original spheroid, the image was eroded to refine the contour of the spheroid. As a result, the spheroid was segmented from the background. A representative image of the overlay of the generated spheroid mask over the original image is shown in Fig.1b. The inner region of the spheroid, characterized by a higher density and, thus, higher darkness due to cells overlap, was further

segmented from the entire spheroid using the active contours region growing technique (Chan and Vese, 2001). Our routine employs the border of the previously detected spheroid masks to initialize the solution and then evolves the curves towards the new boundaries that delimit the inner regions from the surrounding migrated cells. All routines were coded in the MATLAB R2020a environment (MathWorks®, Natick, MA) using built-in function available within the Computer Vision Toolbox.

### 2.10. *Statistical analysis*

Statistical analysis was carried out using GraphPad Prism version 7 (GraphPad Software, San Diego, California, USA), statistical software package. Data were expressed as mean  $\pm$  SEM of different independent experiments. The statistical analysis of the results was performed by Student's t-test for paired samples. Differences between groups were analysed statistically with one-way ANOVA followed by the Tukey HDS *post-hoc* test for multiple comparisons. We set a significance level of 0.05, such that  $p \leq 0.05$  was considered statistically significant.

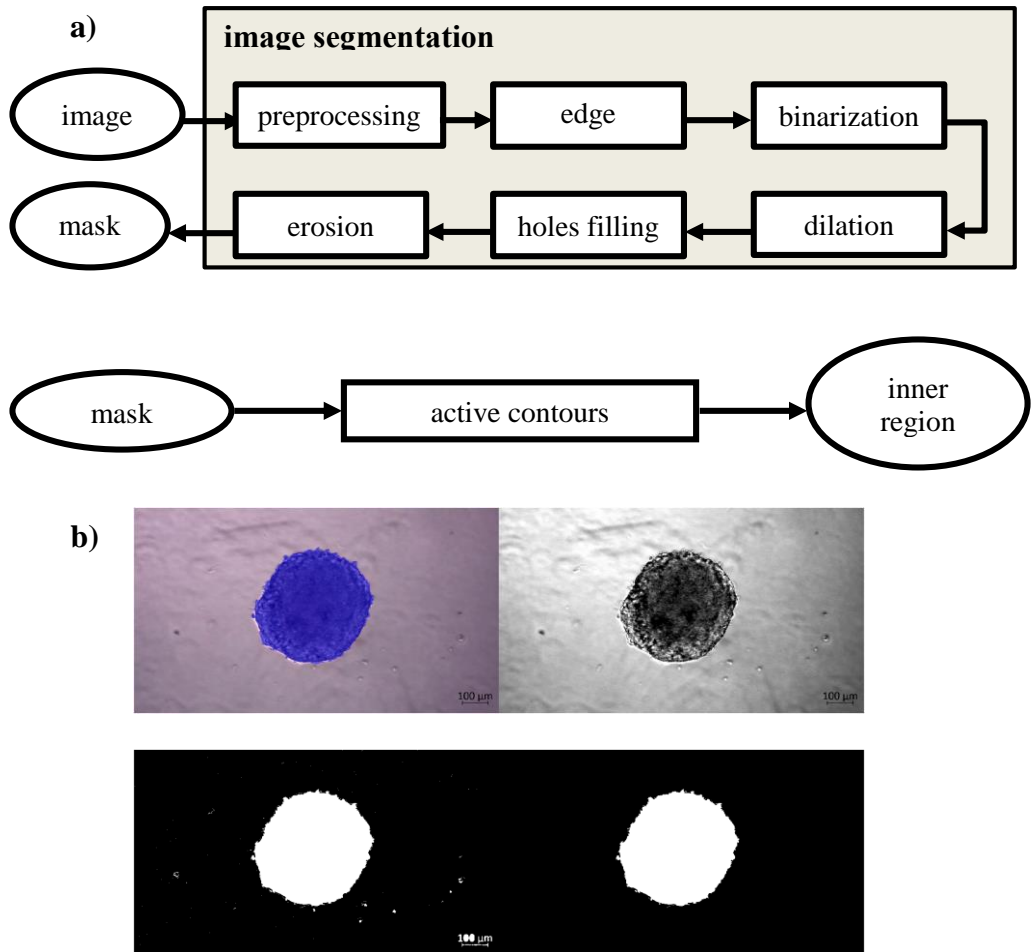


**Fig. 1.** Pipeline employed for spheroid segmentation. a) Routine used to segment spheroids from the background (top panel). Additional routine employed to segment regions of higher cell density within spheroids from migrated cells around (bottom panel). b) Representative image of the overlay of the generated spheroid mask over the original image.

### 3. Results

#### 3.1. *SH-SY5Y and SK-N-DZ cell spheroids cultures*

3D spheroids were derived from SH-SY5Y and SK-N-DZ neuroblastoma cell lines. Bright field microscope images of SH-SY5Y and SK-N-DZ spheroids are shown in Fig. 2. Both cell lines formed well-defined spheroids centrally positioned in each well of the ULA 96-well round bottom plates within 1 day. Overall, the sphericity index of SK-N-DZ 3D constructs was higher than that of SH-SY5Y cells, which typically assumed more elliptical or irregular shapes. However, the shape of both cell type spheroids was retained over time while the size increased, reaching the desired diameter of  $\sim 500 \mu\text{m}$  on day 3 for SK-N-DZ and day 7 for SH-SY5Y spheroids. The different growing rates are consistent with the faster doubling time of SK-N-DZ cells compared to SH-SY5Y, as measured in standard 2D monolayer cultures. Considering that  $500 \mu\text{m}$  have been suggested to be the best choice for initiating experimental studies (Vinci et al., 2012), the starting point ( $t_0$ ) for all cytotoxicity assays was set at day 3 for SK-N-DZ and day 7 for SH-SY5Y spheroids.

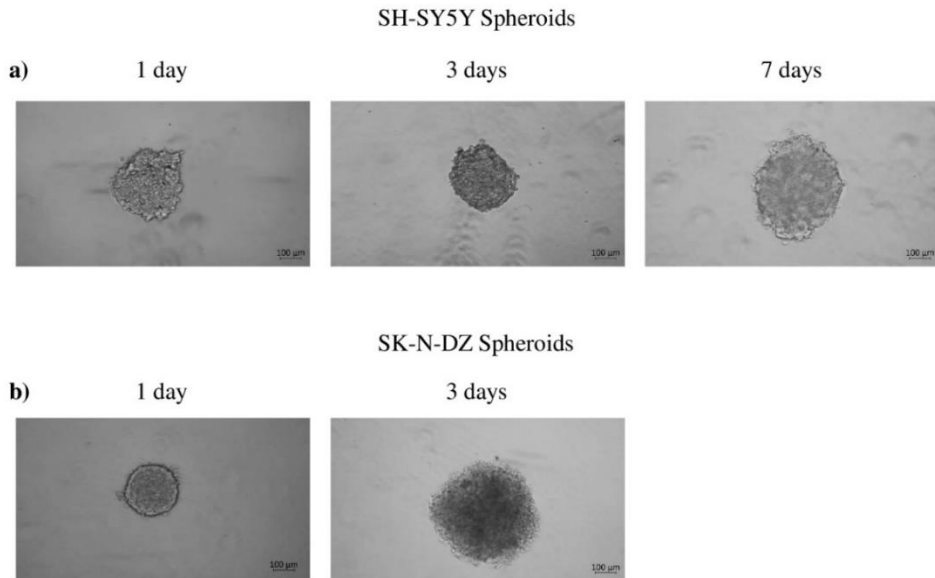


**Fig. 2.** Bright-field images of SH-SY5Y (a) and SK-N-DZ (b) spheroids grown at the indicated time points. Images were obtained using the Light Microscope Zeiss Axio Observer (Zeiss Microscopy, Germany). Scale bars: 100 µm.

### 3.2. *Effect of STE exposure on cell viability*

The cytotoxic effect of STE on SH-SY5Y and SK-N-DZ spheroids was evaluated by ATP assay after 1, 2, 3 and 4 days exposure to determine the molar concentration of mycotoxin able to reach the  $IC_{50}$ . For both cell lines, spheroids exposed to STE (2.5 - 20 µM) revealed a decrease in cell viability in a time- and concentration-dependent manner (data not shown). SH-SY5Y spheroids after 1 and 2 days of STE exposure did not show an  $IC_{50}$  value at the range of concentration tested, while after 3 and 4 days, STE showed  $IC_{50}$  values of 5.18



$\mu\text{M} \pm 3.14$  and  $1.78 \mu\text{M} \pm 1.05$ , respectively. Overall, after 1 day of exposure, STE concentrations ranging from 5 to 20  $\mu\text{M}$  were associated with a significant cell viability reduction ranging from 14% to 38% compared to the control. After 3 and 4 days of exposure, even the lowest STE concentration (2.5  $\mu\text{M}$ ) led to significant viability reductions (39% and 54%, respectively). At the same time points, the highest STE concentrations decreased viability rates to 6% - 11%, respectively. To provide further confirmation, the effect on cell viability induced by 2, 3 and 4 days of exposure to the lowest concentrations of STE (2.5 and 5  $\mu\text{M}$ ) was evaluated by the MTT assay. Based on the results, the  $\text{IC}_{50}$  value was reached only after 4 days of exposure ( $\text{IC}_{50} = 1.43 \mu\text{M} \pm 1.73$ ), while after 2 and 3 days a decrease of about 25% and 35%, respectively, was observed.

Morphological analysis showed that STE exposure resulted in a gradual disaggregation of the spheroids, with cell detachment from the structure at all concentrations and each time point considered (Fig. 3a). Quantitative analysis by assessment of the main body area of the spheroids for the lowest STE concentrations (2.5 and 5  $\mu\text{M}$ ) indicated a significant decrease in the area of the spheroids induced by STE exposure compared to the control (Fig. 3b). At the highest STE concentrations (10 and 20  $\mu\text{M}$ ), the extent of the disaggregation phenomena did not allow to perform a reliable quantitative analysis of the area.

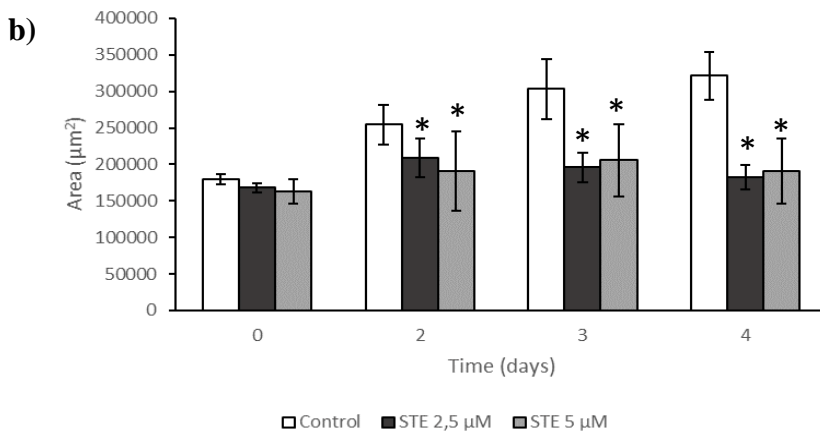
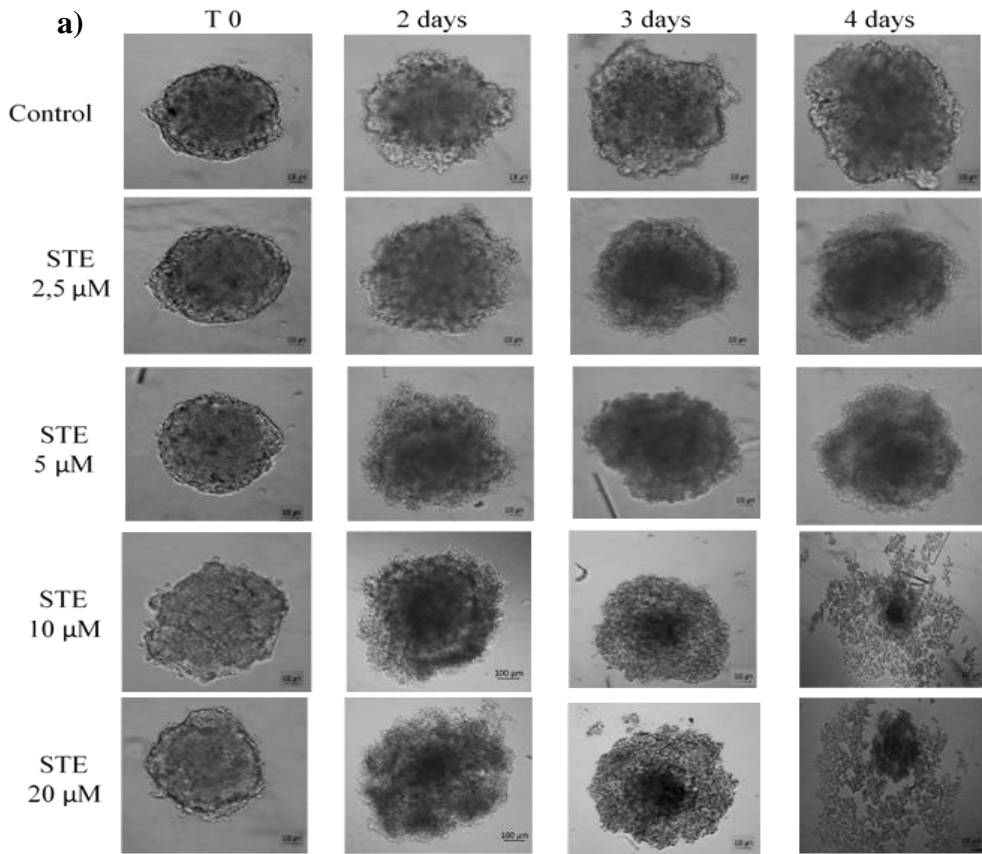
As regards SK-N-DZ spheroids, the ATP assay showed that after 1 and 3 days of exposure, only about 11% - 18% cell mortality was induced by the highest STE concentration (20  $\mu\text{M}$ ) and the  $\text{IC}_{50}$  was reached only after 4 days of exposure ( $\text{IC}_{50} = 9.62 \mu\text{M} \pm 10.38$ ), suggesting a lower susceptibility to STE compared to SH-SY5Y spheroids. Furthermore, the SK-N-DZ spheroids better

retained their shape after STE exposure (Fig. 3c), with a decrease of their area over time, but without measurable changes following treatment (Fig. 3d).

For all following assays, SH-SY5Y spheroids were chosen as 3D cell culture model for testing the mechanisms of action underlying STE-induced toxicity.

### *3.3. STE induces apoptosis in SH-SY5Y spheroids*

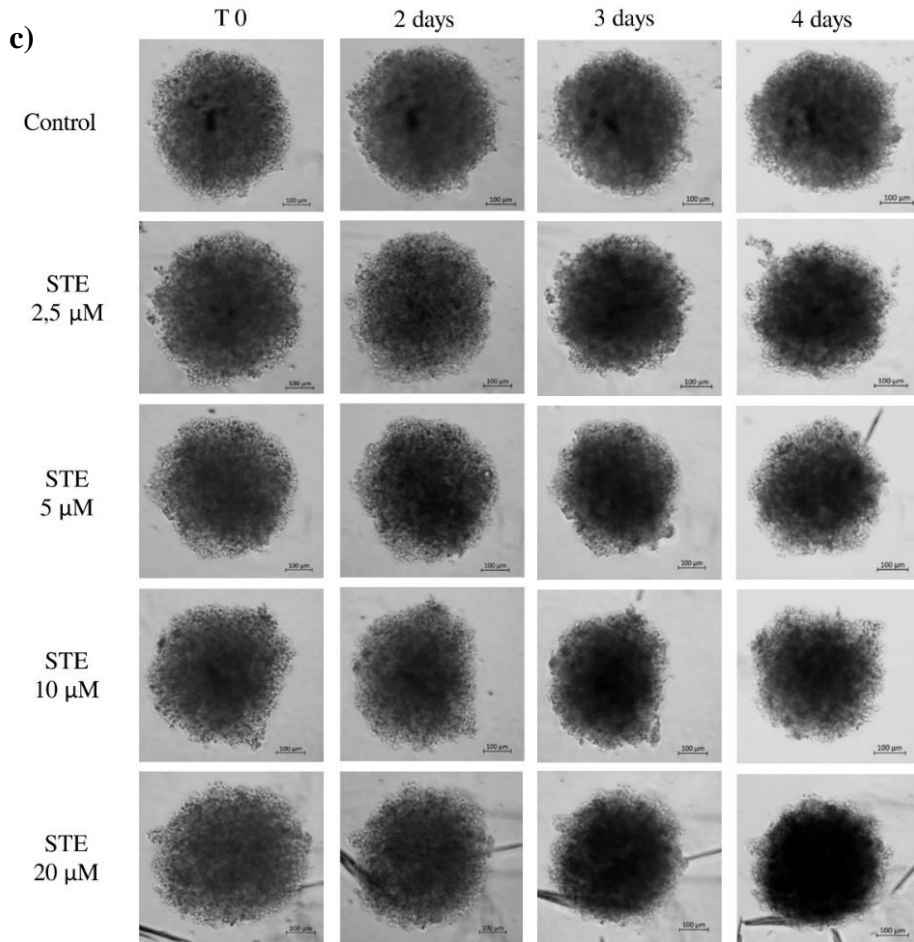
According to the viability assays, STE inhibited cell growth in SH-SY5Y spheroids causing morphological changes strongly suggesting the induction of the apoptosis process. To verify if STE triggered apoptosis, SH-SY5Y spheroids were stained with the apoptotic marker Casp-3 and the proliferation marker Ki-67. Exposure to STE (2.5 and 5  $\mu$ M) for 2 and 3 days showed a decrease in proliferation and an increase in apoptotic cells compared to the control, with a more marked effect after 3 days of exposure (Fig. 4). Representative images of the spheroids exposed to STE 5  $\mu$ M for 2 and 3 days are shown in Fig. 5. To confirm the effect of STE on apoptosis, western blot analysis of cPARP, a known marker of SH-SY5Y cells death, was performed in spheroids exposed to 2.5 and 5  $\mu$ M STE for 3 days (Fig. 6a). As expected, densitometric analysis of the blots indicated that cPARP expression increased in spheroids exposed to STE in a concentration-dependent manner (Fig. 6b).



(caption of the figures on page 353)

## Resultados

---



(caption of the figure on page 353)

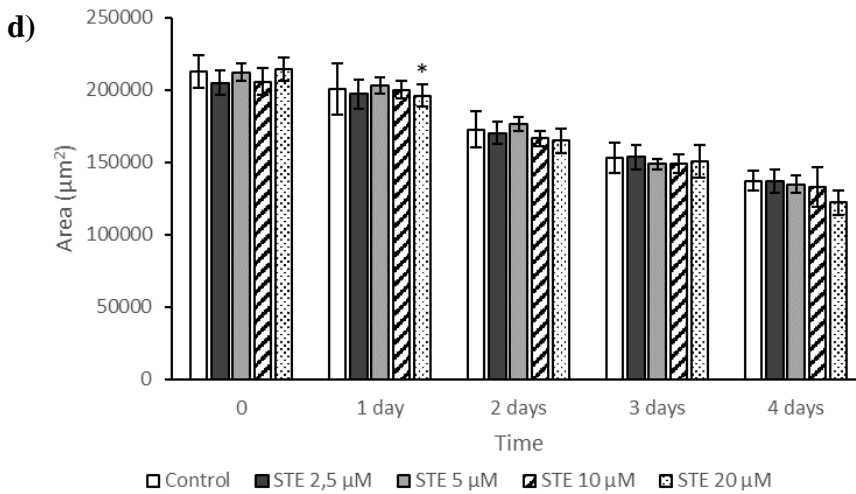


**Fig. 3.** Morphology and volume of human neuroblastoma spheroids after exposure to STE. a) Bright-field images of SH-SY5Y spheroids after 0, 1, 2, 3 and 4 days of exposure to increasing concentrations of STE (2.5 - 20 µM). Scale bar: 100 µM. Images were obtained using the Light Microscope Zeiss Axio Observer (Zeiss Microscopy, Germany). b) Bar chart showing the area growth of SH-SY5Y spheroids exposed to STE (2.5 and 5 µM) for 0, 2, 3 and 4 days. (\*)  $p \leq 0.05$  indicates a significant difference compared to the control. Quantitative analysis was performed using the software Zen Lite version 2.6 (Zeiss Microscopy, Germany). c) Bright-field images of SK-N-DZ spheroids after 0, 1, 2, 3 and 4 days of exposure to increasing concentrations of STE (2.5 - 20 µM). Scale bar: 100 µM. Images were obtained using the Light Microscope Zeiss Axio Observer (Zeiss Microscopy, Germany). d) Bar chart showing the area growth of SK-N-DZ spheroids exposed to STE (2.5 - 20 µM) for 0, 2, 3 and 4 days. Quantitative analysis was performed using the Zen Lite version 2.6 (Zeiss Microscopy, Germany). (\*)  $p \leq 0.05$  indicates a significant difference compared to the control.

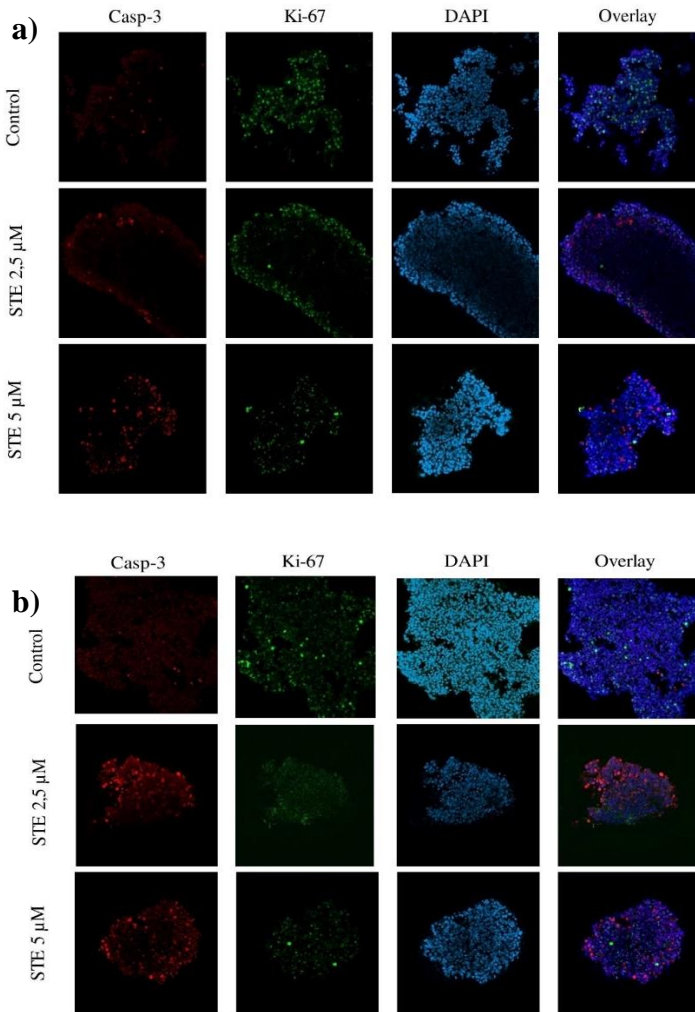


**Fig. 4.** Effect of STE exposure on Casp-3 and Ki-67 by immunofluorescence assay. The SH-SY5Y spheroids were exposed to STE (2.5, and 5  $\mu$ M) for (a) 2 and (b) 3 days, fixed and stained with DAPI to visualize nuclei (blue), anti-Casp-3 antibody as marker of apoptosis (red) and anti-Ki-67 antibody as marker of proliferation (green). Images were obtained by using the confocal fluorescence microscope Zeiss LSM 800 (Zeiss Microscopy, Germany; 25x magnification). The data shown are representative of two independent experiments.

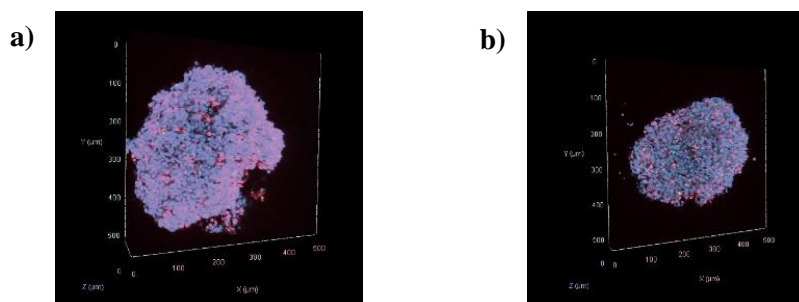


**Fig. 5.** 3D images are representative of SH-SY5Y spheroids exposed to STE 5  $\mu\text{M}$  for (a) 2 and (b) 3 days. Spheroids were exposed to STE and stained with DAPI (blue), the apoptotic marker Casp-3 (red) and the proliferation marker Ki-67 (green). Images were obtained using the software Zen Lite version 3.3 (Zeiss Microscopy, Germany).

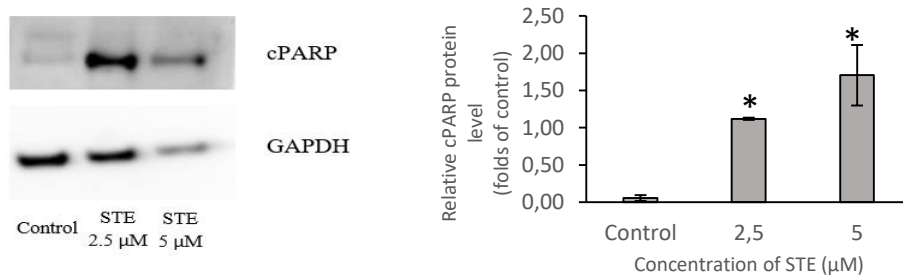


**Fig. 6.** Effect of STE on cPARP expression. SH-SY5Y spheroids were exposed to STE at 2.5 and 5  $\mu\text{M}$  for 3 days. The samples were then subjected to western blot analysis. a) Western blot showing cleaved PARP expression. b) Densitometric analysis of cleaved PARP western blots performed using ImageJ software version 1.53e (Java 1.8.0\_172, USA). The average of the target protein value was normalized to the corresponding GAPDH value and expressed as fold change compared with the solvent control. Data are expressed as mean  $\pm$  SEM of two independent experiments ( $n = 2$ ). (\*)  $p \leq 0.05$  indicates a significant difference compared to the control.

### 3.4. *STE increases intracellular ROS generation in SH-SY5Y spheroids*

There is growing evidence that oxidative stress is a common trigger for many of the effects associated with STE exposure. Therefore, ROS generation in SH-SY5Y spheroids exposed to STE for 1, 2 and 3 days was measured using the ROS-specific fluorescent dye H2-DCFDA. A significant increase in ROS levels was induced in SH-SY5Y spheroids exposed to STE 2.5 and 5  $\mu\text{M}$  for 2 and 3 days. In particular, the increase was found to be time- and concentration-dependent, starting at day 2 for the highest STE concentration tested and at day 3 for the lowest (Fig. 7a).

### 3.5. *STE leads to DNA damage in SH-SY5Y spheroids*

To investigate whether STE exposure caused DNA damage in SH-SY5Y spheroids, the comet assay was performed under alkaline condition. Spheroids exposed to STE 2.5  $\mu\text{M}$  for 3 days showed clearly visible comet tails, an evident indicator of DNA strand breakage (Fig. 8b). Conversely, in the solvent control group, almost all comet heads were concentrated with high-density DNA, accompanied by a smooth margin and intact nuclei (Fig. 8a). The analysis indicated that treatment with STE caused a significant increase in % tail DNA, tail length, and olive tail moment (Table 1). These results suggested that SH-SY5Y spheroids exposed to STE exhibited markedly higher DNA damage than controls.



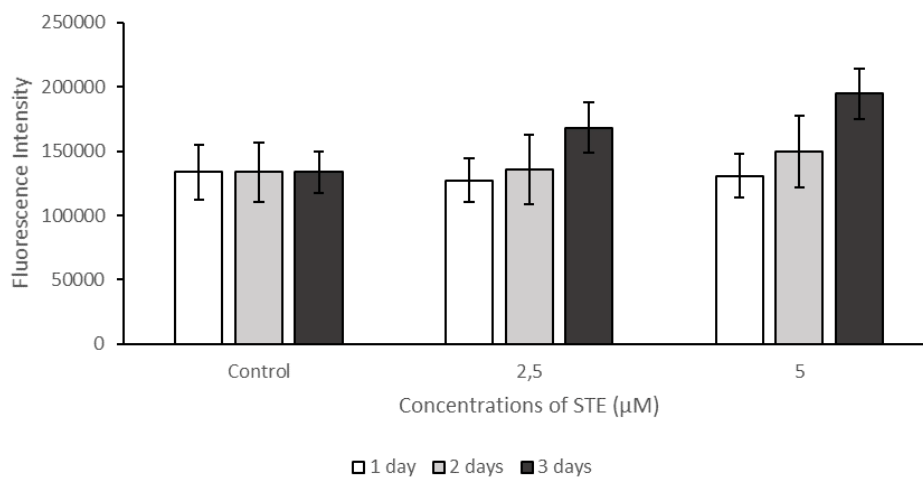


**Fig. 7.** Effect of STE exposure on ROS generation in SH-Y5Y spheroids. Spheroids were exposed to STE (2.5 and 5  $\mu\text{M}$ ) for 1, 2 and 3 days. The ROS generation was assessed by  $\text{H}_2\text{-DCFDA}$  probe. Data are expressed as mean  $\pm$  SEM of two independent experiments ( $n = 2$ ) with 24 replicates each. (\*)  $p \leq 0.05$  indicates a significant difference compared to the control.

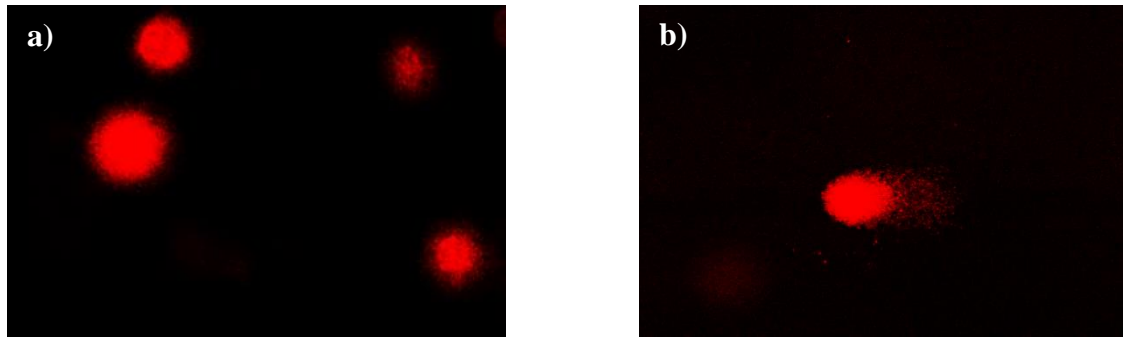


**Fig. 8.** The DNA strand breaks in SH-SY5Y spheroids measured by alkaline comet assay. The cells were treated with the vehicle (a) and 2.5  $\mu\text{M}$  (b) of STE for 3 days. The cells in the single cell suspension were obtained from spheroids by mechanical degradation and enzymatic digestion. Cells were observed under a fluorescent microscope and quantified (20x magnification).

**Table 1.** The tail DNA %, tail length and olive tail moment in SH-SY5Y cells obtained from spheroids exposed to 2.5  $\mu\text{M}$  STE for 3 days. Data represent the means  $\pm$  SEM. (\*)  $p \leq 0.05$  indicates a significant difference compared to the control.

Group	Tail DNA %	Tail length	Olive tail moment
Control	$1.43 \pm 2.17$	$5.55 \pm 1.77$	$0,33 \pm 1.3$
STE 2.5 $\mu\text{M}$	$10.42 \pm 3.27^*$	$62.85 \pm 27.61^*$	$7.33 \pm 3.34^*$

---

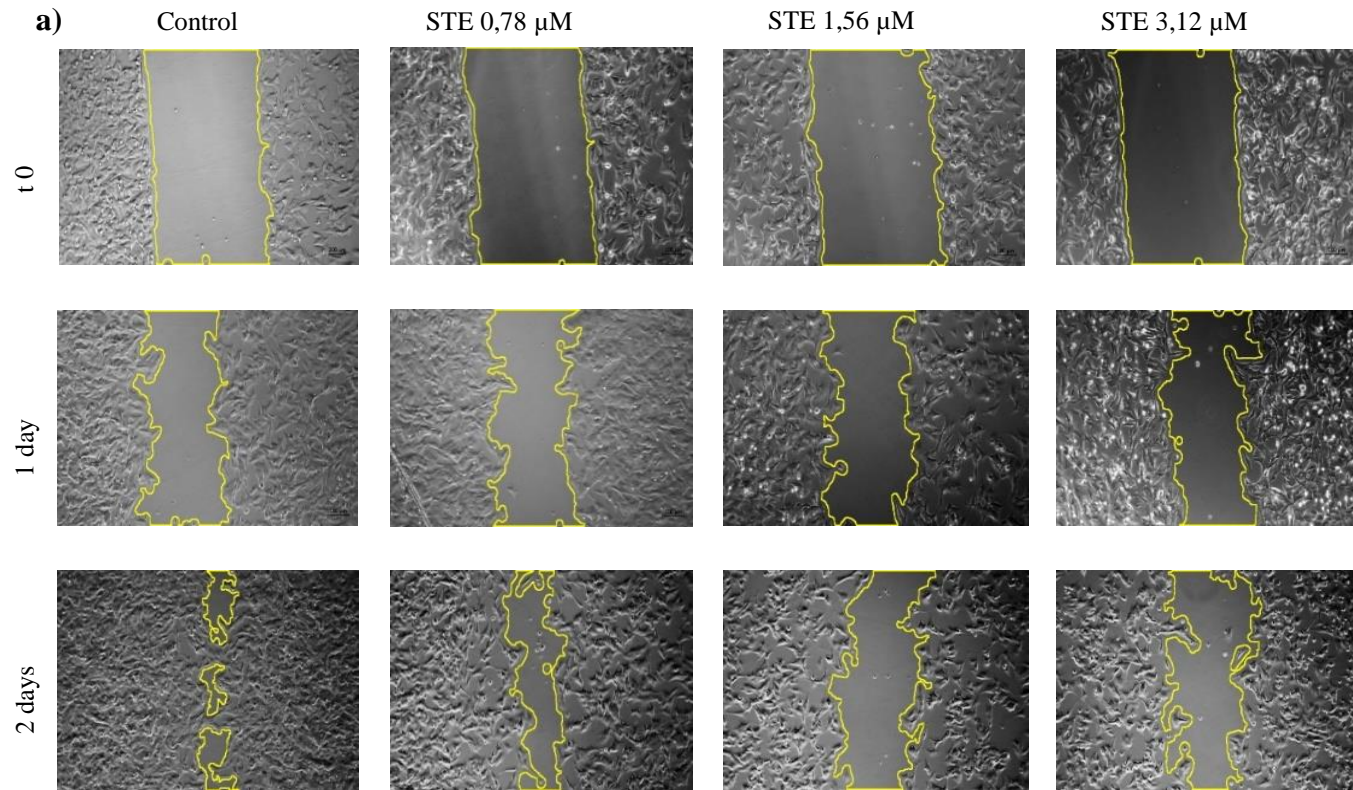
### 3.6. STE interferes with SH-SY5Y cell motility in 2D and 3D models

Finally, considering that the ability of cells to migrate is essential for many physiological processes, the effect of STE on SH-SY5Y cell migration in cell culture monolayers (2D) and spheroids (3D) was also evaluated. In SH-SY5Y cells monolayer, both wound healing assay and transwell assay demonstrated that cells exposed to STE (0.78, 1.56 and 3.12  $\mu\text{M}$ ) for 2 days had an equal or lower migration rate than control cells. In particular, based on the wound healing assay, the area uncovered by cells significantly decreased over the time in all sample groups. However, if on the one hand an almost total closure of the wound was reached in control cells, on the other a statistically significant increase in the area uncovered by cells was observed after exposure to STE at the highest concentrations (1.56 and 3.12  $\mu\text{M}$ ; Figs. 9a and b). Similarly, the transwell migration assay showed that STE exposure did not increase the number of migrated cells, but slightly lowered it, although with no statistical significance (Figs. 9c and d).

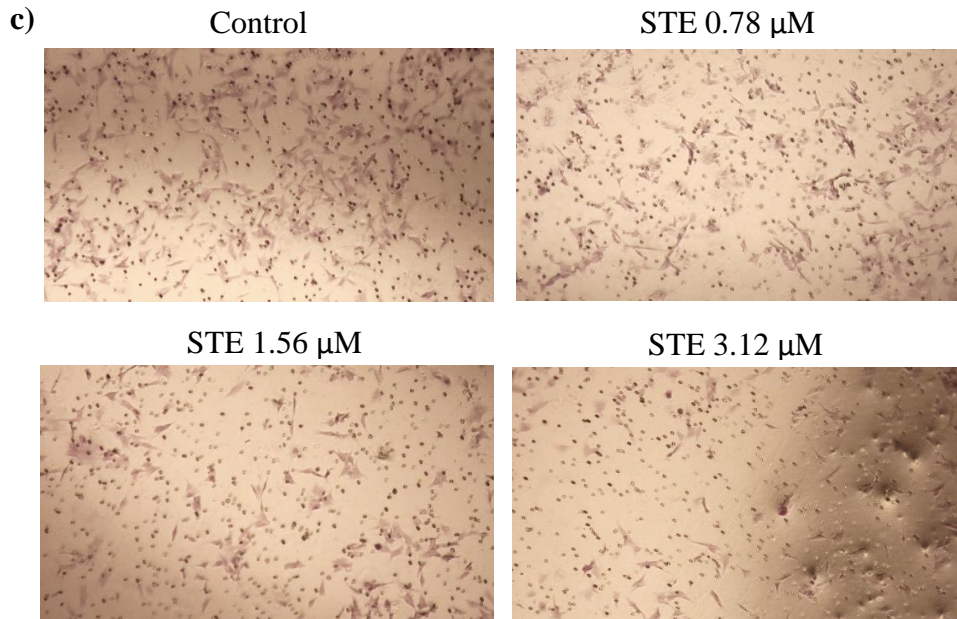
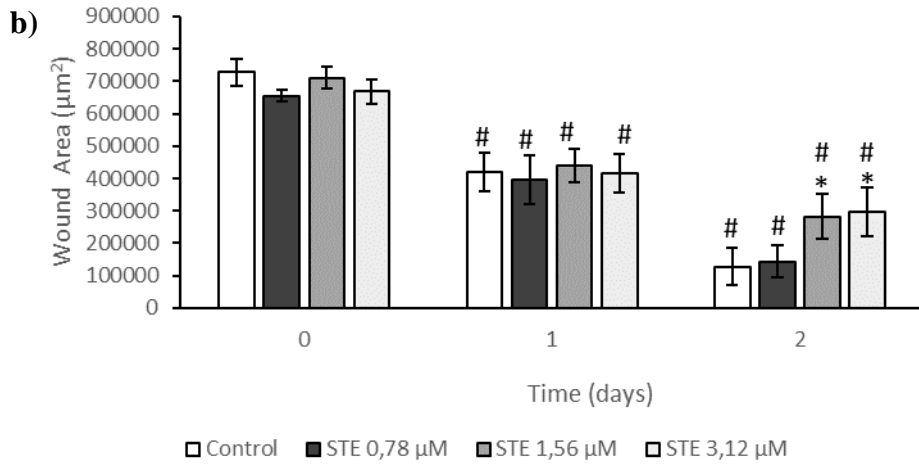
The 3D spheroid-based migration assay further confirmed our previous results in the 2D system. Spheroid migration was monitored for up to 3 days at 1-day intervals and although slightly less cell migration was evident in STE-exposed spheroids compared to controls, no statistically significant differences were found between the two groups (Figs. 10a-c). Western blot analysis of the matrix metalloproteinase 9 (MMP9), involved in the degradation of the extracellular matrix as a prerequisite for cellular migration, confirmed this observation and indicated that MMP9 protein expression level was decreased by STE exposure, although not in a statistically significant manner (Fig. 10d).

## Resultados

---



(caption of the figure on page 362)



(Caption of the figures on page 362)

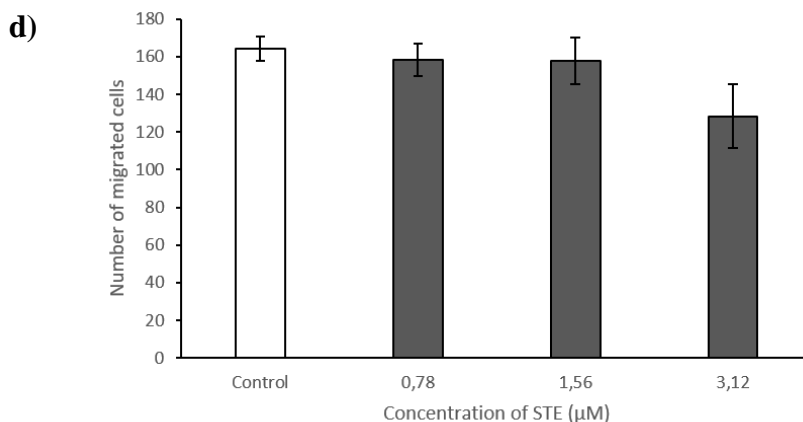
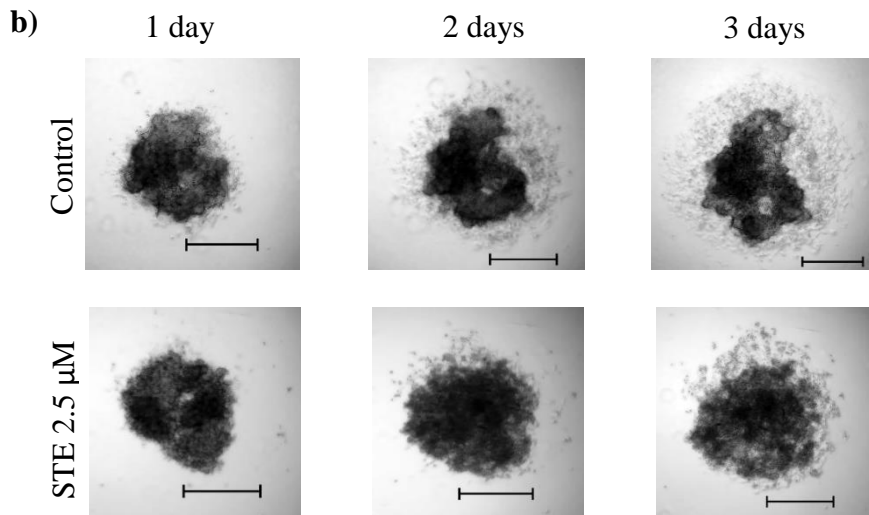
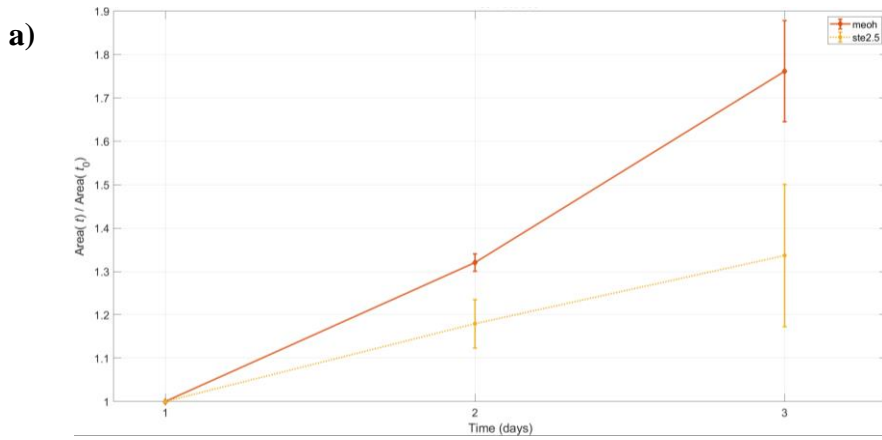


**Fig. 9.** Effect of STE (0.78, 1.56 and 3.12 µM) on cell migration in SH-SY5Y cells monolayer (2D). a) Representative microscopic images showing the effect of STE on cell migration in the wound healing migration assay (10x magnification). Cells were seeded in each compartment of the silicone culture insert and, after its removal, cells were photographed for evidence of cell migration 0, 1 and 2 days after the addition of the mycotoxin. b) Bar chart showing the wound closure expressed as the remaining area uncovered by the cells over the time. The area that remained clear of cells was quantified using ImageJ software version 1.53e (Java 1.8.0\_172, USA). Data are expressed as mean  $\pm$  SEM of three independent experiments ( $n = 3$ ). Three visual fields were analysed per sample in each independent experiment. (\*)  $p \leq 0,05$  indicates a significant difference with respect to the corresponding solvent control; (#)  $p \leq 0,05$  indicates a significant difference respect to the corresponding concentration at time 0 h. c) Representative microscopic images of cells that migrated through the pores of the transwell in the transwell migration assay (10x magnification). Cells exposed to STE for 2 days were seeded upper transwell chambers, incubated for 1 day, fixed and stained with crystal violet. d) Bar chart showing the number of cells that migrated through the transwell in the transwell migration assay. The number of cells that migrated through the transwell was calculated using the ImageJ software 1.53e (Java 1.8.0\_172, USA). Data are expressed as mean  $\pm$  SEM of two independent experiments ( $n = 2$ ) with 2 replicates each. Four-five visual fields were analysed per replicate in each independent experiment. No significant differences were observed between cells exposed to STE and control.



(Caption of the figures on the next page)

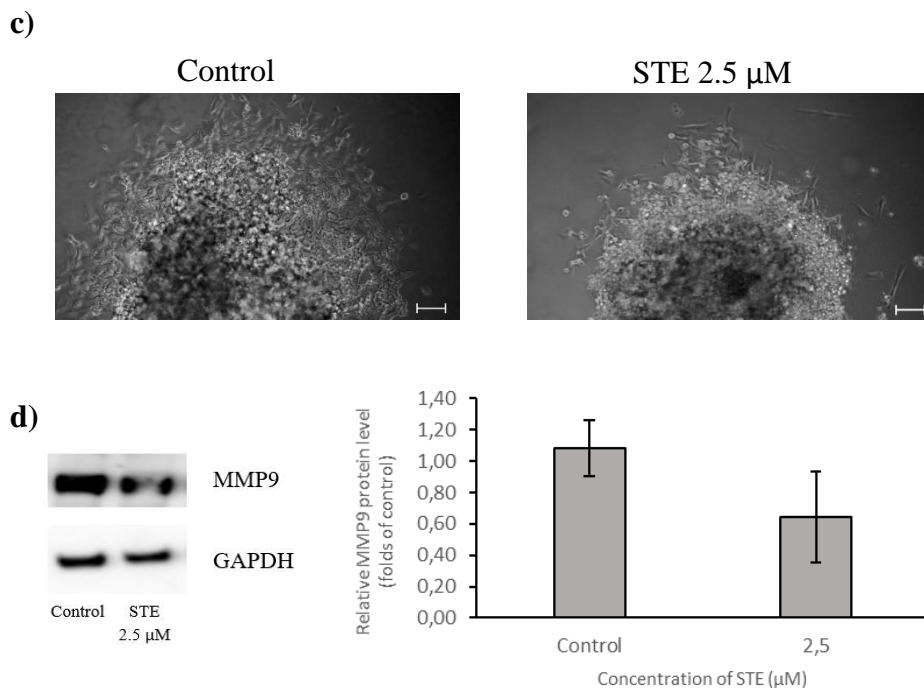


**Fig.10.** Effect of STE 2.5  $\mu$ M on cell migration in SH-SY5Y spheroids (3D). a-b) Spheroids were placed on gelatin-coated plates and exposed to 2.5  $\mu$ M STE. Control was treated with the vehicle. Images were captured for 3 days at intervals of 1 day using the inverted light microscope Zeiss Primo Vert equipped with a Zeiss camera (Axiocam 208 color, Zeiss Microscopy, Germany) at 4 $\times$  magnification and analysed with the software MATLAB R2020a (MathWorks®, Natick, MA). Scale bar: 500  $\mu$ m. c) Details of cell migration in spheroids after 3 days of exposure obtained using the inverted light microscope Zeiss Primo Vert equipped with a Zeiss camera (Axiocam 208 color, Zeiss Microscopy, Germany) at 10 $\times$  magnification. Scale bar: 100  $\mu$ m. d) Western blot showing MMP9 expression and its densitometric analysis performed using Image J software version 1.53e (Java 1.8.0\_172, USA). The average of the target protein value was normalized to the corresponding GAPDH value and expressed as fold change compared with the solvent control. Data are expressed as mean  $\pm$  SEM of two independent experiments ( $n = 2$ ). No significant differences were observed between spheroids exposed to STE and control.



#### 4. Discussion

In recent years, great strides have been made in the risk assessment of several mycotoxins. However, studies aimed at evaluating mycotoxins' cytotoxicity mainly relies on *in vitro* 2D cell models, affected by several limitations and poor predictability of *in vivo* conditions. On the contrary, 3D spheroids represent a more physiologically relevant and innovative *in vitro* tool for obtaining more realistic and trustworthy results (Mazzoleni et al., 2009).

In this study, we developed for the first time a viable and repeatable 3D culture model for the assessment of the cytotoxic effect of the mycotoxin STE. In pilot studies, we compared different techniques for generating spheroids (data not shown). The ULA 96-well round bottom plate was found to be the ideal method, least time consuming and generating the most compact, uniform and reproducible single spheroid/well. Spheroids were generated using SH-SY5Y and SK-N-DZ human neuroblastoma cells and suitable conditions were established to grow cell spheroids of approximately 500  $\mu\text{m}$  in diameter.

Spheroids were exposed to increasing concentrations of STE and morphological changes, as well as cell viability, were recorded and measured. Results showed that STE induced a more pronounced mortality in SH-SY5Y compared to SK-N-DZ spheroids, revealing significant differences in sensitivity towards STE between cell lines. Based on our results, despite their preliminary character, it may be implied that the lack of MYCN amplification in SH-SY5Y cell line makes it more sensitive to STE. This agrees with the ability of MYCN to confer cellular resistance to apoptosis (Goldsmith and Hogarty, 2005). Similarly, Cuperus et al. (2008) showed a different sensitivity to fenretinide, a

vitamin A analogue, between MYCN-amplified and MYCN single copy cell lines, further suggesting the role of MYCN in cell susceptibility.

In addition, and as assessed by morphological analysis, SH-SY5Y spheroids failed to maintain their canonical shape and started to display cell disaggregation, a phenomena that became more evident at the higher concentrations. We speculate that extracellular matrix (ECM) could be digested upon STE treatment. Conversely, SK-N-DZ spheroids retained their shape, supporting that ECM was still intact.

The SH-SY5Y cells grown in spheroid cultures demonstrated considerably greater resistance to the toxic effect of STE exposure compared to 2D cell cultures. Based on our previous results, viability was lower in SH-SY5Y cells grown in monolayer cultures ( $IC_{50} = 0.52 \mu\text{M} \pm 0.05$ ) compared to spheroids ( $IC_{50} = 5.18 \mu\text{M} \pm 3.14$ ) after exposure up to 3 days (Zingales et al., 2020a). Our findings agree with literature evidence reporting that the same degree of sensitivity of the 2D system did not translate into 3D culture systems, resulting in higher  $IC_{50}$  values in the latter (Baek et al., 2016; De Simone et al., 2018; Mikhail et al., 2013; Mueller et al., 2014; Salehi et al., 2017). This discrepancy can be attributed to the presence in 3D spheroids of pronounced intracellular junctions, mimicking physiological barriers, as well as a dense ECM with small pores, which influence xenobiotic transport by decreasing its penetration (Goodman et al., 2008; Lee et al., 2009). Contrarily, the absence of a 3D organization in 2D systems can lead to an overestimation of cellular toxicity.

One of our main goals was to compare the results obtained in the present study with our previous findings on SH-SY5Y monolayer cell cultures, thus addressing potential differences between 2D and 3D SH-SY5Y cultures in

detecting STE toxicity. For these assays, two concentrations of STE were tested (2.5 and 5  $\mu\text{M}$ ) based on their cytotoxic effects on SH-SY5Y spheroids, while being lower than the  $\text{IC}_{50}$  values at the times of exposure selected for the assays (2 and 3 days). Moreover, 2.5 and 5  $\mu\text{M}$  are within or close to the range of the estimated STE total intake through cereal consumption (from 0.77 nM to 4.78  $\mu\text{M}/\text{day}$ ; Zingales et al., 2020b). Our previous findings reported that the loss of cell viability resulting from the exposure of SH-SY5Y cells to STE was due to the induction of an apoptotic process (Zingales et al., 2020a). SH-SY5Y spheroids exposed to STE exhibited cell apoptotic increase. In detail, spheroids exposed to STE and stained with the apoptotic marker Casp-3 and the proliferation marker Ki-67 showed an increase in apoptosis as well as a decrease in proliferation. As further proof, elevated protein expression levels of cPARP were observed after STE exposure. Cleavage of PARP, generated by the caspases 3 activated during apoptosis, has become a useful hallmark of this type of cell death (Qvarnstrom et al., 2009).

Migration assays along with proliferation and apoptosis assays allowed a better understanding of the cytotoxic mechanisms of STE. As a result of decreased proliferation and increased apoptosis, mainly cytostasis was observed, both in the 2D system and in the 3D spheroids. Although STE did not induce a statistically significant inhibition of migration, a trend towards a decrease in migration was confirmed by the wound healing assay, transwell migration, 3D migration and western blot, further proving the cytotoxic nature of STE.

In the apoptotic process a crucial role is played by ROS. Elevated cellular ROS levels leads to the loss of mitochondrial membrane potential, which causes the release of pro-apoptotic factors and thus DNA breakage, nuclear chromatin

condensation, and apoptosis (Brodska and Holoubek, 2011; Takahashi et al., 2004). Exposure of SH-SY5Y spheroids to STE resulted in increased ROS levels, confirming our previous results on the 2D system (Zingales et al., 2020b). However, while in SH-SY5Y monolayer cells ROS were induced starting from the lowest STE concentration tested (0.78  $\mu\text{M}$ ) after 1 day of exposure, in 3D spheroids the ROS levels augmentation was time- and concentration-dependent, with a significant increase after 2 days of exposure for the highest STE concentration (5  $\mu\text{M}$ ) and after 3 days for the lowest (2.5  $\mu\text{M}$ ), while no changes were observed after 1 day (Zingales et al., 2020b). Similarly, with respect to DNA damage, lower concentrations and exposure times were sufficient to cause DNA double strand breaks in the 2D system compared to the 3D system (Zingales et al., 2021).

To the best of our knowledge, this is the first study reporting the toxic effect of STE in a 3D model. Overall, our findings indicate that STE causes cytotoxic effects by inducing apoptosis, increasing intracellular ROS levels and triggering DNA damage on SH-SY5Y cells in both 2D and 3D cell cultures. The comparison of results obtained in monolayer and spheroid cultures demonstrated the important influence of the microenvironment and of the 3D tissue structure in toxicology investigation. In particular, the assessment of cytotoxicity in spheroids rather than monolayer cultures is expected to more accurately reflect *in vivo*-like cell behaviour. In spite of the obvious advantages of 3D models over 2D models, there have so far been only a few attempts to use 3D cellular systems for cytotoxicity testing and even fewer for mycotoxins studies. With improved *in vitro* experimental models and enhanced availability of spheroid-specific consumables and high-content imaging platforms that make

spheroid analysis easier, less *in vivo* follow-up will be needed, in accordance with the 3R strategy (replace, reduce, refine).

### **Acknowledgments**

This research has been supported by the Generalitat Valenciana pre-doctoral grant "Santiago Grisolia (GRISOLIAP/2018/092) CPI-18-117" and by the Spanish Ministry of Science and Innovation project (PID2020-115871RB-I00-ALI). The work was also supported by ERC Starting grant (ERC-StG) MICRONEX project (UERI17, PI E Cimetta).

### **Conflict of interest statement**

The authors declare that there are no conflicts of interest.

### **References**

Baek, N., Seo, O.W., Kim, M., Hulme, J., An, S.S., 2016. Monitoring the effects of doxorubicin on 3D-spheroid tumor cells in real-time. *Onco Targets Ther* 9, 7207-7218. doi: 10.2147/OTT.S112566

Brodzka, B., Holoubek, A., 2011. Generation of reactive oxygen species during apoptosis induced by DNA-damaging agents and/or histone deacetylase inhibitors. *Oxid Med Cell Longev* 2011, 253529. doi: 10.1155/2011/253529

Cao, X., Li, X., Li, J., Niu, Y., Shi, L., Fang, Z., et al., 2018. Quantitative determination of carcinogenic mycotoxins in human and animal biological matrices and animal-derived foods using multi-mycotoxin and analyte-specific high performance liquid chromatography-tandem mass spectrometric methods. *J Chromatogr B* 1073, 191-200. doi: 10.1016/j.jchromb.2017.10.006

Chan, T. F., Vese, L. A., 2001. Active contours without edges. *IEEE Trans Image Process* 10, 266-277.

Cuperus, R., Tytgat, G.A., Leen, R., Brites, P., Bras, J., Caron, H.N., et al., 2008. Pleiotropic effects of fenretinide in neuroblastoma cell lines and multicellular tumor spheroids. *Int J Oncol* 32, 1011-1019.

De Simone, U., Roccio, M., Gribaldo, L., Spinillo, A., Caloni, F., Coccini, T., 2018. Human 3D Cultures as Models for Evaluating Magnetic Nanoparticle CNS Cytotoxicity after Short- and Repeated Long-Term Exposure. *Int J Mol Sci* 19. doi: 10.3390/ijms19071993

EFSA, 2013. European food safety authority (efsa) panel on contaminants in food chain (CONTAM), scientific opinion on the risk for public and animal health related to the presence of sterigmatocystin in food and feed. *EFSA J* 11 (6), 3254.

Fujii, K., Kurata, H., Odashima, S., Hatsuda, Y., 1976. Tumor induction by a single subcutaneous injection of sterigmatocystin in newborn mice. *Cancer Res* 36, 1615-1618.

Gao, W., Jiang, L., Ge, L., Chen, M., Geng, C., Yang, G., et al., 2015. Sterigmatocystin-induced oxidative DNA damage in human liver-derived cell line through lysosomal damage. *Toxicol In Vitro* 29, 1-7. doi: 10.1016/j.tiv.2014.08.007

- Goldsmith, K.C., Hogarty, M.D., 2005. Targeting programmed cell death pathways with experimental therapeutics: opportunities in high-risk neuroblastoma. *Cancer Lett* 228, 133-141. doi: 10.1016/j.canlet.2005.01.048
- Goodman, T.T., Ng, C.P., Pun, S.H., 2008. 3-D tissue culture systems for the evaluation and optimization of nanoparticle-based drug carriers. *Bioconj Chem* 19, 1951-1959. doi: 10.1021/bc800233a
- Hirschhaeuser, F., Menne, H., Dittfeld, C., West, J., Mueller-Klieser, W., Kunz-Schughart, L.A., 2010. Multicellular tumor spheroids: an underestimated tool is catching up again. *J Biotechnol* 148, 3-15. doi: 10.1016/j.jbiotec.2010.01.012
- Hutanasu, C., Sfarti, C., Trifan, A., Cojocariu, C., Singeap, A.M., Spac, A., et al., 2011. High levels of sterigmatocystin in patients with chronic liver diseases. *Rev Med Chir Soc Med Nat Iasi* 115, 33-37.
- Kanopoulos, N., Vasanthavada, N., Baker, R.L., 1988. Design of an image edge detection filter using the Sobel operator. *IEEE J of Solid-State Circuits* 23, 358–367.
- Kapalczynska, M., Kolenda, T., Przybyla, W., Zajackowska, M., Teresiak, A., Filas, V., et al., 2018. 2D and 3D cell cultures - a comparison of different types of cancer cell cultures. *Arch Med Sci* 14, 910-919. doi: 10.5114/aoms.2016.63743
- Langhans, S.A., 2018. Three-Dimensional in Vitro Cell Culture Models in Drug Discovery and Drug Repositioning. *Front Pharmacol* 9, 6. doi: 10.3389/fphar.2018.00006
- Lee, J., Lilly, G.D., Doty, R.C., Podsiadlo, P., Kotov, N.A., 2009. In vitro toxicity testing of nanoparticles in 3D cell culture. *Small* 5, 1213-1221. doi: 10.1002/smll.200801788

Liu, Y., Du, M., Zhang, G., 2014. Proapoptotic activity of aflatoxin B1 and sterigmatocystin in HepG2 cells. *Toxicol Rep* 1, 1076-1086. doi: 10.1016/j.toxrep.2014.10.016

Maltman, D.J., Przyborski, S.A., 2010. Developments in three-dimensional cell culture technology aimed at improving the accuracy of in vitro analyses. *Biochem Soc Trans* 38, 1072-1075. doi: 10.1042/BST0381072

Mazzoleni, G., Di Lorenzo, D., Steimberg, N., 2009. Modelling tissues in 3D: the next future of pharmaco-toxicology and food research? *Genes Nutr* 4, 13-22. doi: 10.1007/s12263-008-0107-0

Mikhail, A.S., Etezadi, S., Allen, C., 2013. Multicellular tumor spheroids for evaluation of cytotoxicity and tumor growth inhibitory effects of nanomedicines in vitro: a comparison of docetaxel-loaded block copolymer micelles and Taxotere(R). *PLoS One* 8, e62630. doi: 10.1371/journal.pone.0062630

Mueller, D., Kramer, L., Hoffmann, E., Klein, S., Noor, F., 2014. 3D organotypic HepaRG cultures as in vitro model for acute and repeated dose toxicity studies. *Toxicol In Vitro* 28, 104-112. doi: 10.1016/j.tiv.2013.06.024

Nath, S., Devi, G.R., 2016. Three-dimensional culture systems in cancer research: Focus on tumor spheroid model. *Pharmacol Ther* 163, 94-108. doi: 10.1016/j.pharmthera.2016.03.013

Pati, F., Gantelius, J., Svahn, H.A., 2016. 3D Bioprinting of Tissue/Organ Models. *Angew Chem Int Ed Engl* 55, 4650-4665. doi: 10.1002/anie.201505062

Purchase, I.F., Van der Watt, J.J., 1973. Carcinogenicity of sterigmatocystin to rat skin. *Toxicol Appl Pharmacol* 26, 274-281. doi: 10.1016/0041-008x(73)90262-7



---

Qvarnstrom, O.F., Simonsson, M., Eriksson, V., Turesson, I., Carlsson, J., 2009. gammaH2AX and cleaved PARP-1 as apoptotic markers in irradiated breast cancer BT474 cellular spheroids. *Int J Oncol* 35, 41-47. doi:

10.3892/ijo\_00000311

Salehi, F., Behboudi, H., Kavooosi, G., Ardestani, S.K., 2017.

Monitoring ZEO apoptotic potential in 2D and 3D cell cultures and associated spectroscopic evidence on mode of interaction with DNA. *Sci Rep* 7, 2553.

doi: 10.1038/s41598-017-02633-z

Schwab, M., 2004. MYCN in neuronal tumours. *Cancer Lett* 204, 179-187. doi: 10.1016/S0304-3835(03)00454-3

Skardal, A., Shupe, T., Atala, A., 2016. Organoid-on-a-chip and body-on-a-chip systems for drug screening and disease modeling. *Drug Discov Today* 21, 1399-1411. doi: 10.1016/j.drudis.2016.07.003

Stampar, M., Tomc, J., Filipic, M., Zegura, B., 2019. Development of in vitro 3D cell model from hepatocellular carcinoma (HepG2) cell line and its application for genotoxicity testing. *Arch Toxicol* 93, 3321-3333. doi:

10.1007/s00204-019-02576-6

Takahashi, A., Masuda, A., Sun, M., Centonze, V.E., Herman, B., 2004. Oxidative stress-induced apoptosis is associated with alterations in mitochondrial caspase activity and Bcl-2-dependent alterations in mitochondrial pH (pH<sub>m</sub>). *Brain Res Bull* 62, 497-504. doi:

10.1016/j.brainresbull.2003.07.009

Vesonder, R.F., Horn, B.W., 1985. Sterigmatocystin in dairy cattle feed contaminated with *Aspergillus versicolor*. *Appl Environ Microbiol* 49, 234-235.

Vinci, M., Gowan, S., Boxall, F., Patterson, L., Zimmermann, M., Court, W., et al., 2012. Advances in establishment and analysis of three-dimensional tumor spheroid-based functional assays for target validation and drug evaluation. *BMC Biol* 10, 29. doi: 10.1186/1741-7007-10-29

Wang, S., Su, X., Xu, M., Xiao, X., Li, X., Li, H., et al., 2019. Exosomes secreted by mesenchymal stromal/stem cell-derived adipocytes promote breast cancer cell growth via activation of Hippo signaling pathway. *Stem Cell Res Ther* 10, 117. doi: 10.1186/s13287-019-1220-2

Weiswald, L.B., Bellet, D., Dangles-Marie, V., 2015. Spherical cancer models in tumor biology. *Neoplasia* 17, 1-15. doi: 10.1016/j.neo.2014.12.004

Zingales, V., Fernandez-Franzon, M., Ruiz, M.J., 2020a. The role of mitochondria in sterigmatocystin-induced apoptosis on SH-SY5Y cells. *Food Chem Toxicol* 142, 111493. doi: 10.1016/j.fct.2020.111493

Zingales, V., Fernandez-Franzon, M., Ruiz, M.J., 2020b. Sterigmatocystin-induced cytotoxicity via oxidative stress induction in human neuroblastoma cells. *Food Chem Toxicol* 136, 110956. doi: 10.1016/j.fct.2019.110956

Zingales, V., Fernandez-Franzon, M., Ruiz, M.J., 2021. Sterigmatocystin-induced DNA damage triggers cell-cycle arrest via MAPK in human neuroblastoma cells. *Toxicol Mech Methods*, 1-10. doi: 10.1080/15376516.2021.1916801

Zouaoui, N., Mallebrera, B., Berrada, H., Abid-Essefi, S., Bacha, H., Ruiz, M.J., 2016. Cytotoxic effects induced by patulin, sterigmatocystin and beauvericin on CHO-K1 cells. *Food Chem Toxicol* 89, 92-103. doi: 10.1016/j.fct.2016.01.010

## **4.GENERAL DISCUSSION**

### **DISCUSSION GENERAL**



#### 4. DISCUSIÓN GENERAL

En la presente Tesis Doctoral se evaluó el efecto citotóxico de la STE individualmente en las líneas celulares SH-SY5Y y HepG2, y en combinación con el NIV en las células HepG2. A continuación, se evaluaron los mecanismos de toxicidad de la STE en las células SH-SY5Y, ya que el número de estudios sobre el efecto de la STE en el sistema neuronal es muy limitado. Concretamente, se determinó el estrés oxidativo mediante la generación de ROS y LPO. Tras observar un incremento del estrés oxidativo en las células SH-SY5Y expuestas a la STE, el siguiente objetivo que se planteó fue evaluar el sistema de defensa intracelular enzimático (GPX, GST, CAT y SOD) y no enzimático (GSH), así como el efecto protector de la QUE, un antioxidante de la dieta que se encuentra en una amplia variedad de alimentos. A continuación, se evaluaron los efectos tóxicos de la STE a través de posibles alteraciones del ciclo celular, de la respuesta inflamatoria, daño al ADN, inducción de apoptosis/necrosis y la alteración del potencial de membrana mitocondrial. Por último, teniendo en cuenta que los efectos citotóxicos observados en cultivos en monocapa convencionales no siempre se reproducen adecuadamente la complejidad del microambiente *in vivo*, la citotoxicidad de la STE se estudió en modelos de cultivo celular tridimensionales (3D) de neuroblastoma (esferoides), con el fin de proporcionar información más detallada sobre la citotoxicidad de la STE a través de un sistema que se asemeja al comportamiento celular *in vivo*.

#### 4.1. Viabilidad celular

##### 4.1.1. Efectos tóxicos de las micotoxinas individuales

Se evaluó la citotoxicidad de la STE en las células HepG2 y SH-SY5Y durante un periodo de exposición de 24, 48 y 72 h. Los parámetros de citotoxicidad que se utilizaron fueron el método de la sal de tetrazolio (MTT) y el Rojo Neutro (RN). Mientras el primero permite relacionar la viabilidad celular con la actividad metabólica mitocondrial, el segundo se basa en la alteración lisosomal tras la exposición a sustancias tóxicas.

La STE disminuyó la viabilidad celular en las células SH-SY5Y de manera dependiente de la concentración y del tiempo de exposición, con valores de  $IC_{50}$  entre  $0,48 \pm 0,09 \mu\text{M}$  y  $> 25 \mu\text{M}$ . Tanto la función mitocondrial (MTT) como la lisosomal (RN) se alteraron tras la exposición a la STE. Sin embargo, no se obtuvieron valores de  $IC_{50}$  para la STE en las células HepG2 durante los tres tiempos de exposición y concentraciones ensayadas (de 0,78 a 50  $\mu\text{M}$ ), lo que sugiere que las células SH-SY5Y son más sensibles a la STE que las células HepG2.

Los resultados obtenidos están en concordancia con los datos obtenidos en la bibliografía, donde se puede observar una gran variabilidad de susceptibilidad a la STE entre diferentes líneas celulares y valores de  $IC_{50}$  que oscilan entre 3,7  $\mu\text{M}$  y 286,1  $\mu\text{M}$ , siendo la línea celular A549 la más sensible y la HepG2 la menos sensible a esta micotoxina (Anninou et al., 2014; Bungler et al., 2004). Esta variabilidad de datos se debe a que los valores de  $IC_{50}$  dependen del método ensayado, el tiempo de exposición y la línea celular empleada. Los resultados obtenidos con los métodos de toxicidad aguda *in vitro* pueden contribuir a la elección de las concentraciones preliminares necesarias en ensayos

*in vivo* que se utilizan para el establecimiento de los límites máximos de estas micotoxinas en alimentos y piensos.

#### **4.1.2. Efectos tóxicos de combinaciones de micotoxinas**

En una dieta completa y equilibrada que contenga una variedad de alimentos diferentes, la posibilidad de exposición simultánea a más de una micotoxina es alta. Además, teniendo en cuenta el hecho de que los hongos micotoxigénicos son capaces de producir más de una micotoxina y que los alimentos y piensos pueden estar infectados por diversas especies de hongos, se puede sospechar la presencia de varias micotoxinas en un mismo alimento. Por ello, es importante evaluar los efectos de las combinaciones de micotoxinas, ya que el efecto tóxico de una micotoxina podría verse potenciado cuando se encuentra de manera simultánea con otras micotoxinas. Por lo tanto, la exposición simultánea o secuencial a múltiples micotoxinas podría dar lugar a efectos adversos sobre la salud del consumidor, los cuales suponen un riesgo mayor que la ingesta de una sola micotoxina, dependiendo de la naturaleza de sus posibles interacciones (antagónicas, sinérgicas o aditivas).

A continuación, se evaluaron los efectos citotóxicos de la STE en combinación binaria con el NIV. Ambas micotoxinas son producidas por especies de hongos predominantes en climas cálidos y húmedos, de modo que se pueden encontrar de simultáneamente en productos alimenticios. Para los estudios de las mezclas de micotoxinas se seleccionó el método MTT y se utilizaron las células HepG2 a las que se expusieron las combinaciones binarias durante 24, 48 y 72 h. Posteriormente, para determinar el tipo de interacción entre las micotoxinas, se aplicaron dos modelos matemáticos diferentes, el

método de las isobolas, basado en el índice de combinación (IC) introducido por Chou (2006) y Chou and Talalay (1984), y la herramienta Combenefit, que predice la superficie de respuesta de no interacción basada en la respuesta de un solo agente frente a la respuesta medida.

Los resultados obtenidos muestran que la viabilidad de la combinación de STE y NIV disminuyó más que la de la STE ensayada de forma individual y también a las concentraciones más bajas de NIV a las 24 y 48 h de exposición. Sin embargo, no se observaron diferencias frente a las concentraciones más altas de NIV, ni a todas las concentraciones ensayadas a las 72 h de exposición. Aplicando el método de las isobolas se obtuvieron interacciones diferentes dependiendo de la combinación, la concentración y los tiempos ensayados, siendo el efecto aditivo y sinérgico los observados con mayor frecuencia. A pesar de eso, el método Combenefit mostró un efecto antagónico a la concentración de NIV de 1,26  $\mu\text{M}$ , probablemente debido a una competencia entre las dos micotoxinas por el mismo receptor, lo cual resultó en un efecto menor del esperado.

Los ensayos utilizados permiten conocer el tipo de interacción entre las combinaciones de diferentes sustancias relacionando la concentración y el efecto producido. Sin embargo, no permiten conocer el mecanismo de acción de dicho efecto (Chou, 2006). Las fluctuaciones observadas son de difícil explicación debido a la complejidad de los mecanismos implicados y a los procesos bioquímicos desconocidos (Ruiz et al., 2011). El efecto aditivo/sinérgico observado tras de la exposición de las células HepG2 a algunas combinaciones de las micotoxinas es de gran importancia debido a que puede suponer un riesgo potencial asociado a la concurrencia de estas micotoxinas en los alimentos, lo



que indica que la evaluación del comportamiento toxicológico de una única micotoxina puede dar lugar a la subestimación de su toxicidad potencial.

#### 4.2. Estrés oxidativo

Los estudios de viabilidad celular con la STE han puesto de manifiesto los efectos tóxicos en los cultivos celulares, ya sea individualmente o en combinación. Debido a que la disminución de la viabilidad celular se debe a procesos moleculares, se llevaron a cabo estudios de la posible interacción con los componentes y mecanismos de acción celulares. Por ello, se eligieron tres concentraciones de STE (0,78, 1,56 y 3,12  $\mu\text{M}$ ), teniendo en cuenta las concentraciones encontradas anteriormente en los productos alimenticios y el consumo medio de cereales en Europa. En particular, según los datos reportados por la Autoridad Europea de Seguridad Alimentaria (EFSA, 2013), se han detectado niveles en el rango de 0,7 a 4300  $\mu\text{g}/\text{kg}$  de STE detectado en cereales y teniendo en cuenta que el consumo de cereales en Europa es de 132  $\text{kg}/\text{año}$  (FAOSTAT, 2013), la ingesta total estimada de STE oscila entre 0,77  $\text{nM}$  y 4,78  $\mu\text{M}/\text{día}$ . Las tres concentraciones seleccionadas en los ensayos se incluyen en este rango. Además, la selección de estas tres concentraciones se debió al hecho de que mostraron efectos citotóxicos en las células SH-SY5Y, y todas ellas son inferiores a las  $\text{IC}_{50}$  obtenidas mediante los ensayos de citotoxicidad.

En primer lugar, se planteó estudiar si la toxicidad inducida por STE podía ser debida a su capacidad de generar sustancias oxidantes. La producción de especies reactivas de oxígeno (ROS) en la célula juega un papel importante en diferentes rutas de señalización celular. Agentes exógenos como las micotoxinas

pueden contribuir a la producción incontrolada de éstas e incrementar el estrés oxidativo que a su vez puede dañar los lípidos de las membranas, las proteínas y el ADN celulares.

Los resultados obtenidos en las células SH-SY5Y demostraron que la STE no produce un aumento temprano de las ROS; sin embargo, se observó un incremento en la producción intracelular de ROS citoplasmáticas y mitocondriales se observó después de 24 h de exposición. Este efecto ha sido corroborado por otros autores en diversas líneas celulares (Gao et al., 2015; Liu et al., 2014). Tampoco se observó ningún aumento temprano en la generación de ROS en las células HepG2 expuestas a STE durante 120 minutos. Únicamente se observó un incremento significativo respecto al control tras 45 minutos de exposición a la mezcla de 0,08  $\mu\text{M}$  NIV + 0,78  $\mu\text{M}$  STE.

Una de las consecuencias más estudiadas producida por las ROS es la peroxidación lipídica (LPO) de los lípidos de membrana, cuyos productos son citotóxicos. Tras la exposición de las células SH-SY5Y a STE durante 24 h, el aumento observado de la LPO pone de manifiesto la capacidad de STE para interactuar con los lípidos de las membranas. Los resultados obtenidos suponen que la generación de ROS está implicada en la citotoxicidad de STE y que se ha producido LPO como consecuencia de la producción de ROS en las células SH-SY5Y.

Para demostrar la implicación del estrés oxidativo en la citotoxicidad inducida por STE, se estudió el efecto de la STE sobre otros marcadores de estrés oxidativo, cuya actividad se modifica por una gran variedad de estímulos relacionados con el estrés. En concreto, se evaluó la expresión génica de las enzimas HO-1 y NOS-2 y la translocación nuclear del factor de transcripción

NF- $\kappa$ B en las células SH-SY5Y tras 24 h de exposición a la STE. Los resultados obtenidos demostraron que dependiendo de la concentración de la STE se induce una sobreexpresión de los niveles de ARNm de HO-1 y NOS-2 y un aumento de la translocación nuclear del factor de transcripción NF- $\kappa$ B. El aumento de los niveles de expresión de HO-1 y la activación de la translocación nuclear de NF- $\kappa$ B son una prueba de la respuesta adaptativa al aumento del estrés oxidativo (Lee et al., 2005); además, la alteración de la señalización de NO a través del aumento de la expresión de NOS-2 está relacionada con la muerte celular y daño a los ácidos nucleicos y proteínas (Allen and Bayraktutan, 2009), por lo que el estrés oxidativo se puede considerar un mecanismo relacionado con la citotoxicidad producida por esta micotoxina en las células SH-SY5Y.

### **4.3 Sistemas de defensa antioxidante**

Tras los resultados obtenidos de disminución de la viabilidad celular e incremento del estrés oxidativo producido por la STE en las células SH-SY5Y, se procedió a estudiar la eficacia del sistema de defensa antioxidante intracelular frente al estrés oxidativo. Para ello, se determinó tanto el mecanismo enzimático como el no enzimático. Asimismo, se evaluó el efecto del flavonol quercetina (QUE) tras 24 h de exposición de las células SH-SY5Y a la STE.

#### **4.3.1 Niveles de glutatión**

El glutatión (GSH) forma parte de las líneas de defensa antioxidante intracelular no enzimática y protege a las células y tejidos frente al daño oxidativo. Por ello, la depleción de niveles de GSH es un marcador indicativo de estrés oxidativo. Se ha demostrado que los niveles intracelulares de GSH

intervienen en diferentes funciones celulares como la reparación del ADN, el ciclo celular, la regulación de rutas de señalización y la regeneración de antioxidantes exógenos.

Los resultados obtenidos tras la exposición a las concentraciones más altas de STE ensayadas (1,56 y 3,12  $\mu\text{M}$ ) en este estudio mostraron una disminución significativa de los niveles de GSH y un aumento del contenido de GSSG.

A continuación, para determinar el papel antioxidante del GSH frente a la exposición de la STE se aplicó la L-butionina-[S,R] sulfoximina (BSO), un reductor del GSH, y la N-acetilcisteína (NAC), un promotor de GSH, en combinación con la micotoxina. Concretamente, las células se pretrataron con 60  $\mu\text{M}$  de BSO o 1 mM de NAC durante 48 h y posteriormente se expusieron a STE 0,78, 1,56 y 3,12  $\mu\text{M}$ . Se determinaron los niveles de GSH y se compararon los resultados con los obtenidos en las células no pretratadas. Al pretratar las células con BSO, se observó una disminución del 45% en los niveles de GSH con respecto al control, así como al comparar las células pretratadas con BSO de las no pretratadas, se observó una disminución de los niveles de GSH entre un 41% y un 79%. Del mismo modo se compararon los resultados obtenidos al pretratar las células con NAC respecto al control y se observó un incremento del 16% en los niveles de GSH. En las células expuestas a STE 0,78 y 1,56  $\mu\text{M}$ , el pretratamiento con NAC incrementó los niveles de GSH al 25% y al 51% con respecto a las células no pretratadas. Sin embargo, con el aumento de las concentraciones de STE, este efecto citoprotector de la NAC disminuyó, hasta no mostrar efectos cuando las células se expusieron a 3,12  $\mu\text{M}$  de STE.

### 4.3.2 Actividades enzimáticas

El sistema enzimático de primera línea de defensa frente a los radicales libres está compuesto principalmente por la glutatión peroxidasa (GPx), la glutatión-S-transferasa (GST), la catalasa (CAT) y la superóxido dismutasa (SOD).

Los resultados obtenidos tras la exposición a la STE durante 24 h en las células SH-SY5Y mostraron una disminución de la actividad enzimática de la GPx del 45% y del 47% a las concentraciones 0,78 y 1,56  $\mu\text{M}$  de STE, respectivamente, mientras que a la concentración más alta se observó un aumento del 18%. Teniendo en cuenta que la GPx trabaja simultáneamente con la CAT para eliminar  $\text{H}_2\text{O}_2$ , se estudió la actividad de la CAT, la cual no produjo diferencias o disminuyó ligeramente respecto al control. Del mismo modo, la actividad de la SOD se redujo significativamente en función de las concentraciones de STE expuestas en las células SH-SY5Y. Finalmente, respecto a la familia de enzimas de la GSTs que cataliza la conjugación del GSH con diferentes sustratos, protegiendo a las células de daños y detoxificando los xenobióticos. Los resultados mostraron que a 1,56 y 3,12  $\mu\text{M}$  de STE la actividad de la GST disminuye, mientras que a la concentración más baja no se observó actividad. La falta de estimulación de la actividad enzimática tras la exposición a la STE sugiere que esta enzima no participa en la detoxificación de la STE en las células SH-SY5Y. A la luz de estos resultados, cabe suponer que las células SH-SY5Y son incapaces de contrarrestar el estrés oxidativo producido por la STE, como sugiere la pérdida de actividad observada de todas las enzimas antioxidantes, lo que lleva a una mayor intensificación y predisposición de las células al daño oxidativo.

En las células expuestas a la STE, el pretratamiento con BSO indujo una disminución adicional de la actividad de la GPx y de la GST, mientras que se observó un incremento de la actividad de la SOD y la CAT respecto al control, lo que sugiere que en presencia de BSO se produce una generación adicional de H<sub>2</sub>O<sub>2</sub>. Por tanto, por un lado el pretratamiento con BSO aumentó la predisposición de las células al daño oxidante inducido por la STE y por otro el pretratamiento con NAC mostró un efecto citoprotector en las células SH-SY5Y expuesta a STE. En particular, el incremento de los niveles de GSH inducido por el pretratamiento con NAC, resultó en un incremento de la actividad enzimática relacionada con el GSH (GPx y GST). Se observó un aumento en la actividad de la GPx a 0,78 y 1,56  $\mu$ M de STE, mientras que la actividad de la GST aumentó en las células expuestas a 3,12  $\mu$ M de STE, lo que sugiere que a la concentración más alta de STE, el pretratamiento con NAC ayuda en la detoxificación de la STE en las células SH-SY5Y. Este hecho puede deberse al incremento de los niveles de GSH, así como a sus propiedades antioxidantes y directas de eliminación de radicales libres (Zafarullah et al., 2003).

### 4.3.3 Quercetina

La ingesta dietética de antioxidantes es una forma plausible y eficaz de aumentar y fortalecer los sistemas de defensa antioxidantes endógenos, ya que muchos antioxidantes de la dieta actúan como eliminadores de radicales libres, lo que resulta en una citoprotección frente al daño oxidativo. La QUE es un flavonol presente en los frutos rojos y otras bayas con efecto antioxidante. Con el objetivo de evaluar el efecto citoprotector de la QUE, se determinó el efecto en la viabilidad celular. Para ello, las células SH-SY5Y se pretrataron con 10  $\mu$ M de QUE durante 2 h y posteriormente se expusieron a STE durante 24 h. Los

resultados obtenidos mediante el ensayo del MTT demostraron que tras pretratar las células con QUE la viabilidad se incrementa en las células expuesta a STE, respecto de las células sin pretratar. A continuación, se procedió a la evaluación de la producción intracelular de ROS. Los datos obtenidos mostraron que el pretratamiento con la QUE disminuye la generación intracelular de ROS inducida por la STE. Nuestros resultados concuerdan con la bibliografía existente que muestra que la QUE es un potente antioxidante capaz de reducir la muerte celular inducida por diferentes micotoxinas al inhibir el aumento intracelular de las ROS (Ghadiri et al., 2019; Gitika et al., 2006; Periasamy et al., 2016). Asimismo, el pretratamiento con QUE disminuyó la sobreexpresión de NOS-2 inducida por la STE. En cambio, en cuanto a la enzima HO-1, la QUE redujo su expresión solo en las células expuestas a la menor concentración de STE, mientras que indujo un aumento a las concentraciones más altas. Este hecho puede interpretarse como una mejora del sistema de defensa antioxidante celular inducido por la QUE en presencia de altas concentraciones de micotoxina. Por último, el pretratamiento de las células SH-SY5Y con la QUE seguido de la exposición a la STE produjo una menor activación de la translocación nuclear del factor de transcripción NF- $\kappa$ B en comparación con las células no pretratadas. Este efecto podría deberse a la capacidad antioxidante de la QUE para reducir la generación de ROS. De forma similar, este comportamiento ha sido observado en otras líneas celulares tras las exposiciones a otros tipos de micotoxinas (Ramya et al., 2014; Ramya and Padma, 2013). Estos resultados sugieren que la QUE protege a las células SHSY5Y de la citotoxicidad y el estrés oxidativo producidos por la STE, pudiendo su presencia contribuir a la disminución del efecto tóxico de la STE.

#### 4.4 Toxicidad mitocondrial

En condiciones *in vitro*, las células se adaptan metabólicamente a un crecimiento rápido y por esta razón, a pesar de las condiciones aeróbicas, la mayor parte de su energía la obtienen mediante la glucólisis, con una disminución significativa concomitante de los niveles de la fosforilación oxidativa (OXPHOS) (efecto Crabtree). Dado que la galactosa no produce ATP neto a partir de la glucólisis, la sustitución de glucosa por galactosa en el medio de cultivo representa una forma rápida de revertir el efecto Crabtree. Por lo tanto, se forzó a las células SH-SY5Y a usar la OXPHOS reemplazando en el medio de cultivos la glucosa por galactosa. Usando este enfoque, se desarrolló un modelo celular que representa de manera más fiel la fisiología mitocondrial y explora el estado funcional de las mitocondrias de las células SH-SY5Y expuestas a STE (Marroquin et al., 2007). Considerando el aumento de los trastornos metabólicos en los países occidentales, cada vez es más importante comprender cómo las micotoxinas presentes en los alimentos, como la STE, pueden afectar al metabolismo energético celular.

Nuestros resultados mostraron que el cambio en el sustrato provocó un cambio en el comportamiento de crecimiento de las células SH-SY5Y expuestas a concentraciones crecientes de STE. En particular, las células cultivadas con glucosa toleraron hasta 6,24  $\mu\text{M}$  de STE sin una pérdida significativa de la viabilidad celular. Por el contrario, las células cultivadas con galactosa resultaron más susceptibles, con una pérdida significativa de viabilidad a partir de 3,12  $\mu\text{M}$  de STE. Las diferencias en la respuesta entre las células SH-SY5Y cultivadas con glucosa y las cultivadas con galactosa sugieren que la citotoxicidad producida por la STE depende del deterioro mitocondrial. Además, se observó una



disminución significativa en los niveles de ATP en las células SH-SY5Y a partir de una concentración de STE de 3,12  $\mu\text{M}$ , el cual fue equivalente en ambas condiciones de crecimiento. Este hecho sugiere que la STE afecta a la producción de ATP en las células SH-SY5Y, aunque el mecanismo subyacente a este deterioro no depende de la ruta a través de la cual las células obtienen su energía. Teniendo en cuenta que en la condición de OXPHOS, otro requisito crucial para la síntesis de ATP consiste en una cadena transportadora de electrones (CTE) funcional, en experimentos posteriores se evaluó el efecto de la STE sobre la viabilidad celular de las células SH-SY5Y cultivadas en medio suplementado con galactosa en presencia de inhibidores de la CTE. La mayor disminución de la viabilidad celular obtenida cuando las células se expusieron a STE en presencia de rotenona, un inhibidor selectivo del complejo I, pusieron de manifiesto que el mecanismo de citotoxicidad de la STE depende directamente de los cambios en la actividad de la CTE. Sin embargo, no se observaron efectos en presencia de antimicina A, un inhibidor del complejo III, lo que sugiere que este último complejo no está implicado en la toxicidad de la STE. En general, estas observaciones establecen claramente que las mitocondrias juegan un papel fundamental en la actividad citotóxica e identifican a la STE como una micotoxina con efecto sobre la mitocondria, con un modo de acción que implica la modulación de la función mitocondrial.

#### **4.5 Muerte celular: apoptosis y necrosis**

Considerando la disfunción mitocondrial tras la exposición a la STE en las células SH-SY5Y y la posible relación de estos efectos con la muerte celular, el siguiente objetivo fue el estudio de la muerte celular por apoptosis y necrosis tras

2 y 24 h de exposición a STE. Después de 2 y 24 h de exposición, la STE no indujo la necrosis de las células SH-SY5Y a ninguna de las concentraciones ensayadas. Sin embargo, los resultados obtenidos mostraron un incremento del porcentaje (de 3,67% a 4,23%) de células en apoptosis temprana tras 2 h de exposición a la STE y un incremento del porcentaje (de 18,43% a 39,08%) de células en apoptosis tardía tras 24 h de exposición respecto al control (1,27% y 3,60%, respectivamente). El incremento de células apoptóticas fue dependiente de la concentración de la STE. Con el fin de obtener una mayor confirmación de nuestros resultados, se analizaron los niveles de expresión de genes codificadores de proteínas implicadas en la apoptosis. En particular, se evaluaron los cambios en los niveles de expresión del ARNm de los genes pro-apoptóticos Bax y Casp-3 y del gen anti-apoptótico Bcl-2. Los resultados obtenidos mostraron que los niveles de expresión del ARNm de Bax y Casp-3 aumentaron tras la exposición a STE, mientras que la expresión de Bcl-2 resultó reprimida en las células SH-SY5Y expuestas a la micotoxina. Estos resultados sugieren que la pérdida de viabilidad celular observada tras la exposición de las células SH-SY5Y a la STE se debe a la inducción de un proceso apoptótico. Nuestros hallazgos son consistentes con otros estudios previos, que demuestran que la apoptosis es un efecto común de la STE en diferentes líneas celulares (Cui et al., 2017; Zhang et al., 2013).

Los mecanismos que pueden dar lugar a la muerte celular por apoptosis tras la exposición a STE pueden ser diferentes. Entre ellos, la muerte celular podría deberse al incremento del estrés oxidativo inducido por la STE. De hecho, la apoptosis es un proceso estrictamente regulado a través de una serie de controles para preservar un equilibrio adecuado entre la muerte y la supervivencia celular y mantener la integridad del genoma (Blatt and Glick, 2001). Uno de los

principales y cruciales disruptores de este equilibrio está representado por el estrés oxidativo, ya que los poros de transición de la permeabilidad mitocondrial (mPT), cuya apertura determina la liberación de factores apoptóticos, son sensibles al estado de reducción-oxidación celular (redox).

#### **4.6 Potencial de membrana mitocondrial ( $\Delta\Psi_m$ )**

El potencial de membrana mitocondrial ( $\Delta\Psi_m$ ) tiene un papel importante en las mitocondrias, siendo la principal fuerza impulsora para la producción de ATP. Por ello y tras ver el papel de las mitocondrias en la toxicidad inducida por la STE, se planteó el objetivo de evaluar el  $\Delta\Psi_m$  tras la exposición de las células SH-SY5Y a la STE. A las 24 h de exposición, no se produjo alteración del  $\Delta\Psi_m$  con ninguna de las concentraciones ensayadas. Sin embargo, en las células HepG2, la exposición a la concentración más alta de STE (3,13  $\mu\text{M}$ ) indujo un aumento significativo del  $\Delta\Psi_m$ . Si bien nuestros resultados previos sugieren que la producción de ATP se ve afectada por la STE, los datos obtenidos muestran que la exposición celular a la micotoxina no produce la disipación del  $\Delta\Psi_m$ . Resultados similares fueron obtenidos por Bohler et al. (2018), quienes mostraron que en las células Jurkat los inhibidores de la CTE, los cuales bloquean el transporte de electrones y, por lo tanto, inhiben la ATP sintetasa, no afectaron al  $\Delta\Psi_m$ .

#### 4.7 Proliferación celular

A continuación, considerando que la alteración de la progresión del ciclo celular es uno de los mecanismos de acción más comunes por los que varias micotoxinas inducen una proliferación celular anormal y teniendo en cuenta que no hay datos que analicen los efectos de STE sobre la progresión del ciclo celular en el sistema neuronal humano, se investigó este efecto en las células SH-SY5Y expuestas a STE. Además, se evaluó el papel de algunas de las vías de señalización intracelular implicadas en la regulación del ciclo celular utilizando inhibidores específicos.

Con el fin de mantener la integridad genómica, las células poseen proteínas reguladoras encargadas de inducir la parada del ciclo celular en los puntos de control ( $G_0/G_1$ , S y  $G_2/M$ ) para poder reparar posibles daños, o en el caso de que estos no puedan ser reparados, inducir la muerte celular (Ishikawa et al., 2006). La proliferación continuada en presencia de daños en el ADN no reparado o reparado de manera inadecuada puede facilitar la propagación de genomas inestables y la adquisición de alteraciones genéticas, lo que puede contribuir significativamente al desarrollo del cáncer. Los resultados obtenidos mostraron una disminución de la población celular en la fase  $G_0/G_1$  acompañada de un incremento de la población celular en las fases S y  $G_2/M$  tras 24 h de exposición a todas las concentraciones ensayadas de STE, lo que se traduce en una parada del ciclo celular en estos puntos. Estos resultados son similares a los obtenidos por otros autores tras la exposición a STE en diversas líneas celulares (Huang et al., 2014; Wang et al., 2013; Zhang et al., 2013). La detención del ciclo celular en las fases S y/o  $G_2/M$  es una respuesta común de la mayoría de las células eucarióticas frente a un riesgo genotóxico. La parada del ciclo celular en

la fase S se relaciona con mecanismos de reparación que evitan que las células entren en mitosis ante un posible daño celular. Asimismo, la parada del ciclo celular por la STE en la fase G<sub>2</sub>/M se puede deber a un proceso adaptativo de supervivencia ante posibles daños en el ADN, con el fin de repararlos.

El ciclo celular es un proceso muy complejo regulado en varios niveles para permitir la detención del ciclo celular cuando se produce daño al ADN (Flatt y Pietenpol 2000; Stewart y Pietenpol 2001). La vía de las proteínas quinasas activadas por mitógeno (MAPK) es una ruta de transducción de señalización intracelular implicada en la regulación del ciclo celular de las células eucarióticas. La familia MAPK regula procesos de mitosis, respuestas a choques osmóticos, citoquinas inflamatorias, cambios de patrones de expresión génica, metabolismo, supervivencia, muerte celular programada genéticamente, lo que permite a las células sobrevivir, proliferar, inducir apoptosis, interactuar con múltiples tipos de células, etc. Estos procesos están implicados en el correcto desarrollo del organismo, así como en su homeostasis. Esta vía viene regulada por la activación de otras subfamilias MAPKs tales como quinasas reguladas por señales extracelulares (ERK) quinasas Jun N-terminal (JNK) y quinasas activada por mitógenos p38 (p38). Por lo tanto, el siguiente objetivo fue el estudio de los mecanismos moleculares subyacentes a la detención del ciclo celular inducidos por la STE a través del uso de inhibidores de las MAPKs. Los resultados mostraron que el pretratamiento de las células SH-SY5Y con los inhibidores de ERK y JNK redujo significativamente el porcentaje de células en la fase S y G<sub>2</sub>/M. La inhibición de la progresión del ciclo celular en la fase G<sub>2</sub>/M también fue anulada parcialmente por la supresión de la actividad de la p38 y de p53 (mediador importante en la fase G<sub>2</sub>/M que controla los daños en el ADN y evita la replicación de las células dañadas). En conjunto, nuestros resultados indicaron

que la detención de la fase S inducida por la STE depende de las rutas ERK y JNK, mientras que la detención de la fase G<sub>2</sub>/M está mediada por las tres rutas MAPK (ERK, JNK y p38) y por el p53. Estos resultados son similares a los obtenidos por otros autores con STE en células Het-1A y GES-1 (Cui et al., 2018; Wang et al., 2013; Xing et al., 2011; Zhang et al., 2013).

#### 4.8 Genotoxicidad

Teniendo en cuenta la disrupción del ciclo celular tras la exposición de las células SH-SY5Y a la STE y su posible contribución al daño del ADN como uno de los posibles mecanismos implicados en este proceso, se evaluó el daño que puede producir la STE en el ADN mediante diferentes técnicas. Por una parte, se realizó el ensayo Cometa, un ensayo que permite determinar el daño genotóxico producido en las células por la rotura de la doble hélice de ADN. Brevemente, mediante una electroforesis la doble hélice del ADN fraccionada se desplaza hacia el ánodo, dando lugar a lo que se conocen como cometas, formados por la cabeza y la cola. Cuanto mayor sea el tamaño de la cola, mayor es el daño genotóxico producido. Tras 24 h de exposición se observó un incremento del daño al ADN dependiente de la concentración de STE, como se demuestra con la presencia de colas de cometa claramente visibles en las células expuestas a la micotoxina. El porcentaje de ADN en la cola aumentó significativamente en un 4,78%, 7,92% y 10,09% tras la exposición a 0,78, 1,56 y 3,12  $\mu$ M de STE respecto al control (1,27%), respectivamente. Por otra parte, se confirma que la STE induce daño al ADN, ya que se observa un incremento de la histona nucleosómica fosforilada ( $\gamma$ H2AX), un marcador bien conocido de roturas a doble cadenas del ADN, así como un incremento de la frecuencia de

micronúcleos (MN) tras la exposición a la STE. Este hecho coincide con la parada del ciclo celular en las fases S y G<sub>2</sub>/M tras 24 h de exposición a la STE en las células SH-SY5Y, por lo que podría sugerirse como un mecanismo de reparación de daños al ADN o apoptosis (previamente demostrada) en el caso de no poderse reparar el daño. Además, de modo similar a nuestros resultados, otros autores demostraron en diferentes líneas celulares las propiedades genotóxicas de la STE (Huang et al., 2014; Jiang et al., 2017; Wang et al., 2015; Wang et al., 2013) .

#### **4.9 Respuesta inflamatoria**

En cuanto al posible efecto de la STE en el sistema inflamatorio, se evaluaron los niveles de expresión de las citoquinas proinflamatorias, el factor de necrosis tumoral alfa (TNF- $\alpha$ ) y la interleuquina-6 (IL-6). Los resultados obtenidos mostraron una disminución de la expresión génica de la IL-6, en las células SH-SY5Y tras la exposición a la STE, mientras que ningún cambio fue inducido con respecto a los niveles de expresión del TNF- $\alpha$ . Los resultados obtenidos para la STE son comparables a los resultados obtenidos por Zhang et al. (2012) en células mPBMC y macrófagos peritoneales, así como en ratones BALB/c. Asimismo, varias micotoxinas han demostrado tener un efecto inmunomodulador negativo sobre la producción de citoquinas (Johannessen et al., 2007). Por lo tanto, los resultados de nuestro estudio, a pesar de su carácter preliminar, sugieren que, al igual que otras micotoxinas, la STE tiene efectos inmunomoduladores negativos, que podrían conducir a la depresión del sistema de defensa sistémico del organismo.

#### 4.10 Citotoxicidad en un modelo de cultivo 3D

Los estudios de evaluación de la citotoxicidad de las micotoxinas se basan principalmente en modelos de cultivo 2D *in vitro*. Si, por un lado, este enfoque es bien aceptado, además de ser conveniente y esencial para probar los efectos de sustancias tóxicas, por otro lado, los efectos citotóxicos observados en cultivos convencionales en monocapa a menudo no reflejan adecuadamente la complejidad del microambiente *in vivo*. Por ello, se planteó el objetivo de desarrollar y optimizar las técnicas y las condiciones de cultivo para obtener un modelo de células neuronales 3D viable (esferoide) con células SH-SY5Y para estudiar los efectos tóxicos causados por la exposición a la STE y compararlos con nuestros resultados obtenidos anteriormente en cultivos celulares en monocapa de células SH-SY5Y. Además, se comparó el efecto de la STE sobre la viabilidad de esferoides obtenidos a partir de otro tipo de células procedentes de neuroblastoma humano, las células SK-N-DZ, las cuales amplifican diferencialmente el protooncogen N-myc (MYCN), con el fin de resaltar las posibles diferencias del efecto de la STE en los dos tipos de líneas celulares de neuroblastoma.

Los resultados mostraron que la STE indujo una mortalidad más pronunciada en los esferoides SH-SY5Y en comparación con los esferoides SK-N-DZ, revelando diferencias significativas en la sensibilidad a la STE entre las líneas celulares que amplifican diferencialmente el MYCN. Este hecho confirma una vez más que líneas celulares diferentes pueden presentar diferente sensibilidad a la STE.

En comparación con los cultivos 2D, los esferoides de SH-SY5Y demostraron una resistencia considerablemente mayor a la STE: mientras que



en las células SH-SY5Y cultivadas en monocapa se obtuvo un valor de  $IC_{50}$  tras 3 días de exposición (72 h) de  $0,52 \mu M$ , en los esferoides de células SH-SY5Y se obtuvo un valor de  $IC_{50}$  de  $5,18 \mu M$ . Nuestros resultados concuerdan con varios estudios que demuestran que no se obtiene el mismo grado de sensibilidad en el sistema 2D y el cultivo 3D, ya que se obtienen valores de  $IC_{50}$  más altos en este último (Baek et al., 2016; De Simone et al., 2018; Mikhail et al., 2013; Mueller et al., 2014; Salehi et al., 2017). Esta discrepancia se puede atribuir a la presencia en los esferoides (3D) de uniones intracelulares pronunciadas, imitando barreras fisiológicas, así como una matriz extracelular densa con poros pequeños, que influye en el transporte de xenobióticos al disminuir su penetración (Goodman et al., 2008; Lee et al., 2009). Por el contrario, la ausencia de una organización 3D en los sistemas 2D puede llevar a una sobreestimación de la toxicidad celular.

Finalmente, se evaluaron los mecanismos de acción subyacentes a la citotoxicidad de la STE en los esferoides de las células SH-SY5Y, con el fin de comparar los resultados obtenidos con nuestros resultados previos. Los resultados obtenidos confirmaron la capacidad de la STE para inducir apoptosis, estrés oxidativo y daño al ADN en las células SH-SY5Y, tanto en cultivos celulares 2D como en 3D. Sin embargo, los esferoides demostraron más resistencia que el cultivo celular en monocapa 2D a los efectos tóxicos de la STE, ya que concentraciones y tiempos de exposición más bajos fueron suficientes para causar efectos tóxicos en el sistema 2D en comparación con el sistema 3D.

En definitiva, la comparación de los resultados obtenidos en cultivos 2D y 3D demostró la importante influencia del microambiente y de la estructura del cultivo 3D en la investigación toxicológica. En particular, la evaluación de la citotoxicidad con esferoides refleja con mayor precisión el comportamiento

celular *in vivo*, debido a que los modelos de cultivos 3D simulan la estructura de los tejidos y los procesos fisiológicos *in vivo*, efecto que no se observa con el sistema de cultivo 2D.

#### 4.11 Referencias

- Allen, C.L., Bayraktutan, U., 2009. Oxidative stress and its role in the pathogenesis of ischaemic stroke. *Int J Stroke* 4, 461-470.
- Anninou, N., Chatzaki, E., Papachristou, F., Pitiakoudis, M., Simopoulos, C., 2014. Mycotoxins' activity at toxic and sub-toxic concentrations: differential cytotoxic and genotoxic effects of single and combined administration of sterigmatocystin, ochratoxin A and citrinin on the hepatocellular cancer cell line Hep3B. *Int J Environ Res Public Health* 11, 1855-1872.
- Baek, N., Seo, O.W., Kim, M., Hulme, J., An, S.S., 2016. Monitoring the effects of doxorubicin on 3D-spheroid tumor cells in real-time. *Onco Targets Ther* 9, 7207-7218.
- Blatt, N.B., Glick, G.D., 2001. Signaling pathways and effector mechanisms pre-programmed cell death. *Bioorg Med Chem* 9, 1371-1384.
- Bohler, P., Stuhldreier, F., Anand, R., Kondadi, A.K., Schlutermann, D., Berleth, N., Deitersen, J., Wallot-Hieke, N., Wu, W., Frank, M., Niemann, H., Wesbuer, E., Barbian, A., Luyten, T., Parys, J.B., Weidtkamp-Peters, S., Borchardt, A., Reichert, A.S., Pena-Blanco, A., Garcia-Saez, A.J., Itskanov, S., van der Blik, A.M., Proksch, P., Wesselborg, S., Stork, B., 2018. The mycotoxin phomoxanthone A disturbs the form and function of the inner mitochondrial membrane. *Cell Death Dis* 9, 286.

- Bunger, J., Westphal, G., Monnich, A., Hinnendahl, B., Hallier, E., Muller, M., 2004. Cytotoxicity of occupationally and environmentally relevant mycotoxins. *Toxicology* 202, 199-211.
- Chou, T.C., 2006. Theoretical basis, experimental design, and computerized simulation of synergism and antagonism in drug combination studies. *Pharmacol Rev* 58, 621-681.
- Chou, T.C., Talalay, P., 1984. Quantitative analysis of dose-effect relationships: the combined effects of multiple drugs or enzyme inhibitors. *Adv Enzyme Regul* 22, 27-55.
- Cui, J., Wang, J., Huang, S., Jiang, X., Li, Y., Wu, W., Zhang, X., 2017. Sterigmatocystin induced apoptosis in human pulmonary cells in vitro. *Exp Toxicol Pathol* 69, 695-699.
- Cui, J., Wang, J., Huang, S., Jiang, X., Li, Y., Wu, W., Zhang, X., 2018. The G2 phase arrest induced by sterigmatocystin is dependent on hMLH1- ERK/p38-p53 pathway in human esophageal epithelium cells in vitro. *Food Chem Toxicol* 115, 205-211.
- De Simone, U., Roccio, M., Gribaldo, L., Spinillo, A., Caloni, F., Coccini, T., 2018. Human 3D Cultures as Models for Evaluating Magnetic Nanoparticle CNS Cytotoxicity after Short- and Repeated Long-Term Exposure. *Int J Mol Sci* 19.
- EFSA, 2013. European food safety authority (efsa) panel on contaminants in food chain (CONTAM), scientific opinion on the risk for public and animal health related to the presence of sterigmatocystin in food and feed. *EFSA J* 11 (6), 3254.
- FAOSTAT, 2013. Food Balance Sheet. <http://faostat.fao.org>.

- Flatt PM, Pietsenpol JA. 2000. Mechanisms of cell-cycle checkpoints: at the crossroads of carcinogenesis and drug discovery. *Drug Metab Rev.* 32(3–4): 283–305.
- Gao, W., Jiang, L., Ge, L., Chen, M., Geng, C., Yang, G., Li, Q., Ji, F., Yan, Q., Zou, Y., Zhong, L., Liu, X., 2015. Sterigmatocystin-induced oxidative DNA damage in human liver-derived cell line through lysosomal damage. *Toxicol In Vitro* 29, 1-7.
- Ghadiri, S., Spalenza, V., Dellaflora, L., Badino, P., Barbarossa, A., Dall'Asta, C., Nebbia, C., Girolami, F., 2019. Modulation of aflatoxin B1 cytotoxicity and aflatoxin M1 synthesis by natural antioxidants in a bovine mammary epithelial cell line. *Toxicol In Vitro* 57, 174-183.
- Gitika, B., Sai Ram, M., Sharma, S.K., Ilavazhagan, G., Banerjee, P.K., 2006. Quercetin protects C6 glial cells from oxidative stress induced by tertiary-butylhydroperoxide. *Free Radic Res* 40, 95-102.
- Goodman, T.T., Ng, C.P., Pun, S.H., 2008. 3-D tissue culture systems for the evaluation and optimization of nanoparticle-based drug carriers. *Bioconjug Chem* 19, 1951-1959.
- Huang, S., Wang, J., Xing, L., Shen, H., Yan, X., Wang, J., Zhang, X., 2014. Impairment of cell cycle progression by sterigmatocystin in human pulmonary cells in vitro. *Food Chem Toxicol* 66, 89-95.
- Ishikawa, K., Ishii, H., Saito, T., 2006. DNA damage-dependent cell cycle checkpoints and genomic stability. *DNA Cell Biol* 25, 406-411.
- Jiang, X., Wang, J., Xing, L., Shen, H., Lian, W., Yi, L., Zhang, D., Yang, H., Liu, J., Zhang, X., 2017. Sterigmatocystin-induced checkpoint adaptation depends on Chk1 in immortalized human gastric epithelial cells in vitro. *Arch Toxicol* 91, 259-270.

- Johannessen, L.N., Nilsen, A.M., Lovik, M., 2007. Mycotoxin-induced depletion of intracellular glutathione and altered cytokine production in the human alveolar epithelial cell line A549. *Toxicol Lett* 168, 103-112.
- Lee, J., Lilly, G.D., Doty, R.C., Podsiadlo, P., Kotov, N.A., 2009. In vitro toxicity testing of nanoparticles in 3D cell culture. *Small* 5, 1213-1221.
- Lee, Y.M., Cheng, P.Y., Hong, S.F., Chen, S.Y., Lam, K.K., Sheu, J.R., Yen, M.H., 2005. Oxidative stress induces vascular heme oxygenase-1 expression in ovariectomized rats. *Free Radic Biol Med* 39, 108-117.
- Liu, Y., Du, M., Zhang, G., 2014. Proapoptotic activity of aflatoxin B1 and sterigmatocystin in HepG2 cells. *Toxicol Rep* 1, 1076-1086.
- Marroquin, L.D., Hynes, J., Dykens, J.A., Jamieson, J.D., Will, Y., 2007. Circumventing the Crabtree effect: replacing media glucose with galactose increases susceptibility of HepG2 cells to mitochondrial toxicants. *Toxicol Sci* 97, 539-547.
- Mikhail, A.S., Eetezadi, S., Allen, C., 2013. Multicellular tumor spheroids for evaluation of cytotoxicity and tumor growth inhibitory effects of nanomedicines in vitro: a comparison of docetaxel-loaded block copolymer micelles and Taxotere(R). *PLoS One* 8, e62630.
- Mueller, D., Kramer, L., Hoffmann, E., Klein, S., Noor, F., 2014. 3D organotypic HepaRG cultures as in vitro model for acute and repeated dose toxicity studies. *Toxicol In Vitro* 28, 104-112.
- Periasamy, R., Kalal, I.G., Krishnaswamy, R., Viswanadha, V., 2016. Quercetin protects human peripheral blood mononuclear cells from OTA-induced oxidative stress, genotoxicity, and inflammation. *Environ Toxicol* 31, 855-865.
- Ramyaa, P., Krishnaswamy, R., Padma, V.V., 2014. Quercetin modulates OTA-induced oxidative stress and redox signalling in HepG2 cells - up regulation of

- Nrf2 expression and down regulation of NF-kappaB and COX-2. *Biochim Biophys Acta* 1840, 681-692.
- Ramyaa, P., Padma, V.V., 2013. Ochratoxin-induced toxicity, oxidative stress and apoptosis ameliorated by quercetin--modulation by Nrf2. *Food Chem Toxicol* 62, 205-216.
- Ruiz, M.J., Macakova, P., Juan-Garcia, A., Font, G., 2011. Cytotoxic effects of mycotoxin combinations in mammalian kidney cells. *Food Chem Toxicol* 49, 2718-2724.
- Salehi, F., Behboudi, H., Kavooosi, G., Ardestani, S.K., 2017. Monitoring ZEO apoptotic potential in 2D and 3D cell cultures and associated spectroscopic evidence on mode of interaction with DNA. *Sci Rep* 7, 2553.
- Stewart ZA, Pietenpol JA. 2001. p53 signaling and cell cycle checkpoints. *Chem Res Toxicol*. 14(3): 243–263.
- Wang, J., Huang, S., Xing, L., Cui, J., Tian, Z., Shen, H., Jiang, X., Yan, X., Wang, J., Zhang, X., 2015. Sterigmatocystin induces G1 arrest in primary human esophageal epithelial cells but induces G2 arrest in immortalized cells: key mechanistic differences in these two models. *Arch Toxicol* 89, 2015-2025.
- Wang, J., Huang, S., Xing, L., Shen, H., Yan, X., Wang, J., Zhang, X., 2013. Role of hMLH1 in sterigmatocystin-induced G(2) phase arrest in human esophageal epithelial Het-1A cells in vitro. *Toxicol Lett* 217, 226-234.
- Xing, X., Wang, J., Xing, L.X., Li, Y.H., Yan, X., Zhang, X.H., 2011. Involvement of MAPK and PI3K signaling pathway in sterigmatocystin-induced G(2) phase arrest in human gastric epithelium cells. *Molecular Nutrition & Food Research* 55, 749-760.
- Zafarullah, M., Li, W.Q., Sylvester, J., Ahmad, M., 2003. Molecular mechanisms of N-acetylcysteine actions. *Cell Mol Life Sci* 60, 6-20.

- Zhang, D., Cui, Y., Shen, H., Xing, L., Cui, J., Wang, J., Zhang, X., 2013. Sterigmatocystin-induced DNA damage triggers G2 arrest via an ATM/p53-related pathway in human gastric epithelium GES-1 cells in vitro. *PLoS One* 8, e65044.
- Zhang, Y., Yao, Z.G., Wang, J., Xing, L.X., Xia, Y., Zhang, X.H., 2012. Effects of sterigmatocystin on TNF-alpha, IL-6 and IL-12 expression in murine peripheral blood mononuclear cells and peritoneal macrophages in vivo. *Mol Med Rep* 5, 1318-1322.





# **5.CONCLUSION**

## CONCLUSIONES



## 5. CONCLUSIONES

1. Las revisiones bibliográficas realizadas ponen de manifiesto que la información sobre la toxicidad de la esterigmatocistina y el nivalenol es limitada, por lo cual se deben realizar más estudios que permitan una adecuada evaluación del riesgo toxicológico.
2. La esterigmatocistina no reduce la viabilidad celular de manera significativa en las células HepG2. Sin embargo, la combinación de la esterigmatocistina con el nivalenol induce una disminución más pronunciada de la viabilidad celular respecto a la producida por la esterigmatocistina de forma individual. Dicha combinación binaria produce principalmente efectos sinérgicos y aditivos, dependiendo de la concentración de cada micotoxina y de la fracción afectada (*fa*) en la mezcla, aunque también se observan efectos antagónicos a la concentración de nivalenol de 1,26  $\mu\text{M}$ .
3. La esterigmatocistina presenta citotoxicidad en las células SH-SY5Y. El efecto citotóxico aumenta con la concentración y el tiempo de exposición, con valores de  $\text{IC}_{50}$  desde  $0,48 \pm 0,09 \mu\text{M}$  hasta  $> 25 \mu\text{M}$ .
4. La esterigmatocistina incrementa el estrés oxidativo en las células SH-SY5Y mediante la producción de especies reactivas de oxígeno citoplasmáticas y mitocondriales, además de producir peroxidación lipídica, observándose un efecto significativo a partir de la concentración 0,78  $\mu\text{M}$ .
5. El estrés oxidativo producido por la esterigmatocistina en las células SH-SY5Y causa una disminución del glutatión y una alteración de la actividad enzimática antioxidante de la glutatión peroxidasa, glutatión transferasa,

- catalasa y superóxido dismutasa. El pretratamiento con el antioxidante exógeno quercetina protege a las células SH-SY5Y de la citotoxicidad y el estrés oxidativo generado por la esterigmatocistina.
6. El cambio en el metabolismo energético generado a nivel mitocondrial en las células SH-SY5Y altera la proliferación celular dependiendo de la concentración de la micotoxina. Este cambio sugiere que la esterigmatocistina modifica la actividad mitocondrial.
  7. La esterigmatocistina no altera el potencial de membrana mitocondrial en las células SH-SY5Y, pero desencadena el proceso de apoptosis, daño al ADN y está implicada en la disrupción del ciclo celular.
  8. La esterigmatocistina presenta un efecto inmunomodulador negativo mediante la disminución de la expresión génica de citoquinas pro-inflamatorias.
  9. La esterigmatocistina presenta citotoxicidad en los esferoides de células SH-SY5Y, causando desagregación celular tras su exposición. La citotoxicidad aumenta con la concentración y el tiempo de exposición, sin embargo, los esferoides (3D) son más resistentes que el cultivo celular en monocapa (2D) a los efectos citotóxicos producido por la esterigmatocistina. La inducción de estrés oxidativo, apoptosis y daño al ADN en los esferoides expuestos a la esterigmatocistina corroboran sus propiedades citotóxicas.
  10. La esterigmatocistina supone un riesgo tóxico potencial de salud pública. Se debería realizar más estudios sobre mecanismos de toxicidad en modelos tridimensionales (esferoides y organoides) ya que son modelos que simulan de forma más realista las condiciones *in vivo*.

## 5. CONCLUSIONS

1. The bibliographic reviews carried out show that data regarding sterigmatocystin and nivalenol toxicity are limited, therefore more studies are recommended to establish an adequate risk assessment.
2. Sterigmatocystin does not significantly reduce cell viability in HepG2 cells. However, the combination of sterigmatocystin with nivalenol induces a more pronounced decrease in viability than sterigmatocystin. The binary combination produces mainly synergistic and additive effects, depending on the concentration of each mycotoxin as well as the fraction affected ( $f_a$ ), although antagonistic effects are also observed at the 1.26  $\mu\text{M}$  nivalenol concentration.
3. Sterigmatocystin exhibits cytotoxic effects in SH-SY5Y cells. Cytotoxicity increases with concentration and exposure time, with  $\text{IC}_{50}$  values ranging from  $0.48 \pm 0.09 \mu\text{M}$  to  $> 25 \mu\text{M}$ .
4. Sterigmatocystin increases oxidative stress in SH-SY5Y cells through the production of cytoplasmic and mitochondrial reactive oxygen species and lipid peroxidation, inducing a significant effect starting from 0.78  $\mu\text{M}$ .
5. Oxidative stress induced by sterigmatocystin in SH-SY5Y cells causes a decrease in glutathione levels and an alteration of the antioxidant enzymatic activities of glutathione peroxidase, glutathione transferase, catalase and superoxide dismutase. Pre-treatment with the exogenous antioxidant quercetin protects SH-SY5Y cells from sterigmatocystin-induced cytotoxicity and oxidative stress.

6. Change in energy metabolism in SH-SY5Y cells exposed to increasing concentrations of sterigmatocystin causes a different cell growth behaviour, suggesting that the etiology of sterigmatocystin cytotoxicity is related to mitochondrial deterioration.
7. Sterigmatocystin does not alter the mitochondrial membrane potential in SH-SY5Y cells, but it triggers the apoptosis process, causes DNA damage, and is involved in cell cycle disruption.
8. Sterigmatocystin has a negative immunomodulatory effect, as highlighted by the decrease in gene expression of pro-inflammatory cytokines.
9. Sterigmatocystin induces cytotoxic effects in SH-SY5Y cell spheroids, causing cell disaggregation following exposure. Cytotoxicity increases with concentration and exposure time, being spheroids more resistant than 2D monolayer cell culture to the cytotoxic effects produced by sterigmatocystin. Induction of oxidative stress, apoptosis, and DNA damage in spheroids exposed to sterigmatocystin further corroborates its cytotoxic properties.
10. Sterigmatocystin represents a health hazard for public health, therefore, further toxicological studies are needed mainly in three-dimensional models (spheroids and organoids) for obtaining more realistic and trustworthy results.

**ANEXO I**  
**DIFUSIÓN DE RESULTADOS**







## Review

# Sterigmatocystin: Occurrence, toxicity and molecular mechanisms of action – A review

Veronica Zingales<sup>\*</sup>, Mónica Fernández-Franzón, Maria-José Ruiz

Laboratory of Food Chemistry and Toxicology, Faculty of Pharmacy, University of Valencia, Av. Vicent Andrés Estellés S/n, 46100, Valencia, Spain

## ARTICLE INFO

## Keywords:

Sterigmatocystin  
Occurrence in food  
Biosynthetic and metabolic pathway  
Mechanisms of action  
Toxicity

## ABSTRACT

The mycotoxin sterigmatocystin (STE) is produced mainly by *Aspergillus* fungi. It has been reported to occur in grains and grain-based products, cheese, coffee, spices and beer. The STE is a known biogenic precursor of aflatoxin B1, sharing with it several structural and biological similarities. The STE has been shown to be hepatotoxic and nephrotoxic in animals and it has been classified as possible human carcinogen (group 2B) by IARC. The STE has been reported to cause a marked decrease in cell proliferation in different mammalian cells. Data available on literature suggest that the cellular mechanisms underlying STE-induced toxicity include the induction of oxidative stress, mitochondrial dysfunction, apoptosis, cell cycle arrest, as well as alteration of immune system function and activation of different signalling pathways. Moreover, STE resulted to be genotoxic, being able to form DNA-adducts and induce DNA damage. Despite its strong cytotoxicity, no risk assessments have been still carried out by authorities due to the lack of toxicity data, so research on STE toxicological impact is still going on. This review reports information available regarding STE toxicity and its related mechanisms of action with the aim of updating information regarding last researches on this mycotoxin.

## 1. Generalities

Sterigmatocystin (STE) is a polyketide mycotoxin produced by several fungal species belonging to the genera *Aspergillus*, *Bipolaris*, *Botryotrichum*, *Humicola* and *Penicillium*. The main producers are *Aspergillus* fungi, such as *A. flavus*, *A. parasiticus*, *A. nidulans* and *A. versicolor*, from whose cultures STE was isolated by the first time in 1954 (Gruber-Dorminger et al., 2017; Rank et al., 2011). Fungi capable of producing STE are common food and feed contaminants, with a consequent strong economic impact for the biotechnological, agricultural and food industries (Wagacha and Muthomi, 2008). *Aspergillus flavus* and *A. parasiticus* are among the main species responsible for maize and peanuts contamination (Rank et al., 2011). Moreover, in tropical countries, *A. flavus* seems to be the fungus with the highest contamination rate for rice grains both in field and in post-harvest, probably due to the high temperatures and high relative humidity recorded throughout the year in these countries. On the other hand, *A. versicolor* shows a low but more stable presence during the growing season (Katsurayama et al., 2018; Reddy et al., 2009).

Previous studies performed on *A. nidulans* revealed that STE production coincides in time with the sexual development, as demonstrated

by the lack of STE production in loss-of-function mutants of sexual development regulators (Bayram and Braus, 2012; Dyer and O’Gorman, 2012). Coupling of these two processes might provide an evolutionary advantage. The mycotoxin production during the sexual development seems to allow the producer organism to defend its sexual structures from fungivores or to successfully compete against other organisms and thereby protect its environmental niche. Furthermore, it has been shown that the interconnection of the sexual development and STE production can be modulated by certain environmental factors, repressing or activating sexual- or asexual-development and/or secondary metabolism (Amon et al., 2018).

With regards to STE occurrence, in literature limited information is available on the presence of STE in food and feed. During the last 50 years only few surveys on the natural occurrence of STE in food and feed were performed and were partly carried out in the 1970s–1980s with less sophisticated techniques and relatively high limits of detection (LODs), often in the range 20–50 µg/kg. An improvement of the methods was obtained between 1979 and 1985, resulting in a LOD of 10 µg/kg in corn matrix and 2 µg/kg in cheese matrix (Francis et al., 1985; Gorst-Allman and Steyn, 1979). Since the late 1990s more advanced techniques have been employed for the determination of STE in food, up to

<sup>\*</sup> Corresponding author. Laboratory of Toxicology, Faculty of Pharmacy, University of Valencia, Av. Vicent Andrés Estellés, s/n, 46100, Burjassot, Valencia, Spain.  
E-mail address: [vezin@uv.es](mailto:vezin@uv.es) (V. Zingales).



## Review

Occurrence, mitigation and *in vitro* cytotoxicity of nivalenol, a type B trichothecene mycotoxin – Updates from the last decade (2010–2020)Veronica Zingales<sup>\*</sup>, Mónica Fernández-Franzón, Maria-José Ruiz

Laboratory of Food Chemistry and Toxicology, Faculty of Pharmacy, University of Valencia, Av. Vicent Andrés Estellés s/n, 46100, Valencia, Spain

## ARTICLE INFO

Handling Editor: Dr. Jose Luis Domingo

## Keywords:

Nivalenol  
Trichothecene mycotoxin  
Occurrence  
Mitigation  
*In vitro* toxicity

## ABSTRACT

The present review aims to give an overview of the literature of the last decade (2010–2020) concerning the occurrence of the type B trichothecene mycotoxin nivalenol (NIV) and its *in vitro* toxicity, with the purpose of updating information regarding last researches on this mycotoxin. The most recent studies on the possible methods for preventing *Fusarium* spp. growth and NIV production are also discussed. Recently, various environmental factors have been shown to influence strongly NIV occurrence. However, *Fusarium* spp. of the NIV genotype have been found almost worldwide. With regard to NIV cytotoxicity, NIV has been reported to cause a marked decrease in cell proliferation in different mammalian cells. In particular, the recent data suggest that organs containing actively proliferating cells represent the main targets of NIV. Moreover, NIV resulted to cause immunosuppression, gastrointestinal toxicity and genotoxicity. However, sufficient evidence of carcinogenicity in humans is currently lacking, and the International Agency for Research on Cancer (IARC) classifies it as a group 3 carcinogen. Further researches and the discovery of effective treatment strategies to prevent NIV contamination and to counteract its toxicity are urgently required against this common food-borne threat to human health and livestock.

## 1. Introduction

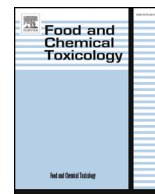
Mycotoxins are toxic secondary metabolites produced by different types of fungi, belonging mainly to the *Aspergillus*, *Penicillium* and *Fusarium* genera. Several *Fusarium* species are known to be the causal agents of *Fusarium* head blight (FHB) and *Fusarium* crown rot (FCR; also known as foot and root rot), two of the most devastating diseases that affect small grain cereal production worldwide. During the infection process, *Fusarium* spp. biosynthesize different mycotoxins that can compromise food safety, including trichothecenes, zearalenone (ZEA) and fumonisins (Mesterhazy, 2020).

Trichothecenes family is divided into four subgroups (A–D), depending on the chemical structure (Krska et al., 2001). Whereas type C and D trichothecenes occur rarely in food and feed, type A and B trichothecenes are toxicologically the most important and extensively studied groups, being frequently found as contaminants in various commodities. Type A trichothecenes include T-2 toxin (T-2), its acetylated derivative HT-2 toxin (HT-2) and their precursors, such as diacetoxyscirpenol (DAS) and neosolaniol (NEO); whereas type B trichothecenes include nivalenol (NIV), deoxynivalenol (DON) and their

acetylated derivatives, 4-acetylnivalenol (fusarenone X or 4-ANIV), 3-acetyldeoxynivalenol (3-ADON), and 15-acetyldeoxynivalenol (15-ADON) (McCormick et al., 2011). In general, in Europe, type B trichothecenes are mainly produced by *F. culmorum* and *F. graminearum*, while *F. poae* is a well-known species for the biosynthesis of NIV, DAS, T-2 and HT-2 toxins (Edwards et al., 2012).

The NIV is a member of type B trichothecenes produced by several *Fusarium* species. The NIV has frequently been observed in agricultural products. Compared to DON, another type B trichothecene from which it differs only by an additional hydroxyl group at the C-4 position, NIV ingested orally by animals is more toxic. However, although dietary exposure to NIV has been associated with an increased incidence of oesophageal and gastric carcinomas (Hsia et al., 2004), the International Agency for Research on Cancer (IARC) has classified NIV as Group 3 (unclassifiable as to carcinogenicity in humans), due to its inadequate evidence of carcinogenicity in experimental animals (IARC, 1993). Nevertheless, NIV warrants particular attention because of its frequency of contamination and its immunotoxicity and haematotoxicity in mammals (SCF, 2000).

<sup>\*</sup> Corresponding author. Laboratory of Toxicology, Faculty of Pharmacy, University of Valencia, Av. Vicent Andrés Estellés, s/n, 46100, Burjassot, Valencia, Spain.  
E-mail address: [vezin@uv.es](mailto:vezin@uv.es) (V. Zingales).



## Cytotoxic effects of individual and combined sterigmatocystin and nivalenol on liver hepatocellular carcinoma cells

Veronica Zingales<sup>\*,1</sup>, Clarissa Fedeli<sup>1</sup>, Mónica Fernández-Franzón, Maria-José Ruiz

Laboratory of Food Chemistry and Toxicology, Faculty of Pharmacy, University of Valencia, Av. Vicent Andrés Estellés s/n, 46100, Valencia, Spain

### ARTICLE INFO

**Keywords:**  
Mycotoxins  
Cytotoxicity  
Interactions  
Isobolograms  
Combeneft

### ABSTRACT

Since humans are exposed to different mycotoxins through daily intake, there is increasing concern about the adverse effects of the interactions between them. Cytotoxicity of sterigmatocystin (STE) and nivalenol (NIV) alone and in combination in human hepatocarcinoma (HepG2) cells was evaluated by MTT assay. Furthermore, ROS production and alteration of  $\Delta\Psi_m$  as mechanisms of action were assessed. Cells were treated with concentrations ranging from 0.15 to 5  $\mu\text{M}$  for NIV and from 0.78 to 50  $\mu\text{M}$  for STE individually and in binary combinations. The combination ratio between the mixture STE + NIV was 10:1. The  $\text{IC}_{50}$  values of NIV ranged from 0.96 to 0.66  $\mu\text{M}$ , whereas no  $\text{IC}_{50}$  values were obtained for STE at any time tested. For the combinations studied, synergistic, antagonistic and additive effects were obtained with the two type of analyses performed, the isobologram analysis and the Combeneft method. No relevant effects on ROS and  $\Delta\Psi_m$  were observed. In conclusion, predictive models based on combination data could help to better understand the interactions between mycotoxins and their implications in food safety assessment. However, a further analysis of the molecular mechanism underlying these interactive effects is required.

### 1. Introduction

Mycotoxins are secondary toxic metabolites produced by filamentous fungi. They are widespread in food and feed and their presence could be considered a significant global concern for human health (Luongo et al., 2006). In fact, the natural co-occurrence of different mycotoxins has been detected in several commodities. However, data on combined toxic effects of mycotoxins are limited and health risk assessments are usually based on one single mycotoxin exposure (Liu et al., 2014; Wan et al., 2013; Yang et al., 2017).

Nivalenol (NIV), a mycotoxin produced by various species of *Fusarium* fungi, belongs to the trichothecenes group, a family with a common tetracyclic, sesquiterpenoid 12,13 epoxytrichothec-9-ene ring system. *Fusarium* fungi are, probably, the most prevalent toxin-producing fungi commonly found on cereals grown in temperate regions of America, Europe and Asia (Luongo et al., 2006). In Europe the highest concentrations of NIV in food, feed and unprocessed grains were found in oats, maize, barley, wheat and their products (EFSA, 2013a).

Sterigmatocystin (STE) has been found in cereal grains and grain commodities following the fungal contamination at the storage stage (EFSA, 2013b). However, in the literature, there is a relatively little information on the occurrence of STE in food and feed.

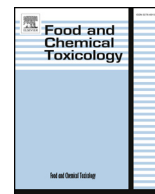
Based on current evidence, NIV and STE individually can produce different toxic effects. The NIV is able to induce cytotoxicity, oxidative stress, genotoxicity and apoptosis in human and animal cells (Nagashima, 2018). Moreover, this trichothecene showed several inhibitory effects on primary metabolism of eukaryotic cells, including inhibition of DNA and protein synthesis as well as mitochondrial function (Arunachalam and Doohan, 2013; Rocha et al., 2005). The NIV could be also associated to many other chronic effects in humans, such as gastrointestinal, hepatic, respiratory, dermal alterations and immunosuppression (Berek et al., 2001; Ferreira Lopes et al., 2017; Smith et al., 2017, 2018; Yang et al., 2017).

With regard to STE mycotoxin, it showed cytotoxic as well as oxidant activities (Liu et al., 2014; Zingales et al., 2019; Zouaoui et al., 2016). Furthermore, it has been shown to be able to inhibit ATP synthesis and impair cell cycle (Huang et al., 2014; Kawai et al., 1984). The STE is a carcinogenic mycotoxin produced mainly by *Aspergillus* and *Penicillium* species of fungi (Anninou et al., 2014; Liu et al., 2014). The International Agency for Research on Cancer (IARC, 1987) has classified STE as a possible human carcinogen (group 2B).

Since a complete and balanced diet normally contains a variety of different foods, the consequent possibility of exposure to more than one mycotoxin is high (EFSA, 2013a, 2013b). The growing research effort of

\* Corresponding author. Laboratory of Toxicology, Faculty of Pharmacy, University of Valencia, Av. Vicent Andrés Estellés, s/n, 46117, Burjassot, Valencia, Spain.  
E-mail address: [vezin@uv.es](mailto:vezin@uv.es) (V. Zingales).

<sup>1</sup> These authors have contributed equally to the study, and thus may be regarded as the first author.



## Sterigmatocystin-induced cytotoxicity *via* oxidative stress induction in human neuroblastoma cells



Veronica Zingales\*, Mónica Fernández-Franzón, Maria-José Ruiz

Laboratory of Food Chemistry and Toxicology, Faculty of Pharmacy, University of Valencia, Av. Vicent Andrés Estellés s/n, 46100, Valencia, Spain

### ARTICLE INFO

**Keywords:**  
Sterigmatocystin  
Cytotoxicity  
Oxidative stress  
Glutathione  
SH-SY5Y cells

### ABSTRACT

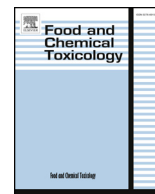
Sterigmatocystin (STE) is a mycotoxin produced by fungi of the genus *Aspergillus*. Considering that the effect of STE on neuronal system has not been well studied, the aim of the present study consists to investigate the cytotoxic effects of STE in human neuroblastoma (SH-SY5Y) cells. Moreover, the role of oxidative stress and intracellular defense systems was assessed by evaluating reactive oxygen species (ROS) generation, lipid peroxidation (LPO) and antioxidant no-enzymatic (GSH) levels and enzymatic (GPx, GST, CAT and SOD) activity. Our results revealed that STE decreased cell viability in a dose and time-dependent manner. Furthermore, after 24 h of exposure, STE induced an increase in ROS generation and LPO at all concentrations tested (0.78, 1.56 and 3.12  $\mu\text{M}$ ), as well as a depletion of GSH levels, an increase in GSSG content and a decrease in GSH/GSSG ratio at the highest concentrations. The activity of all antioxidant enzymes resulted to be also decreased. Additionally, an enhance of the oxidative damage was caused by BSO, a GSH depletor, while NAC, a GSH precursor, showed a scavenger activity. Our findings suggest that STE could injure SH-SY5Y cells via oxidative stress and highlight the antioxidant role of the glutathione system.

### 1. Introduction

Mycotoxins are toxic secondary metabolites of low-molecular-weight produced by filamentous fungi. They are characterized by their potential to cause adverse health effects in humans and animals following consumption of contaminated foods or feedstuffs (Bennett and Klich, 2003; Hussein and Brasel, 2001). The high prevalence of mycotoxin-contaminated food has led to focus the scientific attention on the study of mycotoxins (Marin et al., 2013; Murugesan et al., 2015). In addition to the serious public health problems produced by these fungal toxins, significant economic losses are also associated with mycotoxin contamination due to decreased market value of contaminated food (Wu, 2006). Sterigmatocystin (STE) is a mycotoxin produced mainly by fungi belonging to the genus *Aspergillus*. It was isolated by the first time in 1954 from *A. vesicolor* cultures (Díaz Nieto et al., 2018). Although in the literature only limited information is available on the occurrence of STE in food and feed, it has been reported to occur in grains and grain-based products following fungal contamination during the post-harvest stage (Versilovskis et al., 2007). Sterigmatocystin has been occasionally reported to occur also in cheese, green coffee beans, spices, nuts and beer (EFSA, 2013; Versilovskis and De Saeger, 2010; Versilovskis et al., 2009). Acute toxicity, cytotoxicity, mutagenicity and carcinogenicity have been associated with STE exposure. Many studies showed that STE

is able to induce tumours in animal models (Huang et al., 2004; Xing et al., 2007). In Mongolian gerbils it has been demonstrated that long-term administration of STE can induce intestinal metaplasia in the gastric mucosa (Kusunoki et al., 2011; Ma et al., 2003). Recently, STE was detected also in urine and plasma of patients with documented hepatocellular carcinoma (Cao et al., 2018). In light of all this, STE has been classified in the Group 2B (possible human carcinogen) by the International Agency for Research on Cancer (IARC, 1987; Pitt et al., 2012). *In vitro* studies demonstrated that STE exerts its cytotoxic effects through different mechanisms of action. Cell cycle arrest and DNA damage may represent two of the common toxic effects of STE (Anninou et al., 2014; Huang et al., 2014; Liu et al., 2014). Gao et al. (2015) suggested that oxidative stress plays a crucial role in STE-induced DNA damage in HepG2 cells. Oxidative stress occurs when the production of reactive oxygen species (ROS) exceeds the antioxidant capacity of cells to scavenge ROS. As consequent effect, lipid peroxidation, DNA fragmentation, protein oxidation and, in presence of elevated ROS levels, genome changes are induced (Cooke et al., 2003; Devasagayam et al., 2004). However, mammalian cells are equipped with a protective endogenous antioxidant system formed by no-enzymatic antioxidant such as the glutathione (GSH) and enzymatic protective systems such as glutathione peroxidase (GPx), glutathione S-transferase (GST), superoxide dismutase (SOD) and catalase (CAT). The

\* Corresponding author. Laboratory of Toxicology, Faculty of Pharmacy, University of Valencia, Av. Vicent Andrés Estellés, s/n, 46117, Burjassot, Valencia, Spain.  
E-mail address: [vezin@uv.es](mailto:vezin@uv.es) (V. Zingales).



# The role of mitochondria in sterigmatocystin-induced apoptosis on SH-SY5Y cells

Veronica Zingales\*, Mónica Fernández-Franzón, Maria-José Ruiz

Laboratory of Food Chemistry and Toxicology, Faculty of Pharmacy, University of Valencia, Av. Vicent Andrés Estellés s/n, 46100, Valencia, Spain

## ARTICLE INFO

**Keywords:**  
Sterigmatocystin  
SH-SY5Y cells  
Cytotoxicity  
Mitochondria  
Apoptosis

## ABSTRACT

Mitochondria are cellular organelles involved in many crucial functions, such as generation of energy (ATP) and initiation of apoptosis. The aim of the present study was to evaluate the role of mitochondria in the toxicity induced by sterigmatocystin (STE), a mycotoxin produced by fungi of the genus *Aspergillus*, on SH-SY5Y cells. Our results showed that STE exposure decreased cell viability in a time- and concentration-dependent manner by MTT assay and caused mitochondrial dysfunction, as highlighted by the increase of STE cytotoxicity in cells forced to rely on mitochondrial oxidative phosphorylation. Furthermore, intracellular ATP depletion and increased mitochondrial reactive oxygen species were also observed. Since mitochondria play a pivotal role in apoptosis, the induction of this process in response to STE exposure was decided to study. Our results showed an increase in apoptotic cell population by flow cytometry, further confirmed by the up-regulation of the expression levels of the pro-apoptotic genes *Bax* and *Casp-3* and the down-regulation of the anti-apoptotic gene *Bcl-2* by qPCR technique. Taken together, our results provide novel insights in the signalling pathways of the cell death process induced by STE in SH-SY5Y cells, highlighting the key role played by mitochondria in STE toxicity.

## 1. Introduction

Mitochondria are key cellular organelles known to guarantee many physiological processes, such as cell proliferation and differentiation, production of cellular energy, signal transduction and cell death. Alterations of one or more of these functions can lead to cellular stress and impairment of cell viability. In particular, the synthesis of high-energy molecules, mainly adenosine-5'-triphosphate (ATP), is a crucial process for cell survival. Considering that ATP synthesis from ADP and inorganic phosphate ( $P_i$ ) involves a complex reaction network, any process that disturbs or blocks it results in a reduction of the ATP generation. In eukaryotic cells, mitochondria produce ATP through oxidative phosphorylation (OXPHOS), a process that involves the electron transport chain (ECT), a series of protein complexes and electron carrier molecules embedded in the inner mitochondrial membrane. The ECT pumps protons out of the mitochondrial matrix into the intermembrane space, generating an electrochemical gradient and, consequently, a membrane potential ( $\Delta\Psi_m$ ), used to synthesize ATP. However, in *in vitro* conditions, cell lines are metabolically adapted to growth rapidly and, for this reason, they derive most of their energy from glycolysis rather than OXPHOS, a phenomenon known as the Crabtree effect (Marroquin et al., 2007; Rodríguez-Enriquez et al., 2001). Evidence suggests that the Crabtree effect can be reversed by

culturing cells in galactose as the main fuel source; these conditions abolish net yield of ATP from glycolysis and, correspondingly, cells are forced to rely on mitochondrial OXPHOS (Rossignol et al., 2004). The substitution of galactose for glucose in the culture medium is used as a method not only to shift the energy metabolism toward OXPHOS, but also as an expeditious way to determine mitochondrial toxicity and reveal mitochondrial dysfunction (Marroquin et al., 2007). Several chronic diseases, including neurodegenerative diseases such as Parkinson's and Alzheimer's, are associated to mitochondrial dysfunction. The latter is characterized by losing efficiency in the ECT and reduction in ATP synthesis (Karbowski and Neutzner, 2012). To date, a lot of mitochondrial toxins are known (Wallace and Starkov, 2000). Among these, natural products, such as the *Streptomyces*-derived ETC inhibitor antimycin A or mycotoxins, have been recognized to contribute to the occurrence of mitochondrial dysfunction (Islam et al., 2018). Mycotoxins are toxic secondary metabolites that can occur in a variety of food and feed. They are produced by a number of fungal genera, primarily *Aspergillus*, *Penicillium*, *Alternaria* and *Fusarium* genus (Marin et al., 2013). Sterigmatocystin (STE) is a mycotoxin mainly produced by several species of the genus *Aspergillus*. Because this genus of fungi grows under a wide range of environmental conditions, including at low and high temperature (4–40 °C), fungal contamination may occur at various points in the food chain, such as the pre- and post-harvest

\* Corresponding author. Laboratory of Toxicology, Faculty of Pharmacy, University of Valencia, Av. Vicent Andrés Estellés, s/n, 46117, Burjassot, Valencia, Spain.  
E-mail address: [vezin@uv.es](mailto:vezin@uv.es) (V. Zingales).

<https://doi.org/10.1016/j.fct.2020.111493>

Received 27 January 2020; Received in revised form 31 May 2020; Accepted 2 June 2020

Available online 14 June 2020

0278-6915/ © 2020 Elsevier Ltd. All rights reserved.

RESEARCH ARTICLE



# Sterigmatocystin-induced DNA damage triggers cell-cycle arrest *via* MAPK in human neuroblastoma cells

Veronica Zingales, Mónica Fernández-Franzón and Maria-José Ruiz 

Laboratory of Food Chemistry and Toxicology, Faculty of Pharmacy, University of Valencia, Valencia, Spain

## ABSTRACT

Sterigmatocystin (STE) is a common mycotoxin found in food and feed. Many studies showed that STE is genotoxic. However, up to now, the potential genotoxicity of STE on human neuronal system remains unknown. In this study, we explored the effect of STE on DNA damage and cell-cycle progression on human neuroblastoma SH-SY5Y cells exposed to various concentrations of STE (0.78, 1.56 and 3.12  $\mu\text{M}$ ) for 24 h. The results indicated that STE exposure induced DNA damage, as evidenced by DNA comet tails formation and increased  $\gamma\text{H2AX}$  foci. Additionally, genotoxicity was confirmed by micronuclei (MN) analysis. Furthermore, we found that STE exposure led to cell-cycle arrest at the S and the G<sub>2</sub>/M phase. Considering the important role played by MAPK and p53 signaling pathways in cell-cycle arrest, we explored their potential involvement in STE-induced cell-cycle arrest by using specific inhibitors. The inhibition of JNK and ERK resulted to attenuate S and G<sub>2</sub>/M arrest, whereas the inhibition of p38 and p53 attenuated only STE-induced S phase arrest. In conclusion, the present study demonstrates that STE induced DNA damage and triggered MAPK and p53 pathways activation, resulting in cell-cycle arrest at the S and the G<sub>2</sub>/M phase.

## ARTICLE HISTORY

Received 20 January 2021  
Revised 8 April 2021  
Accepted 8 April 2021

## KEYWORDS

Sterigmatocystin; SH-SY5Y cells; genotoxicity; DNA damage; cell cycle

## 1. Introduction

Sterigmatocystin (STE) is a toxic secondary fungal metabolite mainly produced by *Aspergillus versicolor* and *A. nidulans* fungi. The STE producing fungi have been frequently isolated from several foodstuffs, with a consequent strong economic impact for the biotechnological, agricultural and food industries. However, in literature only limited information is available on the presence of STE in food and feed (Zingales et al. 2020c). Due to the limited STE occurrence data, STE is not included in the European Commission Regulation (EC) no. 1881/2006, which established maximum levels for certain contaminants in foodstuffs to ensure animal and public health, as well as agricultural productivity (Commission Regulation 2006). However, efforts are focused on this mycotoxin to establish a better risk assessment. In fact, epidemiological evidence highlighted the existence of associations between STE exposure and the risk of cancer development. A large number of studies performed in China revealed that STE may be a putative etiological factor for gastric carcinoma, as suggested by the strong positive correlations existing between high levels of STE contamination in foodstuffs and a higher incidence of gastric cancer (Lou et al. 1995; Zhang X et al. 2003; Tian and Liu 2004; Hutanasu et al. 2011). Furthermore, STE has been shown to be hepatotoxic and nephrotoxic in animal models. Accordingly, in light of the animal studies performed and of the cases of human cancer analyzed as far, STE has been classified in the group

2B (possibly carcinogenic to humans) by the International Agency for Research on Cancer (IARC 1987; Pitt et al. 2012).

It has been generally accepted that one of the most common mechanism of action through which many carcinogenic mycotoxins induce abnormal cell proliferation and carcinogenesis consists in the alteration of cell-cycle progression. For example, the ochratoxin A (OTA), a nephrotoxic mycotoxin associated to urinary tract tumors, was shown to inhibit cell-cycle progression at the G<sub>2</sub> phase in human gastric epithelium GES-1 cells and at the G<sub>2</sub>/M phase in V79 Chinese hamster lung fibroblast, whereas cell-cycle arrest in G<sub>0</sub>/G<sub>1</sub> phase was detected in human liver cancer cells (HepG2) exposed to OTA and OTA + beauvericin (BEA), indicating that different effects on cell-cycle distribution can be induced in different cell lines (Palma et al. 2007; Cui et al. 2010; Juan-Garcia et al. 2019). Cell-cycle arrest in G<sub>2</sub>/M phase has been observed to be caused also by T-2 toxin in HepG2 cells and by zearalenone (ZEA) in human colon cancer cells (Abid-Essefi et al. 2004; Taroncher et al. 2020). Additionally, ZEA has been shown to induce G<sub>1</sub> phase arrest in human peripheral blood mononuclear cells (hPBMCs) (Banjerdpongchai et al. 2010). Similar results were obtained in hPBMCs exposed to OTA (Liu J et al. 2012).

The cell-cycle arrest is frequently a consequence of DNA damage that can be caused by environmental or metabolic factors. Indeed, in the presence of DNA damage, cells respond by undergoing cell-cycle arrest, to minimize the replication of damaged DNA and prevent the transmission of